UNIVERSIDAD COMPLUTENSE DE MADRID

FACULTAD DE CIENCIAS FÍSICAS

TESIS DOCTORAL

Límites fundamentales en metrología cuántica

Fundamental Limits In Quantum Metrology

MEMORIA PARA OPTAR AL GRADO DE DOCTOR

PRESENTADA POR

José Luis Romero Hervás

DIRIGIDA POR

Luis Lorenzo Sánchez Soto
Ángel Santiago Sanz Ortiz

Fundamental Limits in Quantum Metrology

Límites Fundamentales en Metrología Cuántica

Memoria para optar al grado de Doctor

presentada por

José Luis Romero Hervás

UNIVERSIDAD COMPLUTENSE DE MADRID

FACULTAD DE CIENCIAS FÍSICAS

Directores

Luis Lorenzo Sánchez Soto y Ángel Santiago Sanz Ortiz

Programa de Doctorado en Física

Agradecimientos

Han sido unos años intensos, llenos de desafíos y aprendizajes que me han permitido crecer mucho tanto a nivel académico como personal. Aunque este camino ha supuesto un gran reto, también ha sido enormemente gratificante. Quiero expresar mi agradecimiento a mis directores, Ángel y Luis, por haberme dado la oportunidad de embarcarme en esta aventura. Asimismo, agradezco a todas las personas de la Universidad de Palacky por su cálida acogida durante mi estancia allí, especialmente a Marek y a Jarda. Por último, gracias a mis padres por estar siempre ahí.

Contents

Resumen xii

Abstract xiii

1 Introduction to Quantum Metrology **1**

1.1 Introduction 1

1.2 Mathematical Preliminaries 5

1.2.1 Classical estimation 5

1.2.2 Quantum Metrology 9

1.2.3 SU(2) parametrized processes 12

1.3 Quantum Metrology Overview 17

1.3.1 Heisenberg Scaling 18

1.3.2 Multiparameter Quantum Metrology 20

1.3.3 Bayesian Quantum Metrology 22

1.3.4 Global Quantum Metrology 24

1.3.5 Machine Learning 25

1.3.6 Other topics 26

2 Publications **29**

2.1 Project 1: Corrections to the quantum Cramér-Rao bound 29

2.2 Project 2: Majora constellation and robust states for SU(2) sensing 32

2.3 Project 3: Multi-parameter estimation and super-resolution 33

3 Conclusions and Future Outlook **36**

Bibliography **39**

Resumen

Esta tesis se compone de tres proyectos que abordan diversos problemas en metrología cuántica.

El primer proyecto se centra en el cálculo de correcciones de orden superior a la cota cuántica de Cramér-Rao (QCRB). Si bien la QCRB establece un límite inferior para el error cuadrático medio (MSE) en el régimen asintótico de un gran número de repeticiones experimentales, no proporciona información sobre la velocidad de convergencia ni sobre el MSE en escenarios con recursos finitos. En este trabajo, se derivan analíticamente correcciones de orden $1/\nu^2$ y superiores al MSE, donde ν representa el número de repeticiones, lo que ofrece una descripción más precisa del comportamiento preasintótico del MSE. Este enfoque, novedoso en la literatura por su naturaleza analítica dentro del paradigma frecuentista, revela que dichas correcciones dependen explícitamente de la medida cuántica implementada. Este hallazgo pone de manifiesto diferencias cruciales entre medidas que son equivalentes en el límite asintótico. Análogamente, al depender de momentos de orden superior de los estados cuánticos, estas correcciones permiten distinguir entre familias de estados que eran indistinguibles bajo la aproximación asintótica. También se analiza la cota de Bhattacharyya y su conexión con estas correcciones, lo que clarifica su utilidad práctica. Estos resultados son de gran relevancia para el diseño de protocolos de estimación óptimos en escenarios con recursos limitados, que son la norma en la práctica.

El segundo proyecto explora la conexión entre la representación de Majorana, la distribución multipolar y la sensibilidad a rotaciones en sistemas con simetría SU(2). La representación de Majorana permite una visualización geométrica de los estados cuánticos y la distribución multipolar cuantifica esa geometría desde un punto de vista invariante SU(2), la cual está íntimamente ligada a la sensibilidad de los estados para detectar transformaciones SU(2). En un primer trabajo, se encuentra una fórmula analítica para los multipolos en función de la constelación de Majorana para la transición entre un estado coherente y un estado N00N, y se caracteriza la distribución multipolar que emerge al maximizar un multipolo específico, lo que revela una estructura de múltiples picos que evoluciona hacia la del estado N00N, entre otros resultados. En un segundo trabajo, la investigación se enfoca en los denominados Random Majorana States, generados mediante la selección aleatoria de puntos sobre la esfera de Bloch. Estos estados se estudian en profundidad de manera numérica y se observa que son robustos frente al ruido desde un punto de vista metrológico. Finalmente, se colaboró con un grupo experimental que generó estos estados utilizando el momento angular orbital de la luz y los empleó para la detección experimental de rotaciones.

El tercer proyecto aborda el problema de la estimación simultánea del centroide y la separación

entre dos fuentes puntuales incoherentes, un problema de gran relevancia en superresolución espacial. Este problema adquirió renovada atención a partir de 2016, cuando un análisis desde la perspectiva de la metrología cuántica demostró que, mediante la implementación de medidas adecuadas, es posible estimar la separación entre las fuentes con una precisión que no depende de su proximidad. Este es un caso paradigmático de estimación multiparamétrica donde las medidas óptimas para cada parámetro individual son mutuamente incompatibles, lo que impide saturar la QCRB de forma conjunta. En este trabajo, se deriva analíticamente una familia de medidas óptimas que permiten extraer la máxima información simultánea sobre el centroide y la separación. Aunque la existencia de tales medidas se había hipotetizado numéricamente para funciones de dispersión de punto (PSF) particulares, la contribución principal de este trabajo radica en la derivación analítica de sus expresiones, válidas para PSFs arbitrarias. Además, se demuestra que estas medidas no son únicas, lo que ofrece una flexibilidad adicional para su implementación experimental.

Abstract

This thesis consists of three projects that address various problems in quantum metrology.

The first project focuses on the calculation of higher-order corrections to the quantum Cramér-Rao bound (QCRB). While the QCRB establishes a lower bound for the mean squared error (MSE) in the asymptotic regime of a large number of experimental repetitions, it provides no information on the convergence speed or the MSE in scenarios with finite resources. In this work, corrections of order $1/\nu^2$ and higher to the MSE are analytically derived, where ν represents the number of repetitions, offering a more precise description of the pre-asymptotic behavior of the MSE. This approach, novel in the literature for its analytical nature within the frequentist paradigm, reveals that these corrections explicitly depend on the implemented quantum measurement. This finding highlights crucial differences between measurements that are equivalent in the asymptotic limit. Analogously, by depending on higher-order moments of the quantum states, these corrections allow for distinguishing between families of states that were indistinguishable under the asymptotic approximation. The Bhattacharyya bound and its connection to these corrections are also analyzed, clarifying their practical utility. These results are relevant for designing optimal estimation protocols in resource-limited scenarios, which are the norm in practice.

The second project explores the connection between the Majorana representation, the multipolar distribution, and the sensitivity to rotations in systems with SU(2) symmetry. The Majorana representation allows for a geometric visualization of quantum states, and the multipolar distribution quantifies this geometry from an SU(2)-invariant standpoint, which is intimately linked to the sensitivity of the states for detecting SU(2) transformations. In a first work, an analytical formula is found for the multipoles as a function of the Majorana constellation for the transition between a coherent state and a N00N state, and the multipolar distribution that emerges when maximizing a specific multipole is characterized, revealing a multi-peaked structure that evolves towards that of the N00N state, among other results. In a second work, the research focuses on the so-called Random Majorana States, generated by randomly selecting points on the Bloch sphere. These states are studied in depth numerically, and they are observed to be robust against noise from a metrological standpoint. Finally, a collaboration was carried out with an experimental group that generated these states using the orbital angular momentum of light and used them for the experimental detection of rotations.

The third project addresses the problem of the simultaneous estimation of the centroid and separation between two incoherent point sources, a problem of great relevance in spatial super-resolution. This problem gained renewed attention starting in 2016, when an analysis from the perspective of

quantum metrology showed that, by implementing appropriate measurements, it is possible to estimate the separation between the sources with a precision that does not depend on their proximity. This is a paradigmatic case of multiparameter estimation where the optimal measurements for each individual parameter are mutually incompatible, which prevents the joint saturation of the QCRB. In this work, a family of optimal measurements is analytically derived that allows for the simultaneous extraction of maximum information about the centroid and the separation. Although the existence of such measurements had been numerically hypothesized for particular point spread functions (PSFs), the main contribution of this work lies in the analytical derivation of their expressions, which are valid for arbitrary PSFs. Furthermore, it is shown that these measurements are not unique, which offers additional flexibility for their experimental implementation.

1

Introduction to Quantum Metrology

1.1 Introduction

In physics, our understanding of the world hinges on our ability to measure it. Physical theories are validated or refuted through measurements, making metrology not just a technical practice but a cornerstone of the scientific method. Measurement serves as the crucial interface between theoretical constructs and observable reality. However, this interface is not a mere passive mirror of nature; its power lies in our ability to interpret data and extract precise knowledge. This interpretative process depends critically on estimation tools. Without them, testing hypotheses and advancing our understanding of the universe would be impossible.

Traditionally, in classical metrology it was assumed that all measurement errors stemmed from environmental disturbances or technical imperfections. In principle, it was believed that any desired level of precision could be achieved by sufficiently minimizing these noise sources. However, the advent of quantum mechanics fundamentally transformed this viewpoint, revealing the existence of fundamental limits to the precision of any estimation, even under ideal conditions, imposed by the inherently probabilistic nature of quantum systems.

In this context, quantum metrology emerges as the discipline that studies the ultimate limits in the estimation of physical parameters when the underlying system obeys the laws of quantum mechanics. Far from being mere restrictions, these quantum limits act as guides that allow us to design innovative protocols. These protocols leverage intrinsically quantum properties, such as entanglement, to achieve

precisions unattainable by classical methods.

The potential applications of quantum metrology span a broad and promising spectrum of fields:

- **High-precision timekeeping:** The application of quantum principles is catalyzing advances in the field of atomic clocks. Particularly, leveraging entanglement between atoms and their precise manipulation are key to improving the performance of these devices [1–3]. These developments are crucial for future applications requiring precise global synchronization and advanced navigation systems.

- **Enhanced spectroscopy:** Spectroscopy, a fundamental tool for analyzing the composition of matter, also benefits enormously from advances in quantum metrology. Protocols are being actively developed that use nonclassical light, such as entangled or squeezed states, to overcome the noise limitations inherent in classical light sources and thus improve sensitivity in the detection of chemical species [4–7]. These techniques open new avenues for the precise analysis of exoplanet atmospheres, where the signal is extremely faint, aiming to identify biomarkers or characterize their composition with high precision [8].

- **Bioimaging:** The field of medical diagnostics and biological imaging is beginning to explore the potential of quantum techniques to overcome the limitations of conventional methods. Protocols are being investigated that leverage the quantum properties of light to obtain images with higher resolution or contrast, even with a reduced number of photons, which could minimize damage to sensitive biological samples [9, 10]. These approaches promise to improve the ability to visualize biological structures and facilitate the early detection of diseases, as explored in studies on quantum decoherence in contexts relevant to Positron Emission Tomography (PET) [11].

- **Defense and navigation:** High-precision inertial navigation systems based on atom interferometry are being developed, with the capability for multi-axis measurements under various dynamic conditions [12, 13]. Institutions such as the U.S. Naval Research Laboratory (NRL) are working on these technologies to reduce drift in navigation systems and decrease reliance on GPS [14].

- **Weak-field detection:** The ability to measure very weak magnetic, electric, or gravitational fields with extreme precision is another of the great promises of quantum metrology. Sensors based on quantum principles, such as trapped-ion crystals or diamond defects (Nitrogen-Vacancy, or NV, centers), are being developed, demonstrating improved sensitivity for detecting minute displacements or nanoscale electric fields [15–17]. These technologies have great potential for application in fields such as neuroscience (e.g., for magnetoencephalography) and geophysics,

through gravitational mapping for subsurface studies [18].

- **High-resolution imaging:** Optical microscopy faces the fundamental barrier of the diffraction limit, but quantum super-resolution techniques offer ways to transcend it [19]. Strategies such as leveraging photon antibunching, complemented by machine learning to optimize acquisition and processing, are demonstrating the ability to improve image quality and speed, resulting in sharper observation of subcellular-scale structures [20–22].

- **Experimental tests of fundamental theories:** The high sensitivity of quantum sensors is being exploited in the search for dark matter candidates, such as axions, through the detection of their interactions with ordinary matter [23, 24]. Experiments are also being conducted to identify dark energy effects, and sensor networks are being designed to investigate large-scale phenomena, ranging from molecules to massive quantum systems, in order to explore the nature of gravity and search for new physics [25–29].

While some branches of quantum technologies [30–32], such as quantum cryptography [33–35] or computing [36], often generate considerable media attention [37] but are in more nascent stages of development for large-scale applications, quantum metrology has already demonstrated concrete and high-impact applications. A paradigmatic example is its contribution to the detection of gravitational waves in observatories like LIGO [38, 39]. Nevertheless, significant challenges persist, such as the practical implementation of robust protocols in the presence of noise and the scalability of quantum systems.

Among the most significant open challenges in quantum metrology are:

- **Noise, loss, and decoherence:** It is crucial to design protocols that remain effective with current technology and realistic imperfections. A case in point is LIGO: after suppressing classical noise to near-fundamental levels, squeezed-vacuum injection delivered quantum-enhanced sensitivity, with the attainable gain ultimately limited by optical losses and phase noise [38].

- **Theoretical limits and general tools:** Many current techniques have been developed under the idealization of infinite resources. We still lack tools to accurately describe more realistic scenarios that consider finite resources, losses, and imperfect measurements. Additionally, the exploration of new developments, such as global scenarios, or the use of machine learning, is very promising. Within these theoretical challenges, multiparameter estimation is particularly relevant. When it is necessary to simultaneously estimate more than one parameter, fundamental incompatibilities can arise that limit the achievable joint precision. This problem is conceptually more complex, and our understanding of it is still partial.

- **Entangled quantum states and measurements:** The efficient generation, manipulation, and detection of quantum states remain a major experimental challenge for all quantum technologies, especially concerning the construction of scalable systems.

This thesis is part of the collective effort to understand and overcome the fundamental limits in quantum estimation. Through three independent but interconnected projects, we address different key aspects of the discipline:

- **Corrections to the quantum Cramér-Rao bound:** In experimental practice, available resources are inherently finite. However, a large part of theoretical developments in quantum metrology are made under the assumption of the asymptotic regime of infinite resources. This work provides analytical tools to understand how precision behaves in the pre-asymptotic regime, thus providing useful information for the design of realistic experiments.

- **Majorana constellation and robust states for SU(2) sensing:** Numerous physical processes relevant in metrology, such as phase estimation or magnetometry, can be modeled by transformations of the SU(2) group. In this thesis, we investigate the geometric structure of the quantum states relevant for these tasks through the Majorana representation and the multipolar distribution. We also propose random states that exhibit high robustness against noise, which, furthermore, have been experimentally implemented in collaboration with another research group.

- **Multiparameter estimation and super-resolution:** One of the great theoretical challenges in quantum metrology is the precise and simultaneous estimation of multiple parameters. In this context, we propose a protocol that allows achieving maximum precision in the simultaneous estimation of the centroid and separation of two incoherent sources. These advances are particularly relevant in applications such as astronomy or microscopy of delicate objects, where direct manipulation of the observed object is not feasible.

This thesis is presented in the format of a compilation of publications. The dissertation is organized as follows: Section 1.2 introduces the fundamental theoretical concepts and tools required to understand the presented work. Next, Section 1.3 provides a review of the state of the art in quantum metrology. The core of this thesis consists of the original research articles, which are presented in Chapter 2. For clarity, the chapter is subdivided into three thematic sections, each introduced by a brief overview that outlines its objectives and main contributions. Finally, Chapter 3 presents the overall conclusions of this work and delineates the future lines of research arising from it.

1.2 Mathematical Preliminaries

In this section, we will introduce the fundamental tools used in the articles that make up this thesis. The purpose is to facilitate the understanding of the results presented in those works. Although each article includes a brief introduction to these tools, a certain familiarity on the part of the reader is often assumed. Consequently, this section is conceived as a detailed complement to the introductions of the articles.

1.2.1 Classical estimation

Estimation theory is a well-established branch of statistics. Given the breadth and depth of the field, this section will concentrate specifically on the concepts and tools most relevant to the developments that follow. The material presented is drawn from foundational works that can be found in the literature [40–45].

Let us consider a physical system whose description depends on an unknown parameter θ. This system is, in general, subject to fluctuations or noise, which implies that repeated measurements of it will, in general, lead to different results. An illustrative example could be the estimation of a parameter characterizing a radio signal, which can be affected by atmospheric conditions during its propagation from the emitter to the receiver. In the context of this thesis, the main interest lies in noise of a fundamental nature. Specifically, we will assume that the parameter θ characterizes a quantum system, and that the randomness inherent in the measurements originates from the principles of quantum mechanics.

The outcome of the experiment is represented by the random variable X, which follows a family of probability distributions $p(x|\theta)$, parametrized by θ, the quantity to be estimated. In what follows, we will assume that we have access to this probability distribution, which is plausible in situations where well-founded theoretical models allow for its calculation. However, in practice, real systems, subject to various sources of noise and imperfections, can deviate significantly from the predictions of available theoretical models. Even if a model is available, it might behave like a "black box"; that is, the dependence of the probability on the parameter θ might not be a simple analytical function. In the absence of a precise theoretical model, the probability function $p(x|\theta)$ can be obtained through experimental characterization of the system. This is the typical case in the development and calibration of sensors, where one has control over the parameter θ. Following the previous example of the radio signal, one could emit a signal with a fixed value of θ and observe the results at the receiver. By repeating the experiment a large number of times, it is possible to construct $p(x_i|\theta)$ empirically, approximating it by the relative frequency of occurrence of the outcome x_i.

Typically, the experiment is repeated ν times. For a given sequence of trials we denote the counts of each possible outcome $\{x_1, x_2, \ldots, x_N\}$ as $\{\nu_1, \nu_2, \ldots, \nu_N\}$, where $\nu_1+\nu_2+\cdots+\nu_N = \nu$. Assuming that individual measurements are statistically independent, a premise that will be maintained throughout this thesis, the probability of obtaining a specific set of outcomes $\{\nu_1, \nu_2, \ldots, \nu_N\}$ is given by the multinomial distribution:

$$p(\nu_1, \nu_2, \ldots, \nu_N|\theta) = \frac{\nu!}{\nu_1!\nu_2!\cdots\nu_N!} p(x_1|\theta)^{\nu_1} p(x_2|\theta)^{\nu_2} \ldots p(x_N|\theta)^{\nu_N}. \tag{1.1}$$

The combinatorial prefactor accounts for the different orders in which the outcomes x_i can occur to produce the observed set $\{\nu_1, \nu_2, \ldots, \nu_N\}$.

Within the frequentist paradigm of estimation, the primary objective is to infer the value of the parameter θ from the experimental data $\{\nu_1, \nu_2, \ldots, \nu_N\}$. This translates into obtaining an estimate θ_{est} that is as close as possible to the true value of θ, given the available data. This approach will be adopted in the present thesis. It is worth mentioning the existence of alternative approaches, such as the Bayesian one, in which the result of the inference is not a point value θ_{est}, but a probability distribution $p(\theta|\nu_1, \nu_2, \ldots, \nu_N)$ for the parameter θ, conditioned on the observed experimental results.

In the frequentist framework, inference is performed using a function called an estimator, $\hat{\theta}(x)$. This function assigns an estimated value θ_{est} to each possible set of experimental outcomes $\{\nu_1, \nu_2, \ldots, \nu_N\}$:

$$\theta_{\text{est}} = \hat{\theta}(\nu_1, \nu_2, \ldots, \nu_N). \tag{1.2}$$

Naturally, we seek estimators that provide precise estimates. To quantify the quality of an estimator, it is necessary to define a loss function that measures the error made in the estimation. An intuitive choice for the loss function could be the absolute error $|\hat{\theta}(x) - \theta|$. However, for reasons of mathematical tractability, the squared error $[\hat{\theta}(x) - \theta]^2$ is commonly used. This choice implies that large errors contribute more significantly to the overall measure of imprecision than small errors, unlike the absolute error which penalizes them linearly.

This leads to the definition of the mean squared error (MSE), which is the expected value of this squared error, averaged over all possible experimental outcomes, for a fixed value of the parameter θ:

$$\text{MSE}[\hat{\theta}(x)]_\theta = \langle[\hat{\theta}(x) - \theta]^2\rangle = \sum_{x\in\{\nu_1\cdots,\nu_N\}} p(x|\theta)[\hat{\theta}(x) - \theta]^2. \tag{1.3}$$

Here, the notation $\langle\cdot\rangle$ denotes the average value with respect to $p(x|\theta)$. Once the MSE is defined, different objectives can be set in choosing an estimator. For example, one could seek an estimator

that minimizes the worst-case scenario; i.e., that minimizes the quantity

$$\sup_{\theta\in\Theta} \mathrm{MSE}[\hat{\theta}(x)]_\theta, \tag{1.4}$$

where Θ represents the set of all possible values that the parameter θ can take. This approach, known as minimax, is useful when it is crucial to avoid very poor estimates, even if it means not achieving the maximum possible precision for most values of θ. A closely related idea appears in radiotherapy: small, realistic uncertainties in patient setup or tissue properties can degrade the delivered dose distribution, so that some regions receive more or less than intended. To mitigate such extreme outcomes, planning employs robust optimization, including worst-case (minimax) formulations [46].

An ideal situation would arise if it were possible to find an estimator $\hat{\theta}(x)$ that minimizes the $\mathrm{MSE}[\hat{\theta}(x)]_\theta$ for all possible values of $\theta \in \Theta$. However, this problem, in general, has no solution; i.e., such a universally optimal estimator does not exist. For any proposed estimator, it is possible to find another that offers better performance for certain specific values of θ. The space of all possible estimators is, in this sense, too broad. To make progress, it is necessary to restrict the class of estimators considered. This leads us to a second approach, which involves considering unbiased estimators. An unbiased estimator is one whose expected value coincides with the true value of the parameter for all θ:

$$\langle\hat{\theta}(x)\rangle = \theta. \tag{1.5}$$

For this class of unbiased estimators, there is a fundamental result known as the (classical) Cramér-Rao bound (CCRB). This bound establishes a lower limit for the achievable MSE:

$$\mathrm{MSE}[\hat{\theta}(x)]_\theta \geq \frac{1}{\nu F(\theta)}, \tag{1.6}$$

where $F(\theta)$ is the so-called classical Fisher information (CFI), defined as:

$$F(\theta) = \sum_{i=1}^{N} p(x_i|\theta) \left[\frac{\partial_\theta p(x_i|\theta)}{p(x_i|\theta)}\right]^2. \tag{1.7}$$

The existence of such a bound is of great practical utility, as it informs about the maximum theoretically achievable precision. If an estimation protocol leads to a precision bound higher than that required for a particular application, this indicates the need to modify or change said protocol. However, the bound does not guarantee that the estimation precision is actually achievable; therefore, the CCRB acts as a first criterion for discarding strategies, but evaluating the actual performance of the estimator remains necessary.

Although the concept of an unbiased estimator is theoretically attractive and allows for considerable analytical progress, its practical applicability is often limited to idealized examples. In most real problems, finding unbiased estimators may not be feasible. Even if they could be found, the ultimate goal remains the minimization of the MSE. An estimator that, even if biased, delivers consistently low MSE over the range of possible parameter values may be preferable to an unbiased estimator with high MSE.

In practice, estimators such as the maximum likelihood estimator (MLE) are frequently used. The MLE depends solely on the probability $p(x|\theta)$, so if this function is available, the estimator is, in principle, accessible. However, the apparent simplicity of this approach often conceals significant numerical challenges, especially if the function $p(x|\theta)$ has a complex structure.

As mentioned above, the CCRB is formulated as a bound for unbiased estimators. However, its utility extends considerably beyond this restriction, making it a widely used tool in practice. In the asymptotic limit, when the number of experimental repetitions ν tends to infinity, the CCRB becomes a bound for any estimator, whether unbiased or not. More precisely, for any reasonable estimator $\hat{\theta}(x)$, it holds that:

$$\mathrm{MSE}[\hat{\theta}(x)]_\theta \geq \frac{1}{\nu F(\theta)} + \mathcal{O}\left(1/\nu^2\right). \tag{1.8}$$

This result is of great importance, as it not only establishes the maximum achievable precision in the limit of a large number of resources but also indicates how to achieve it. It can be shown that the MLE, which, as introduced, is a generally accessible estimator (with the aforementioned numerical caveats), saturates this bound in the limit $\nu \to \infty$. That is, the goal of obtaining the minimum possible MSE for all values of θ is, in fact, achievable in this asymptotic limit. In general, when seeking an estimator, this property of asymptotic efficiency (saturating the CCRB) is highly desirable. It is important to note that not all estimators satisfy it.

In this thesis, the CCRB and its quantum analog, the QCRB (which will be introduced in the next section), will be understood in this asymptotic sense: as the maximum precision achievable in the limit $\nu \to \infty$.

All the theory presented so far can be generalized to the case of estimating multiple parameters. Let $\boldsymbol{\theta} = (\theta_1, \cdots, \theta_M)$ be the vector of parameters to be estimated, and $\hat{\boldsymbol{\theta}}(x) = (\hat{\theta}_1(x), \cdots, \hat{\theta}_M(x))$ be the vector of their corresponding estimators. In the limit $\nu \to \infty$, a generalization of the CCRB is obtained in the form:

$$\mathrm{MSE}[\hat{\boldsymbol{\theta}}(x)]_{\boldsymbol{\theta}} \succeq \frac{1}{\nu}\boldsymbol{F}^{-1}(\boldsymbol{\theta}) + \mathcal{O}\left(1/\nu^2\right). \tag{1.9}$$

In this expression, $\boldsymbol{A} \succeq \boldsymbol{B}$ means that the matrix $\boldsymbol{A} - \boldsymbol{B}$ is positive semidefinite, $\mathrm{MSE}[\hat{\boldsymbol{\theta}}(x)]$ is the MSE matrix of the estimation error, and $\boldsymbol{F}(\boldsymbol{\theta})$ is the Fisher information matrix. Their elements are

given by:

$$\begin{aligned} \mathrm{MSE}[\hat{\boldsymbol{\theta}}(x)]_{ij} &= \langle [\hat{\theta}_i(x) - \theta_i][\hat{\theta}_j(x) - \theta_j] \rangle, \\ \boldsymbol{F}_{ij}(\boldsymbol{\theta}) &= \left\langle \frac{\partial_{\theta_i} p(x|\boldsymbol{\theta})}{p(x|\boldsymbol{\theta})} \frac{\partial_{\theta_j} p(x|\boldsymbol{\theta})}{p(x|\boldsymbol{\theta})} \right\rangle . \end{aligned} \tag{1.10}$$

For practical purposes, this implies that the MSE of the estimation of each individual parameter is bounded. In particular, for the estimation of the parameter θ_i, we have:

$$\mathrm{MSE}[\hat{\theta}_i(x)]_{\boldsymbol{\theta}} \geq \frac{1}{\nu} [\boldsymbol{F}^{-1}(\boldsymbol{\theta})]_{ii} + \mathcal{O}\left(1/\nu^2\right). \tag{1.11}$$

That is, bounds are obtained for the precision with which the different parameters can be estimated, determined by the diagonal elements of the inverse of the Fisher information matrix $\boldsymbol{F}(\boldsymbol{\theta})$.

As in the single-parameter case, this multiparameter bound is asymptotically achievable by the MLE and represents the fundamental limit to precision in the simultaneous estimation of multiple parameters in the regime of a large number of measurements.

1.2.2 Quantum Metrology

The fundamental concepts of quantum metrology that will be presented in this section can be found in various reviews [47–50], as well as some PhD theses [51–53].

In the context of quantum metrology, the probability distribution $p(x|\theta)$, which governs experimental outcomes, originates from a measurement performed on a quantum system. Let $\rho(\theta)$ be a density matrix that depends on the parameter θ to be estimated, and let $\Pi = \{\Pi_1, \ldots, \Pi_N\}$ be a set of measurement operators describing a Positive Operator-Valued Measure (POVM). Then, the probability of obtaining outcome x_i is given by Born's rule:

$$p(x_i|\theta) = \mathrm{Tr}\left[\rho(\theta)\Pi_i\right]. \tag{1.12}$$

The dependence of the quantum state on the parameter θ generally arises from some physical process. A paradigmatic case, and one of great relevance in this thesis, is the unitary encoding of the parameter. In this scenario, the quantum state evolves according to $\rho(\theta) = U(\theta)\rho_0 U^\dagger(\theta)$, where ρ_0 is the initial state of the system and $U(\theta)$ is a unitary transformation that depends on the parameter, and can be expressed as $U(\theta) = \exp(-i\theta X)$, where X is a Hermitian operator generating the transformation.

As discussed in the previous section on classical metrology, the main interest lies in the asymptotic limit $\nu \to \infty$, where the CCRB establishes a fundamental bound on estimation precision. Therefore, in the quantum realm, the objective is to determine the POVM Π that maximizes the classical Fisher information $F(\theta)$ for a given state $\rho(\theta)$. A larger $F(\theta)$ will imply a tighter CCRB (lower minimum achievable MSE).

Given a quantum state $\rho(\theta)$, maximizing the CFI over all possible POVMs leads to the concept of quantum Fisher information (QFI), denoted by $Q[\rho(\theta)]$:

$$Q[\rho(\theta)] = \sup_{\Pi} F[\rho(\theta), \Pi]. \tag{1.13}$$

This optimization gives rise to the quantum Cramér-Rao bound (QCRB):

$$\mathrm{MSE}[\hat{\theta}(x)] \geq \frac{1}{\nu Q[\rho(\theta)]} + \mathcal{O}\left(1/\nu^2\right). \tag{1.14}$$

The QFI is given by the expression $Q[\rho(\theta)] = \mathrm{Tr}\left[L(\theta)^2 \rho(\theta)\right]$, where $L(\theta)$ is the operator known as the symmetric logarithmic derivative (SLD). The SLD is implicitly defined through the relation:

$$\partial_\theta \rho(\theta) = \frac{1}{2}[L(\theta)\rho(\theta) + \rho(\theta)L(\theta)]. \tag{1.15}$$

Thus, to achieve the maximum theoretically possible precision, it would suffice to implement the optimal POVM, Π_{opt}, the one for which $F[\rho(\theta), \Pi_{\mathrm{opt}}] = Q[\rho(\theta)]$, when measuring the system. However, there is an important subtlety: this optimal POVM, in general, depends on the true value of the parameter θ. In a real experimental situation, the objective is precisely to infer this true value, which implies that, a priori, θ is not known, and therefore, the measurement $\Pi_{\mathrm{opt}}(\theta)$ cannot be directly implemented.

This difficulty leads to two main scenarios. First, there may be situations where considerable prior information about the parameter is available; that is, it is known that θ lies within a relatively narrow range, bounded by θ_{min} and θ_{max}. In such a case, one can choose to use the POVM corresponding to the mean value of the interval, $(\theta_{\mathrm{max}} + \theta_{\mathrm{min}})/2$, or to some other prior estimate. In this regime, the theory of the local QCRB applies reasonably well. Second, the situation may arise where the interval of possible values for θ is very wide. In this case, some initial, possibly suboptimal, POVM will have to be employed. However, if, as data are acquired and more information about θ is obtained, the measurement strategy is adjusted using updated estimates of the parameter, $\Pi(\theta_{\mathrm{est}})$, it can be shown that, in the asymptotic limit $\nu \to \infty$, it is also possible to saturate the QCRB. Such strategies are known as adaptive strategies.

Throughout this thesis, we will generally assume that we are in a regime where it is reasonable to suppose that we have access to a POVM close to the optimal one, or that adaptive strategies can be employed to reach it asymptotically. When this assumption is not valid, we enter the domain of so-called global quantum metrology, a very active field of research today [54].

Once we have the QFI, one last step remains to obtain the maximum possible precision. For this, we seek the initial state ρ_0 that maximizes the QFI. The value obtained from this QCRB is the maximum precision allowed by nature (recall, in the asymptotic regime, where both QCRB and CCRB are valid). In particular, for the unitary case and when the initial state is pure $\rho_0 = |\psi_0\rangle \langle\psi_0|$, which will be the primary case treated in this thesis, we have the following expression for the QFI:

$$Q[e^{-i\theta X}\rho_0 e^{i\theta X}] = 4 \langle\psi_0| [X - \langle X\rangle]^2 |\psi_0\rangle \ . \tag{1.16}$$

Note that there is no dependence on θ as one might expect. This is something particular to the unitary case. The state that maximizes this expression is simply a superposition of the maximum and minimum eigenstates of the generator X.

As in the classical case, the above formalism can be extended to the estimation of vectorial parameters $\boldsymbol{\theta} = (\theta_1, \cdots, \theta_M)$. However, a fundamental complication arises now. The direct generalization of the QFI to the multiparameter case, defined through the quantum Fisher information matrix (QFIM):

$$\boldsymbol{Q}_{ij}(\boldsymbol{\theta}) = \frac{1}{2} \mathrm{Tr}\{\rho(\boldsymbol{\theta})[L_i(\boldsymbol{\theta})L_j(\boldsymbol{\theta}) + L_j(\boldsymbol{\theta})L_i(\boldsymbol{\theta})]\}, \tag{1.17}$$

where $L_i(\boldsymbol{\theta})$ are the SLDs corresponding to the parameter θ_i, gives rise to a multiparameter QCRB:

$$\mathrm{MSE}[\hat{\theta}_i(x)]_{\boldsymbol{\theta}} \geq \frac{1}{\nu}[\boldsymbol{Q}^{-1}]_{ii} + \mathcal{O}\left(1/\nu^2\right). \tag{1.18}$$

The problem lies in the fact that this multiparameter bound, based on the QFIM of the SLDs, is not generally saturable. That is, in general, there is no single POVM that allows simultaneously achieving the precision dictated by $\boldsymbol{Q}(\boldsymbol{\theta})$ for all parameters. The underlying reason is that the optimal individual measurement for estimating parameter θ_i may not commute with the optimal individual measurement for estimating parameter θ_j. Except in special cases (e.g., commuting SLDs), this typically leads one to consider a "trade-off" or compromise in the choice of the measurement strategy.

This nonsaturability has motivated the search for other information matrices and tighter bounds, with the ultimate goal of obtaining a tight bound, i.e., one for which an implementable measurement strategy exists that saturates it. Multiparameter quantum metrology is a very active field of research today. However, for the purposes of this thesis, we will primarily rely on results that have recently

appeared in the literature and offer an alternative approach to this problem [55]. This leads us to define the "information regrets":

$$\Delta_j = \sqrt{\frac{\boldsymbol{Q}_{jj} - \boldsymbol{F}_{jj}}{\boldsymbol{Q}_{jj}}}. \tag{1.19}$$

These quantities quantify how far one is from achieving the maximum possible precision (given by $\boldsymbol{Q}_{jj}$) for the estimation of the j-th parameter, when using a POVM that attempts to estimate all parameters simultaneously (giving rise to a classical Fisher information matrix $\boldsymbol{F}$). Recall that there always exists a POVM Π that allows, for a particular parameter j, $\boldsymbol{F}_{jj} = \boldsymbol{Q}_{jj}$ to hold. However, when estimating several parameters simultaneously, it is generally not possible to achieve this for all of them with the same measurement.

Eq. (1.19) leads to an uncertainty relation for any pair of parameters:

$$\Delta_j^2 + \Delta_k^2 - 2\sqrt{1-\tilde{c}_{jk}^2}\sqrt{(1-\Delta_j)(1-\Delta_k)} \;\leq\; 2 - \tilde{c}_{jk}^2. \tag{1.20}$$

In the specific case that will be studied in this thesis we have that $\tilde{c}_{jk} \to 1$ at the parameter value of interest. This is the maximal value of $\tilde{c}_{jk}$ and signals a regime of maximal incompatibility between the two parameters. In this limit, the trade-off simplifies to

$$\Delta_j^2 + \Delta_k^2 \leq 1. \tag{1.21}$$

Pushing one parameter to its quantum limit ($\Delta_j = 0$) forces the other to carry no information ($\Delta_k = 1$), and vice versa. Intermediate points ($0 < \Delta_j, \Delta_k < 1$) reflect different allocations of precision between the two estimates.

1.2.3 SU(2) parametrized processes

The content developed in this section, as well as extensions and more detailed treatments, can be found in [56–63]. In the context of the present thesis, a case of particular relevance will be where the unitary transformation $U(\theta)$ encoding the parameter belongs to the SU(2) group. These transformations are expressed as $U(\theta) = e^{-i\theta J_{\mathbf{n}}}$, where $J_{\mathbf{n}} = \mathbf{J}\cdot\mathbf{n}$ represents the component of the angular momentum operator $\mathbf{J} = (J_x, J_y, J_z)$ along the direction specified by the unit vector $\mathbf{n}$.

The irreducible representations of the SU(2) group are characterized by the quantum number S, which corresponds to the spin. We will focus mainly on systems where S is a fixed value. A generic

state in this representation can be written in the angular momentum basis as:

$$|\psi\rangle = \sum_{m=-S}^{S} \psi_m |S, m\rangle , \tag{1.22}$$

where $|S, m\rangle$ are the usual eigenstates of J^2 and J_z. Systems with a fixed value of S frequently appear in experimental physics. A prominent example is a set of N spin-1/2 bosons, whose collective states must belong to the symmetric subspace. This symmetric subspace is isomorphic to a total spin space $S = N/2$. Even for particles that are not bosons, the symmetric subspace can often be the subspace of physical interest [64]. It is important to note that it is not necessary for each elementary component (qubit) to correspond to an electronic "spin"; it is sufficient for it to be a two-level system. In practice, systems such as atoms trapped in optical lattices, photons propagating in waveguides, or superconducting qubits can implement this spin model.

Another important physical system whose description falls within the SU(2) formalism is the polarization of light. The polarization state of a monochromatic light beam is described by the Stokes vector $\mathbf{S} = (S_1, S_2, S_3)$. Upon quantization, the components of this vector satisfy the same commutation relations as those of the su(2) Lie algebra. Consequently, the action of any linear optical element on the polarization state is modeled as a rotation $U \in \mathrm{SU}(2)$.

Representing a quantum state by its coefficients ψ_m in the $|S, m\rangle$ basis is not the most intuitive way to visualize its geometric properties or its behavior under rotations. It is at this point that the Majorana representation offers an alternative and powerful perspective. This representation establishes a correspondence between a spin-S state and a set of $2S$ (unordered) points on the surface of a unit sphere. We can map every state to the following polynomial in the complex variable z:

$$f_\psi(z) = \sum_{m=-S}^{S} \psi_m (-1)^{S+m} \sqrt{\binom{2S}{S+m}} z^{S+m}, \tag{1.23}$$

which can be factored into its $2S$ complex roots:

$$f_\psi(z) = C(z - z_1)(z - z_2) \cdots (z - z_{2S}). \tag{1.24}$$

These complex roots can be mapped onto the unit sphere by a stereographic projection from the south pole, so each z_i is related to a point on the unit sphere through $z_i = \tan(\Theta_i/2)e^{i\Phi_i}$, where (Θ_i, Φ_i) are the usual spherical coordinates (with $\Theta_i \in [0, \pi]$ and $\Phi_i \in [0, 2\pi)$). This effectively provides a one-to-one map between any pure state of spin S and a configuration of $2S$ points on the unit sphere. These points are commonly known as the Majorana "stars", and their distribution on the sphere is

called the Majorana "constellation".

Although at first glance the Majorana representation is simply a mapping between two parameterizations of the quantum state, it possesses properties that make it particularly useful. One of the most important is that, under the action of a transformation $U(\theta) = e^{-i\theta J_{\mathbf{n}}} \in \mathrm{SU}(2)$ on the state $|\psi\rangle$, the associated Majorana constellation rotates rigidly on the unit sphere. Specifically, an SU(2) rotation of angle θ around the axis $\mathbf{n}$ applied to the quantum state translates into an ordinary geometric rotation of the constellation of stars by the same angle θ and around the same axis $\mathbf{n}$. This property contrasts with the transformation of the coefficients ψ_m, whose change under an SU(2) rotation does not usually have a direct geometrical interpretation.

Another relevant property relates the distribution of the stars to the expectation value of the spin. In general, the mean value of the spin operator $\langle\psi| J_{\mathbf{n}} |\psi\rangle$ tends to be larger in directions $\mathbf{n}$ where there is a concentration of stars. Conversely, if the Majorana constellation is very dispersed, one will have $\langle\psi| J_{\mathbf{n}} |\psi\rangle \approx 0$ for all directions $\mathbf{n}$. These properties illustrate how the Majorana representation can offer geometrical intuition about the properties of spin states.

As mentioned, we will be interested in estimating the parameter θ after a rotation $U = e^{-iJ_{\mathbf{n}}\theta}$ around an axis $\mathbf{n}$. Throughout this thesis, we will consider the case where the axis of rotation $\mathbf{n}$ is arbitrary. To illustrate what types of states are useful for this task, let us consider the two contrasting Majorana constellations in Fig. (1.1). In the first state (a coherent state), all stars are concentrated at a single point. If we rotate this state around an axis passing through that point, the constellation (and thus the state) remains unchanged. In contrast, the second state (a king state: a state with the highest possible isotropy order for a given S (this will be clarified below)), with its widely dispersed stars, will visibly change under rotations around any axis. This intuitively suggests that states well-suited for detecting arbitrary rotations must have Majorana constellations distributed quite uniformly over the sphere, ensuring sensitivity in all directions.

The sensitivity of a quantum state to detect a rotation with an arbitrary axis is an invariant property under SU(2) transformations (when considering all rotation axes, it is irrelevant whether we rotate the initial state). Therefore, to quantify it, we need a description of the state's geometric properties that is invariant under SU(2) transformations. For this, we introduce the multipolar distribution. Any quantum state ρ of a spin S system can be expanded in the basis of irreducible tensor operators T_{kq}

$$\rho = \sum_{k=0}^{2S} \sum_{q=-K}^{K} \rho_{kq} T_{kq}, \tag{1.25}$$

where the T_{kq} form an orthonormal basis $\mathrm{Tr}\left[T_{kq} T^{\dagger}_{k'q'}\right] = \delta_{kk'}\delta_{qq'}$. From the coefficients ρ_{kq} of this expansion, the multipole of order K, denoted by ρ_K^2, is defined as the sum of the squared moduli of

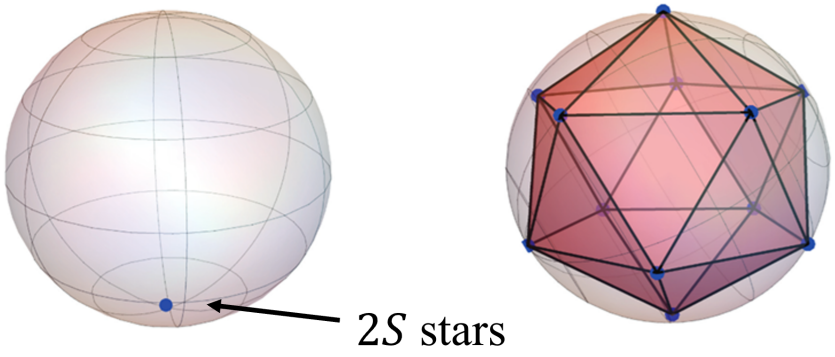

Figure 1.1: Majorana constellations corresponding to a coherent state (left) and king state (right)

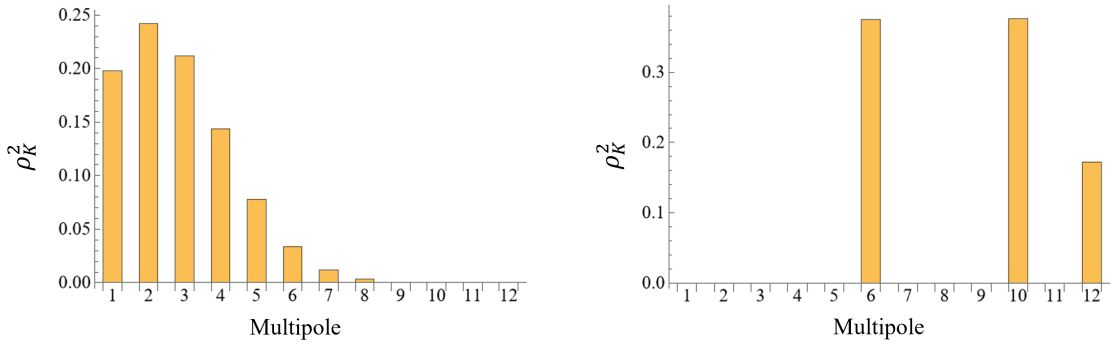

Figure 1.2: Multipolar distributions corresponding to a coherent state (left) and a king state (right)

the coefficients for a fixed order K:

$$\rho_K^2 \equiv \sum_{q=-K}^{K} |\rho_{Kq}|^2. \tag{1.26}$$

The set of these multipoles constitutes the multipolar distribution, which is invariant under rotations. For the pure states we will study, this distribution is normalized, $\sum_{k=0}^{2S} \rho_k^2 = 1$, which allows a direct comparison between different states. The multipole of order $K = 0$ is constant, so it is omitted in the analyses.

The multipolar distribution provides information about the geometric structure of the state at different scales. Low-order multipoles (small k) are linked to the "coarse" features of the constellation, which are described by the low-order moments of the spin operator, $\langle J_{\mathbf{n}}^i \rangle$. In contrast, high-order multipoles (large k) quantify the "fine" details and the complexity of the star distribution, associated with higher-order moments. This correspondence is clearly illustrated by the states in Fig. (1.1): the coherent state, with all its stars concentrated, exhibits a multipolar distribution with most of its weight in the lower orders, as shown in Fig. (1.2). Conversely, the king state, with its highly

dispersed constellation, exhibits null values for the first multipoles, with the weight of the distribution concentrated in the higher orders.

In general, there is a heuristic that associates the multipolar distribution with the degree of "quantumness" of the state: those with distributions concentrated in low multipoles are considered more "classical", while a higher population in high multipoles is usually interpreted as a manifestation of more pronounced quantum properties. This idea is based on the observation of limiting cases, such as the coherent state (considered the most classical) and states like the king state (which maximize certain quantumness metrics and exhibit populated high multipoles).

However, despite this intuitive interpretation and the usefulness of these extreme cases, it is important to emphasize that the exact mathematical relationship between the Majorana constellation, the multipolar distribution, and the moments $\langle J_{\mathbf{n}}^{i} \rangle$ is, in general, non-trivial. For example, the ρ_K^2 multipoles cannot take arbitrary values, as upper bounds exist for each order K. Consequently, not just any set of values $\{\rho_K^2\}$ that satisfies the normalization condition can originate from a physically realizable quantum state. Furthermore, experience shows that if a state is generated randomly, its resulting multipolar distribution is usually complex and often difficult to interpret in simple geometric terms.

The multipolar distribution, with the properties and nuances discussed, plays a central role in the second project of this thesis. In the first paper, the connection between the multipolar distribution and the Majorana constellation will be investigated in detail. In the second paper, the multipolar distribution will be employed, along with other metrics, to characterize the properties of the so-called "Random Majorana States", which are states generated by the random selection of stars on the Bloch sphere.

To quantify the suitability of a state in detecting an arbitrary rotation, a relevant metric is the average value of the QCRB over all possible rotation axes:

$$\frac{1}{4\pi} \int_{\mathcal{S}_2} \frac{1}{4\mathfrak{m}_2(\mathbf{n})} \, d\Omega, \tag{1.27}$$

where $d\Omega$ is the area element on the surface of the sphere $\mathcal{S}_2$ and $\mathfrak{m}_2(\mathbf{n}) \equiv \left\langle (J_{\mathbf{n}} - \langle J_{\mathbf{n}} \rangle)^2 \right\rangle$ is the variance of the generator along the axis $\mathbf{n}$. It can be shown that the states that minimize this quantity, are those that satisfy the following conditions:

$$\langle \psi_0 | \, J_{\mathbf{n}} \, | \psi_0 \rangle = 0, \tag{1.28}$$

$$\langle \psi_0 | \, J_{\mathbf{n}}^2 \, | \psi_0 \rangle = \text{constant}. \tag{1.29}$$

A state for which the first k_0 moments $\langle\psi_0| J_{\mathbf{n}}^k |\psi_0\rangle$ do not contain directional information is called isotropic up to order k_0. At first glance, a state with $\langle\psi_0| J_{\mathbf{n}} |\psi_0\rangle = 0$ might seem completely unpolarized. However, this apparent lack of polarization in the first moment does not imply a total absence of directional structure. A quantum state satisfying $\langle\psi_0| J_{\mathbf{n}} |\psi_0\rangle = 0$, unlike a classical unpolarized state, can still harbor directional information in its higher-order moments. This phenomenon is known as hidden polarization.

The result that isotropic states beyond $k = 2$ are optimal for detecting arbitrary rotations (according to the averaged QCRB) is, at first glance, counterintuitive. If isotropy is, indeed, a desirable property for this task, why is the optimality condition limited to order $k = 2$? Shouldn't higher-order isotropy confer an additional metrological advantage? The study of this apparent paradox is one of the topics that will be addressed in the first project of this thesis.

Finally, it is important to highlight the direct mathematical connection between the isotropy of a state and its multipolar distribution: a state is isotropic up to order k_0 if, and only if, all its multipoles ρ_k^2 are null for $1 \leq k \leq k_0$. This relationship is consistent with the interpretation of the multipolar distribution discussed earlier, where constellations more distributed over the sphere (and therefore more isotropic) tend to exhibit low values in the first multipoles.

1.3 Quantum Metrology Overview

To conclude, we provide in this section a brief overview of the state of the art in quantum metrology, begining with its historical development and surveying key contemporary topics. Its scope is intentionally broad, designed to complement rather than duplicate the specific background information found in the introductions of the research articles that constitute this thesis.

Consequently, this chapter serves as a supplementary resource for readers interested in the wider scientific landscape. A detailed reading is not a prerequisite for understanding the core contributions presented in the subsequent articles. Necessarily, this review is selective given the breadth of the field; for example, the extensive experimental work is only briefly mentioned. For a comprehensive treatment of various topics, we refer the reader to the numerous excellent reviews [48–50, 54, 64–77] and recent doctoral theses [52, 53, 78–86].

The birth of quantum metrology occurs when the principles of quantum mechanics are incorporated into the classical framework of estimation. Since measurements in quantum systems are inherently probabilistic and can perturb the state of the system, both new fundamental limits to precision and new strategies to overcome them emerge. The tools of classical metrology are extended to the quantum domain through the introduction of the quantum Fisher information (QFI) and the quantum Cramér-

Rao bound (QCRB). These formalisms were developed by authors such as Helstrom and Holevo during the 1970s and 1980s [87, 88].

A fundamental driving force for the development of quantum metrology was the search for the detection of gravitational waves (GWs). The need to measure extremely small physical effects, predicted by General Relativity, forced consideration of the limits imposed by quantum mechanics on the precision of measurements. These GWs, whose existence was postulated by Albert Einstein in 1916, were the subject of a prolonged debate about their physical reality, with questions raised as to whether they were a mere mathematical artifact or physically measurable entities; even Einstein himself harbored doubts about this at certain times [89, 90].

In this context of seeking maximum sensitivity for the detection of phenomena as elusive as GWs, crucial concepts such as the standard quantum limit (SQL) and the Heisenberg limit (HL) began to emerge. Initially, these limits were often derived heuristically, using arguments based on Heisenberg's uncertainty relation or error propagation. For example, the SQL for harmonic oscillators, relevant in resonant GW detectors, was analyzed in pioneering works such as those by Giffard [91] and Caves et al. [92]. Subsequently, strategies were proposed to overcome the SQL using nonclassical states of light, such as those presented by Caves [93] or Bondurant and Shapiro [94], which led to the coining of the term "Heisenberg limit" by Holland and Burnett [95]. Although the tools of quantum estimation theory, such as the QCRB, had already been developed by authors like Helstrom, it was later that QCRB became established as the standard measure for rigorously formalizing and determining the achievable sensitivity in metrological schemes and defining their fundamental limits.

After decades of intense technological and theoretical development, large-scale interferometric observatories such as LIGO, VIRGO, and GEO600 were built. These efforts culminated in 2015 with the first direct detection of a gravitational wave [96], event GW150914, by the LIGO and Virgo collaborations [97]. Currently, to further increase the precision of these detectors, squeezed states of light are routinely used to detect GWs [98–101]. This technique was first implemented in GEO600 [39] and later by LIGO [102].

1.3.1 Heisenberg Scaling

One of the main attractions of quantum metrology is the possibility of achieving the so-called "Heisenberg scaling". In a classical metrological scheme, the variance of the estimator, or mean squared error (MSE), reduces, at best, reciprocally to the number of resources ν used (e.g., the number of photons or experimental repetitions), which is known as SQL or "shot-noise" limit, where precision scales as $1/\sqrt{\nu}$.

As we mentioned, in the latter part of the last century, there appeared a shared consensus that,

by using quantum resources, a substantial improvement to this bound could be obtained. Using often heuristic approaches, without yet generally resorting to the QFI formalism, the possibility of achieving a precision scaling on the order of $1/\nu$ was observed, which would imply an MSE reduction proportional to $1/\nu^2$. The precise definition of the number of resources used, ν, can be subtle, but paradigmatic examples include the number of repetitions of an experiment, the total measurement time, or the number of repetitions of a parameter encoding process in the probe state. Achieving this Heisenberg scaling would have profound practical implications, as it would not be a simple improvement by a constant factor over classical protocols, but a fundamentally different dependence of precision on available resources.

The first works in this direction explored the use of nonclassical states of light. For example, Caves proposed the use of squeezed states to improve the sensitivity of interferometers [93]. In that work, he considered sending a squeezed state of light, instead of vacuum, into the normally unused input port of the interferometer. By doing so, the photon counting error can be reduced at the expense of increasing the radiation pressure error, or vice versa. Although this work does not explicitly achieve Heisenberg scaling, it represents a crucial conceptual advance towards overcoming the limits imposed by standard quantum noise through the use of quantum resources.

Other contemporary works also explored these ideas from different perspectives, such as the analysis of SU(2) and SU(1,1) interferometers presented by Yurke et al. [103]. The article demonstrated, in principle, the possibility of achieving a phase sensitivity approaching $1/\nu$, where ν is the total number of photons. This scaling corresponds to the Heisenberg limit.

The understanding of how to achieve this scaling was consolidated with subsequent works, which analyzed in detail the role of entanglement and the number of systems involved [104–107]. In the context of estimating a parameter encoded by unitary evolution, it has been shown that highly entangled states such as GHZ (Greenberger-Horne-Zeilinger) or N00N states, and their generalizations, are capable of producing this Heisenberg scaling [105]. It is relevant to note that this same scaling can, in principle, be obtained through strategies of multiple passes of the probe state through the system encoding the parameter. This suggests an interesting interchangeability of resources: the use of states with a high degree of entanglement could, in certain scenarios, be replaced by a longer interaction or sensing time.

This $1/\nu$ Heisenberg scaling is particularly attractive, but its attainment is based on the consideration of unitary evolutions, i.e., in the absence of noise. In the real world, quantum systems are inevitably subjected to decoherence and various sources of noise, which raises the fundamental question of whether Heisenberg scaling can be maintained in realistic scenarios. This issue has been, and continues to be, one of the main focuses of research in quantum metrology.

Although the promise of Heisenberg scaling is considerable, a more detailed analysis considering noisy systems has revealed that, in practice, this scaling tends to disappear in the face of many common types of noise [108]. Nevertheless, notable exceptions exist. For example, it has been shown that in the presence of non-Markovian noise, certain strategies can preserve an improvement in scaling beyond the SQL [109]. Similarly, under specific noise conditions in frequency estimation, the limitations imposed by the SQL can also be overcome [110].

Given the fragility of Heisenberg scaling in the presence of noise, an active line of research focuses on developing techniques to recover it or, at least, to obtain a substantial improvement over classical protocols in noisy environments. Among these techniques, the use of auxiliary systems (ancillas), with which the probe state is entangled, and the application of quantum error correction (QEC) protocols stand out. Entanglement with ancillas can offer additional protection to the probe state, improving the final precision [111]. For its part, QEC actively seeks to identify and correct errors induced by noise, allowing, in principle, for the recovery of Heisenberg scaling or, at the very least, a significant improvement in precision [112–114].

While the complete recovery of Heisenberg scaling in the presence of generic noise is a considerable and often unattainable challenge, it is important to note that, even in noisy scenarios, quantum metrology can offer an advantage in the form of a constant factor improvement in precision over classical protocols. Various works have demonstrated the possibility of achieving the HL or improving the SQL through QEC adapted to the specific noise of the system [114–117]. For example, in the context of gravitational wave detection, an improvement in sensitivity has been achieved using quantum states of light (squeezed states), in accordance with theoretical predictions. Such advances are crucial, as they demonstrate the feasibility of implementing protocols with a quantum advantage using current technology [98].

Finally, it is relevant to mention that research on the Heisenberg limit is not solely confined to the impact of noise. Other aspects, such as the intrinsic limitations of the QCRB (which is an asymptotic bound), have also been studied. When the number of repetitions is not sufficiently large, or when considering simultaneous estimation of multiple parameters, it is necessary to refine the analysis of Heisenberg scaling, which may lead to the introduction of correction factors or a reconsideration of optimal strategies [118, 119].

1.3.2 Multiparameter Quantum Metrology

Another topic of great relevance in quantum metrology is multiparameter estimation. While classical multiparameter estimation already brings new concepts (e.g., statistical correlations), quantum scenarios add specifically nonclassical obstacles: noncommuting parameter generators and measure-

ment incompatibility. As a result, joint optimality is not guaranteed and practical strategies typically balance precision across parameters.

Given its fundamental importance and practical implications, multiparameter quantum metrology has been the subject of intense research, reflected in various recent reviews that address this topic from different perspectives [70, 71, 120, 121]. The need to simultaneously estimate multiple parameters arises naturally in a wide range of practical applications. Notable examples include three-dimensional magnetometry, which seeks to determine the three components of a magnetic field [122]; the estimation of multiple optical phases, crucial in advanced interferometry and in the characterization of complex systems [123, 124]; the joint estimation of a phase and its diffusion, relevant in scenarios where phase noise is not negligible [125]; the characterization of multidimensional fields, where the parameters to be estimated may correspond to different components or properties of the field [126, 127]; and super-resolution, which aims to overcome classical diffraction limits by precisely estimating multiple spatial parameters [128].

Analogous to the single-parameter case, the fundamental objective in multiparameter estimation is to determine the maximum achievable precision. However, this ultimate precision limit is not always analytically calculable, except for simple systems, which has motivated the development of various bounds. A crucial distinction from single-parameter metrology is that, while the single-parameter QCRB is always saturable, its generalization to the multiparameter case gives rise to bounds that, in general, are not [129, 130]. In fact, the non-commutativity inherent to quantum observables in the multiparameter scenario leads to the definition of different versions of the QCRB—most notably those based on the symmetric (SLD) and the right logarithmic (RLD) derivatives [131].

Despite not always being a tight bound, the QCRB based on the SLD is frequently analytically calculable in various situations. This tractability has facilitated its study and application, making it one of the most investigated bounds in practice. The question of when the SLD-CRB is saturable, i.e., when the precision it specifies can be achieved, has been a central research topic. Various works have explored the conditions under which this occurs, analyzing the role of commutativity between SLD operators, the influence of the extended Hilbert space, and the implications for different types of probe states and measurements [132–138]. Likewise, connections between the SLD-CRB and other fundamental bounds, such as the Holevo bound, as well as its relationship with the dimensionality of the probe state and measures of quantum incompatibility, have been investigated [139–142].

The realization that the SLD-CRB is not, in general, a tight bound in the multiparameter scenario has spurred the study of tighter bounds. Among them, the Holevo Cramér-Rao bound (HCRB) stands out as being the asymptotically achievable bound through collective measurements [143]. Although the HCRB is fundamentally tighter than the SLD-CRB, its calculation usually requires numerical

methods, and its analytical expression is known only for particular cases [144–147].

Although the HCRB is, in principle, achievable, a collective measurement acting on a possibly infinite number of copies of the quantum system may be necessary [148, 149]. This considerably limits its practical applicability, preventing it, in general, from being considered a tight bound in realistic experimental scenarios.

Another relevant bound in multiparameter estimation is that of Nagaoka [144]. Initially conceived for two parameters, it has recently been generalized, under the name "Nagaoka-Hayashi" to an arbitrary number of parameters [150, 151]. Although it was thought that this bound might be tight, recent works have shown that this is not the case, highlighting the influence of the extended Hilbert space on its achievability [152].

Like the HCRB, calculating the Nagaoka-Hayashi bound generally requires numerical methods. Fortunately, it has been possible to mathematically reformulate both the HCRB and the Nagaoka-Hayashi bound as convex optimization problems, specifically as semidefinite programs (SDPs) [150, 153, 154]. This formulation is of great practical importance, as SDPs can be solved efficiently, although the numerical nature of the solution may limit the insights obtained [155, 156].

The ideal goal, however, would be to obtain not only bounds but also the maximum achievable precision and the measurement strategy that achieves it, all in a numerically tractable manner. Significant efforts are being made in this direction, such as those seeking to unify the theory of precision bounds for multiparameter estimations through conic programming [157]. These approaches not only focus on state estimation but also on the fundamental question of what the optimal probe state is for a given quantum channel [158].

An alternative approach that has recently emerged is based on "uncertainty relations" for multiparameter estimation. These relations, inspired by Heisenberg's uncertainty relations, establish bounds on the classical Fisher information that can be simultaneously achieved for each parameter [55]. A notable advantage of this method is that the resulting bounds are usually analytically simpler to calculate. The relationship between these uncertainty-based bounds and the more traditional Cramér-Rao-type bounds has also been studied [159]. Other novel approaches include the study of implementing an arbitrary number of observables with a single measurement [160] and the use of randomized measurements [161].

1.3.3 Bayesian Quantum Metrology

As we have already mentioned, statistical estimation theory, which serves as the basis for metrology, can be conceptually divided into two major approaches: frequentist and Bayesian [162, 163]. In the frequentist paradigm, the parameter of interest is considered a fixed but unknown quantity, whose

value is intended to be inferred from observational data. On the other hand, the Bayesian approach models the parameter as a random variable, characterized by a prior probability distribution that reflects initial knowledge about said parameter. This prior distribution is updated using Bayes' rule as new information from measurements is incorporated.

Both paradigms offer different ways of approaching the estimation problem, each with its own strengths and weaknesses. One of the main criticisms of the Bayesian approach lies in the influence that the a priori distribution exerts on the final conclusions, especially when the number of data points is limited. In practice, this prior distribution is not always accessible or easy to determine objectively, which can introduce a certain degree of subjectivity into the analysis [164]. Despite this, and although most works in quantum metrology have traditionally been developed from a frequentist perspective, there has been a notable surge in Bayesian techniques in recent years.

It is important to note that, in the limit of a large number of experimental repetitions (asymptotic limit), both approaches tend to converge in their results. However, when a finite number of resources are available, the predictions and optimal strategies derived from each paradigm can diverge significantly.

The first Bayesian analyses in the context of quantum metrology date back to the 1970s, developing in parallel with the frequentist approach. Pioneering works such as those by Helstrom, Personick, Holevo, and Yuen and Lax laid the foundations for applying Bayesian principles to parameter estimation in quantum systems [87, 131, 165–167]. In these initial works, the quantum minimum mean squared error (MMSE) estimator is derived, and the formalism is extended to include multiparameter estimation.

As in the classical case, bounds on achievable precision have been derived, given that the exact evaluation of the optimal strategy may not be possible or may require numerical evaluations. Among them, the quantum Ziv-Zakai bounds [168] and the quantum Weiss-Weinstein bounds [169] stand out. These bounds, which generalize their classical counterparts, are tighter than the (Bayesian) QCRB in limited-data regimes or when the likelihood function is not Gaussian. They have been extended to cover waveform estimation [170] and vector parameters [171]. Other bounds also exist, such as those based on the quantum Van Trees inequality [172].

The Bayesian approach has demonstrated growing relevance and applicability in contemporary quantum metrology. In phase estimation, robust strategies against noise have been designed [173]. Quantum thermometry, an area of great activity, has seen the application of Bayesian methods for temperature estimation without detailed prior knowledge [174], or using concepts such as thermodynamic length to optimize inference with limited prior information [175]. These approaches have made it possible to explore the fundamental limits of Bayesian thermometry and develop adaptive strategies

to reach them [176].

The Bayesian paradigm's ability to incorporate prior information and adapt to measurement results makes it particularly suitable for real-time protocol optimization. This has been exploited in quantum imaging for super-resolution through adaptive multiparameter estimation [177], and in experimental demonstrations confirming the significant precision improvements obtainable with these techniques, for example, in gravimetry with cold atoms [178, 179]. Rigorous benchmarking of these protocols, considering the influence of the prior and the finite number of measurements, is a crucial aspect for validating their practical utility [180].

From a theoretical perspective, Bayesian quantum metrology continues to expand. The ultimate precision limits in multiparameter scenarios, such as in magnetometry, have been investigated [122], and unifying conceptual frameworks for different types of parameters are being developed. A notable example is the extension of metrology beyond phase and location parameters towards "quantum scale parameter estimation" for quantities like decay rates or temperatures, where inherent symmetries of the problem play a fundamental role [181–183]. Connections with other quantum information concepts, such as coherence, are being used to better understand the origin of quantum advantage [184]. Furthermore, techniques are being developed for the systematic design of optimal protocols that jointly optimize the probe state and the measurement [185].

1.3.4 Global Quantum Metrology

A particularly active area of research today, which fundamentally relies on Bayesian metrology, is so-called global quantum sensing. For a recent review, see reference [54].

As mentioned, in the frequentist approach, the central quantity is the QCRB, which is evaluated pointwise in the parameter space. This implies that, generally, the optimization of the probe state and the measurement is performed for a specific value of the parameter. While this strategy is effective when very precise prior information about the parameter is available—allowing optimization at the central point of a narrow range—the optimal state and measurement found are, in general, only valid for that particular point. For different values of the parameter, the optimal strategy will differ.

However, in practice, such detailed prior information is often not available, and a sensing strategy is required that is optimal, or at least robust, for a wide range of the parameter. A paradigmatic example of this is found in phase estimation: while the locally optimal state is the well-known N00N state, if complete initial ignorance of the phase is assumed, the globally optimal state is the so-called sine state [48]. This does not imply that the QCRB cannot be reached in the asymptotic limit, as adaptive strategies can be employed, where the measurement is adjusted as more information about the parameter is obtained.

Nevertheless, this leaves open the fundamental question of what state and what measurement to use initially, when little or no information is yet available. This is precisely the domain of the global approach, where the Bayesian paradigm has been most commonly used to address this issue. Various works have explored this global approach from a Bayesian perspective, for example, in the context of quantum thermometry [186], in establishing strict hierarchies for global estimation strategies [187], or by analyzing the role of symmetry and geometry in the design of global quantum sensors [183].

Although less common, there are also contributions to the global approach from the frequentist perspective. In the context of many-body systems, for example, the exploitation of critical points—regions where the system undergoes a phase transition—has been investigated to obtain improved sensing precision. While this increase in sensitivity is usually, in principle, restricted to a narrow region around the critical point, strategies have been developed for scenarios where detailed prior information about the parameter to be estimated is not available [188]. Such works have subsequently been extended through the design of modular sensors, which allow for a significant extension of the region where said improved precision is maintained [189].

Finally, other approaches exist that address estimation in global regimes. Probably approximately correct metrology (PAC) is one such technique, where the key quantity is the probability that the parameter estimate lies within a predefined range around its true value [190]. Another relevant approach involves using mutual information as a figure of merit, as opposed to QFI, in order to study Heisenberg scaling from a global perspective [191].

1.3.5 Machine Learning

Machine learning (ML), although having recently gained public notoriety with the advent of large language models, is a tool with a well-established track record in the field of physics [192, 193]. In quantum metrology, its application has experienced notable growth, opening new avenues for protocol optimization and overcoming experimental limitations [194].

An area of special interest is Bayesian estimation, where ML methods have proven effective. It has been proposed to reformulate Bayesian estimation as a classification task, allowing Neural Networks (NNs) to perform inference efficiently and, in certain cases, surpass standard calibration methods, especially when available data are limited [195]. These NNs not only facilitate direct inference but can also be trained to act as robust and fast heuristics in the adaptive design of experiments, a crucial component in Bayesian estimation, where the optimal choice of the next experimental step is fundamental to maximizing acquired information [196, 197].

Reinforcement learning (RL) is another ML technique with significant potential in this domain. It has been successfully employed in optimizing experimental design for adaptive quantum estimation,

where the RL agent learns to select the sensor's control parameters. A promising approach is "model-aware RL", where prior knowledge about the system's model is assumed and incorporated into the agent's training process. This can lead to superior control strategies and more efficient training compared to model-free approaches [198].

The combination of these ML techniques has led to even more comprehensive developments. For example, multiparameter quantum estimation protocols have been designed where a deep RL agent, which makes decisions concerning adaptive control, is combined with a deep neural network that performs Bayesian updating. Such integrated "model-free" architectures, trained directly with experimental data, have demonstrated the ability to outperform standard calibration strategies in realistic scenarios with limited resources, such as in the simultaneous estimation of multiple optical phases in photonic circuits [199].

Another recent application of these techniques is in the classification of images with sub-Rayleigh resolution subject to photon shot noise. In this context, hybrid algorithms have been proposed that integrate physical preprocessing of the optical field—performed through spatial mode demultiplexing (SPADE)—with computational postprocessing carried out by machine learning algorithms. This approach has demonstrated the ability to classify images that would be indistinguishable using conventional direct imaging techniques, operating under conditions of severe diffraction and extremely weak light signals [200].

1.3.6 Other topics

There are other areas of research in quantum metrology that, while may be considered more tangential or specific, offer valuable insights and address particular challenges in the pursuit of maximum precision.

A first set of works has focused on deepening the understanding of fundamental tools, such as the QFI and QFIM, and their possible anomalous behaviors. It has been discovered, for example, that the QFI can exhibit discontinuities when the range of the density operator changes [201, 202]. These discontinuities, and the possible non-invertibility (singularity) of the QFIM, have important metrological implications, as they can invalidate the employment of the standard QCRB [203]. The conditions for continuity of the QFI have been studied [204], and strategies have been proposed to overcome the singularity of the QFIM, such as the use of sequential measurements, where information is accumulated over a sequence of local interactions and measurements, thereby overcoming the limitations imposed by an insufficient number of independent measurement outcomes [205]. Work such as that developed during the doctoral period of the author of this thesis, although not explicitly included here, has also addressed the issue of QFIM singularities [206].

The correct interpretation of data and the diagnosis of imperfections in quantum sensors have also been studied, for example, by using generalized Cramér-Rao bounds to assess the quality of data postprocessing and detect possible biases in estimation [207, 208].

In the search for new metrological strategies and harnessing of quantum resources, innovative proposals have emerged. Postselected quantum metrology, for example, explores the use of pre-measurements to filter quantum states before the final measurement intended to extract information about the parameter. It has been shown that these filtered states can concentrate information, which is particularly useful in the presence of limited resources or noisy detectors, and this advantage has been linked to the negativity of certain quasiprobability distributions [209, 210]. In fact, a general theory of compression channels for postselected quantum metrology has been developed [211]. Another particular technique to optimize the so-called null or near-null measurements, which are known to allow the saturation of the QFI, are displaced-null measurements, proposed to address distinguishability problems that arise when the measurement reference is too close to the actual state of the system [212]. Additionally, other approaches explore the use of quantum contextuality as a resource to increase estimation precision [213]. Symmetry has also been identified as a fundamental resource, enabling the preparation of mixed quantum states with advantageous metrological properties [214]. Finally, quantum speed limits also play a crucial role, as they impose fundamental restrictions on the achievable temporal resolution in the detection of dynamic signals [215].

Quantum metrology also faces specific challenges in particular estimation problems and in the development of more general theoretical tools. An example is parameter estimation when the measurement strategy itself depends on the unknown parameter, which requires treatment beyond the standard QCRB [216, 217]. The presence of nuisance parameters, which affect precision but are not of direct interest, has also been addressed, giving rise to semiparametric quantum metrology [133, 218]. Generalizations of the symmetric logarithmic derivative SLD, such as the bound based on the maximum logarithmic derivative, which combines the SLD and the right logarithmic derivative, have been proposed [219]. The estimation of high-dimensional unitary transformations is another complex problem, where protocols that saturate the QCRB are sought [220]. Beyond parameter estimation, methods have been developed to certify the dimensionality of quantum systems based on experimental evidence [221]. Finally, the concept of "QFI power" has been introduced to characterize the ability of a quantum evolution to generate QFI, especially starting from states with initially null QFI [222].

From a more practical and computational perspective, software tools have been developed to facilitate calculations and simulations in quantum metrology, such as the QuanEstimation toolkit [223]. Furthermore, strategies are being actively investigated to optimize sensing protocols considering the limitations of real laboratories. Approaches such as end-to-end variational quantum sensing, which

uses parameterized quantum circuits and neural networks, seek to jointly optimize state preparation, interaction, and estimation [224]. Similarly, specific dynamics, such as quantum resonances, are being explored to improve metrology in the presence of noise and with limited controls [225].

2

Publications

2.1 Project 1: Corrections to the quantum Cramér-Rao bound

As discussed in the mathematical preliminaries section, the QCRB constitutes a bound for the MSE of an estimator that is only guaranteed to be attainable in the asymptotic limit of an infinite number of repetitions. Therefore, it does not, in general, provide direct information about the actual MSE when a finite number of resources is available. This is an intrinsic feature of the classical Cramér-Rao bound, which is inherited by its quantum generalization.

Despite this fundamental limitation, the QCRB has established itself as the most widely used tool in quantum metrology. This prevalence is due to a pragmatic balance: on the one hand, its analytical tractability has enabled substantial theoretical progress, with a vast literature dedicated to its calculation for various systems, scenarios, and types of noise; on the other hand, the bound shows a remarkable correspondence with experimental results when the number of resources is reasonably large. It is this combination of theoretical manageability and empirical relevance that has made it the preferred figure of merit in the field.

However, in recent years, the quantum metrology community has begun to incorporate tools from classical statistics that go beyond the Cramér-Rao approach, enriching the available theoretical arsenal. The recent rise of Bayesian techniques, as well as the emergence of works adopting minimax or PAC perspectives, are clear examples of this trend. This adoption process has been gradual. On one hand, it involves the incorporation of tools that, while part of the standard toolkit of advanced statistics like Bayesian and minimax perspectives, are less straightforward than the Cramér-Rao approach. On the other hand, there are even more specialized theories, such as the higher-order asymptotic

theory that will be used in this work, whose presence is limited even in standard statistical textbooks, placing them on a plane far removed from the typical training of a physicist.

The limitations of the first-order asymptotic approach, represented by the QCRB, have direct practical implications: In the quest for maximum precision, selecting the optimal POVM is crucial. The QCRB states that any measurement that saturates the bound, i.e., that makes the CFI equal to the QFI, is optimal. This leads to an ambiguity, as, in general, it does not identify a unique strategy, but rather an entire family of POVMs that are indistinguishable and equivalent from this perspective. More precisely, there may exist a family of POVMs $\Pi(\phi)$, parameterized by a parameter ϕ, such that $F(\Pi(\phi), \rho(\theta)) = Q(\rho(\theta))$ for all ϕ.

Analogously, this ambiguity extends to the choice of the optimal probe state. Let us consider the estimation of an arbitrary SU(2) transformation of the form $U(\theta) = e^{-i\theta J_{\mathbf{n}}}$ acting on an initial pure state $|\psi_0\rangle$. The QFI is given by:

$$Q\left(U(\theta)\,|\psi_0\rangle\,\langle\psi_0|\,U^\dagger(\theta)\right) = 4\,\langle\psi_0|\,(J_{\mathbf{n}} - \langle J_{\mathbf{n}}\rangle)^2\,|\psi_0\rangle \equiv 4\mathfrak{m}_2(\mathbf{n}) \tag{2.1}$$

If the goal is to optimize performance over all possible directions $\mathbf{n}$, one seeks to minimize the average of the QCRB over the sphere:

$$\frac{1}{4\pi}\int_{\mathcal{S}_2} \frac{1}{4\mathfrak{m}_2(\mathbf{n})}\, d\Omega \tag{2.2}$$

where $d\Omega$ is the area element on the surface of the sphere $\mathcal{S}_2$. This quantity is minimized by states that satisfy the following conditions:

$$\langle\psi_0|\,J_{\mathbf{n}}\,|\psi_0\rangle = 0 \tag{2.3}$$

$$\langle\psi_0|\,J_{\mathbf{n}}^2\,|\psi_0\rangle = \text{constant} \tag{2.4}$$

That is, by states that are isotropic to second order. However, there are generally many states that satisfy these two conditions, with the QCRB offering no criterion to choose among them.

In the work presented in this section, these two issues are addressed by calculating higher-order corrections (as an expansion in powers of $1/\nu$, where ν denotes the number of trials) to the MSE predicted by the QCRB. The central idea is that these corrections allow us to discriminate between strategies (states and measurements) that were equivalent in the eyes of the QCRB, revealing that some are preferable to others in the finite-resource regime. As we will see, the calculation of these corrections involves certain technical subtleties, as their value depends on the specific estimator used, the possible presence of a bias of order $1/\nu$, and whether the probabilities of certain measurement outcomes vanish at the true value of the parameter. Beyond resolving the ambiguity in the choice of

optimal strategies, the derived expressions provide a more accurate approximation of the actual MSE before the asymptotic limit is reached, which can be of great practical use by reducing the need to resort to numerical simulations.

We will also introduce the Bhattacharyya bound, a classical bound that adds corrections to the CCRB, thereby tightening it. In its standard form, the bound applies to unbiased estimators; however, in practice the estimators of interest are typically biased, which limits its non-asymptotic usefulness. For this reason, the corrections it provides are primarily relevant in the limit $\nu \to \infty$, where they can be understood as a lower bound to those obtained via second-order asymptotics. A quantum extension of this bound is known, enabling optimization over all POVMs.

This section is composed of two papers. The first is a letter in which we introduced these concepts for the first time. The second reiterates the explanations in greater depth, conducts numerical simulations to test these expressions, and delves into some of the associated technical difficulties. Finally, the Bhattacharyya bound and its relationship to them are also examined.

Beyond the Quantum Cramér-Rao Bound

J. R. Hervas,[1] A. Z. Goldberg,[2] A. S. Sanz,[1] Z. Hradil,[3] J. Řeháček,[3] and L. L. Sánchez-Soto[1,4,5]
[1]*Departamento de Óptica, Facultad de Física, Universidad Complutense, 28040 Madrid, Spain*
[2]*National Research Council of Canada, 100 Sussex Drive, Ottawa, Ontario K1N 5A2, Canada*
[3]*Department of Optics, Palacký University, 17. listopadu 12, 771 46 Olomouc, Czech Republic*
[4]*Institute for Quantum Studies, Chapman University, Orange, California 92866, USA*
[5]*Max-Planck-Institut für die Physik des Lichts, 91058 Erlangen, Germany*

(Received 8 July 2024; accepted 10 December 2024; published 10 January 2025)

The quantum Cramér-Rao bound (QCRB) stands as a cornerstone of quantum metrology. Yet, akin to its classical counterpart, it provides only local information and overlooks higher-order details. We leverage the theory of higher-order asymptotics to circumvent these issues, providing corrections to the performance of estimators beyond the QCRB. While the QCRB often yields a whole family of optimal states and several optimal measurements, our approach allows us to identify optimal states and measurements within the family that are otherwise equivalent according to the QCRB alone; these are requisite for optimal metrology before reaching the asymptotic limit. These results are especially pertinent when dealing with unitary processes.

DOI: 10.1103/PhysRevLett.134.010804

Introduction—Quantum metrology is a rapidly growing field that leverages the principles of quantum physics to achieve extremely precise measurements [1–6]. Today, quantum metrology offers significant advantages in terms of precision, sensitivity, and noise reduction. These benefits are driving remarkable advancements in both fundamental and applied research.

The cornerstone of frequentist quantum metrology, the quantum Cramér-Rao bound (QCRB), sets a lower bound on the minimum mean square error (MSE) of an estimator for a parameter encoded in a state [7,8]. The inverse of the QCRB is a measure for the state's sensitivity under small variations of a parameter, known as the quantum Fisher information (QFI) [9].

Despite the prevalence of the QFI in quantum information, its implications have to be taken with a grain of salt. First, the associated QCRB is only asymptotically attainable, leading to apparent violations of the bound when few measurement samples are available [10,11]. More importantly, the QFI is tailored for local estimation scenarios rather than global ones, where both the location and size of the parameter neighborhood remain unknown. It has been noticed that the MSE of global estimation problems can significantly differ from local strategies [12–16]. Additionally, the QCRB suggests that the best strategy is to use all available resources in a single measurement [17]. However, as the number of resources increases, so does the required prior knowledge about the parameter, a problem that can be circumvented by using a Bayesian approach [18–20].

In this Letter, we will address additional issues that, while highly relevant, have remained largely unexplored. For single-parameter estimation, multiple measurements can saturate the QCRB [21,22], raising the question of which one measurement to prefer over the rest. The QCRB also has limitations when determining the optimal state for sensing a unitary transformation. As a representative example, consider the simplest case of rotations in SU(2): a whole family of optimal states is known to exist when all rotation axes are taken into consideration [23–26].

This Letter handles these limitations by leveraging the theory of higher-order asymptotics. This theory extends beyond the central limit theorem, providing corrections based on the number of trials, which are crucial for a *bona fide* statistical inference [27]. By properly incorporating these corrections, we can distinguish between states and measurements that appear equivalent according to the QCRB. Additionally, the corrections are essential for evaluating performance in real-world scenarios with finite resources. Although tools from the theory of higher-order asymptotics are well established in the statistical literature and have been applied in the context of quantum hypothesis testing [28], their application in quantum metrology offers a ripe opportunity for progress.

Higher-order asymptotics—We consider the canonical scenario of quantum metrology in which we want to estimate the value of a single real parameter θ from the

outcomes of ν independent measurements. Let $p(x|\theta)$ be the probability that in any given round the measurement will result in the outcome x, given that the value of the parameter is θ (we take x as a discrete random variable, but the continuous case can be dealt with in a similar way). In the quantum domain, the measurement setting is described by the positive operator-valued measure (POVM) $\Pi_x \geq 0$, with $\sum_x \Pi_x = \mathbb{1}$, and the probabilities are given by Born's rule $p(x|\theta) = \mathrm{Tr}[\varrho_\theta \Pi_x]$.

To report a value of the parameter θ, a proper estimator $\hat{\theta}(x)$ must be used. This is a function of the obtained measurement results x. The quantity of central interest is the MSE of $\hat{\theta}(x)$, which for estimators that approach the classical Cramér-Rao bound (CCRB) can generally be expanded as [29]

$$\mathrm{MSE}[\hat{\theta}(x)] = \frac{1}{\nu}\frac{1}{F_x(\theta)} + \frac{1}{\nu^2}\left[\Gamma(\theta) + b^2(\theta) + 2\frac{b'(\theta)}{F_x(\theta)}\right] + \mathcal{O}\left(\frac{1}{\nu^3}\right), \tag{1}$$

where the classical Fisher information (CFI) is $F_x(\theta) = \sum_x p(x|\theta)[\partial_\theta p(x|\theta)/p(x|\theta)]^2$ and $b(\theta)$ denotes the bias to order $1/\nu$: $\langle \hat{\theta}(x) - \theta \rangle = b(\theta)/\nu + \mathcal{O}(1/\nu^2)$, with $\langle \hat{\theta}(x) \rangle = \sum_x p(x|\theta)\hat{\theta}(x)$. The function $\Gamma(\theta)$ depends on the particular estimator. Actually, a vast number of estimators have been formulated by proposing *ad hoc* functions $\hat{\theta}(x)$ [10]. One of the most widely adopted is the maximum likelihood estimator (MLE), defined as $\hat{\theta}_{\mathrm{MLE}}(x) = \arg\max_\theta p(\theta|x)$. Here, the likelihood $p(\theta|x)$ must be interpreted as the probability of θ being the true value given the data x. For this estimator, the function $\Gamma(\theta)$ takes the value [29]

$$\Gamma(\theta) = -\frac{1}{F_x(\theta)} + \frac{\gamma_{02}(\theta) - 2\gamma_{21}(\theta) + \gamma_{40}(\theta)}{F_x^3(\theta)} + \frac{\frac{1}{2}\gamma_{11}^2(\theta) - [\gamma_{11}(\theta) - \gamma_{30}(\theta)]^2}{F_x^4(\theta)}, \tag{2}$$

and $b(\theta) = -\gamma_{11}/[2\nu F_x^2(\theta)]$, with

$$\gamma_{rs}(\theta) = \sum_x p(x|\theta)\left[\frac{\partial_\theta p(x|\theta)}{p(x|\theta)}\right]^r \left[\frac{\partial^2_{\theta\theta} p(x|\theta)}{p(x|\theta)}\right]^s. \tag{3}$$

For unbiased estimators, the MSE reduces to the variance, and the $1/\nu$ term gives the time-honored classical Cramér-Rao bound (CCRB). Similar expresions for other estimators can be found in [29]; nonetheless, no estimator is universally guaranteed to minimize all the $1/\nu^2$ contributions in Eq. (1); which one is best depends on the particular problem at hand. This differs markedly from the usual asymptotic case, where the CCRB sets the fundamental limit, independent of the estimator.

To establish a fundamental limit, we must first restrict the allowed estimators. It is reasonable to compare estimators that are unbiased to order $1/\nu$; i.e., $b(\theta) = 0$. This is not a significant loss of generality, since for any $\hat{\theta}(x)$ one can always build a bias-corrected version as $\hat{\theta}^*(x) = \hat{\theta}(x) - b(\hat{\theta}(x))/\nu$. In this case, the MSE takes the following value

$$\mathrm{MSE}[\hat{\theta}(x)] = \frac{1}{\nu F_x(\theta)} + \frac{\Gamma(\theta)}{\nu^2} + \mathcal{O}\left(\frac{1}{\nu^3}\right). \tag{4}$$

Interestingly, Rao [29–32] showed that the MLE minimizes $\Gamma(\theta)$, thus setting a fundamental limit similar to the CCRB and confirming that the MLE is distinctive among all estimators that reach the CCRB. With this in mind, we henceforth focus on the MLE.

Problem setting—To gain further insights into these corrections, we consider an SU(2) rotation $R = \exp(i\theta J_{\boldsymbol{n}})$, parametrized by its rotation axis $\mathbf{n}$ and angle θ. Here, $J_{\boldsymbol{n}} = \mathbf{J}\cdot\mathbf{n}$, with $\mathbf{J}$ being the generators of the rotation, which satisfy the commutation relations of the Lie algebra $\mathfrak{su}(2)$. The irreducible representations of this algebra are labeled by J and are spanned by the states $|J, m\rangle$, which are the simultaneous eigenstates of $\mathbf{J}^2$ and J_3. These states form a basis for a $(2J+1)$-dimensional Hilbert space, denoted by $\mathcal{H}_J$. In what follows, we assume that we have a pure state $|\psi\rangle \in \mathcal{H}_J$ that undergoes the rotation R, resulting in $|\psi_\theta\rangle = R|\psi\rangle$.

QCRB-optimal states—If the axis of rotation is fixed, we can always take $\mathbf{n}$ as being directed along the z axis. The optimal probe states according to the QCRB for estimating the angle are those maximizing the variance of J_3: they are the NOON states $R(|J, J\rangle + |J, -J\rangle)/\sqrt{2}$ [33].

When the rotation axis is an arbitrary $\mathbf{n}$, one can find states that minimize the QCRB averaged over all possible rotation axes

$$\frac{1}{4\pi}\int_{\mathcal{S}_2} \frac{1}{4\mathfrak{m}_2(\mathbf{n})} d\Omega, \tag{5}$$

where $d\Omega$ is the surface area element on the unit sphere $\mathcal{S}_2$ and we use the notation $\mathfrak{m}_k(\mathbf{n}) = \langle (J_{\boldsymbol{n}} - \langle J_{\boldsymbol{n}} \rangle)^k \rangle$ for the kth central moment (that, in general, depends on $\mathbf{n}$ and on the initial state $|\psi\rangle$). Here, we have taken into account that the QFI, which is obtained by optimizing the CFI over all possible measurements, reduces to $Q_\psi(\mathbf{n}) = 4\mathfrak{m}_2(\mathbf{n})$ for pure states.

The optimal states minimizing the averaged QCRB are those that satisfy $\langle J_{\boldsymbol{n}} \rangle = 0$ and $\langle J_{\boldsymbol{n}}^2 \rangle = \text{constant}$: $\mathfrak{m}_2(\mathbf{n})$ is thus isotropic and the states do not carry information in their first two moments. In general, for a given J, various states can fulfill these conditions, making the optimal states not unique [26]. Furthermore, there are states with isotropic higher-order moments $\mathfrak{m}_k(\mathbf{n})$, raising the question of whether the QCRB is overlooking relevant higher-order information [34,35].

Another motivation for states with isotropic higher-order moments comes from a connection between QFI and fidelity. Under unitary evolution, a state's fidelity with itself is given, to lowest order, by $|\langle\psi|e^{i\theta J_{\mathbf{n}}}|\psi\rangle|^2 = 1-\theta^2 Q_\psi(\mathbf{n})$, such that states with the largest QFI are those that change the most rapidly with small unitaries; as was previously established. If we extend the fidelity calculation to higher orders and average over all axes $\mathbf{n}$, we now find that the fidelity that deviates the most rapidly from unity to next order in θ is the one for states with $\mathfrak{m}_k$ independent from $\mathbf{n}$ for the next order k (see Sec. I in Supplemental Material [36]). This is true for any unitary transformation (e.g., crowning Fock states for displacement sensing) and suggests that higher-order isotropic states emerge in a natural and unexplored way.

QCRB-optimal measurements—We study these higher-order corrections using a measurement whose CFI attains the QFI, so they can be understood as higher-order corrections to the QCRB. The requirements for a measurement to attain the QFI in the pure state case were given in a particularly simple form in the Appendix E of Ref. [22].

For unitary evolution with generator $J_{\mathbf{n}}$, the optimal measurement is characterized by a set of two projectors $\Pi_\pm = |\Phi_\pm\rangle\langle\Phi_\pm|$

$$|\Phi_\pm(\theta)\rangle = \frac{1}{2}\left[(1+e^{i\phi_\pm})|\psi_\theta\rangle + \frac{(1-e^{i\phi_\pm})}{\sqrt{\mathfrak{m}_2}}(J_{\boldsymbol{n}}-\langle J_{\boldsymbol{n}}\rangle)|\psi_\theta\rangle\right], \tag{6}$$

that depends on a single free parameter $\phi_+ = \phi_- + \pi$ (see Sec. II in [36]). This represents a family of measurements that are equivalently optimal according to the QCRB, but that may be further optimized when considering higher-order asymptotics. Note that due to periodicity, it is enough to consider the range $[-\pi/2, 0]$.

There is a subtlety often overlooked in quantum metrology: when considering $p(x|\theta)$, the value of θ on which the measurement depends must be treated as a constant, say θ_0. For example, $p(x_+|\theta) = |\langle\psi_\theta|\Phi_+(\theta_0)\rangle|^2$, and the dependence on θ is only through the state, not the measurement, even when we assume $\theta_0 = \theta$. It follows that the resulting probabilities, $|\langle\psi_\theta|\Phi_\pm(\theta_0)\rangle|^2$, only sum up to one when $\theta = \theta_0$. This implies that we have to extend our measurement, because the MLE presupposes a valid probability distribution that must arise from a true POVM. However, modifying the POVM can affect the performance of real estimators, such as the MLE, even when $\theta = \theta_0$. This is because the MLE relies on $p(x|\theta)$ as a function of θ, and any modification to the POVM alters this dependence.

We will consider two ways of addressing this issue, which are essentially exhaustive. The first method is to replace one of the initial projectors, say $|\Phi_-(\theta_0)\rangle\langle\Phi_-(\theta_0)|$, with $\Pi_2 = \mathbb{1} - |\Phi_+(\theta_0)\rangle\langle\Phi_+(\theta_0)|$. When $\theta = \theta_0$, this is equivalent to the $\Pi_\pm$ measurement, but when $\theta \neq \theta_0$, Π_2 absorbs the missing probability.

The second approach involves extending the two initial measurements by introducing a set of POVM elements $\{\Pi_3, \Pi_4, \ldots\}$, with associated probabilities $\{p(x_3|\theta), p(x_4|\theta), \ldots\}$ that are zero when $\theta = \theta_0$. Interestingly, the performance at $\theta = \theta_0$ is unaffected by this extension. To see why, note that the MLE is the value of θ that maximizes $\sum_x \nu_x \ln[p(x|\theta)]$, where ν_x is the number of measurement outcomes for x. At $\theta = \theta_0$, only the outcomes ν_+ and ν_- are observed, meaning the MLE is independent of the extended elements. In principle, it is possible to imagine other types of extensions, but they would be a combination of these two. While these two extensions both approach the QCRB, we will see that their second-order corrections are different.

Results—In what follows, we assume that $\theta_0 = 0$ without loss of generality. First, we study the extension $\Pi_2 = \mathbb{1} - |\Phi_+(0)\rangle\langle\Phi_+(0)|$. In this case, $\Gamma(0) = \cot^2\phi_+/8\mathfrak{m}_2$, which is minimal and equal to zero when $\phi_+ = -\pi/2$, revealing the optimal measurement. The optimal ϕ_+ is the one where $p(x_+|0) = p(x_-|0) = 1/2$, that is, the "fair coin" case. To understand why this is the case, note that CCRB is attained in the asymptotic limit because the MLE tends to a Gaussian distribution. Convergence to a Gaussian is faster for a fair coin than for a biased coin. This rate of convergence is reflected in the $1/\nu^2$ correction terms.

As the term $1/\nu^2$ cancels out for all second-order unpolarized states, we are naturally interested in the $1/\nu^3$ corrections to look for optimal probe states among the QCRB-optimal family. These next-order corrections have not been explored in detail in the statistical literature, so we calculate them explicitly. For this, we employ the method described in [40]. This involves expanding the equation for the MLE in powers of $\hat{\theta}_{\mathrm{MLE}}$ and then using the Lagrange-Bürmann inversion formula [41] to obtain the inverse series for $\hat{\theta}_{\mathrm{MLE}}$ as a function of the experimental output. Details are provided in [36] (Sec. III). Noting that $\phi_+ = -\pi/2$, which is fixed by $\Gamma(0)$, we get

$$\begin{aligned}\mathrm{MSE}\left[\hat{\theta}^*_{\mathrm{MLE}}(x)\right]_{\theta=0} &= \frac{1}{4\mathfrak{m}_2\nu} \\ &+ \frac{138\mathfrak{m}_2^4 + 79\mathfrak{m}_2^2\mathfrak{m}_4 + \mathfrak{m}_2(30\mathfrak{m}_3^2 - 3\mathfrak{m}_6) + 26\mathfrak{m}_4^2}{768\mathfrak{m}_2^5\nu^3} \\ &+ \mathcal{O}\left(\frac{1}{\nu^4}\right).\end{aligned} \tag{7}$$

Note that this MSE depends on $\mathbf{n}$. This expression can be readily evaluated to assess how quickly one approaches the QCRB and a method's performance before reaching the asymptotic limit without the need for numerical methods. We also provide the formulas for the MLE (without bias correction) in [36] (Sec. III).

We proceed with the family of QCRB-optimal states, with $\langle J_{\boldsymbol{n}}\rangle = 0$ and $\langle J_{\boldsymbol{n}}^2\rangle = \text{constant}$. The average over the

sphere of the $1/\nu^3$ term in Eq. (7) is minimized by states with $\langle J_{\boldsymbol{n}}^3\rangle = 0$ and $\langle J_{\boldsymbol{n}}^4\rangle =$ constant (see Sec. IV in [36]), confirming our intuition of the superiority of states whose higher-order moments $\mathbf{m}_k$ are independent from $\mathbf{n}$ among the family of states that are isotropic to second order. We have thus found general strategies for selecting optimal measurements and states for preasymptotic metrology from among those that are optimal in the asymptotic limits.

We next consider the second extension that adds extra POVM elements with vanishing probabilities at $\theta = 0$; as aforementioned, the performance does not depend on their choice. Using Eq. (1) yields an incorrect expression for the second-order corrections. This is because, in general, they are not appliable at points where probabilities approach zero [note that $\Gamma(0)$ diverges at $\phi_+ = 0$ where $p(x_-|0) = 0$ in the previous POVM extension]. We discuss this in more detail in [36], Sec. V. As Eq. (1) fails, we perform an asymptotic expansion as before to find, up to order $1/\nu^2$

$$\mathrm{MSE}[\hat{\theta}_{\mathrm{MLE}}(x)]_{\theta=0} = \frac{1}{4\mathbf{m}_2\nu} + \frac{\mathbf{m}_2^3(14\csc^2\phi_+ - 5) - \mathbf{m}_2\mathbf{m}_4 + 3\mathbf{m}_3^2}{32\mathbf{m}_2^4\nu^2} + \mathcal{O}\left(\frac{1}{\nu^3}\right). \quad (8)$$

We observe that the optimal measurement and states correspond to $\phi_+ = -\pi/2$ and $\langle J_{\boldsymbol{n}}^3\rangle = 0$, respectively, as before, although there is no longer an advantage in having $\langle J_{\boldsymbol{n}}^4\rangle =$ constant. While the statistical literature considers probabilities approaching zero to be highly pathological, this is a common scenario in quantum metrology. Note also that the definition of the fundamental quantity $\Gamma(\theta)$ loses its meaning, as it relies on Eq. (1) being valid.

We tested this expression numerically. For that, we calculated the average over a grid of $\mathbf{n}$ values of the second order corrections

$$\nu^2\left[\langle\hat{\theta}_{\mathrm{MLE}}^2(x)\rangle - \frac{1}{4\mathbf{m}_2\nu}\right]. \quad (9)$$

The results are shown in Fig. 1, where we can see how the numerical MSE average converges to the theoretical value given by Eq. (8).

As we have seen, these techniques are useful because they reveal information not captured by the QCRB: they provide the rate of convergence to the QCRB and allow for a better assessment of the performance before reaching the asymptotic limit, as well as identify optimal measurements and states that appear equivalent according to the QCRB. This additional information comes with certain costs: there is some dependence on the estimators, the need to specify how the POVM is extended, and the breakdown of the general theory when probabilities approach zero. Regarding the first issue, it is inherent to the problem—after all, the QCRB (and also the CCRB) is a simplification of a complex estimation process. If we want more detailed information, we must accept these caveats. As for the other two issues, a few comments can be made: when dealing with full-rank density matrices, there is no need to extend the measurement, and probabilities generally do not approach zero, thus eliminating the problem. Moreover, it is possible to derive expressions that remain valid when probabilities approach zero, as we have shown, making it feasible to extend Eq. (1) to account for this.

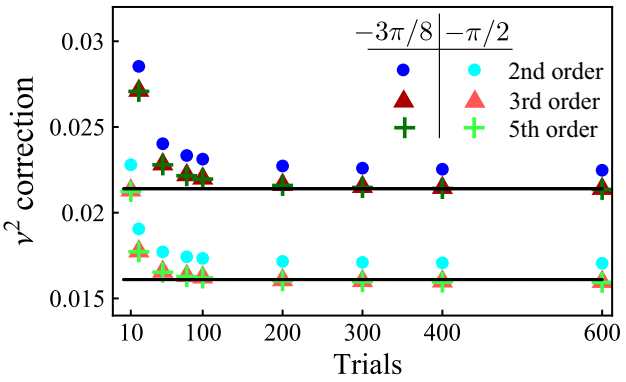

FIG. 1. $1/\nu^2$ corrections at $\theta = 0$, for a different number of trials, of the MSE averaged over the sphere for the second POVM extension. We compare states isotropic to the second, third, and fifth order, and measurements with $\phi_+ = -\pi/2$ and $\phi_+ = -3\pi/8$. The black lines denote the average over all $\mathbf{n}$ of Eq. (8) for third order isotropic states, and the two measurements ($\phi_+ = -\pi/2$ bottom, $\phi_+ = -3\pi/8$ top). We used 300 grid points and the states belong to $J = 6$.

We have presented two possible ways to extend the POVM, raising the question of which method is superior or what the differences are. If the goal is to achieve optimal measurement across a wide range of θ values, it is advisable to have a POVM consisting of many elements. These elements should likely include projections onto the subspaces of $J_{\boldsymbol{n}}^2|\psi_\theta\rangle$, $J_{\boldsymbol{n}}^3|\psi_\theta\rangle$, $J_{\boldsymbol{n}}^4|\psi_\theta\rangle$, and so on. This approach ensures that even when θ varies significantly, information can still be extracted from the new state, which will have components in these subspaces. This concept was demonstrated in the problem of incoherent imaging [42,43], where expanding the POVM with projectors onto subspaces of powers of the generator allowed for achieving the QCRB over a broader region. Therefore, the second extension is our recommended approach.

On the other hand, when we are very close to the true value, the first extension shows that we can eliminate the $1/\nu^2$ terms, resulting in extremely fast convergence to the QCRB. However, this extension fails to attain the QCRB if we move far away from the true value because

$$\frac{1}{F_x(\theta)} = \frac{1}{4\mathbf{m}_2} + \frac{1}{4}\left(\frac{\mathbf{m}_4}{\mathbf{m}_2^2} - 1\right)\theta^2 + \mathcal{O}(\theta^3), \quad (10)$$

and the θ^2 term is always positive and the average is independent of the state.

In the first-order approach, the QCRB serves as a metric for comparing two states in a straightforward manner. However, the QCRB provides only a oversimplified view. Extending beyond the first order offers a more comprehensive perspective, albeit at the expense of simplicity.

Concluding remarks—The QCRB, while having vital importance in quantum metrology, also exhibits certain deficiencies due to its local character. In this Letter, we have focused on three aspects: its inability to distinguish among a set of measurements that saturate it, its incapacity to differentiate optimal states for an arbitrary unitary transformation, and the fact that it provides information exclusively about the asymptotic limit.

We have considered higher-order corrections to the QCRB that allow us to assess performance before reaching the asymptotic limit. These corrections also enabled us to identify an optimal measurement and distinguish between states that appeared indistinguishable according to the QCRB.

Our results apply to any unitary transformation, with the general case handled by considering the generators of the group $\mathrm{SU}(n)$ instead of the usual angular momentum operators.

This work has only scratched the surface of the potential uses of higher-order asymptotic theory in quantum metrology. While our primary focus was on frequentist estimation, these techniques are equally applicable in the Bayesian framework. Extensions to the multiparameter case are also feasible and are expected to yield interesting results. Additionally, moving beyond the examination of pure states and unitary transformations, a promising avenue for future research involves extending these concepts to encompass general transformations and density matrices. Moreover, a more thorough investigation of scenarios where probabilities approach zero—a common instance in quantum metrology—looks intriguing. The multitude of potential applications suggests that these techniques can play a crucial role in advancing quantum metrology.

Acknowledgments—We acknowledge discussions with A. Smerzi, L. Pezzè, A. Datta, M. Barbieri, and M. Evans at an early stage of this work. A. Z. G. acknowledges that the NRC headquarters is located on the traditional unceded territory of the Algonquin Anishinaabe and Mohawk people, as well as support from the NRC Quantum Sensors Challenge program. This publication has received financial support from the QuantEra program (Project ApresSF) and from the Agencia Española de Investigación (Grant No. PID2021-127781NB-I00). L. L. S. S. was supported in part by Grant No. NSF PHY-1748958 to the Kavli Institute for Theoretical Physics (KITP).

[1] M. G. A. Paris, Quantum estimation for quantum technology, Int. J. Quantum. Inform. **07**, 125 (2009).
[2] V. Giovannetti, S. Lloyd, and L. Maccone, Advances in quantum metrology, Nat. Photonics **5**, 222 (2011).
[3] M. Szczykulska, T. Baumgratz, and A. Datta, Multiparameter quantum metrology, Adv. Phys. X **1**, 621 (2016).
[4] J. S. Sidhu and P. Kok, Geometric perspective on quantum parameter estimation, AVS Quantum Sci. **2**, 014701 (2020).
[5] E. Polino, M. Valeri, N. Spagnolo, and F. Sciarrino, Photonic quantum metrology, AVS Quantum Sci. **2**, 024703 (2020).
[6] F. Albarelli, M. Barbieri, M. G. Genoni, and I. Gianani, A perspective on multiparameter quantum metrology: From theoretical tools to applications in quantum imaging, Phys. Lett. A **384**, 126311 (2020).
[7] C. W. Helstrom, *Quantum Detection and Estimation Theory* (Academic, New York, 1976).
[8] A. S. Holevo, *Probabilistic and Statistical Aspects of Quantum Theory*, Quaderni Monographs No. 1 (Ed. della Normale, Pisa, 2011).
[9] D. Petz and C. Ghinea, Introduction to quantum Fisher information, in *Quantum Probability and Related Topics* (World Scientific, Singapore, 2011), Vol. 27, pp. 261–281.
[10] S. M. Kay, *Fundamentals of Statistical Signal Processing* (Prentice-Hall, Englewood Cliffs, NJ, 1993).
[11] H. L. Van Trees, *Detection, Estimation, and Modulation Theory* (Wiley, New York, 2001).
[12] M. Hayashi, Comparison between the Cramer-Rao and the mini-max approaches in quantum channel estimation, Commun. Math. Phys. **304**, 689 (2011).
[13] M. J. W. Hall and H. M. Wiseman, Heisenberg-style bounds for arbitrary estimates of shift parameters including prior information, New J. Phys. **14**, 033040 (2012).
[14] W. Górecki, R. Demkowicz-Dobrzański, H. M. Wiseman, and D. W. Berry, π-corrected Heisenberg limit, Phys. Rev. Lett. **124**, 030501 (2020).
[15] W. Górecki and R. Demkowicz-Dobrzański, Multiparameter quantum metrology in the Heisenberg limit regime: Many-repetition scenario versus full optimization, Phys. Rev. A **106**, 012424 (2022).
[16] G. Chesi, A. Riccardi, R. Rubboli, L. Maccone, and C. Macchiavello, Protocol for global multiphase estimation, Phys. Rev. A **108**, 012613 (2023).
[17] M. Zwierz, C. A. Pérez-Delgado, and P. Kok, General optimality of the Heisenberg limit for quantum metrology, Phys. Rev. Lett. **105**, 180402 (2010).
[18] J. Rubio, P. Knott, and J. Dunningham, Non-asymptotic analysis of quantum metrology protocols beyond the Cramér–Rao bound, J. Phys. Comm. **2**, 015027 (2018).
[19] J. Rubio and J. Dunningham, Quantum metrology in the presence of limited data, New J. Phys. **21**, 043037 (2019).
[20] M. Gessner and A. Smerzi, Hierarchies of frequentist bounds for quantum metrology: From Cramer-Rao to Barankin, Phys. Rev. Lett. **130**, 260801 (2023).
[21] S. L. Braunstein and C. M. Caves, Statistical distance and the geometry of quantum states, Phys. Rev. Lett. **72**, 3439 (1994).
[22] S. Kurdzialek and R. Demkowicz-Dobrzanski, Measurement noise susceptibility in quantum estimation, Phys. Rev. Lett. **130**, 160802 (2023).
[23] P. Kolenderski and R. Demkowicz-Dobrzanski, Optimal state for keeping reference frames aligned and the platonic solids, Phys. Rev. A **78**, 052333 (2008).

[24] G. Björk, A. B. Klimov, P. De La Hoz, M. Grassl, G. Leuchs, and L. L. Sánchez-Soto, Extremal quantum states and their Majorana constellations, Phys. Rev. A **92**, 031801 (R) (2015).
[25] D. Baguette, F. Damanet, O. Giraud, and J. Martin, Anticoherence of spin states with point-group symmetries, Phys. Rev. A **92**, 052333 (2015).
[26] A. Z. Goldberg, A. B. Klimov, G. Leuchs, and L. L. Sánchez-Soto, Rotation sensing at the ultimate limit, J. Phys. Photonics **3**, 022008 (2021).
[27] J. K. Ghosh, *Higher Order Asymptotics*, NSF-CBMS Regional Conference Series in Probability and Statistics (Institute of Mathematical Statistics, Alexandria, VA, 1994).
[28] N. Datta, Y. Pautrat, and C. Rouzé, Second-order asymptotics for quantum hypothesis testing in settings beyond I.I.D.—Quantum lattice systems and more, J. Math. Phys. (N.Y.) **57**, 062207 (2016).
[29] C. R. Rao, Criteria of estimation in large samples, Sankhya **25**, 189 (1963).
[30] C. R. Rao, Asymptotic efficiency and limiting information, in *Proceedings of the Fourth Berkeley Symposium on Mathematical Statistics and Probability, Volume 1: Contributions to the Theory of Statistics* (University of California Press, 1961), Vol. 4, pp. 531–546.
[31] C. R. Rao, Apparent anomalies and irregularities in maximum likelihood estimation (with discussion), Sankhya **24**, 73 (1962), http://hdl.handle.net/10263/296.
[32] C. R. Rao, Efficient estimates and optimum inference procedures in large samples, J. R. Stat. Soc. Ser. B **24**, 46 (1962).
[33] J. P. Dowling, Quantum optical metrology—The lowdown on high-N00N states, Contemp. Phys. **49**, 125 (2008).
[34] J. Martin, S. Weigert, and O. Giraud, Optimal detection of rotations about unknown axes by coherent and anticoherent states, Quantum **4**, 285 (2020).
[35] I. Gianani, M. G. Genoni, and M. Barbieri, Assessing data postprocessing for quantum estimation, IEEE J. Sel. Top. Quantum Electron. **26**, 1 (2020).
[36] See Supplemental Material at http://link.aps.org/supplemental/10.1103/PhysRevLett.134.010804, which includes Refs. [37–39].
[37] W.-K. Tung, *Group Theory in Physics* (World Scientific, Philadelphia, 1985).
[38] M. Tsang, Conservative classical and quantum resolution limits for incoherent imaging, J. Mod. Opt. **65**, 1385 (2018).
[39] Y. Ye and X.-M. Lu, Quantum Cramér-Rao bound for quantum statistical models with parameter-dependent rank, Phys. Rev. A **106**, 022429 (2022).
[40] J. B. S. Haldane and S. M. Smith, The sampling distribution of a maximum-likelihood estimate, Biometrika **43**, 96 (1956).
[41] M. Abramowitz and I. A. Stegun, *Handbook of Mathematical Functions: With Formulas, Graphs and Mathematical Tables* (Dover, New York, 1972).
[42] M. Tsang, R. Nair, and X.-M. Lu, Quantum theory of superresolution for two incoherent optical point sources, Phys. Rev. X **6**, 031033 (2016).
[43] J. Rehacek, M. Paúr, B. Stoklasa, Z. Hradil, and L. L. Sánchez-Soto, Optimal measurements for resolution beyond the Rayleigh limit, Opt. Lett. **42**, 231 (2017).

Higher-order corrections to the quantum Cramér-Rao bound

J. R. Hervas [1], A. Z. Goldberg [2], A. S. Sanz [1], Z. Hradil [3], J. Řeháček [3] and L. L. Sánchez-Soto [1,4,5]

[1] *Departamento de Óptica, Facultad de Física, Universidad Complutense, 28040 Madrid, Spain*

[2] *National Research Council of Canada, 100 Sussex Drive, Ottawa, Ontario K1N 5A2, Canada*

[3] *Department of Optics, Palacký University, 17. listopadu 12, 771 46 Olomouc, Czech Republic*

[4] *Institute for Quantum Studies, Chapman University, Orange, California 92866, USA*

[5] *Max-Planck-Institut für die Physik des Lichts, 91058 Erlangen, Germany*

(Received 8 May 2025; accepted 29 July 2025; published 20 August 2025)

Quantum Fisher information and the associated quantum Cramér-Rao bound (QCRB) are fundamental tools in frequentist quantum metrology, offering both analytical simplicity and practical precision limits for parameter estimation. The QCRB sets a lower bound on the mean square error (MSE) in the idealized limit of infinite measurement trials ($\nu \to \infty$). Here we perform a systematic expansion in powers of $1/\nu$ to refine MSE estimates in realistic, finite-resource scenarios. These corrections reveal differences between measurements that appear equally optimal under the QCRB. They also help to distinguish among multiple optimal state families for estimating an unknown unitary transformation. Additionally, we explore the Bhattacharyya bound and its quantum counterpart, which constrain these corrections. Our results are relevant for preasymptotic metrology, enabling optimized protocols with limited resources without reliance on numerical simulations.

DOI: 10.1103/ltz3-163t

I. INTRODUCTION

Metrology is the science of devising methods to extract the most precise possible estimates of quantities in nature. The ultimate limits in this endeavor are governed by the laws of physics, with quantum mechanics being the most fundamental theoretical framework. By harnessing uniquely quantum phenomena, such as entanglement and squeezing, quantum metrology surpasses the precision of classical methods, making it an ever-growing field of research [1–9].

Parameter estimation has traditionally been approached from two primary perspectives: Frequentist and Bayesian [10]. Rooted in different interpretations of probability, these frameworks provide different insights into parameter estimates and associated uncertainties. While they converge in the asymptotic limit of a large number of measurements, this has led to the mistaken belief that they are interchangeable in quantum metrology. In reality, they embody fundamentally different paradigms.

Our main interest here is in the frequentist scheme, where the quantum Cramér-Rao bound (QCRB) plays a pivotal role, establishing a fundamental lower bound on the mean square error (MSE) of any estimator. It is formulated in terms of the quantum Fisher information (QFI), which quantifies the sensitivity of a quantum state to infinitesimal changes in the parameter, thereby dictating the ultimate precision achievable [11].

The QCRB is widely employed for its elegant blend of analytical tractability, theoretical significance, and practical relevance. It not only drives theoretical advancements but also provides insights into the fundamental limits of estimation precision in real-world experiments.

Nevertheless, despite its prevalence in quantum information, the implications of the QCRB must be taken with a grain of salt. Notably, it is only asymptotically attainable in the limit of infinitely many measurements $\nu \to \infty$. The performance with limited trials remains largely *terra incognita*, although several intriguing results have recently emerged [12–15].

Another challenge is that the QFI is designed for local estimation rather than global scenarios, where both the location and size of the parameter neighborhood are unknown. It has been realized that the MSE in global estimation can differ significantly from that in local strategies [16–18].

Moreover, while the QCRB indicates that concentrating all resources on a single measurement is the optimal strategy, this approach paradoxically requires increasingly precise prior knowledge of the parameter as resources increase. The scaling predicted by the QCRB is corroborated by a Bayesian analysis, aside from a numerical constant [19,20].

To overcome some of these limitations, alternative bounds have been introduced in classical statistics, including the Hammersley-Chapman-Robbins bound [21], the Bhattacharyya bound [22], the Barankin bound [23], and the more general Abel bounds [24]. Similarly, a hierarchy of lower bounds on estimator variance has been explored by imposing additional unbiasedness constraints in the quantum domain [25].

Recently, we have addressed these challenges by leveraging the theory of higher-order asymptotics [26]. Extending beyond the central limit theorem, this framework provides trial-dependent corrections essential for *bona fide* statistical

inference [27]. In this paper, we build upon this approach to explore additional largely unexplored issues.

For instance, in single-parameter estimation, multiple measurements can saturate the QCRB [28], raising the question of which measurement should be preferred over the rest. We shall demonstrate that $O(1/\nu^2)$ corrections serve to distinguish among them.

The QCRB also presents ambiguousness when determining the optimal state for sensing a unitary transformation. A notable example is the case of rotations in SU(2), where a whole family of optimal states exists when considering all possible rotation axes [29–32]. Here, too, higher-order terms allow us to distinguish between states that are otherwise equivalent under the QCRB.

These findings are instrumental for preasymptotic metrology, enabling the design of optimal protocols well before reaching the asymptotic limit. Since the $O(1/\nu^2)$ corrections depend solely on the quantum state, they allow for straightforward analytical calculations without requiring numerical simulations. In a rapid measurement, where $\nu \sim 10$–100 samples can be taken before costs incur or the system changes, this type of correction becomes extremely valuable.

The QCRB is founded on the concept of the symmetric logarithmic derivative (SLD) [33]. The Bhattacharyya bound (BB), in both its classical and quantum formulations, seeks to enhance the QCRB by extending the order of the derivative, making it intrinsically connected to these higher-order corrections. We will demonstrate that it establishes a lower bound for such corrections, offering deeper insights into the fundamental limits of precision in quantum estimation.

This paper is organized as follows. Section II presents the essential background in estimation theory, laying the foundations for the discussions that follow. In Sec. III we examine in detail the previously mentioned limitations of the QCRB. Section IV introduces the theory of higher-order asymptotics, which provides a refined framework for analyzing $O(1/\nu^2)$ corrections. In this context, Sec. V explores the BB and its connections with $O(1/\nu^2)$ terms. We then present its quantum counterpart and analyze its relation with the classical case. Finally, we summarize our findings and present our conclusions in Sec. VI.

II. BACKGROUND

To ensure a self-contained presentation, we briefly outline the key concepts of estimation theory relevant to our discussion. Throughout the paper we restrict ourselves to the case of single-parameter estimation. For further details, we refer the reader to the relevant literature [34,35].

A. Classical estimation theory

To extract information from a physical system, one must perform measurements. The results of such an experiment are represented by a random variable X, which follows a family of probability distributions $p(x|\theta)$, parametrized by θ, the quantity to be estimated. We take X as a discrete variable that can take on N possible values, forming the sample space $S = \{x_1, \ldots, x_N\}$. The continuous case can be addressed in a similar manner.

Typically, the experiment is repeated ν times, yielding a set of ν outcomes $\{\mathbf{x}_1, \ldots, \mathbf{x}_\nu\}$, where each $\mathbf{x}_i \in S$. These trials are assumed to be independent and identically distributed. The assumption of identical distribution means that each trial is governed by the same parameter θ, while independence implies that the joint distribution of all these trials factorizes

$$p(\mathbf{x}|\theta) = \prod_{i=1}^{\nu} p(\mathbf{x}_i|\theta), \tag{2.1}$$

where $\mathbf{x} = (\mathbf{x}_1, \ldots, \mathbf{x}_\nu)^\top$ and the superscript $\top$ denotes the transpose.

If we denote by ν_i the number of times each x_i occurs in $\mathbf{x}$, with $\nu_1 + \nu_2 + \ldots + \nu_N = \nu$, then the probability distribution governing $\{\nu_1, \ldots, \nu_N\}$ is given by a multinomial distribution

$$p(\nu_1, \ldots, \nu_N|\theta) = \frac{\nu!}{\nu_1!\nu_2!\cdots\nu_N!} p(x_1|\theta)^{\nu_1} \cdots p(x_N|\theta)^{\nu_N}. \tag{2.2}$$

Because $\{\nu_1, \ldots, \nu_N\}$ is a sufficient statistic, it retains all the information contained in the full sample $\mathbf{x}$. In practice, this representation is typically preferred for computational purposes.

The goal is to infer the value of θ from the observed data. To achieve this, we employ an estimator $\hat{\theta}(\mathbf{x})$, which is a function of the observed data only. To quantify the performance of this estimator, we need a loss function that measures the error in the estimation. The most common choice is the squared error $[\hat{\theta}(\mathbf{x}) - \theta]^2$, which leads to the concept of the MSE [36]:

$$\mathrm{MSE}[\hat{\theta}(\mathbf{x})] = \langle[\hat{\theta}(\mathbf{x}) - \theta]^2\rangle = \sum_{\mathbf{x}} p(\mathbf{x}|\theta)[\hat{\theta}(\mathbf{x}) - \theta]^2, \tag{2.3}$$

where $\langle\cdot\rangle$ denotes the expectation value with respect to the probability distribution $p(\mathbf{x}|\theta)$.

Ideally, we seek an estimator $\hat{\theta}(\mathbf{x})$ that minimizes the MSE for all possible values of θ. However, this is generally not achievable because the optimal estimator may explicitly depend on the true value of the parameter θ, which is unknown [34]. To proceed further, it is necessary to constrain the class of estimators we consider. This leads to the concept of an unbiased estimator, which is defined as an estimator whose expectation value is equal to the true value of the parameter: $\langle\hat{\theta}(\mathbf{x})\rangle = \theta$.

For unbiased estimators, the classical Cramér-Rao bound (CCRB) establishes a lower bound on the MSE (note that in this case, the MSE coincides with the standard notion of variance):

$$\mathrm{MSE}[\hat{\theta}(\mathbf{x})] \geqslant \frac{1}{\nu\,\mathsf{F}_x(\theta)}, \tag{2.4}$$

where $\mathsf{F}_x(\theta)$ is the classical Fisher information (CFI), defined as [37]

$$\mathsf{F}_x(\theta) = \sum_{i=1}^{N} p(x_i|\theta)\left[\frac{\partial_\theta p(x_i|\theta)}{p(x_i|\theta)}\right]^2. \tag{2.5}$$

Geometrically, the CFI defines a curvature on the statistical manifold of probability distributions, quantifying how distinguishable different parametrized distributions are. A higher

curvature enables more precise parameter estimation. Moreover, the CFI is intrinsically linked to the statistical distance between probability distributions. In particular, for two neighboring distributions, $p(x|\theta)$ and $p(x|\theta + d\theta)$, the infinitesimal statistical distance is given by

$$ds^2 = \mathsf{F}_x(\theta)\, d\theta^2. \tag{2.6}$$

This expression underscores the role of the CFI in shaping the local geometry of the parameter space, establishing a natural scale for parameter estimation.

This unbiasedness constraint facilitates significant analytical progress, allowing the identification of estimators that saturate the bound in specific cases. Even if no estimator fully saturates the bound, it serves as a guiding principle for finding estimators with a lower MSE.

However, this progress is often confined to textbook examples. In most real-world scenarios, identifying unbiased estimators might be impractical. Furthermore, even if such estimators were available, the primary objective remains minimizing the MSE. A biased estimator that achieves a substantially lower MSE is preferable to an unbiased one with a higher MSE [38].

The CCRB is not merely a bound for unbiased estimators; it provides a fundamental lower limit on the MSE for any estimator, whether biased or unbiased, in the asymptotic limit $\nu \to \infty$. This asymptotic optimality is a highly desirable property, ensuring that with sufficient resources, the MSE reaches its theoretical minimum.

B. Quantum estimation theory

In the quantum version, the probe state is represented by a density operator ϱ. The single parameter θ is encoded via a quantum channel $\mathcal{E}_\theta$, whose action on the state ϱ is the transformation $\mathcal{E}_\theta[\varrho] = \varrho_\theta$ [39]. For simplicity, we will restrict our attention to unitary channels, so that $\varrho_\theta = U_\theta \varrho U_\theta^\dagger$, with the unitary operator U_θ expressed as $U_\theta = \exp(-i\theta\, G)$, where G is a selfadjoint operator that is called the generator of the transformation.

To estimate θ, we perform a measurement that is represented by some positive operator-valued measure (POVM) $\{\Pi_x\}$ [40]. Then the probability of obtaining outcome x_i is given by the time-honored Born rule [41]:

$$p(x_i|\theta) = \mathrm{Tr}(\varrho_\theta \Pi_{x_i}). \tag{2.7}$$

The goal is to optimally select both the POVM $\{\Pi_x\}$ and the initial state ϱ such that the resulting probability distribution $p(x|\theta)$ is highly sensitive to the parameter θ, enabling its precise estimation. This translates into optimizing ϱ and $\{\Pi_x\}$ to achieve the lowest possible CCRB or, equivalently, the highest possible $\mathsf{F}_x(\theta)$. Maximizing the CFI ensures that with sufficient resources, we attain the minimum possible MSE.

Given a quantum state ϱ_θ, maximizing the CFI over all possible POVMs leads to the concept of the QFI, which can be expressed as [11]

$$\mathsf{Q}_\varrho(\theta) = \sup_{\{\Pi_x\}} \mathsf{F}_x(\theta), \tag{2.8}$$

and the associated QCRB:

$$\mathrm{MSE}[\hat{\theta}(\mathbf{x})] \geqslant \frac{1}{\nu\, \mathsf{Q}_\varrho(\theta)}. \tag{2.9}$$

Helstrom, using elementary arguments [33], showed an explicit way to compute $\mathsf{Q}_\varrho(\theta)$:

$$\mathsf{Q}_\varrho(\theta) = \mathrm{Tr}(\varrho_\theta L_\theta^2), \tag{2.10}$$

where L_θ is the SLD, defined implicitly via

$$\frac{\partial \varrho_\theta}{\partial \theta} = \frac{1}{2}\{\varrho_\theta, L_\theta\}, \tag{2.11}$$

and $\{\cdot,\cdot\}$ is the anticommutator $\{A, B\} = AB + BA$.

The QFI is intimately connected with the distinguishability of a probe for small variations of the parameter [42]. The distinguishability between two states, ϱ and ϱ', can be quantified by the normalized Bures distance [43] $D_\mathrm{B}(\varrho|\varrho') = \sqrt{1 - F(\varrho|\varrho')}$, where $F(\varrho|\varrho') = [\mathrm{Tr}(\sqrt{\sqrt{\varrho}\,\varrho'\,\sqrt{\varrho}})]^2$ is the fidelity [44]. Then, given two states ϱ_θ and $\varrho_{\theta+d\theta}$, obtained by an infinitesimal change in the parameter, one has [5]

$$D_\mathrm{B}^2(\varrho_\theta|\varrho_{\theta+d\theta}) = \tfrac{1}{8}\mathsf{Q}_\varrho(\theta)\, d\theta^2, \tag{2.12}$$

except for pointwise differences when ϱ_θ changes rank [45,46]. Therefore, the more distinguishable a state is from neighboring states in the manifold, the greater the QFI and the sensitivity of the state to the parameter θ, much as in the classical case.

The next step after calculating the QFI is to find the initial state ϱ that maximizes it, thereby optimizing both the measurement and the state. In the general case where θ enters through a quantum channel, this leads to the concept of the channel QFI [47]. In the unitary case with pure states, the state that maximizes the QFI is simply a superposition of the eigenstates corresponding to the largest and smallest eigenvalues of the generator [48]:

$$|\psi_\mathrm{opt}\rangle = \frac{1}{\sqrt{2}}(|g_\mathrm{max}\rangle + |g_\mathrm{min}\rangle). \tag{2.13}$$

III. LIMITATIONS OF THE CRAMÉR-RAO BOUND

The first limitation of the QCRB has already been mentioned: It only provides information about the achievable performance in the asymptotic limit of infinite resources, $\nu \to \infty$. Yet in practical scenarios, resources are always finite. This raises a critical question: How many trials, ν, are required for the QCRB to accurately approximate the actual MSE? More precisely, for a finite number of trials ν, what is the true MSE? We will explore this in Sec. IV. We turn to two additional limitations that, despite their relevance, have received less attention within the community. We will use the lens of rotation sensing for illustration.

A. Ambiguity in optimal states

Let us consider the illustrative example of a rotation $R = \exp(i\theta J_{\boldsymbol{n}}) \in \mathrm{SU}(2)$, parametrized by its rotation axis $\mathbf{n}$ and angle θ. Here $J_{\boldsymbol{n}} = \mathbf{J}\cdot\mathbf{n}$, with $\mathbf{J}$ being the generators of the rotation, which satisfy the commutation relations of the Lie algebra $\mathfrak{su}(2)$. The irreducible representations of this algebra are labeled by J and are spanned by the states

$|J,m\rangle$, which are the simultaneous eigenstates of $\mathbf{J}^2$ and J_z. These states form a basis for a $(2J+1)$-dimensional Hilbert space, denoted by $\mathcal{H}_J$. In what follows, we assume a pure state $|\psi\rangle \in \mathcal{H}_J$ that undergoes the rotation R, resulting in $|\psi_\theta\rangle = R\,|\psi\rangle$.

For a fixed $\mathbf{n}$ (which we can take as the z axis without loss of generality) and a fixed J, the states that maximize the QFI (and minimize the QCRB) are the time-honored NOON states [49]:

$$|\psi\rangle = \frac{1}{\sqrt{2}}(|J,J\rangle + |J,-J\rangle), \tag{3.1}$$

in agreement with (2.13). In the context of magnetometry, these correspond to the Greenberg-Horne-Zeilinger (GHZ) states [50]. These optimal (pure) states verify $\mathsf{Q}_\varrho(\theta) = 4\mathfrak{m}_2(\mathbf{n})$, independent of θ, where we adopt throughout the notation

$$\mathfrak{m}_k(\mathbf{n}) = \langle\psi|(J_{\boldsymbol{n}} - \langle J_{\boldsymbol{n}}\rangle)^k|\psi\rangle \tag{3.2}$$

for the kth central moment of the generator $J_{\boldsymbol{n}}$.

When the axis $\mathbf{n}$ is not fixed, an optimal state should perform well for any arbitrary $\mathbf{n}$. A reasonable criterion is to minimize the average QCRB over all rotation axes; i.e.,

$$\frac{1}{4\pi}\int_{\mathcal{S}_2}\frac{1}{4\mathfrak{m}_2(\mathbf{n})}\,d\Omega \equiv \frac{1}{4}\overline{\frac{1}{\mathfrak{m}_2}}, \tag{3.3}$$

with the bar denoting such an average over the unit sphere $\mathcal{S}_2$. The states that optimize this average are second-order isotropic, meaning their first two moments are independent of the rotation axis: $\langle J_{\boldsymbol{n}}\rangle = 0$ and $\langle J_{\boldsymbol{n}}^2\rangle = \text{const}$ [51]. These states are not necessarily unique for a given J. Additionally, higher-order isotropic states exist [52,53], raising the question of whether increasing isotropy further reduces the $O(1/\nu^2)$ terms of the MSE.

Higher-order isotropic states naturally emerge when analyzing the fidelity between a quantum state and its rotated counterpart [54]:

$$\begin{aligned}|\langle\psi|e^{iJ_{\boldsymbol{n}}\theta}|\psi\rangle|^2 &= 1 - \mathfrak{m}_2\theta^2 + \tfrac{1}{12}\big(3\mathfrak{m}_2^2 + \mathfrak{m}_4\big)\theta^4 \\ &\quad + \tfrac{1}{360}\big(10\mathfrak{m}_3^2 - 15\mathfrak{m}_2\mathfrak{m}_4 - \mathfrak{m}_6\big)\theta^6 + O(\theta^7).\end{aligned} \tag{3.4}$$

Our goal is to identify the states that, when averaged over all rotation axes $\mathbf{n}$, minimize this fidelity; i.e., those that undergo the largest change. To achieve this, we analyze the average behavior of each order in θ separately.

(i) *Second-order*. This term is proportional to the QFI. The average value $\overline{\mathfrak{m}}_2$ is maximized by states satisfying $\langle J_{\boldsymbol{n}}\rangle = 0$; that is, first-order isotropic [32].

(ii) *Fourth-order*. Among first-order isotropic states, the optimal ones are those that further minimize the next-order term. Since $\langle J_{\boldsymbol{n}}\rangle = 0$, we have $\mathfrak{m}_k = \langle J_{\boldsymbol{n}}^k\rangle$. However, it can be readily shown that $\overline{\langle J_{\boldsymbol{n}}^k\rangle} = \text{const}$ and, consequently, $\overline{\mathfrak{m}}_4$ is constant and independent of the state.

For the term $\overline{\mathfrak{m}_2^2}$ we use Jensen's inequality to show that

$$\frac{1}{4\pi}\int_{\mathcal{S}_2}\langle J_{\boldsymbol{n}}^k\rangle^2\,d\Omega \geqslant \left(\frac{1}{4\pi}\int_{\mathcal{S}_2}\langle J_{\boldsymbol{n}}^k\rangle\,d\Omega\right)^2 = \text{const}. \tag{3.5}$$

Therefore, this term is minimized by states with $\mathfrak{m}_2 = \text{const}$. This condition is satisfied by second-order isotropic states, making them the optimal choice at this order.

(iii) *Sixth-order*. Applying the same reasoning, the optimal states at this order are those that minimize $\overline{\mathfrak{m}_3^2}$. This requirement is satisfied by third-order isotropic states.

In Appendix A we provide a mathematical proof that this pattern continues to arbitrary orders, demonstrating that higher-order isotropic states are always optimal at minimizing fidelity under rotation.

B. Ambiguity in optimal measurements

For the CFI to match the QFI, a specific POVM must be used. This POVM is generally not unique. Despite its importance, this issue has received relatively little attention in the quantum metrology community. Research in this field typically focuses on the QFI itself, with the assumption that any measurement achieving it is sufficient.

The conditions that a POVM must satisfy to ensure that the CFI equals the QFI were recently expressed in a particularly simple form in Ref. [55]. Building on this formulation, Ref. [28] derived the most general form of such a POVM for pure states, which is the case we consider here.

Accordingly, let us define

$$|\pm\rangle = \frac{1}{\sqrt{2}}\left[|\psi_{\theta_0}\rangle \mp \frac{1}{\sqrt{\mathfrak{m}_2}}(J_{\boldsymbol{n}} - \langle J_{\boldsymbol{n}}\rangle)|\psi_{\theta_0}\rangle\right], \tag{3.6}$$

where θ_0 is the value at which the measurement is evaluated. The most general quantum measurement that attains the QFI is given by a set of projectors $\Pi_i = \lambda_i|\Phi_i\rangle\langle\Phi_i|$ onto the states

$$|\Phi_i\rangle = \frac{1}{\sqrt{2}}(|+\rangle + e^{i\phi_i}|-\rangle), \tag{3.7}$$

such that $\sum_i \lambda_i = 2$ and $\sum_i \lambda_i e^{i\phi_i} = 0$.

We focus on the simplest case of two projectors, with $\lambda_1 = \lambda_2 = 1$. This yields a family of measurements parametrized by an angle ϕ_+,

$$\begin{aligned}&|\Phi_\pm(\theta_0)\rangle \\ &\quad = \frac{1}{2}\left[(1+e^{i\phi_\pm})|\psi_{\theta_0}\rangle + \frac{(1-e^{i\phi_\pm})}{\sqrt{\mathfrak{m}_2}}(J_{\boldsymbol{n}} - \langle J_{\boldsymbol{n}}\rangle)|\psi_{\theta_0}\rangle\right],\end{aligned} \tag{3.8}$$

where $\phi_- = \phi_+ - \pi$.

A subtle but often overlooked point in quantum metrology is that when considering the probability distribution $p(x|\theta)$, the parameter θ_0 that influences the measurement must be treated as a fixed constant, even when $\theta_0 = \theta$. As a consequence, the resulting probabilities, $|\langle\psi_\theta|\Phi_\pm(\theta_0)\rangle|^2$, sum to unity only when $\theta = \theta_0$. Actually, a simple calculation shows

that

$$p(x_+|\theta)+p(x_-|\theta)=1+\frac{\mathfrak{m}_2^3+\mathfrak{m}_3^2-\mathfrak{m}_2\mathfrak{m}_4}{4\mathfrak{m}_2}(\theta-\theta_0)^4+O(\theta^5). \tag{3.9}$$

This implies that we must extend our measurement. However, modifying the POVM can affect the performance of real estimators, such as the maximum likelihood estimator (MLE), even when $\theta=\theta_0$. We will consider two ways of addressing this issue.

The first method is to replace one of the initial projectors, say, $|\Phi_-(\theta_0)\rangle\langle\Phi_-(\theta_0)|$, with $\Pi_2=\mathbb{1}-|\Phi_+(\theta_0)\rangle\langle\Phi_+(\theta_0)|$. When $\theta=\theta_0$, this is equivalent to the $\Pi_\pm$ measurement, but when $\theta\neq\theta_0$, Π_2 absorbs the missing probability, ensuring a complete POVM.

The second approach involves extending the two initial measurements by introducing a set of POVM elements $\{\Pi_3,\Pi_4,\ldots\}$, with associated probabilities $\{p(x_3|\theta),p(x_4|\theta),\ldots\}$ that are zero when $\theta=\theta_0$. In principle, other types of extensions might be conceived, but they would essentially be combinations of these two. While both extensions achieve the QCRB, we will demonstrate that their second-order corrections differ.

IV. BEYOND THE ASYMPTOTIC LIMIT

A. Higher-order asymptotics

A wide variety of estimators have been formulated by proposing ad hoc functions [34,35]. Among these, one of the most widely adopted is the MLE, largely due to its turn-the-crank nature. Popularized by Fisher [56], the MLE provides a general-purpose method that can be readily applied across a broad range of problems without requiring problem-specific tuning. It is defined as

$$\hat{\theta}_{\mathrm{MLE}}(\mathbf{x})=\arg\max_\theta p(\mathbf{x}|\theta). \tag{4.1}$$

Here the likelihood $p(\mathbf{x}|\theta)$ must be interpreted as the probability of θ being the true value given the dataset $\mathbf{x}$. This estimator just picks the value of θ that makes $\mathbf{x}$ the most likely observation; in other words, *it bets on the winner.*

Under mild regularity conditions, the MLE enjoys desirable asymptotic properties: It is consistent, asymptotically efficient, and normally distributed as the sample size grows [57]. Thus, in the regime of abundant resources, one can be confident in achieving the minimum possible MSE. Nevertheless, many estimators are known to reach the CCRB asymptotically, raising the question of why one should be preferred over another.

In a series of influential papers, Rao addressed this question [58–60] (for additional perspectives, see also Refs. [61,62]). For any efficient estimator, the MSE can always be expanded as

$$\mathrm{MSE}[\hat{\theta}(\mathbf{x})]=\frac{1}{\nu}\frac{1}{\mathsf{F}_x(\theta)}+\frac{1}{\nu^2}\left[\Gamma(\theta)+b^2(\theta)+2\frac{b'(\theta)}{\mathsf{F}_x(\theta)}\right]+O\left(\frac{1}{\nu^3}\right), \tag{4.2}$$

where $b(\theta)/\nu=\langle\hat{\theta}(\mathbf{x})-\theta\rangle$ is the bias of order $O(1/\nu)$ and $\Gamma(\theta)$ is an estimator-dependent function. Specifically, for the MLE, we have

$$b(\theta)=-\frac{1}{2\nu}\frac{\gamma_{11}}{\mathsf{F}_x^2(\theta)},$$
$$\Gamma(\theta)=-\frac{1}{\mathsf{F}_x(\theta)}+\frac{\gamma_{02}(\theta)-2\gamma_{21}(\theta)+\gamma_{40}(\theta)}{\mathsf{F}_x^3(\theta)}+\frac{\frac{1}{2}\gamma_{11}^2(\theta)-[\gamma_{11}(\theta)-\gamma_{30}(\theta)]^2}{\mathsf{F}_x^4(\theta)}, \tag{4.3}$$

with

$$\gamma_{rs}(\theta)=\sum_{i=1}^N p(x_i|\theta)\left[\frac{\partial_\theta p(x_i|\theta)}{p(x_i|\theta)}\right]^r\left[\frac{\partial_\theta^2 p(x_i|\theta)}{p(x_i|\theta)}\right]^s. \tag{4.4}$$

In general, no single estimator minimizes the $O(1/\nu^2)$ terms in Eq. (4.2). To establish a fundamental bound at this order, it is necessary to restrict the analysis to estimators that are unbiased up to $O(1/\nu)$. More precisely, while comparisons could be made between estimators with the same bias $b(\theta)$, the most natural approach is to consider the strictly unbiased case, where $b(\theta)=0$ [27]. This restriction does not result in a significant loss of generality, as any estimator $\hat{\theta}(\mathbf{x})$ can be transformed into a bias-corrected version

$$\hat{\theta}^*(\mathbf{x})=\hat{\theta}(\mathbf{x})-\frac{b[\hat{\theta}(\mathbf{x})]}{\nu}, \tag{4.5}$$

which is unbiased to order $O(1/\nu)$ [60].

In this case, the MSE takes the form:

$$\mathrm{MSE}[\hat{\theta}^*(\mathbf{x})]=\frac{1}{\nu\,\mathsf{F}_x(\theta)}+\frac{\Gamma(\theta)}{\nu^2}+O\left(\frac{1}{\nu^3}\right). \tag{4.6}$$

In this way, $\Gamma(\theta)$ appears as a second-order correction to the CCRB. The key result established by Rao is that the MLE is the unique estimator that minimizes $\Gamma(\theta)$. This highlights the distinguished status of the MLE among all efficient estimators, not just in terms of first-order efficiency but also in minimizing second-order error contributions.

B. First POVM extension

Even once the MLE is chosen as the estimator, one must still choose among POVM strategies. First, we calculate $\Gamma(\theta)$ for the first POVM extension, $p(x_2|\theta)=1-p(x_+|\theta)$. We assume without loss of generality that $\theta_0=0$ from now on. In this case, one gets

$$\Gamma(0)=\frac{\cot^2\phi_+}{8\mathfrak{m}_2}. \tag{4.7}$$

The minimum value of $\Gamma(0)$ is zero when $\phi_+=-\pi/2$, identifying this as the optimal measurement setting. At this value, the probabilities satisfy $p(x_+|0)=p(x_2|0)=1/2$, corresponding to a fair coin scenario. In this case, the CCRB is attained asymptotically because the MLE converges to a Gaussian distribution. This convergence occurs more rapidly when the underlying distribution resembles a fair coin, compared to a biased one. This difference is captured in the $O(1/\nu^2)$ correction terms, which are smaller for the fair coin case, indicating faster asymptotic efficiency.

If we do not fix the measurement at $\phi_+ = -\pi/2$, then one could in principle average over all rotation axes to identify the states that minimize $\Gamma(\theta)$, among those that are optimal according to the QCRB. However, for these states $\langle J_{\boldsymbol{n}}\rangle = 0$ and $\langle J_{\boldsymbol{n}}^2\rangle = \mathfrak{m}_2 = \text{const}$, so this term is the same for all of them. Interestingly, the measurement with $\phi_+ = -\pi/2$ is also optimal according to the Fisher information measurement noise susceptibility, a recently introduced concept that quantifies a measurement's resilience to noise [28].

It is also interesting to analyze the standard MLE, without bias correction. The $O(1/\nu^2)$ correction is given by

$$\Gamma(0) + b^2(0) + 2\frac{b'(0)}{\mathsf{F}_x(0)} = \frac{\mathfrak{m}_2^2[2\cos(2\phi_+) + 5]\csc^2(\phi_+) + \mathfrak{m}_4}{16\mathfrak{m}_2^3}. \tag{4.8}$$

As before, the measurement that minimizes this expression is $\phi_+ = -\pi/2$. With this choice, a remaining $O(1/\nu^2)$ term from the bias derivative appears, $(3\mathfrak{m}_2^2 + \mathfrak{m}_4)/(16\nu^2\mathfrak{m}_2^3)$, which is always positive.

1. Third-order corrections

Since we can set $\Gamma(0) = 0$ by choosing $\phi_+ = -\pi/2$, we then look at the next term $O(1/\nu^3)$ in the expansion. With the measurement fixed, we calculate these corrections following the procedure in Ref. [63].

The very same definition of the MLE; that is, $\max_\theta\{\nu_+ \ln[p(x_+|\theta)] + \nu_2 \ln[p(x_2|\theta)]\}$, implies

$$\frac{\nu_+}{p(x_+|\theta)}\frac{dp(x_+|\theta)}{d\theta} + \frac{\nu_2}{p(x_2|\theta)}\frac{dp(x_2|\theta)}{d\theta} = 0. \tag{4.9}$$

We substitute a Taylor series expansion for $p(x_+|\theta)$

$$p(x_+|\theta) = \frac{1}{2} - \sqrt{\mathfrak{m}_2}\,\theta + \frac{(3\mathfrak{m}_2^2 + \mathfrak{m}_4)\theta^3}{6\sqrt{\mathfrak{m}_2}} + O(\theta^4) \tag{4.10}$$

into the MLE equation (4.9):

$$0 = -4\delta_+\sqrt{\mathfrak{m}_2} - 4\mathfrak{m}_2\nu\,\theta - \frac{2\delta_+(5\mathfrak{m}_2^2 - \mathfrak{m}_4)}{\sqrt{\mathfrak{m}_2}}\theta^2 + O(\theta^3), \tag{4.11}$$

where we have used the variable δ_+ defined as $\nu_+ = \delta_+ + \nu/2$, since we will need to take the limit $\nu \to \infty$ and require the remaining terms to be small compared to ν. We invert this series to obtain the value of θ_{MLE}. This can be done using the Lagrange-Bürmann inversion formula [64,65]; the result reads

$$\hat{\theta}^2_{\text{MLE}}(\mathbf{x}) = \frac{\delta_+^2}{\mathfrak{m}_2\nu^2} + \frac{\delta_+^4(3\mathfrak{m}_2^2 + \mathfrak{m}_4)}{3\mathfrak{m}_2^3\nu^4} - \frac{\delta_+^5(\mathfrak{m}_2^3 - \mathfrak{m}_2\mathfrak{m}_4 + \mathfrak{m}_3^2)}{4\mathfrak{m}_2^4\nu^5} + \cdots. \tag{4.12}$$

This expression can be used to estimate the value of $\hat{\theta}^2_{\text{MLE}}(\mathbf{x})$ as a function of the experimental outcomes ν_+. Finally, we take the expectation value $\langle\theta^2_{\text{MLE}}(\mathbf{x})\rangle$. The quantities $\langle\delta_+^k\rangle$ are the central moments of a binomial distribution with a fair coin [66], given by $\langle\delta_+^2\rangle = \nu/4$, $\langle\delta_+^4\rangle = \nu(3\nu - 2)/16$ and $\langle\delta_+^6\rangle = [15(\nu - 2)\nu + 16]/64$. For odd k, they are 0. Substituting and performing an expansion in powers of $1/\nu$, we arrive at

$$\text{MSE}[\hat{\theta}_{\text{MLE}}(\mathbf{x})]_{\theta=0} = \frac{1}{4\mathfrak{m}_2\nu} + \frac{3\mathfrak{m}_2^2 + \mathfrak{m}_4}{16\mathfrak{m}_2^3\nu^2} + \frac{219\mathfrak{m}_2^4 + 133\mathfrak{m}_2^2\mathfrak{m}_4 + \mathfrak{m}_2(30\mathfrak{m}_3^2 - 3\mathfrak{m}_6) + 35\mathfrak{m}_4^2}{768\mathfrak{m}_2^5\nu^3} + O\left(\frac{1}{\nu^4}\right). \tag{4.13}$$

We can refine our search for optimal states by considering the $O(1/\nu^3)$ terms, since the $O(1/\nu^2)$ term does not distinguish between different optimal states. When averaging over all possible rotation axes, the only state-dependent terms in $O(1/\nu^3)$ are $30\mathfrak{m}_2\overline{\mathfrak{m}_3^2}$ and $35\overline{\mathfrak{m}_4^2}$. As we previously observed, both of these terms are minimized by fourth-order isotropic states. This reveals that not all states that were second-order isotropic are equivalent: The MLE favors higher-order isotropic states.

2. Third-order corrections with bias correction

We next consider the MSE of the bias-corrected MLE estimator. We expand $b(\hat{\theta}) = b(0) + a_1\hat{\theta} + a_2\hat{\theta}^2 + a_3\hat{\theta}^3$ in $\langle[\hat{\theta}(\mathbf{x}) - b(\hat{\theta}(\mathbf{x}))/\nu]^2\rangle$. Note that $b(0) = 0$ for $\phi_+ = -\pi/2$. We obtain a lengthy expression in terms of $\langle\hat{\theta}^k(\mathbf{x})\rangle$. The details can be seen in the Appendix B. The final result is

$$\text{MSE}[\hat{\theta}^*_{\text{MLE}}(\mathbf{x})]_{\theta=0} = \frac{1}{4\mathfrak{m}_2\nu} + \frac{84\mathfrak{m}_2^4 - 11\mathfrak{m}_2^2\mathfrak{m}_4 + 3\mathfrak{m}_2(-10\mathfrak{m}_3^2 + \mathfrak{m}_6) - 28\mathfrak{m}_4^2}{768\mathfrak{m}_2^5\nu^3} + O\left(\frac{1}{\nu^4}\right). \tag{4.14}$$

When searching for the optimal states for detecting an arbitrary rotation, we find that the only nonconstant terms are $\overline{\mathfrak{m}_3^2}$ and $\overline{\mathfrak{m}_4^2}$. Unlike the standard MLE case, where fourth-order isotropic states were optimal, here they are actually the worst choices, because these nontrivial terms contribute with negative coefficients. To our knowledge, states that are second-order isotropic but exhibit *anti-isotropic* behavior at higher orders have not been studied.

3. Preasymptotic performance

We turn to an important application: estimating performance before reaching the asymptotic limit; a regime where the QCRB provides limited guidance.

It is crucial to emphasize that discussing the MSE of the MLE (or any estimator) in the low-trial regime is meaningless without specifying prior information about the parameter. In particular, the admissible range of values for θ must be clearly defined by the experimental context.

To illustrate this, we analyze the behavior of the MLE using the previous POVM extension, with $\phi_+ = -\pi/2$, which is a binomial model. Similar qualitative conclusions would apply in more general multinomial scenarios. The key idea is that, given an observed outcome ν_+, the MLE estimates θ

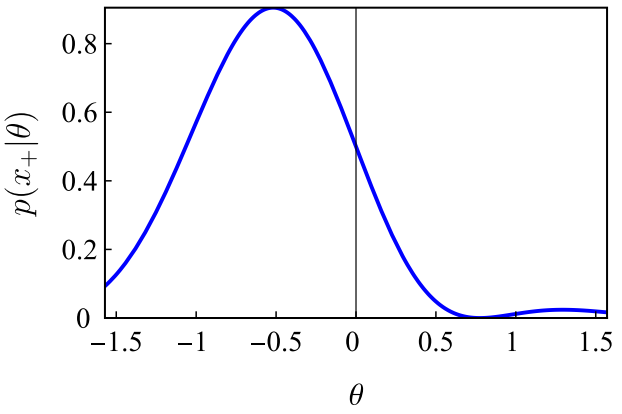

FIG. 1. Probability $p(x_+|\theta)$ for a coherent state (with $J = 3$) pointing along the z axis, after being rotated by an angle θ around the x axis: $|\psi_\theta\rangle = e^{-\theta J_x}|J, J\rangle$.

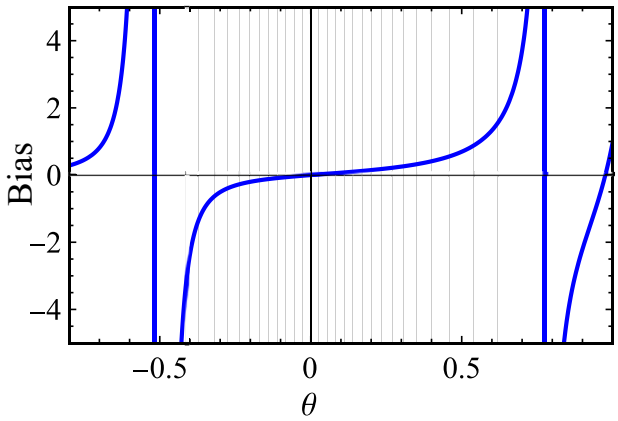

FIG. 3. Bias $b(\theta)$ for the same state as in Fig. 1. The vertical lines indicate the values of θ returned by the MLE for the different experimental outputs.

by setting $p(x_+|\theta) = \nu_+/\nu$, as it follows from Eq. (4.9), after substituting $\nu = \nu_+ + \nu_2$ and $p(x_2|\theta) = 1 - p(x_+|\theta)$. Alternatively, this result follows from the invariance property of the MLE and the fact that for a binomial distribution, the MLE for the coin's q value is simply $\hat{q} = \nu_+/\nu$. If this value does not exist, then it returns the closest value.

Figure 1 illustrates the behavior of $p(x_+|\theta)$ for a coherent state pointing in the z axis, rotated around the x axis $|\psi_\theta\rangle = e^{-\theta J_x}|J, J\rangle$ with $J = 3$. This example will serve as a guiding thread throughout the discussion. The maximum detectable range of θ is limited by the region where the function does not turn around (i.e., where the derivative remains nonzero). If the function were to turn around, then the MLE would yield multiple values of θ, making the problem unidentifiable.

The importance of prior information can be stressed by considering a single trial ($\nu = 1$ and $\nu_+ = 1$). The MLE equation simplifies to $\arg\max_\theta p(x_+|\theta)$. If $\nu_2 = 1$, then the MLE instead maximizes $1 - p(x_+|\theta)$, leading to the lowest possible θ. These extrema may coincide with the range beyond which the model becomes unidentifiable, but this is not always the case. If the system rotates slightly beyond this range, then it becomes impossible to detect, making the effective range smaller in practice.

Figure 2 illustrates how the MSE varies with the choice of prior range for θ. Comparing the full range with a reduced 80% interval, the results reveal a strong dependence of the MSE on the assumed prior. Further narrowing the range to 50% would reduce the MSE even further.

Since we have to choose a range, and there is no single correct answer, the most natural choice is simply to take the maximum range. We have observed that for all states (not just for our example) the bias diverges near the edges, rendering bias correction unfeasible. A practical workaround is to either exclude these boundary regions or apply a cutoff beyond which bias correction is no longer applied.

A more natural approach, though, is simply to restrict the θ range to avoid the divergence. This is illustrated in Fig. 3, where we restrict the range to 80% to avoid falling into the diverging region. The figure shows the bias $b(\theta)$, and how the MLE assigns values of θ based on different experimental results ($\nu = 30$), with $p(x_+|\theta) = 0, 1/30, 2/30, \ldots, 1$. Owing to the 80% threshold, some of the equations lack solutions, causing several solution lines to cluster at the boundaries. This behavior follows directly from the original definition of the MLE.

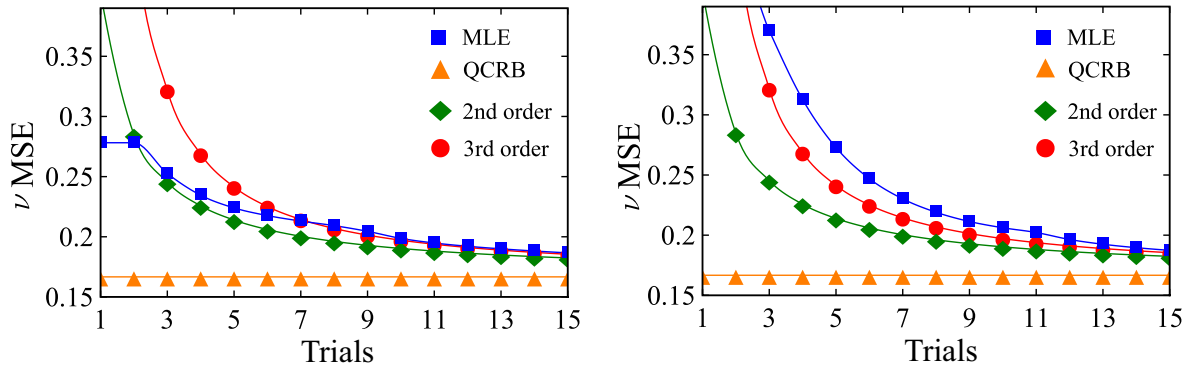

FIG. 2. MSE of the MLE as a function of the number of trials for the same state as in Fig. 1. In the left panel, the parameter θ is restricted to 80% of its maximum admissible range, while in right panel, the full range is considered. The plots also show the QCRB and the approximations given by equation (B6), including corrections up to orders up to orders $1/\nu^2$ and $1/\nu^3$.

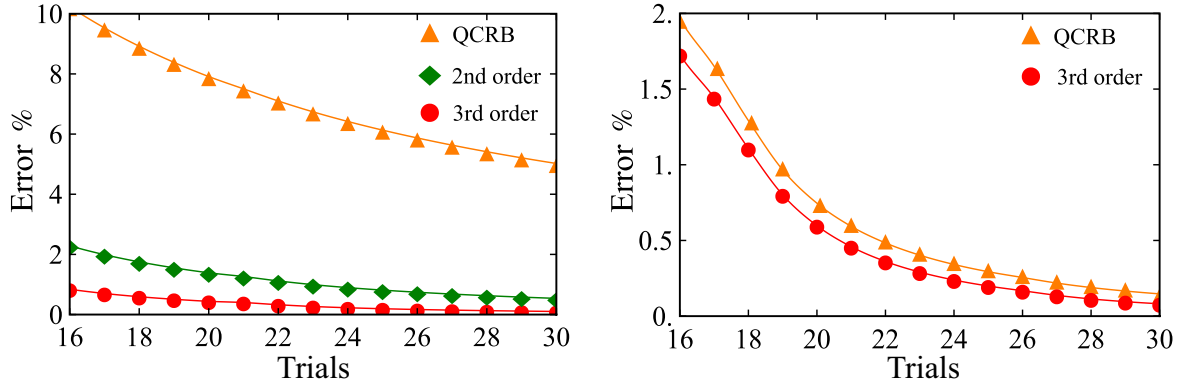

FIG. 4. Relative error in the MSE when using the MLE with different approximations. The left panel shows results for the standard MLE, while the right panel presents the bias-corrected MLE. Insets within each panel illustrate the specific approximation method used for the first POVM extension.

To assess the usefulness of our analytical corrections, Fig. 4 shows the percentage error when approximating the MSE using the QCRB alone versus including $O(1/\nu^2)$ and $O(1/\nu^3)$ corrections. This is calculated as $|\mathrm{MSE}_{\mathrm{approx}} - \mathrm{MSE}|/\mathrm{MSE}$. For the standard MLE, these corrections significantly improve accuracy over the QCRB. For the bias-corrected MLE, the corrections have little impact because eliminating the $O(1/\nu^2)$ term causes the MSE to converge to the QCRB much faster. In general, whether a $O(1/\nu^3)$ or even $O(1/\nu^2)$ correction is relevant or not depends on the specific context.

A final numerical validation of our expressions can be performed by computing $\nu^2[\langle\hat{\theta}^2(\mathbf{x})\rangle - 1/\mathfrak{m}_2\nu]$ and similarly for third order. In Appendix B we show how the theoretical values of these corrections are in excellent agreement with the numerical results.

C. Second POVM extension

This case is more complex than the previous one. The key insight is that, according to Eq. (4.2), the corrections $O(1/\nu^2)$ depend on the derivative of the bias; specifically, on its behavior in a neighborhood of the point of interest.

The MLE equation for this extension $\{\Pi_3, \Pi_4, \ldots\}$, with probabilities $\{p(x_3|\theta), p(x_4|\theta), \ldots\}$ that are zero at $\theta = 0$, is $\max_\theta \sum_x \nu_x \ln[p(x|\theta)]$.

At $\theta = 0$, we have $\nu_3, \nu_4, \ldots = 0$, as the corresponding outcomes have zero probability. As a result, the MLE depends solely on $p(x_+|\theta)$ and $p(x_-|\theta)$, assuming it is maximized at $\theta = 0$. This is somewhat counterintuitive, because the bias $b(\theta)$, for $\theta \neq 0$, clearly depends on the chosen extension, which in turn should influence its derivative and, consequently, the MSE at $\theta = 0$. This highlights how probabilities that approach zero can introduce subtle complications in the analysis.

In fact, attempting to compute second-order corrections using only $p(x_+|\theta)$ and $p(x_-|\theta)$ leads to incorrect results. One possible approach is to introduce a third outcome, defining $p(x_3|\theta) = 1 - p(x_1|\theta) - p(x_2|\theta)$, but this produces an inaccurate expression. More generally, this theoretical framework breaks down at these points and the fundamental quantity $\Gamma(\theta)$ loses its significance. We discuss this in the next subsection.

We proceed by computing these corrections following the same approach used to determine the $O(1/\nu^3)$ terms in the previous case. The procedure is largely similar, with two key differences. First, we have $x_+ = \delta_+ + \nu\cos^2(\phi_+/2)$, as we do not fix the value of ϕ_+. This also changes the form of the $\langle\delta_+^k\rangle$; specifically, we obtain $\langle\delta_+^2\rangle = \frac{1}{4}\nu\sin^2\phi_+$, $\langle\delta_+^3\rangle = -\frac{1}{4}\nu\sin^2\phi_+\cos\phi_+$, and $\langle\delta_+^4\rangle = \frac{1}{32}\nu\sin^2\phi_+[3(2-\nu)\cos(2\phi_+) + 3\nu + 2]$. The second change arises after substituting these terms into Eq. (4.12), where terms involving δ_+ are in the denominator. To eliminate them and subsequently compute the mean values of δ_+^k, we must first expand in powers of $1/\nu$ before proceeding further. The details can be found in Appendix B. This leads us to

$$\mathrm{MSE}[\hat{\theta}_{\mathrm{MLE}}(\mathbf{x})]_{\theta=0} = \frac{1}{4\mathfrak{m}_2\nu} + \frac{\mathfrak{m}_2^3(14\csc^2\phi_+ - 5) - \mathfrak{m}_2\mathfrak{m}_4 + 3\mathfrak{m}_3^2}{32\mathfrak{m}_2^4\nu^2} + O\left(\frac{1}{\nu^3}\right). \tag{4.15}$$

As in the previous case, the measurement that minimizes the order $O(1/\nu^2)$ is $\phi_+ = -\pi/2$.

Regarding the optimal states, when taking the mean value, the only term that does not remain constant is $\overline{\mathfrak{m}_3^2}$, which is minimized by third-order isotropic states. This result aligns with the MLE without bias correction. However, upon calculating the next correction, we find that the fourth-order isotropic states are the worst, and the best states would be those that maximize the value of $\overline{\mathfrak{m}_4^2}$. The calculation is lengthy, we defer its full derivation to Appendix B.

As with the previous POVM extension, we test the corrections using the same rotated coherent state as before and also fix $\phi_+ = -\pi/2$. Here we take the maximum admissible range for θ, as bias correction is not meaningful in this regime. In Fig. 5 we compare the error predicted by the QCRB with the error obtained from (4.15). As before, the expressions provide significant insight. As previously noted, the relevance of corrections of order $O(1/\nu^2)$ or $O(1/\nu^3)$ ultimately depend on the particular context.

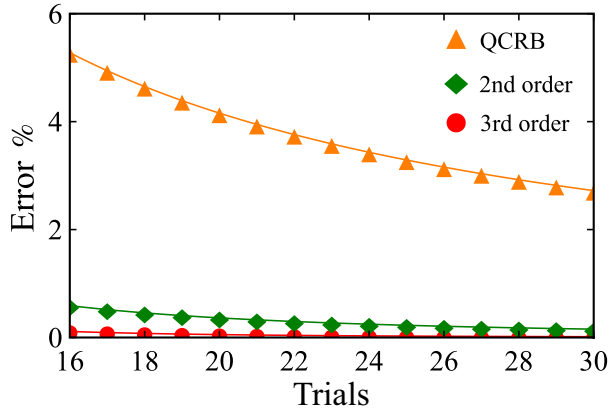

FIG. 5. Relative error in the MSE when using the MLE with the approximations indicated in the inset, computed using Eq. (4.15), for the second POVM extension.

D. The problem of vanishing probabilities

Before tackling the complications of vanishing probabilities, let us first consider a simpler case that clarifies the core issue. Returning to the first POVM extension with $\phi_+ = 0$, we find $p(x_2|0) = 0$, indicating a probability that vanishes at $\theta = 0$. Unlike the more complex scenario where the outcome space grows rapidly with ν, here the number of possible outcomes is limited to $\nu + 1$, and the MLE is determined by solving $p(x_+|\theta) = \nu_+/\nu$.

In Fig. 6, we show the MSE and the bias of the MLE for a NOON state (3.1), though this choice does not play a particularly special role in the analysis. On the right side of the plot, the QCRB is attained and the MLE remains unbiased, as it happens in the asymptotic limit. However, as θ approaches zero, clear deviations emerge: The MSE diverges from the asymptotic trend, and the estimator becomes biased. This behavior persists even as ν increases: Larger ν merely shrinks the region of deviation but does not eliminate it.

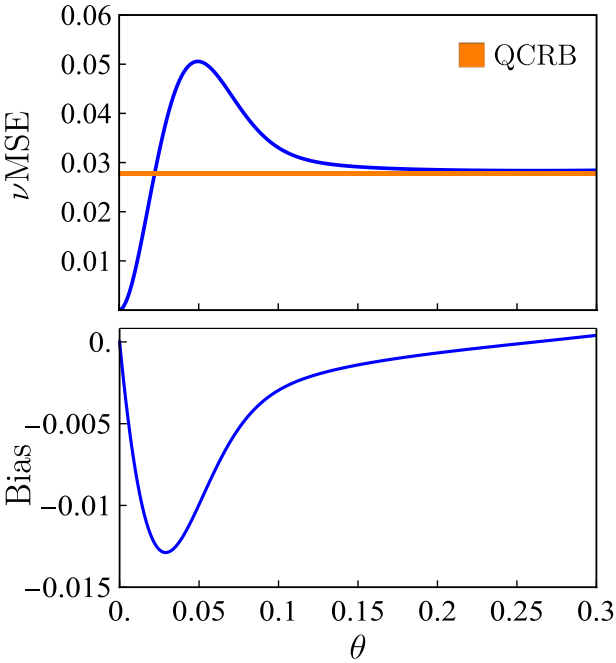

FIG. 6. MSE and bias of the MLE for the estimation of the rotation angle around the z axis with a NOON state (3.1). The number of trials is $\nu = 30$, although this behavior is observed for arbitrarily high values of ν.

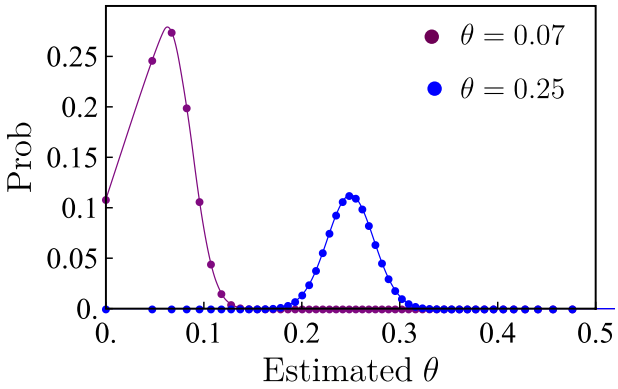

FIG. 7. Probability distribution of the MLE for the true values $\theta = 0.07$ and $\theta = 0.25$ with $\nu = 30$ trials for the same NOON state as in Fig. 6.

To understand this behavior, Fig. 7 shows the probability distribution of the MLE when the true values of the parameter are $\theta = 0.07$ and $\theta = 0.25$. In the first case, the distribution is still far from a Gaussian, whereas in the second case it already closely approximates one. No matter how large we make ν, we can always find a sufficiently small θ for which the MLE has not yet converged to a Gaussian distribution. This explains the *bump* observed in Fig. 6: The system has simply not yet reached the asymptotic regime. The fact that the MSE becomes 0 at $\theta = 0$ is specific to this particular example. It arises because at $\theta = 0$ the experiment can only return one result. Since the MLE assigns $\theta = 0$ to this outcome, the MSE is necessarily zero, as the estimator is always correct in this specific case.

Now let us examine the case of $p(x_+|\theta)$ and $p(x_-|\theta)$. When $\theta = 0$, we attain the QCRB, as previously observed, and we do not encounter the same issues as in the previous example. To analyze this further, let us consider the simplest possible extension: $p(x_3|\theta) = 1 - p(x_+|\theta) - p(x_-|\theta)$. The choice of this particular extension is not crucial, as the argument we are about to make holds for any other extension as well.

The MSE of the MLE can be decomposed into two distinct components:

$$\begin{aligned}\mathrm{MSE}[\hat{\theta}_{\mathrm{MLE}}(\mathbf{x})] = &\sum_{\substack{\nu_3=0\\ \nu_+,\nu_-}} [\hat{\theta}_{\mathrm{MLE}}(\nu_+,\nu_-,\nu_3)-\theta]^2 p(\nu_+,\nu_-,0)\\ &+\sum_{\substack{\nu_3=1\\ \nu_+,\nu_-}}^{\nu} [\hat{\theta}_{\mathrm{MLE}}(\nu_+,\nu_-,\nu_3)-\theta]^2 p(\nu_+,\nu_-,\nu_3)\\ &\equiv \Delta_0 + \Delta. \end{aligned} \tag{4.16}$$

Consider a sufficiently large ν such that, at $\theta = 0$, we are already in the asymptotic regime (e.g., $\nu \sim 30$ is often sufficient). In this case, the MSE is given by Δ_0, with $\Delta = 0$. Now, if we choose a small nonzero value for θ while keeping ν

fixed, then the probability that the outcome ν_3 does not occur in the experiment is given by

$$\sum_{\nu_+,\nu_-} p(\nu_+, \nu_-, 0) = [1 - p(x_3|\theta)]^\nu \simeq (1 - \theta^4)^\nu. \quad (4.17)$$

For a fixed ν, we can always take θ small enough that the probability of observing ν_3 becomes negligible. As a result, the contribution from Δ can be made arbitrarily small, since the relevant probabilities vanish while the MLE remains bounded. By continuity of the MSE, this implies that the QCRB is saturated in the limit of small θ.

Now, keeping this small fixed θ, let us increase ν until $[1 - p(x_3|\theta)]^\nu \simeq 0$. This marks the asymptotic regime for this value of θ, where the MSE converges to $1/\mathsf{F}_x(\theta)$. In this limit, $\Delta_0 \simeq 0$, and the MSE is dominated entirely by the contribution from Δ. Between the initial regime and this asymptotic limit, there exists a transition region in which the CCRB is not attained.

For any fixed ν, there always exists a range of θ values lying within the transition region between the asymptotic regime and the QCRB value at $\theta = 0$. In this transition region, the qualitative behavior of vanishing probabilities resembles that shown in Fig. 6, with one key difference: At $\theta = 0$, the MSE reaches the QCRB rather than dropping to zero.

It is noteworthy that this seemingly pathological phenomenon is, in fact, likely to be common in quantum metrology. Unless the density matrix is full rank, it is typical for its support to change as the parameter varies. While this behavior has been previously observed [67,68], to the best of our knowledge, its underlying origin has not been thoroughly investigated nor has its generality across quantum estimation problems been fully recognized.

V. BHATTACHARYYA BOUND

This section revisits the BB [22]. While it provides less detail than higher-order asymptotic theories, it still offers a rigorous lower bound. A key advantage is its quantum extension, allowing direct evaluation from the state without searching for the optimal POVM, making calculations much simpler.

A. Classical Bhattacharyya bound

We begin with the derivation of the classical Bhattacharyya bound (CBB), presenting a general framework that encompasses this bound and extends to the multiparameter case.

Consider a probability distribution $p(\mathbf{x}|\boldsymbol{\theta})$ that depends on a set of parameters $\boldsymbol{\theta} = \{\theta_1, \cdots, \theta_n\}$ and let $\hat{\boldsymbol{\theta}}(\mathbf{x}) = \{\hat{\theta}_1(\mathbf{x}), \ldots, \hat{\theta}_n(\mathbf{x})\}$ be the corresponding estimators. Let us set $\Delta\hat{\theta}_i = \hat{\theta}_i(\mathbf{x}) - \langle\hat{\theta}_i(\mathbf{x})\rangle$. Define the quantities

$$y_i = \Delta\hat{\theta}_i - A_{im}c_m, \quad (5.1)$$

where A_{im} is an arbitrary matrix with real entries and c_m is a vector that can depend on both $\mathbf{x}$ and $\boldsymbol{\theta}$. Throughout, we adopt the Einstein summation convention when no ambiguity arises. We construct a positive semidefinite matrix with matrix elements

$$y_i y_j = (\Delta\hat{\theta}_i - A_{im}c_m)(\Delta\hat{\theta}_j - A_{jp}c_p). \quad (5.2)$$

Averaging with respect to the probability distribution $p(\mathbf{x}|\boldsymbol{\theta})$ preserves the positive semidefinitess,

$$\begin{aligned}\langle\Delta\hat{\theta}_i\Delta\hat{\theta}_j\rangle &\geqslant \langle\Delta\hat{\theta}_i c_p\rangle A_{jp} + A_{im}\langle\Delta\hat{\theta}_j c_m\rangle - A_{im}\langle c_m c_p\rangle A_{jp} \\ &= (TA^\top + AT^\top - AHA^\top)_{ij}, \end{aligned} \quad (5.3)$$

where the matrices T and C have elements

$$T_{ij} = \langle\Delta\hat{\theta}_i\, c_j\rangle, \quad C_{ij} = \langle c_i\, c_j\rangle. \quad (5.4)$$

The left-hand side in Eq. (5.3) is the covariance matrix. Our goal is to minimize the sum of its diagonal entries, which corresponds to minimizing the total variance. To achieve the tightest bound, we take the trace of both sides and differentiate with respect to the elements A_{ij}, yielding the optimal choice $A = TC^{-1}$. Substituting into (5.3), we obtain

$$\mathrm{Cov}[\hat{\boldsymbol{\theta}}(\mathbf{x})] \geqslant TC^{-1}T^\top. \quad (5.5)$$

Since for general estimators we have $\mathrm{MSE}[\hat{\boldsymbol{\theta}}(\mathbf{x})]_{ij} = \mathrm{Cov}[\hat{\boldsymbol{\theta}}(\mathbf{x})]_{ij} + \langle\delta\hat{\theta}_i\rangle\langle\delta\hat{\theta}_j\rangle$, where the deviation from the true parameter value is given $\delta\hat{\theta}_i = \hat{\theta}_i(\mathbf{x}) - \theta_i$ and $\delta\hat{\boldsymbol{\theta}} = \{\delta\hat{\theta}_1, \delta\hat{\theta}_2, \cdots \delta\hat{\theta}_n\}$, we then have

$$\mathrm{MSE}[\hat{\boldsymbol{\theta}}(\mathbf{x})] \geqslant TC^{-1}T^\top + \langle\delta\hat{\boldsymbol{\theta}}\rangle\,\langle\delta\hat{\boldsymbol{\theta}}^\top\rangle, \quad (5.6)$$

which lets us derive different classical bounds. For unbiased estimators, the bias term disappears and T becomes independent of the estimator.

We now focus on the single-parameter case with unbiased estimators and choose the c_k to arrive at the CBB

$$c_k = \frac{1}{p(\mathbf{x}|\theta)}\frac{d^k p(\mathbf{x}|\theta)}{d\theta^k}. \quad (5.7)$$

The CBB of order k corresponds to the kth derivative. For instance, the second-order CBB takes the form

$$\mathrm{MSE}[\hat{\theta}(\mathbf{x})] \geqslant \frac{1}{C_{11}} + \frac{C_{12}^2}{C_{11}\big(C_{11}C_{22} - C_{12}^2\big)}. \quad (5.8)$$

The term $1/C_{11}$ corresponds to the standard CCRB, while the extra term, which is always positive, is a correction that makes it tighter. In some cases, the CCRB is too optimistic because no unbiased estimator can achieve it. Nonetheless, an unbiased estimator might still exist that saturates the higher-order CBB. A classic example is estimating the square of the mean of a Gaussian distribution: Although the CCRB can be saturated for the mean itself, no unbiased estimator achieves it for the square. Yet, an unbiased estimator does exist that saturates the second-order CBB [57].

As formulated above, the theory applies to the full probability distribution; i.e., over ν trials. For the term C_{11}, which is the CFI, we simply have that $C_{11} = \nu c_{11}$. The other quantities scale as [57]

$$\begin{aligned} C_{12} &= \nu c_{12}, \quad C_{13} = \nu c_{13}, \quad C_{22} = \nu\big[c_{22} + 2(\nu-1)c_{11}^2\big], \\ C_{23} &= \nu[c_{23} + 6(\nu-1)c_{12}c_{11}], \\ C_{33} &= \nu\big[c_{33} + 9(\nu-1)\big(c_{22}c_{11} + c_{12}^2\big) + 6(\nu-1)(\nu-2)c_{11}^3\big]. \end{aligned} \quad (5.9)$$

In this way, we get

$$\mathrm{MSE}[\hat{\theta}(\mathbf{x})] \geqslant \frac{1}{\nu}\frac{1}{c_{11}} + \frac{1}{\nu^2}\frac{c_{12}^2}{2c_{11}^4} + \frac{1}{\nu^3}\frac{2c_{11}^2c_{13}^2 + c_{12}^2\left(6c_{11}^3 + 21c_{12}^2 - 3c_{11}c_{22} - 12c_{11}c_{13}\right)}{12c_{11}^7} + O\left(\frac{1}{\nu^4}\right), \tag{5.10}$$

where we have included terms $O(1/\nu^3)$. Note that this bound, to order $O(1/\nu^i)$, is only applicable to estimators that are unbiased to the ith order.

The correction term of order $O(1/\nu^2)$ remains unchanged even when higher-order derivatives are added to the CBB (by introducing additional c_k). However, this is no longer true for terms of order $1/\nu^3$ and beyond.

Importantly, we note that the $O(1/\nu^2)$ term in the CBB is precisely the contribution $\gamma_{11}^2/[2\mathsf{F}_x^4(\theta)]$ appearing in $\Gamma(\theta)$. This terms corresponds to the so-called *naming curvature* [69] and is one of the three positive terms that constitute $\Gamma(\theta)$. As a result, the CBB should be interpreted as a lower bound for the fundamental quantity $\Gamma(\theta)$.

Having understood the nature of the CBB, we can apply it to search for corrections to the QCRB. For the first POVM extension, the $O(1/\nu^2)$ coincides with $\Gamma(0)$; that is, it reduces to $\cot(\phi_+)^2/8\mathfrak{m}_2$. We fix $\phi_+ = -\pi/2$ and calculate the third correction; the result is $(3\mathfrak{m}_2^2 + \mathfrak{m}_4)^2/(384\mathfrak{m}_2^5)$.

For the second POVM extension, things are more complicated. First, we complete the POVM in the simplest possible way: adding a third output $p(x_3|\theta) = 1 - p(x_+|\theta) - p(x_-|\theta)$. The term of order $O(1/\nu^2)$ coincides again with $\Gamma(0)$. However, when calculating the correction of order $O(1/\nu^3)$, the expansion (5.10) is no longer useful. This is because it was derived by taking the limit $\nu \to \infty$, which implicitly assumes that no terms larger than ν exist. In this case we find that $c_{33} \to \infty$ as $\theta \to 0$. To address this, we substitute Eq. (5.9) in the general CBB, assuming the estimator is unbiased to order $O(1/\nu^3)$. We take the limit $\theta \to 0$ and then expand in powers of $1/\nu$, leading to

$$\mathrm{MSE}[\hat{\theta}(\mathbf{x})]_{\theta=0} \geqslant \frac{1}{4\mathfrak{m}_2\nu} + \frac{\cot^2\phi_+}{8\mathfrak{m}_2\nu^2} + \frac{\cot^2\phi_+}{8\mathfrak{m}_2\nu^3} + O\left(\frac{1}{\nu^4}\right). \tag{5.11}$$

This indicates that by choosing the optimal measurement, all correction terms can be eliminated, making the bound tighter.

It is important to highlight that this case is problematic. The derivation of these expressions assumes an estimator unbiased to the order of the calculated correction. However, as shown in Fig. 6, this assumption does not hold (at least for the MLE). When θ is sufficiently small, the bias does not tend to zero, regardless of the value of ν. As we already discussed, dealing with probabilities that approach zero introduces significant difficulties.

B. Quantum Bhattacharyya bound

The quantum Bhattacharyya bound (QBB) was first introduced by Tsuda [70], who also extended other classical bounds useful for nondifferentiable models [71]. Later, Parthasarathy provided a rigorous proof that helped to derive quantum versions of several classical bounds [72].

Another approach, proposed by Brody and coworkers [73–75], used a geometric formulation of quantum mechanics. In this framework, quantum states exist in a real Hilbert space with a complex structure. They derived a series of Bhattacharyya-style bounds for pure quantum states, which depend on the estimator used. To remove this dependence, special types of estimators are needed. More recently, these bounds were extended to general density matrices [76].

In Appendix C we provide an alternative proof that closely parallels the one for the CBB. We summarize here the results. We proceed as in the classical case, defining $Y_i = \Delta X_i - A_{im}L_m$, where $X_i = \sum_{\mathbf{x}} \hat{\theta}_i(\mathbf{x})\Pi_{\mathbf{x}}$ and $\Delta X_i = X_i - \langle\hat{\theta}_i(\mathbf{x})\rangle = \sum_{\mathbf{x}} \Delta\hat{\theta}_i(\mathbf{x})\Pi_{\mathbf{x}}$ and L_m are operators and $\{\Pi_{\mathbf{x}}\}$ is the POVM representing the measurement. Operating much in the same way we arrive at

$$\mathrm{Cov}[\hat{\boldsymbol{\theta}}(\mathbf{x})] \geqslant T Q^{-1} T^{\top}, \tag{5.12}$$

where the matrices T and Q have elements

$$\begin{aligned} T_{ij} &= \tfrac{1}{2}\,\mathrm{Tr}[\varrho^{(\nu)}(\Delta X_i L_j^{\dagger} + L_j \Delta X_i)], \\ Q_{ij} &= \tfrac{1}{2}\,\mathrm{Tr}[\varrho^{(\nu)}(L_i L_j^{\dagger} + L_j L_i^{\dagger})], \end{aligned} \tag{5.13}$$

where $\varrho^{(\nu)}$ is the density matrix corresponding to the ν trials. As in the classical case, we can add the bias to get the MSE.

Equation (5.12) provides a bound for the MSE, but how does it relate to the CBB and, more generally, to other classical bounds derived from Eq. (5.6)? The key idea is that T remains the same as in the classical case when L_k are chosen appropiately. For the QBB we choose them as the kth-order SLDs, ensuring they are Hermitian,

$$\frac{d^k \varrho_\theta^{(\nu)}}{d\theta^k} = \frac{1}{2}\left(L_k \varrho_\theta^{(\nu)} + \varrho_\theta^{(\nu)} L_k\right). \tag{5.14}$$

Also, one can demonstrate that the POVM consisting of eigenvectors of the operator $X = \langle\hat{\theta}(\mathbf{x})\rangle + A_m L_m = \langle\hat{\theta}(\mathbf{x})\rangle + T_k (Q^{-1})_{km} L_m$ saturate the QBB and the other single parameter bounds.

While we aim to apply this bound to pure states, a fundamental issue arises: These operators do not exist for pure states. This becomes evident when taking the second derivatives of the state ϱ_θ,

$$\frac{d^2\varrho_\theta}{d\theta^2} = -J_{\boldsymbol{n}}^2|\psi_\theta\rangle\langle\psi_\theta| - |\psi_\theta\rangle\langle\psi_\theta|J_{\boldsymbol{n}}^2 + J_{\boldsymbol{n}}|\psi_\theta\rangle\langle\psi_\theta|J_{\boldsymbol{n}}. \tag{5.15}$$

Clearly, the last term cannot be produced by an operator of the form L_i as in Eq. (5.14), since it maps from outside the span of ϱ to to outside the span of ϱ. But what does this imply? To gain insight, we introduce a small amount of white noise and then gradually let it approach zero,

$$\varrho_\theta = \frac{1}{1+\varepsilon d}(|\psi_\theta\rangle\langle\psi_\theta| + \varepsilon\mathbb{1}), \tag{5.16}$$

where d is the dimension of the space. The analytical expressions for the L_k may be obtained by the use of the methods in Ref. [77]. It turns out that the nondiagonal terms are 0, so there

is no second-order correction. This is because $\mathrm{Tr}(\varrho L_2 L_1)$ is an imaginary number. A similar thing happens for $i = 4, 6, \ldots$. We continue and calculate the third-order corrections. In that case, we have

$$\frac{d^3\varrho_\theta}{d\theta^3} = \frac{1}{1+\epsilon d}\left(iJ_{\boldsymbol{n}}^3|\psi_\theta\rangle\langle\psi_\theta| + 3iJ_{\boldsymbol{n}}|\psi_\theta\rangle\langle\psi_\theta|J_{\boldsymbol{n}}^2 + \mathrm{c.c.}\right), \tag{5.17}$$

which leads to the following values for q (we use again q instead of Q to denote the $\nu = 1$ case)

$$\begin{aligned} q_{11} &= \frac{4\mathfrak{m}_2}{(1+2\epsilon)(1+d\varepsilon)}, \\ q_{13} &= -\frac{4\left(3\mathfrak{m}_2^2+\mathfrak{m}_4\right)}{(1+2\varepsilon)(1+d\varepsilon)}, \\ q_{22} &= \frac{4\mathfrak{m}_2^2(3\varepsilon^2+3\varepsilon+1)+\mathfrak{m}_4\varepsilon(1+\varepsilon)}{\varepsilon(1+\varepsilon)(1+2\varepsilon)(1+d\varepsilon)}, \\ q_{33} &= \frac{-18\mathfrak{m}_2^3+6\mathfrak{m}_4\mathfrak{m}_2(10\varepsilon+3)-2\mathfrak{m}_3^2(20\varepsilon+9)+4\mathfrak{m}_6\varepsilon}{\varepsilon(1+2\varepsilon)(1+d\varepsilon)}. \end{aligned} \tag{5.18}$$

The rest of the terms involving L_2 are zero. See Appendix D for the scaling of Q.

We calculate the third-order corrections,

$$(Q^{-1})_{11} = \frac{1}{Q_{11}}\left(1+\frac{Q_{13}^2}{Q_{33}-Q_{13}^2}\right). \tag{5.19}$$

To analyze the asymptotic expansion in powers of ν, it is crucial to carefully consider the order in which limits are taken. If we first take the limit $\varepsilon \to 0$, then the third-order corrections vanish. This behavior mirrors what we observed with the CBB in the second POVM extension, where choosing $\phi_+ = -\pi/2$ canceled these corrections.

On the other hand, if we assume ε small, but nonzero, and apply Eq. (5.10) before taking $\varepsilon \to 0$, then we recover a correction that matches the result from the first POVM extension:

$$\mathrm{MSE}[\hat{\theta}(\mathbf{x})]_{\theta=0} \geqslant \frac{1}{4\mathfrak{m}_2\nu} + \frac{\left(3\mathfrak{m}_2^2+\mathfrak{m}_4\right)^2}{384\mathfrak{m}_2^5\nu^3} + O\left(\frac{1}{\nu^4}\right). \tag{5.20}$$

To interpret this, recall that the element Q_{11} corresponds to the QFI. The QBB must be attained by measurements that also achieve the QFI, while minimizing higher-order corrections. This is precisely what we did in the previous section.

When ε is small but finite, the scenario resembles the first POVM extension, where no probabilities vanish. This explains why the QBB corrections match the case with $\phi_+ = -\pi/2$, which cancels the corrections of order $O(1/\nu^2)$.

Conversely, in the second POVM extension, certain probabilities vanish as $\varepsilon \to 0$, preventing higher-order corrections when $\phi_+ = -\pi/2$. This corresponds to $\varepsilon \to 0$ before taking $\nu \to \infty$.

This interplay between limits offers an intuitive explanation of the observed behavior, although a more rigorous treatment is needed to fully characterize the underlying relationships.

This brings us to the practical significance of the CBB (or its quantum analog, the QBB). In the classical case, the CBB naturally arises within the framework of second-order asymptotic theory. Specifically, the $1/\nu^2$ term in the CBB is one of the three components that define the full second-order asymptotic behavior.

The key advantage of the QBB is its ability to determine the minimum possible value of the $1/\nu^2$ term in the CBB. Moreover, it helps to identify the measurements that achieve this minimum within the class of measurements that saturate the QFI.

However, the QBB is not guaranteed to exist in all scenarios. In particular, problems arise when the span of the quantum state changes with the parameter. One possible workaround is to introduce a small amount of white noise and consider the limit as it vanishes. This regularization approach has been shown to recover the corrections associated with both POVM extensions, though a deeper analysis is required to fully understand its scope and limitations.

In summary, the QBB is especially useful for full-rank density matrices. In cases where the rank varies, its applicability is less clear and requires deeper investigation.

VI. CONCLUSIONS AND OUTLOOK

In this work, we have derived $O(1/\nu^2)$ and $O(1/\nu^3)$ corrections to the MSE in quantum metrology, where ν is the number of trials. These corrections improve the accuracy of MSE estimates in the preasymptotic regime.

Our results highlight that these corrections depend on the estimator used. While the QCRB sets a fundamental asymptotic limit, estimator-specific effects emerge in the preasymptotic regime. If we consider estimators unbiased up to order $O(1/\nu)$, then the second-order corrections simplify, revealing a fundamental quantity akin to the QCRB.

We also showed that standard higher-order correction methods may fail when the density matrix's span depends on the parameter. Despite this, we demonstrated that these corrections remain computable. Importantly, they allow us to distinguish measurement strategies that appear equivalent under the QCRB. For instance, measurements achieving the QFI may still exhibit different preasymptotic performance. Additionally, for optimal state families used in detecting unitary transformations, higher-order corrections help refine optimality beyond the asymptotic limit.

Furthermore, we explored the connection between these corrections and the CBB, a tighter bound than the CCRB. We demonstrated that the BB provides a lower limit for these $O(1/\nu^2)$ corrections. Notably, like the QCRB, it has a quantum extension that offers a POVM-independent lower bound on preasymptotic corrections, making it a powerful and easy-to-use tool.

Looking ahead, several research directions arise. A key next step is generalizing the $O(1/\nu^2)$ correction formulas to probability distributions that do not sum to one, a common scenario in practice. This could follow the approach in Ref. [63] but without assuming probability normalization, simplifying calculations by avoiding explicit series inversion.

Another significant direction is extending these results to arbitrary quantum processes and mixed states. Investigating

measurement parametrizations that saturate the QFI in broader scenarios and optimizing them using second-order corrections is also a natural extension.

The role of POVM extensions in parameter estimation accuracy deserves further study. A deeper understanding of their most general forms and implications would be valuable.

Additionally, while our work focuses on frequentist quantum metrology, these techniques could be adapted for Bayesian methods. Extending this approach to multiparameter quantum metrology is, in principle, feasible but potentially challenging, as the asymptotic case remains unresolved and is an active research area [78–81].

In conclusion, while we focused on unitary transformations and pure states, our methods provide a strong analytical foundation for quantum metrology beyond the asymptotic regime. By enabling finite-resource studies without relying on numerical simulations, this approach holds great potential for further theoretical advancements.

ACKNOWLEDGMENTS

We acknowledge discussions with A. Smerzi, L. Pezzè, A. Datta, M. Barbieri, I. Gianani, and M. Evans at an early stage of this work. This publication has received financial support from the QuantEra program (Project ApresSF), from the Agencia Estatal de Investigación (Grant No. PID2021-127781NB-I00), and from Palacký University (Grant No. IGA PRF 2025_005). A.Z.G. acknowledges that the NRC headquarters is located on the traditional unceded territory of the Algonquin Anishinaabe and Mohawk people, as well as support from the NRC Quantum Sensors Challenge program. L.L.S.-S. was supported in part by the Grant No. NSF PHY-1748958 to the Kavli Institute for Theoretical Physics (KITP).

DATA AVAILABILITY

The data that support the findings of this article are not publicly available. The data are available from the authors upon reasonable request.

APPENDIX A: FROM FIDELITY TO HIGHER-ORDER AVERAGES

The fidelity between a state and a slightly rotated version of the state is given by $\mathcal{F}(\theta|\mathbf{n}) \equiv |\langle\psi|e^{i\theta J_n}|\psi\rangle|^2 = 1 - \frac{1}{4}\theta^2 \mathsf{Q}_\psi(\mathbf{n}) + O(\theta^3)$. This means that the states that change most rapidly with small θ are those with maximal QFI and that the states that change the most on average for all rotation axes $\mathbf{n}$ are those with the maximal values of $\int_{\mathcal{S}_2} \mathsf{Q}_\psi(\theta|\mathbf{n})d\Omega$, which are the states with isotropic first-order moments $\langle J_{\boldsymbol{n}}\rangle = \text{const} = 0$. Within this family of states that have such a maximal average QFI, which states have their fidelities decrease the most to next leading order in θ?

We begin by writing

$$\mathcal{F}(\theta) \equiv \frac{1}{4\pi}\int_{\mathcal{S}_2}\mathcal{F}(\theta|\mathbf{n})d\Omega = \frac{1}{4\pi}\int_{\mathcal{S}_2}\left\{\left[\sum_{k=0}^{\infty}\frac{(-1)^k}{(2k)!}\langle\psi|(\theta J_{\boldsymbol{n}})^{2k}|\psi\rangle\right]^2 + \left[\sum_{k=0}^{\infty}\frac{(-1)^k}{(2k+1)!}\langle\psi|(\theta J_{\boldsymbol{n}})^{2k+1}|\psi\rangle\right]^2\right\}d\Omega. \tag{A1}$$

The integrals are all over terms of the form $\int_{\mathcal{S}_2} n_1^j n_2^k n_3^l d\Omega$, which equals $\frac{2\Gamma(\frac{j+1}{2})\Gamma(\frac{k+1}{2})\Gamma(\frac{l+1}{2})}{\Gamma(\frac{1}{2}(j+k+l+3))}$ when each of j, k, and l are even and vanishes otherwise. We can write $\mathcal{F}(\theta) = \sum_{n=0}^{\infty} f_n\theta^{2n}$ and note the first few terms:

$$\begin{aligned}
f_0 &= 1,\\
f_1 &= \frac{1}{4\pi}\int_{\mathcal{S}_2}\left(\langle J_{\mathbf{n}}\rangle^2 - \langle J_{\mathbf{n}}^2\rangle\right)d\Omega = \frac{1}{3}\sum_{i=1}^{3}\left(\langle J_i\rangle^2 - \langle J_i^2\rangle\right) = -\frac{1}{16\pi}\int_{\mathcal{S}_2}\mathsf{Q}_\psi(\mathbf{n})d\Omega,\\
f_2 &= \frac{1}{4\pi}\int_{\mathcal{S}_2}\frac{1}{12}\left(\langle J_{\boldsymbol{n}}^4\rangle - 4\langle J_{\boldsymbol{n}}^3\rangle\langle J_{\boldsymbol{n}}\rangle + 3\langle J_n^2\rangle^2\right)d\Omega,
\end{aligned} \tag{A2}$$

and so on. We see that f_0 is the same for any state. The sum $\sum_{i=1}^3\langle J_i^2\rangle$ is constant for any state because $\sum_{i=1}^3 J_i^2$ is proportional to the identity operator, so f_1 is minimized by states with $\langle J_1\rangle = \langle J_2\rangle = \langle J_3\rangle = 0$, which are first-order isotropic ($\langle J_{\mathbf{n}}\rangle = \text{const}$). Among these states, since $\int_{\mathcal{S}_2} J_{\mathbf{n}}^4 d\Omega$ is proportional to the identity operator [see Eq. (A8) onwards], f_2 simplifies to

$$f_2 = \text{const} + \frac{1}{16\pi}\int_{\mathcal{S}_2}\langle J_{\mathbf{n}}^2\rangle^2 d\Omega \tag{A3}$$

and

$$\frac{1}{4\pi}\int_{\mathcal{S}_2}\langle J_{\mathbf{n}}^2\rangle^2 d\Omega \geqslant \left(\frac{1}{4\pi}\int_{\mathcal{S}_2}\langle J_{\mathbf{n}}^2\rangle d\Omega\right)^2 = \text{const} \tag{A4}$$

has the same lower bound regardless of the state due to $\int_{\mathcal{S}_2} J_{\mathbf{n}}^2 d\Omega$ being proportional to identity [see Eq. (A8) onwards]; this lower bound is achieved if and only if the state obeys $\langle J_{\mathbf{n}}^2\rangle = \text{const}$. This was found using Jensen's inequality that the average of a square is greater than the square of the average, with equality if and only if the quantity being averaged is constant, as above.

To summarize, all states have the same f_0, states that are isotropic to first order have the smallest f_1, states that are isotropic to first and second order have smallest f_2, and so on.

We proceed to prove the general case by induction. Consider that the subleading order in the expansion of $\mathcal{F}(\theta)$ to order $\theta^{2(n-1)}$ is minimized by states that are isotropic to order $n-1$; i.e., by states $|\psi\rangle$ with $\langle J_{\boldsymbol{n}}^k\rangle = \text{const}$ for all $k \in \{0, 1, \cdots, n-1\}$. Then, the terms of order θ^{2n} in the integrand are

$$I_n = \sum_{k=0}^{n} \frac{(-1)^k}{(2k)!}\frac{(-1)^{n-k}}{(2n-2k)!}\langle\psi|J_{\boldsymbol{n}}^{2k}|\psi\rangle\,\langle\psi|J_{\boldsymbol{n}}^{2n-2k}|\psi\rangle + \sum_{k=0}^{n-1}\frac{(-1)^k}{(2k+1)!}\frac{(-1)^{n-k-1}}{(2n-2k-1)!}\langle\psi|J_{\boldsymbol{n}}^{2k+1}|\psi\rangle\,\langle\psi|J_{\boldsymbol{n}}^{2n-2k-1}|\psi\rangle. \tag{A5}$$

Since all the expectation values $\langle J_{\boldsymbol{n}}^k\rangle \equiv c_k$ to order k are independent from $\mathbf{n}$ for $k < n$, all of the c_k with odd values of $k < n$ will vanish. The second sum only retains terms with $2k+1 = 2n-2k-1 = n$ and so only remains if n is odd. The first sum is always a constant times a single expectation value, if n is odd, yielding another constant after integration. We thus have the possibilities:

$$I_n = \begin{cases} \frac{(-1)^{(n-1)/2}}{n!}\left\langle J_{\boldsymbol{n}}^n\right\rangle^2 + 2\sum_{k=0}^{(n-1)/2}\frac{(-1)^k}{(2k)!}\frac{(-1)^{n-k}}{(2n-2k)!}c_{2k}\left\langle J_{\boldsymbol{n}}^{2n-2k}\right\rangle, & n\,\text{odd}, \\ \frac{(-1)^{n/2}}{n!}\left\langle J_{\boldsymbol{n}}^n\right\rangle^2 + 2\sum_{k=0}^{n/2-1}\frac{(-1)^k}{(2k)!}\frac{(-1)^{n-k}}{(2n-2k)!}c_{2k}\left\langle J_{\boldsymbol{n}}^{2n-2k}\right\rangle, & n\,\text{even}. \end{cases} \tag{A6}$$

Performing the integral over the angular coordinates $f_n = \frac{1}{4\pi}\int_{\mathcal{S}_2} I_n d\Omega$ again uses that $\int_{\mathcal{S}_2}(\mathbf{J}\cdot\mathbf{n})^{2n-2k}d\Omega$ is proportional to the identity operator, such that, for all states isotropic to order $n-1$,

$$f_n = \frac{1}{n!^2}\frac{1}{4\pi}\int_{\mathcal{S}_2}\left\langle J_{\mathbf{n}}^n\right\rangle^2 d\Omega + \text{const}. \tag{A7}$$

Such a quantity is uniquely minimized by states with $\langle J_{\mathbf{n}}^n\rangle = \text{const}$. This proves that a state minimizing the axis-averaged fidelity between itself and a rotated version of itself to every order in rotation angle θ up to and including θ^{2n} is a state that is isotropic to order n. None of this proof relies on a particular group structure and so these results apply to any unitary transformation.

Finally, we prove that all averages over the unit sphere $\mathcal{S}_2$ of the type

$$\overline{\langle J_{\boldsymbol{n}}^k\rangle} = \frac{1}{4\pi}\int_{\mathcal{S}_2}\langle J_{\boldsymbol{n}}^k\rangle\, d\Omega, \tag{A8}$$

are independent of the state. Consider the operator

$$O = \int_{\mathcal{S}_2} J_{\boldsymbol{n}}^k\, d\Omega. \tag{A9}$$

Applying an arbitrary rotation $R \in \mathrm{SU}(2)$, we have

$$ROR^\dagger = \int_{\mathcal{S}_2} RJ_{\boldsymbol{n}}^k R^\dagger\, d\Omega = \int_{\mathcal{S}_2}(RJ_{\boldsymbol{n}}R^\dagger)(RJ_{\boldsymbol{n}}R^\dagger)\cdots(R^\dagger J_{\boldsymbol{n}}R)\, d\Omega = \int_{\mathcal{S}_2} J_{\mathbf{n}'}^k\, d\Omega, \tag{A10}$$

where $J_{\mathbf{n}'}$ is simply the rotated angular momentum operator. Because we are integrating over all directions $\mathbf{n}$, $ROR^\dagger = O$. But the only operator that remains invariant under all rotations is an operator proportional to the identity [82], thus

$$\overline{\langle J_{\boldsymbol{n}}^k\rangle} = \text{const}. \tag{A11}$$

APPENDIX B: SERIES EXPANSION OF THE MAXIMUM LIKELIHOOD ESTIMATOR

We expand the two outcomes probabilities around $\theta = 0$, collecting terms up to $O(\theta^6)$; we obtain

$$\begin{aligned} p(x_+|\theta) &= \cos^2\left(\frac{\phi_+}{2}\right) + \theta\sqrt{\mathfrak{m}_2}\sin\phi_+ - \theta^2\mathfrak{m}_2\cos\phi_+ - \frac{\theta^3\left(3\mathfrak{m}_2^2+\mathfrak{m}_4\right)\sin\phi_+}{6\sqrt{\mathfrak{m}_2}} \\ &\quad + \frac{\theta^4\left[3\mathfrak{m}_2^3(1+\cos\phi_+) - \mathfrak{m}_2\mathfrak{m}_4(3-5\cos\phi_+) + 3\mathfrak{m}_3^2(1-\cos\phi_+)\right]}{24\mathfrak{m}_2} + \frac{\theta^5\left(15\mathfrak{m}_2\mathfrak{m}_4 - 10\mathfrak{m}_3^2 + \mathfrak{m}_6\right)\sin\phi_+}{120\sqrt{\mathfrak{m}_2}} \\ &\quad + O(\theta^6), \\ p(x_-|\theta) &= \sin^2\left(\frac{\phi_+}{2}\right) - \theta\sqrt{\mathfrak{m}_2}\sin\phi_+ + \theta^2\mathfrak{m}_2\cos\phi_+ + \frac{\theta^3\left(3\mathfrak{m}_2^2+\mathfrak{m}_4\right)\sin\phi_+}{6\sqrt{\mathfrak{m}_2}} \\ &\quad + \frac{\theta^4\left[3\mathfrak{m}_2^3(1-\cos\phi_+) - \mathfrak{m}_2\mathfrak{m}_4\,(3+5\cos\phi_+) + 3\mathfrak{m}_3^2(1+\cos\phi_+)\right]}{24\mathfrak{m}_2} - \frac{\theta^5(15\mathfrak{m}_2\mathfrak{m}_4 - 10\mathfrak{m}_3^2 + \mathfrak{m}_6)\sin\phi_+}{120\sqrt{\mathfrak{m}_2}} \\ &\quad + O(\theta^6). \end{aligned} \tag{B1}$$

1. First POVM extension

We now focus on the first POVM extension, in which only two outcomes are possible. Their probabilities are $p(x_+|\theta)$ and $p(x_2|\theta) = 1 - p(x_+|\theta)$. The MLE is obtained by using (4.9). We introduce the shorthand $\delta_+ \equiv \nu_+ - \nu/2$ and note that $\nu_2 = \nu - \nu_+$. Fixing $\phi_+ = -\pi/2$, as determined earlier by the minimization of $\Gamma(0)$, we then obtain:

$$\begin{aligned}
&\frac{\nu_+}{p(x_+|\theta)}\frac{dp(x_+|\theta)}{d\,\theta} + \frac{\nu_2}{p(x_2|\theta)}\frac{dp(x_2|\theta)}{d\,\theta} \\
&= -4\delta_+\sqrt{\mathrm{m}_2} - 4\mathrm{m}_2\nu\,\theta + \frac{2\delta_+\left(\mathrm{m}_4 - 5\mathrm{m}_2^2\right)}{\sqrt{\mathrm{m}_2}}\theta^2 + \left[2\mathrm{m}_2^2(\delta_+ - 4\nu) + \frac{2\mathrm{m}_3^2\delta_+}{\mathrm{m}_2} + \frac{2}{3}\mathrm{m}_4(4\nu - 3\delta_+)\right]\theta^3 \\
&\quad + \frac{\left[5\mathrm{m}_2\mathrm{m}_4(13\delta_+ - 3\nu) + 3\mathrm{m}_2^3(5\nu - 48\delta_+) + 5\mathrm{m}_3^2(2\delta_+ + 3\nu) - \mathrm{m}_6\delta_+\right]}{6\sqrt{\mathrm{m}_2}}\theta^4 \\
&\quad + \frac{\left\{\mathrm{m}_2^4(360\delta_+ - 570\nu) + 15\mathrm{m}_2^2\mathrm{m}_4(22\nu - 25\delta_+) + \mathrm{m}_2\left[10\mathrm{m}_3^2(37\delta_+ + 6\nu) - 15\mathrm{m}_3\mathrm{m}_5\delta_+ + 10\mathrm{m}_4^2(\delta_+ - \nu) + \mathrm{m}_6(5\delta_+ - 6\nu)\right]\right\}}{30\mathrm{m}_2}\theta^5 \\
&\quad + O(\theta^6).
\end{aligned} \tag{B2}$$

Formally, this can be written as

$$0 = a_0 + a_1\theta_{\mathrm{MLE}} + a_2\theta_{\mathrm{MLE}}^2 + a_3\theta_{\mathrm{MLE}}^3 + a_4\theta_{\mathrm{MLE}}^4 + a_5\theta_{\mathrm{MLE}}^5 + O\left(\theta_{\mathrm{MLE}}^6\right), \tag{B3}$$

and applying the Lagrange-Bürmann inversion formula [64,65] provides an explicit power-series expansion for θ_{MLE}. Squaring this series yields θ_{MLE}^2,

$$\theta_{\mathrm{MLE}}^2 = \frac{a_0^2}{a_1^2} + \frac{2a_0^3a_2}{a_1^4} + \frac{a_0^4\left(5a_2^2 - 2a_1a_3\right)}{a_1^6} + \frac{2a_0^5\left(7a_2^3 - 6a_1a_2a_3 + a_1^2a_4\right)}{a_1^8} + \frac{a_0^6\left(42a_2^4 - 56a_1a_2^2a_3 + 14a_1^2a_2a_4 + 7a_1^2a_3^2 - 2a_1^3a_5\right)}{a_1^{10}}. \tag{B4}$$

Identifying terms this yields

$$\theta_{\mathrm{MLE}}^2(\mathbf{x}) = \frac{\delta_+^2}{\mathrm{m}_2\nu^2} + \frac{\delta_+^4\left(3\mathrm{m}_2^2 + \mathrm{m}_4\right)}{3\mathrm{m}_2^3\nu^4} - \frac{\delta_+^5\left(\mathrm{m}_2^3 - \mathrm{m}_2\mathrm{m}_4 + \mathrm{m}_3^2\right)}{4\mathrm{m}_2^4\nu^5} + \frac{\delta_+^6\left[315\mathrm{m}_2^4 + 165\mathrm{m}_2^2\mathrm{m}_4 + \mathrm{m}_2\left(30\mathrm{m}_3^2 - 3\mathrm{m}_6\right) + 35\mathrm{m}_4^2\right]}{180\mathrm{m}_2^5\nu^6}. \tag{B5}$$

Because δ_+ follows a centered binomial distribution (i.e., a fair-coin distribution), its even moments are $\langle\delta_+^2\rangle = \nu/4$, $\langle\delta_+^4\rangle = \nu(3\nu - 2)/16$, and $\langle\delta_+^6\rangle = [15(\nu - 2)\nu + 16]/64$, while all odd moments vanish. Substituting these averages and retaining terms up to $O(1/\nu^3)$ we obtain

$$\left\langle\hat{\theta}_{\mathrm{MLE}}^2(\mathbf{x})\right\rangle = \frac{1}{4\mathrm{m}_2\nu} + \frac{3\mathrm{m}_2^2 + \mathrm{m}_4}{16\mathrm{m}_2^3\nu^2} + \frac{219\mathrm{m}_2^4 + 133\mathrm{m}_2^2\mathrm{m}_4 + \mathrm{m}_2\left(30\mathrm{m}_3^2 - 3\mathrm{m}_6\right) + 35\mathrm{m}_4^2}{768\mathrm{m}_2^5\nu^3} + O(1/\nu^4). \tag{B6}$$

To reach this expression we require the series for θ_{MLE} up to fifth order and the $1/\nu$ expansion up to sixth order; higher-order terms do not contribute. Because the estimator is still biased, a positive $1/\nu^2$ term arising from the derivative of the bias survives, highlighting the advantage of employing the bias-corrected estimator.

To obtain the MSE of the bias-corrected estimator we expand $b(\hat{\theta}) = b(0) + a_1\hat{\theta} + a_2\hat{\theta}^2 + a_3\hat{\theta}^3$ in $\langle(\hat{\theta}(\mathbf{x}) - b(\hat{\theta})/\nu)^2\rangle$. Since $b(0) = 0$ for $\phi_+ = -\pi/2$ we obtain

$$\langle\hat{\theta}^2(\mathbf{x})\rangle\left(1 + \frac{a_1^2}{\nu^2} - \frac{2a_1}{\nu}\right) + \langle\hat{\theta}^3(\mathbf{x})\rangle\left(\frac{2a_1a_2}{\nu^2} - \frac{2a_2}{\nu}\right) + \langle\hat{\theta}^4(\mathbf{x})\rangle\left(\frac{a_2^2}{\nu^2} + \frac{2a_1a_3}{\nu^2} - \frac{2a_3}{\nu}\right) + \langle\hat{\theta}^5(\mathbf{x})\rangle\frac{2a_2a_3}{\nu^2} + \langle\hat{\theta}^6(\mathbf{x})\rangle\frac{a_3^2}{\nu^2}. \tag{B7}$$

While the intermediate algebra is omitted here, the same expansion technique used for $\langle\hat{\theta}^2(\mathbf{x})\rangle$ can be repeated to obtain $\langle\hat{\theta}^3(\mathbf{x})\rangle$, $\langle\hat{\theta}^4(\mathbf{x})\rangle$, and higher moments,

$$\left\langle\hat{\theta}_{\mathrm{MLE}}^3(\mathbf{x})\right\rangle = \frac{45\left(\mathrm{m}_2^3 + \mathrm{m}_3^2 - \mathrm{m}_2\mathrm{m}_4\right)}{512\,\mathrm{m}_2^{9/2}\,\nu^3} + O(1/\nu^4); \quad \left\langle\hat{\theta}_{\mathrm{MLE}}^4(\mathbf{x})\right\rangle = \frac{3}{16\,\mathrm{m}_2^2\,\nu^2} + O(1/\nu^3). \tag{B8}$$

Thus, the only contributions that remain at $O(1/\nu^3)$ are

$$\langle(\hat{\theta}_{\mathrm{MLE}}^*(\mathbf{x}))^2\rangle = \left\langle\hat{\theta}_{\mathrm{MLE}}^2(\mathbf{x})\right\rangle\left(1 - \frac{2a_1}{\nu} + \frac{a_1^2}{\nu^2}\right) - \left\langle\hat{\theta}_{\mathrm{MLE}}^4(\mathbf{x})\right\rangle\frac{2a_3}{\nu}. \tag{B9}$$

The $2a_1/\nu$ term cancels the contribution from the bias derivative at $O(1/\nu^2)$. The bias is given by

$$b(\theta) = \frac{1}{8}\left(3 + \frac{\mathrm{m}_4}{\mathrm{m}_2^2}\right)\theta + \frac{3\left(\mathrm{m}_2^3 + \mathrm{m}_3^2 - \mathrm{m}_2\mathrm{m}_4\right)}{16\mathrm{m}_2^{5/2}}\theta^2 + \frac{\left(9\mathrm{m}_2^4 + 15\mathrm{m}_2^2\mathrm{m}_4 + \mathrm{m}_2\left(10\mathrm{m}_3^2 - \mathrm{m}_6\right) + 9\mathrm{m}_4^2\right)}{48\mathrm{m}_2^3}\theta^3 + O(\theta^4). \tag{B10}$$

Inserting these results reproduces Eq. (4.14).

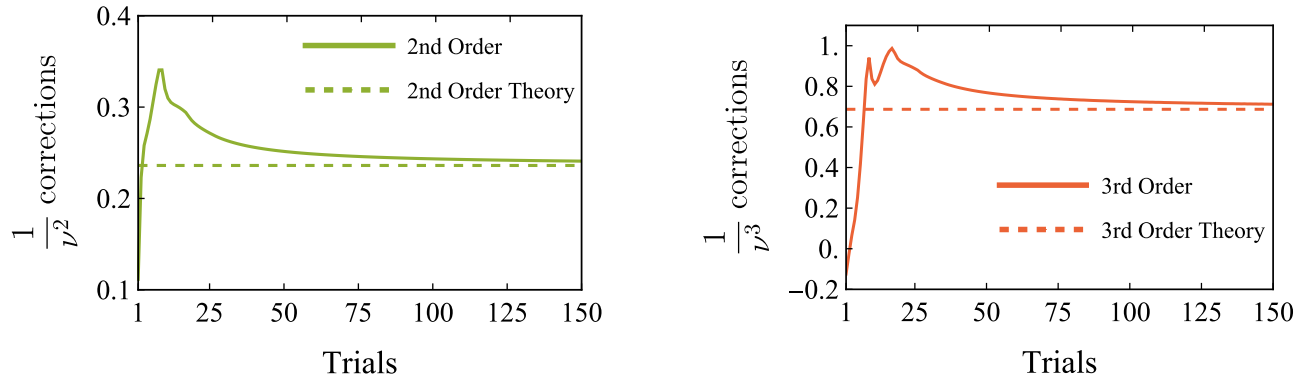

FIG. 8. Numerical validation of the asymptotic coefficients for the first POVM extension, using the uncorrected MLE. The quantum state is that employed in the main text.

For completeness, we present the general ϕ_+-dependent expressions, valid at finite θ, for all quantities entering Eq. (4.2),

$$\begin{aligned}\Gamma(\theta) &= \frac{\cot^2\phi_+}{8\mathrm{m}_2} + \theta\frac{\cot\phi_+\left[\mathrm{m}_2^2\csc^2\phi_+(\cos 2\phi_+ + 7) + 2\mathrm{m}_4\right]}{16\mathrm{m}_2^{5/2}} + O(\theta^2),\\ b(\theta) &= \frac{\cot\phi_+}{4\sqrt{\mathrm{m}_2}} + \frac{\theta}{8}\left(\frac{\mathrm{m}_4}{\mathrm{m}_2^2} + 4\csc^2\phi_+ - 1\right) + O(\theta^2),\\ \frac{1}{\mathsf{F}_x(\theta)} &= \frac{1}{4\mathrm{m}_2} + \frac{\theta^2}{4}\left(\frac{\mathrm{m}_4}{\mathrm{m}_2^2} - 1\right) + O(\theta^3).\end{aligned} \tag{B11}$$

2. Second POVM extension

For the second POVM extension, the use of Eq. (4.2) produces incorrect second-order terms, so we derive them explicitly. Because ϕ_+ is no longer fixed, we redefine $\delta_+ \equiv \nu_+ - \nu\cos^2(\phi_+/2)$. Following the same steps as before, but after inserting the series into Eq. (B4) we expand in powers of $1/\nu$ to remove δ_+ from the denominators. This procedure yields

$$\theta^2_{\mathrm{MLE}}(\mathbf{x}) = \frac{\delta_+^2\csc^2(\phi_+)}{\mathrm{m}_2\nu^2} + \frac{2\delta_+^3\cot(\phi_+)\csc^3(\phi_+)}{\mathrm{m}_2\nu^3} + \frac{\delta_+^4\csc^4(\phi_+)\left\{3\mathrm{m}_2^3[7\cos(2\phi_+)+13]\csc^2(\phi_+) - 2\mathrm{m}_4\mathrm{m}_2 + 6\mathrm{m}_3^2\right\}}{12\mathrm{m}_2^4\nu^4}. \tag{B12}$$

To evaluate the MSE we require the series for θ_{MLE} and the $1/\nu$ expansion only up to fourth order; higher orders leave the result unchanged. The central moments are $\langle\delta_+^2\rangle = \frac{\nu}{4}\sin^2\phi_+$, $\langle\delta_+^3\rangle = -\frac{\nu}{4}\sin^2\phi_+\cos\phi_+$, and $\langle\delta_+^4\rangle = \frac{\nu}{32}\sin^2\phi_+\,[\,3(\nu-2)\cos(2\phi_+) - 3\nu - 2\,]$. Substituting these moments and keeping terms through $O(1/\nu^2)$ reproduces Eq. (4.15).

For completeness, Eq. (4.15) at the optimal setting $\phi_+ = -\pi/2$ reads

$$\mathrm{MSE}[\hat{\theta}_{\mathrm{MLE}}(\mathbf{x})]_{\theta=0} = \frac{1}{4\mathrm{m}_2\nu} + \frac{9\mathrm{m}_2^3 - \mathrm{m}_2\mathrm{m}_4 + 3\mathrm{m}_3^2}{32\mathrm{m}_2^4\nu^2} + O(1/\nu^3). \tag{B13}$$

Proceeding in the same fashion one can derive the $O(1/\nu^3)$ corrections, although the resulting expression is rather cumbersome. Their evaluation requires carrying the series for both θ_{MLE} and the $1/\nu$ expansion to sixth order:

$$\frac{1}{4\mathrm{m}_2\nu} + \frac{9\mathrm{m}_2^3 - \mathrm{m}_2\mathrm{m}_4 + 3\mathrm{m}_3^2}{32\mathrm{m}_2^4\nu^2} + \frac{1719\mathrm{m}_2^6 - 116\mathrm{m}_2^4\mathrm{m}_4 + 6\mathrm{m}_2^3\left(223\mathrm{m}_3^2 + 3\mathrm{m}_6\right) - 5\mathrm{m}_2^2\left(17\mathrm{m}_4^2 + 18\mathrm{m}_3\mathrm{m}_5\right) - 30\mathrm{m}_2\mathrm{m}_3^2\mathrm{m}_4 + 315\mathrm{m}_3^4}{3072\mathrm{m}_2^7\nu^3}$$
$$+ O\left(\frac{1}{\nu^4}\right). \tag{B14}$$

Finally, we reproduce the erroneous second-order expression obtained by applying Eq. (4.2),

$$\Gamma(0) + \frac{2b'(0)}{\mathsf{F}_x(0)} + b(0)^2 = \frac{\mathrm{m}_2^2\csc^2(\phi_+)(2\cos(2\phi_+)+5) + \mathrm{m}_4}{16\mathrm{m}_2^3}. \tag{B15}$$

3. Numerically testing the coefficients of the asymptotic expansions

To validate the expansion coefficients for the first POVM extension, Fig. 8 shows the numerical evaluation of the quantities,

$$\nu^2\left(\langle\hat{\theta}^2(\mathbf{x})\rangle - \frac{1}{\mathrm{m}_2\nu}\right); \quad \nu\left[\nu^2\left(\langle\hat{\theta}^2(\mathbf{x})\rangle - \frac{1}{\mathrm{m}_2\nu}\right) - \frac{3\mathrm{m}_2^2 + \mathrm{m}_4}{16\mathrm{m}_2^3}\right]. \tag{B16}$$

The numerics converge to the analytical predictions, confirming the correctness of the series coefficients.

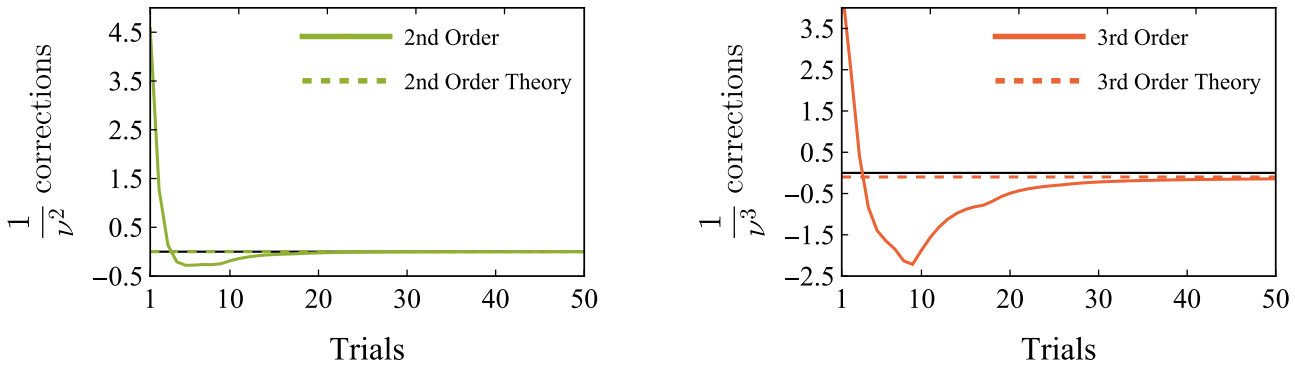

FIG. 9. Numerical validation of the asymptotic coefficients for the bias-corrected MLE in the first POVM extension. The quantum state is that employed in the main text.

Figure 9 repeats the numerical test for the bias-corrected estimator. As predicted, the second-order term vanishes, leaving the third-order correction as the leading contribution. The same verification for the second POVM extension is presented in Fig. 10.

APPENDIX C: PROOF OF THE QUANTUM BHATTACHARYYA BOUND

Let $\{|\omega_{\mathbf{x}}\rangle\}$ be a list of arbitrary states, $\{a_{\mathbf{x}}\}$ a list of arbitrary constants, and $\{\Pi, \hat{\boldsymbol{\theta}}(\mathbf{x})\} = \{\Pi_{\mathbf{x}}, \hat{\theta}_i(\mathbf{x})\}$ a POVM and a set of estimators for the different parameters. By expanding

$$\sum_{\mathbf{x}} \left[\langle \omega_{\mathbf{x}} | a_{\mathbf{x}}^* - \left(\sum_{\mathbf{x}'} \langle \omega_{\mathbf{x}'} | a_{\mathbf{x}'}^* \Pi_{\mathbf{x}'} \right) \right] \Pi_{\mathbf{x}} \left[a_{\mathbf{x}} | \omega_{\mathbf{x}} \rangle - \left(\sum_{\mathbf{x}'} a_{\mathbf{x}'} \Pi_{\mathbf{x}'} | \omega_{\mathbf{x}'} \rangle \right) \right] \geqslant 0 \tag{C1}$$

and using $\sum_{\mathbf{x}} \Pi_{\mathbf{x}} = \mathbb{1}$ we arrive at

$$\Pi_{\mathbf{x}} \delta_{\mathbf{x}\mathbf{x}'} - \Pi_{\mathbf{x}} \Pi_{\mathbf{x}'} \geqslant 0, \tag{C2}$$

with no summation over the index $\mathbf{x}$ implied. This matrix of operators should be understood as an operator acting on the tensor product space $\mathcal{H} \otimes \mathbb{C}^n$, where $\mathcal{H}$ is the Hilbert space in which the states exist and n is the number of elements in the POVM [78], that is, it acts on vectors of kets. More precisely, it would be written as

$$\sum_{\mathbf{x}\mathbf{x}'} \Pi_{\mathbf{x}} \delta_{\mathbf{x}\mathbf{x}'} \otimes |\mathbf{x}\rangle\langle\mathbf{x}'| - \Pi_{\mathbf{x}} \Pi_{\mathbf{x}'} \otimes |\mathbf{x}\rangle\langle\mathbf{x}'| \geqslant 0, \tag{C3}$$

where $|\mathbf{x}\rangle$ is an orthonormal basis of $\mathbb{C}^n$. We now act on the right with $\mathbb{1} \otimes \Delta\hat{\theta}_i(\mathbf{x})$, and on the left with its conjugate transpose. We do the same with $\sqrt{\varrho^{(\nu)}} \otimes \mathbb{1}$. This preserves the positive-definiteness of the operators and the inequality. With that we

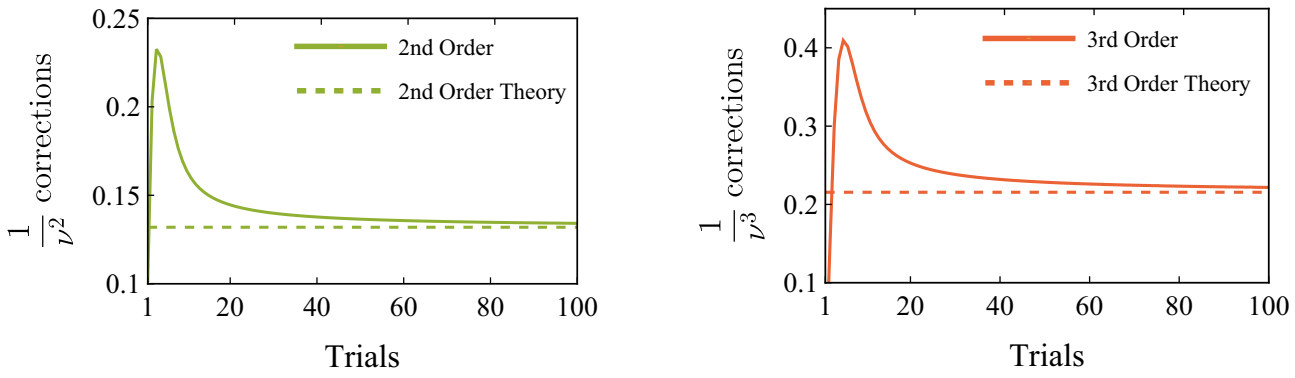

FIG. 10. Numerical validation of the asymptotic coefficients for the second POVM extension. The quantum state is that employed in the main text.

arrive at

$$\sum_{\mathbf{x}} \Delta\hat{\theta}_i(\mathbf{x})\Delta\hat{\theta}_j(\mathbf{x})\sqrt{\varrho^{(\nu)}}\Pi_{\mathbf{x}}\sqrt{\varrho^{(\nu)}} \geqslant \sum_{\mathbf{x},\mathbf{x}'} \Delta\hat{\theta}_i(\mathbf{x})\Delta\hat{\theta}_j(\mathbf{x}')\sqrt{\varrho^{(\nu)}}\Pi_{\mathbf{x}}\Pi_{\mathbf{x}'}\sqrt{\varrho^{(\nu)}}. \tag{C4}$$

We now take the partial trace with the respect to $\mathcal{H}$ and get

$$\mathrm{Cov}[\hat{\boldsymbol{\theta}}(\mathbf{x}), \Pi]_{ij} = \sum_{\mathbf{x}} \Delta\hat{\theta}_i(\mathbf{x})\Delta\hat{\theta}_j(\mathbf{x})\,\mathrm{Tr}(\Pi_{\mathbf{x}}\varrho^{(\nu)}) \geqslant \sum_{\mathbf{x},\mathbf{x}'} \Delta\hat{\theta}_i(\mathbf{x})\Delta\hat{\theta}_j(\mathbf{x}')\,\mathrm{Tr}(\varrho^{(\nu)}\Pi_{\mathbf{x}}\Pi_{\mathbf{x}'}) = \mathrm{Tr}(\varrho^{(\nu)}\Delta X_i\Delta X_j), \tag{C5}$$

where we define the estimator operators $X_i = \sum_{\mathbf{x}} \hat{\theta}_i(\mathbf{x})\Pi_{\mathbf{x}}$ and $\Delta X_i = X_i - \langle\hat{\theta}_i(\mathbf{x})\rangle = \sum_{\mathbf{x}} \Delta\hat{\theta}_i(\mathbf{x})\Pi_{\mathbf{x}}$.

At this point, we may proceed in two ways, depending on whether we want to obtain the symmetric version or the nonsymmetric version of the quantum bounds. First, we show the symmetric version. For that we notice that if we have two matrices such that $A \geqslant B$, then it implies that $\bar{A} \geqslant \bar{B}$, where the bar denotes the complex conjugate. This allows us to write

$$\mathrm{Cov}[\hat{\boldsymbol{\theta}}(\mathbf{x}), \Pi]_{ij} \geqslant \tfrac{1}{2}\,\mathrm{Tr}[\varrho^{(\nu)}(\Delta X_i\Delta X_j + \Delta X_j\Delta X_i)]. \tag{C6}$$

We proceed as in the classical case, defining the operators $Y_i = \Delta X_i - A_{im}L_m$, where L_m are now operators and A_{im} is a real matrix as before. We can build the following positive semidefinite matrix:

$$\mathrm{Tr}[\varrho^{(\nu)}(Y_iY_j^\dagger + Y_jY_i^\dagger)] \geqslant 0, \tag{C7}$$

and substituting

$$\begin{aligned}\frac{1}{2}\,\mathrm{Tr}[\varrho^{(\nu)}(\Delta X_i\Delta X_j + \Delta X_j\Delta X_i)] \geqslant{}& \frac{A_{im}}{2}\,\mathrm{Tr}[\varrho^{(\nu)}(L_m\Delta X_j + \Delta X_jL_m^\dagger)] + \frac{A_{jp}}{2}\,\mathrm{Tr}[\varrho^{(\nu)}(\Delta X_iL_p^\dagger + L_p\Delta X_i)]\\ &- \frac{A_{im}}{2}\,\mathrm{Tr}[\varrho^{(\nu)}(L_mL_p^\dagger + L_pL_m^\dagger)] = (AT^\top + TA^\top - AQA^\top)_{ij},\end{aligned} \tag{C8}$$

where

$$T_{ij} = \tfrac{1}{2}\,\mathrm{Tr}[\varrho^{(\nu)}(\Delta X_iL_j^\dagger + L_j\Delta X_i)], \quad Q_{ij} = \tfrac{1}{2}\,\mathrm{Tr}[\varrho^{(\nu)}(L_iL_j^\dagger + L_jL_i^\dagger)]. \tag{C9}$$

Thanks to symmetrization, everything is real. We find the optimum A as in the classical case by differentiating the trace with respect to A to find the value of A that minimizes it; the result is

$$\mathrm{Cov}[\hat{\boldsymbol{\theta}}(\mathbf{x}), \Pi] \geqslant TQ^{-1}T^\top. \tag{C10}$$

We can add the bias to get the MSE,

$$\mathrm{MSE}[\hat{\boldsymbol{\theta}}(\mathbf{x}), \Pi] \geqslant TQ^{-1}T^\top + \langle\delta\hat{\theta}\rangle\langle\delta\hat{\theta}\rangle^\top. \tag{C11}$$

To derive the nonsymmetric version, we proceed without symmetrizing and do not assume A to be real, arriving at

$$\mathrm{Tr}(\varrho^{(\nu)}\Delta X_i\Delta X_j) \geqslant A_{im}\,\mathrm{Tr}(\varrho^{(\nu)}L_m\Delta X_j) + \mathrm{Tr}(\varrho^{(\nu)}\Delta X_iL_m^\dagger)A_{jm}^* - A_{il}\,\mathrm{Tr}(\varrho^{(\nu)}L_lL_m^\dagger)A_{jm}^* = (AT^\dagger + TA^\dagger - AGA^\dagger)_{ij}, \tag{C12}$$

where now

$$T_{ij} = \mathrm{Tr}(\varrho^{(\nu)}\Delta X_iL_j^\dagger), \quad Q_{ij} = \mathrm{Tr}(\varrho^{(\nu)}L_iL_j^\dagger). \tag{C13}$$

Now, we simply set $A = TQ^{-1}$. We can also assume T to be real. This will in general be the case, as T will have the same value as in the classical version by choosing the L_i appropriately. As in the symmetric case, we get

$$\mathrm{Cov}\big[\hat{\boldsymbol{\theta}}(x), \Pi\big] \geqslant TQ^{-1}T^\top. \tag{C14}$$

Notice that, in general, Q is a complex matrix.

Next, we focus on the symmetric version. Equation (C11) provides a bound for the MSE, but what is its relationship to the CBB or, more generally, to other classical bounds derived from Eq. (5.6)? The key observation is that T takes the same values as in the classical case, provided that the L_i are chosen appropriately. For the QBB, the L_i we select are the higher-order SLDs (5.14). This yields:

$$T_j \equiv T_{1j} = \mathrm{Tr}\left[\left(\frac{d^j}{d\theta^j}\varrho_\theta^{(\nu)}\right)\Delta X\right] = \frac{d^j}{d\theta^j}\langle\hat{\theta}(\mathbf{x})\rangle - \langle\hat{\theta}(\mathbf{x})\rangle\frac{d^j}{d\theta^j}\,\mathrm{Tr}\left(\varrho_\theta^{(\nu)}\right) = \frac{d^j}{d\theta^j}\langle\hat{\theta}(\mathbf{x})\rangle, \tag{C15}$$

which coincides with the T of the CBB. We have omitted the subscript in ΔX_1 since we only have one parameter. Knowing this, since the QBB applies to any POVM, it must be true that

$$\mathrm{Cov}[\hat{\boldsymbol{\theta}}(\mathbf{x}), \Pi] \geqslant TC^{-1}T^\top \geqslant TQ^{-1}T^\top. \tag{C16}$$

Adding the bias, we obtain the version for the MSE

$$\mathrm{MSE}[\hat{\boldsymbol{\theta}}(\mathbf{x}),\Pi] \geqslant TC^{-1}T^{\top} + \langle\delta\hat{\theta}\rangle\langle\delta\hat{\theta}\rangle^{\top} \geqslant TQ^{-1}T^{\top} + \langle\delta\hat{\theta}\rangle\langle\delta\hat{\theta}\rangle^{\top}. \tag{C17}$$

This can be generalized to different classical bounds, for example, choosing $L_i = (\varrho_\theta^{(\nu)})^{-1}\varrho_{\theta_i}^{(\nu)} - \mathbb{1}$ gives the quantum version of the Barankin bound [25]. In the same way, choosing L_i as the SLD for the parameter θ_i we obtain the multiparameter QCRB [72].

The first inequality, Eq. (C2) can be saturated using projective measurements, since in that case $\Pi_{\mathbf{x}}\Pi_{\mathbf{x}'} = \Pi_{\mathbf{x}}\delta_{\mathbf{x}\mathbf{x}'}$. The second inequality, Eq. (C7), is saturated when $Y = 0$; that is, $X = \langle\hat{\theta}(\mathbf{x})\rangle + A_m L_m = \langle\hat{\theta}(\mathbf{x})\rangle + T_k(Q^{-1})_{km}L_m$ (we define $A_{1m} \equiv A_m$ as it is a single parameter). What we do then is to define the POVM Π as the eigenvectors of this operator, and also define a new estimator $\hat{\theta}(x)$ as its eigenvalues. In this way, X saturates the inequality.

APPENDIX D: SCALING OF Q

The derivation of the asymptotic CBB in Eq. (5.10) assumed the scaling relations in Eq. (5.9). We seek to verify whether the scaling of the matrix elements Q_{ij}, matches that of their classical counterparts, C_{ij}.

We begin by analyzing the element Q_{11}, which is well known to scale linearly with the number of trials ν; i.e., $Q_{11} = \nu q_{11}$. This linear dependence arises because the SLD for ν trials, $L_1^{(\nu)}$, acting on the state $\varrho_\theta^{(\nu)}$, is simply the sum of the individual SLDs, L_1. For example, in the case of $\nu = 2$, the derivative of the composite state is given by

$$\partial_\theta\varrho^{(2)} = \partial_\theta\varrho\otimes\mathbb{1} + \mathbb{1}\otimes\partial_\theta\varrho, \tag{D1}$$

and the SLD is given by $L_1^{(2)} = L_1\otimes\mathbb{1} + \mathbb{1}\otimes L_1$. This linear scaling also extends to the off-diagonal elements Q_{1i}. To prove this, let us examine the element Q_{12} for the $\nu = 2$ case, which is given by

$$Q_{12} = \mathrm{Tr}\left[L_1^{(2)}\partial_\theta^2\varrho\right] = \mathrm{Tr}(L_1\otimes\mathbb{1} + \mathbb{1}\otimes L_1)\left(\partial_\theta^2\varrho\otimes\varrho + 2\partial_\theta\varrho\otimes\partial_\theta\varrho + \varrho\otimes\partial_\theta\varrho^2\right). \tag{D2}$$

By invoking the identity $\mathrm{Tr}(\partial_\theta^i\varrho) = 0$ for any integer $i \geqslant 1$, we find that the only terms contributing to the trace are

$$\mathrm{Tr}\left(L_1\partial_\theta^2\varrho\otimes\varrho + \varrho\otimes L_1\partial_\theta^2\varrho\right) = 2q_{12}. \tag{D3}$$

This can be extended to the general case of ν trials, as each of the ν terms composing $L_1^{(\nu)}$ contributes a single q_{1i} to the final trace, confirming the linear scaling $Q_{1i} = \nu q_{1i}$.

The analysis for the Q_{22} term is more involved. Its classical counterpart exhibits a more complex scaling, given by $C_{22} = \nu c_{22} + 2\nu(\nu-1)c_{11}^2$. To determine if Q_{22} follows a similar pattern, we first consider the $\nu = 2$ case, for which we must construct the operator $L_2^{(2)}$ satisfying

$$\tfrac{1}{2}\left[L_2^{(2)}\varrho\otimes\varrho + \varrho\otimes\varrho\, L_2^{(2)}\right] = \left(\partial_\theta^2\varrho\otimes\varrho + 2\partial_\theta\varrho\otimes\partial_\theta\varrho + \varrho\otimes\partial_\theta\varrho^2\right). \tag{D4}$$

The terms $\partial_\theta^2\varrho\otimes\varrho$ and $\varrho\otimes\partial_\theta^2\varrho$ are generated by including the operators $L_2\otimes\mathbb{1}$ and $\mathbb{1}\otimes L_2$ in the construction of $L_2^{(2)}$. The contribution of these components to the QFI element Q_{22} is thus given by

$$\mathrm{Tr}(L_2\otimes\mathbb{1} + \mathbb{1}\otimes L_2)\left(\partial_\theta^2\varrho\otimes\varrho + 2\partial_\theta\varrho\otimes\partial_\theta\varrho + \varrho\otimes\partial_\theta\varrho^2\right). \tag{D5}$$

The only nonzero terms are as follows:

$$\mathrm{Tr}\left(L_2\partial_\theta^2\varrho\otimes\varrho + \varrho\otimes L_2\partial_\theta^2\varrho\right) = 2q_{22}. \tag{D6}$$

This contribution provides the linear scaling component, analogous to the νc_{22} term in the classical case. The quadratic scaling component must therefore arise from the remaining term, $2\partial_\theta\varrho\otimes\partial_\theta\varrho$. By expressing $\partial_\theta\varrho$ in terms of the SLD L_1, this term expands as follows:

$$2\partial_\theta\varrho\otimes\partial_\theta\varrho = \tfrac{1}{2}(L_1\varrho\otimes L_1\varrho + L_1\varrho\otimes\varrho L_1 + \varrho L_1\otimes\varrho L_1 + \varrho L_1\otimes L_1\varrho). \tag{D7}$$

The terms $\frac{1}{2}(L_1\varrho\otimes L_1\varrho + \varrho L_1\otimes\varrho L_1)$ can be generated by an $L_1\otimes L_1$ component in the SLD $L_2^{(2)}$. The contribution of this component to Q_{22} is then given by

$$\mathrm{Tr}(L_1\otimes L_1)\left(\partial_\theta^2\varrho\otimes\varrho + 2\partial_\theta\varrho\otimes\partial_\theta\varrho + \varrho\otimes\partial_\theta^2\varrho\right). \tag{D8}$$

Recalling that $\mathrm{Tr}(L_i\varrho) = 0$ for any i, the only nonvanishing contribution to the trace is as follows:

$$2\,\mathrm{Tr}(L_1\partial_\theta\varrho\otimes L_1\partial_\theta\varrho) = 2q_{11}^2. \tag{D9}$$

However, generating the remaining cross-terms, $L_1\varrho\otimes\varrho L_1 + \varrho L_1\otimes L_1\varrho$, is not straightforward, as they cannot be produced by any simple tensor product of the form $L_i\otimes L_j$. Accounting for these terms would, in principle, require introducing a new operator X into the structure of $L_2^{(2)}$ that satisfies

$$\tfrac{1}{2}(X\varrho\otimes\varrho + \varrho\otimes\varrho X) = \tfrac{1}{2}(L_1\varrho\otimes\varrho L_1 + \varrho L_1\otimes L_1\varrho). \tag{D10}$$

To fully replicate the classical scaling, this new operator would need to yield a contribution of $2q_{11}^2$. However, an explicit demonstration of this result has proven elusive. Given the difficulty of this direct approach, we now turn to an alternative method to validate the asymptotic expressions.

We pursue an alternative approach to show that Eq. (5.10) remains valid to second order under the replacement of c_{ij} with q_{ij}. This method begins by establishing a general inequality between the two quantities. For any list of real constants $\{a_i\}$, it has been shown that [25] that

$$a_i C_{ij} a_j = \left\langle \left(\frac{a_i}{p(x|\theta)} \frac{d^i p(x|\theta)}{d\theta^i} \right)^2 \right\rangle = \sum_k \frac{1}{p(x_k|\theta)} \left[a_i \frac{d^i p(x_k|\theta)}{d\theta^i} \right]^2 = \sum_k \frac{1}{\mathrm{Tr}(\varrho \Pi_k)} \left\{ a_i \,\mathrm{Tr}\left[\frac{1}{2}(L_i \varrho + \varrho L_i)\Pi_k \right] \right\}^2$$
$$\leqslant \sum_k \frac{|\mathrm{Tr}\left[\varrho (a_i L_i)\Pi_k\right]|^2}{\mathrm{Tr}(\varrho \Pi_k)} \leqslant a_i \,\mathrm{Tr}\left[\frac{1}{2}(L_i L_j + L_j L_i)\varrho \right] a_j = a_i Q_{ij} a_j; \tag{D11}$$

that is, $C \preccurlyeq Q$. Notably, this inequality does not guarantee the existence of a single POVM for which equality holds, as the optimal measurement projectors—eigenstates of the operator $a_i L_i$—depend on the specific choice of coefficients a_i. Despite this, the relationship provides a powerful tool for constraining individual matrix elements. By isolating the second-order terms (i.e., setting $a_i = \delta_{i2}$), we find that $C_{22} \leqslant Q_{22}$. Now, in the asymptotic limit $\nu \to \infty$, a measurement that saturates the QFI yields $c_{11} = q_{11}$. For such a measurement, the classical element scales as follows:

$$C_{22} = 2\nu^2 c_{11}^2 = 2\nu^2 q_{11}^2 \leqslant Q_{22}. \tag{D12}$$

Therefore, in the asymptotic limit $\nu \to \infty$, it must hold that $Q_{22} \geqslant 2\nu^2 q_{11}^2$. This lower bound is sufficient to validate the asymptotic expression in Eq. (5.10), since the dominant contribution from the classical term C_{22} to that expression is precisely its leading-order term, $2\nu^2 c_{11}^2$. While this analysis confirms the result to order $O(1/\nu^2)$, a complete determination of higher-order corrections would necessitate a more precise characterization of the scaling for all Q_{ij} elements.

[1] V. Giovannetti, S. Lloyd, and L. Maccone, Quantum metrology, Phys. Rev. Lett. **96**, 010401 (2006).

[2] M. G. A. Paris, Quantum estimation for quantum technology, Int. J. Quantum Inf. **07**, 125 (2009).

[3] V. Giovannetti, S. Lloyd, and L. Maccone, Advances in quantum metrology, Nat. Photon. **5**, 222 (2011).

[4] R. Demkowicz-Dobrzański, M. Jarzyna, and J. Kolodyński, Quantum limits in optical interferometry, Prog. Opt. **60**, 345 (2015).

[5] J. S. Sidhu and P. Kok, Geometric perspective on quantum parameter estimation, AVS Quantum Sci. **2**, 014701 (2020).

[6] F. Albarelli, M. Barbieri, M. G. Genoni, and I. Gianani, A perspective on multiparameter quantum metrology: From theoretical tools to applications in quantum imaging, Phys. Lett. A **384**, 126311 (2020).

[7] E. Polino, M. Valeri, N. Spagnolo, and F. Sciarrino, Photonic quantum metrology, AVS Quantum Sci. **2**, 024703 (2020).

[8] M. Barbieri, Optical quantum metrology, PRX Quantum **3**, 010202 (2022).

[9] A. P. Alodjants, D. V. Tsarev, D. A. Kuts, S. A. Podoshvedov, and S. P. Kulik, Quantum optical metrology, Phys. Usp. **67**, 668 (2024).

[10] G. Casella and R. Berger, *Statistical Inference*, 2nd ed. (Duxbury Thomson Learning, Albany, NY, 2002).

[11] D. Petz and C. Ghinea, Introduction to quantum fisher information, in *Quantum Probability and Related Topics*, Vol. 27 (World Scientific, Singapore, 2011), pp. 261–281.

[12] J. Rubio, P. Knott, and J. Dunningham, Non-asymptotic analysis of quantum metrology protocols beyond the Cramér–Rao bound, J. Phys. Commun. **2**, 015027 (2018).

[13] J. Rubio and J. Dunningham, Quantum metrology in the presence of limited data, New J. Phys. **21**, 043037 (2019).

[14] J. J. Meyer, S. Khatri, D. S. França, J. Eisert, and P. Faist, Quantum metrology in the finite-sample regime, arXiv:2307.06370 [PRX Quantum (to be published)].

[15] W. Salmon, S. Strelchuk, and D. Arvidsson-Shukur, Only classical parameterised states have optimal measurements under least squares loss, Quantum **7**, 998 (2023).

[16] M. Hayashi, Comparison between the Cramér-Rao and the mini-max approaches in quantum channel estimation, Commun. Math. Phys. **304**, 689 (2011).

[17] M. J. W. Hall and H. M. Wiseman, Heisenberg-style bounds for arbitrary estimates of shift parameters including prior information, New J. Phys. **14**, 033040 (2012).

[18] G. Chesi, A. Riccardi, R. Rubboli, L. Maccone, and C. Macchiavello, Protocol for global multiphase estimation, Phys. Rev. A **108**, 012613 (2023).

[19] W. Górecki, R. Demkowicz-Dobrzański, H. M. Wiseman, and D. W. Berry, π-corrected Heisenberg limit, Phys. Rev. Lett. **124**, 030501 (2020).

[20] W. Górecki and R. Demkowicz-Dobrzański, Multiparameter quantum metrology in the Heisenberg limit regime: Many-repetition scenario versus full optimization, Phys. Rev. A **106**, 012424 (2022).

[21] D. G. Chapman and H. Robbins, Minimum variance estimation without regularity assumptions, Ann. Math. Stat. **22**, 581 (1951).

[22] A. Bhattacharyya, On some analogues of the amount of information and their use in statistical estimation, Sankhya: Ind. J. Stat. **8**, 1 (1946).

[23] E. W. Barankin, Locally best unbiased estimates, Ann. Math. Stat. **20**, 477 (1949).

[24] J. S. Abel, A bound on mean-square-estimate error, IEEE Trans. Inf. Theory **39**, 1675 (1993).

[25] M. Gessner and A. Smerzi, Hierarchies of frequentist bounds for quantum metrology: From Cramér-Rao to Barankin, Phys. Rev. Lett. **130**, 260801 (2023).

[26] J. R. Hervas, A. Z. Goldberg, A. S. Sanz, Z. Hradil, J. Řeháček, and L. L. Sánchez-Soto, Beyond the quantum Cramér-Rao bound, Phys. Rev. Lett. **134**, 010804 (2025).

[27] J. K. Ghosh, Higher order asymptotics, in *NSF-CBMS Regional Conference Series in Probability and Statistics* (Institute of Mathematical Statistics, Alexandria, VA, 1994), p. 4153181.

[28] S. Kurdziałek and R. Demkowicz-Dobrzanski, Measurement noise susceptibility in quantum estimation, Phys. Rev. Lett. **130**, 160802 (2023).

[29] P. Kolenderski and R. Demkowicz-Dobrzanski, Optimal state for keeping reference frames aligned and the platonic solids, Phys. Rev. A **78**, 052333 (2008).

[30] G. Björk, A. B. Klimov, P. De La Hoz, M. Grassl, G. Leuchs, and L. L. Sánchez-Soto, Extremal quantum states and their Majorana constellations, Phys. Rev. A **92**, 031801(R) (2015).

[31] D. Baguette, F. Damanet, O. Giraud, and J. Martin, Anticoherence of spin states with point-group symmetries, Phys. Rev. A **92**, 052333 (2015).

[32] A. Z. Goldberg, A. B. Klimov, G. Leuchs, and L. L. Sánchez-Soto, Rotation sensing at the ultimate limit, J. Phys. Photon. **3**, 022008 (2021).

[33] C. W. Helstrom, *Quantum Detection and Estimation Theory* (Academic Press, New York, 1976).

[34] S. M. Kay, *Fundamentals of Statistical Signal Processing* (Prentice-Hall, Englewood Cliffs, NJ, 1993).

[35] H. L. Van Trees, *Detection, Estimation, and Modulation Theory* (Wiley, New York, 2001).

[36] E. L. Lehmann and G. Casella, *Theory of Point Estimation*, 2nd ed. (Springer, New York, 1998).

[37] R. A. Fisher, Theory of statistical estimation, Math. Proc. Cambr. Philos. Soc. **22**, 700 (1925).

[38] J. Shang, H. K. Ng, and B.-G. Englert, Quantum state tomography: Mean squared error matters, bias does not, arXiv:1405.5350 [quant-ph].

[39] I. Chuang and M. Nielsen, *Quantum Computation and Quantum Information* (Cambridge University Press, Cambridge, UK, 2000).

[40] A. S. Holevo, *Probabilistic and Statistical Aspects of Quantum Theory*, Quaderni Monographs No. 1 (Ed. della Normale, Pisa, 2011).

[41] A. Peres, *Quantum Theory: Concepts and Methods* (Kluwer, New York, 2002).

[42] W. K. Wootters, Statistical distance and Hilbert space, Phys. Rev. D **23**, 357 (1981).

[43] D. Bures, An extension of Kakutani's theorem on infinite product measures to the tensor product of semifinite w^*-algebras, Trans. Am. Math. Soc. **135**, 199 (1969).

[44] A. Uhlmann, The "transition probability" in the state space of a *-algebra, Rep. Math. Phys. **9**, 273 (1976).

[45] D. Šafránek, Discontinuities of the quantum Fisher information and the Bures metric, Phys. Rev. A **95**, 052320 (2017).

[46] D. Šafránek, Simple expression for the quantum Fisher information matrix, Phys. Rev. A **97**, 042322 (2018).

[47] J. Liu, M. Zhang, H. Chen, L. Wang, and H. Yuan, Optimal scheme for quantum metrology, Adv. Quantum Tech. **5**, 2100080 (2022).

[48] L. J. Fiderer, J. M. E. Fraïsse, and D. Braun, Maximal quantum Fisher information for mixed states, Phys. Rev. Lett. **123**, 250502 (2019).

[49] J. P. Dowling, Quantum optical metrology—The lowdown on high-N00N states, Contemp. Phys. **49**, 125 (2008).

[50] D. M. Greenberger, M. A. Horne, A. Shimony, and A. Zeilinger, Bell's theorem without inequalities, Am. J. Phys. **58**, 1131 (1990).

[51] E. Serrano-Ensástiga, C. Chryssomalakos, and J. Martin, Quantum metrology of rotations with mixed spin states, Phys. Rev. A **111**, 022435 (2025).

[52] J. Martin, S. Weigert, and O. Giraud, Optimal detection of rotations about unknown axes by coherent and anticoherent states, Quantum **4**, 285 (2020).

[53] J. L. Romero, A. B. Klimov, A. Z. Goldberg, G. Leuchs, and L. L. Sánchez-Soto, Multipoles from Majorana constellations, Phys. Rev. A **109**, 012214 (2024).

[54] C. Chryssomalakos and H. Hernández-Coronado, Optimal quantum rotosensors, Phys. Rev. A **95**, 052125 (2017).

[55] S. Zhou, C.-L. Zou, and L. Jiang, Saturating the quantum Cramér-Rao bound using LOCC, Quantum Sci. Technol. **5**, 025005 (2020).

[56] R. H. Norden, A survey of Maximum Likelihood Estimation, Int. Stat. Rev. **40**, 329 (1972).

[57] A. Papoulis and S. U. Pillai, *Probability, Random Variables, and Stochastic Processes*, 4th ed. (McGraw–Hill, Boston, 2002).

[58] C. R. Rao, Asymptotic efficiency and limiting information, in *Proceedings of the Fourth Berkeley Symposium on Mathematical Statistics and Probability, Volume 1: Contributions to the Theory of Statistics*, Vol. 4 (University of California Press, Los Angeles, 1961), pp. 531–546.

[59] C. R. Rao, Apparent anomalies and irregularities in maximum likelihood estimation (with discussion), Sankhya Ser. A **24**, 73 (1962).

[60] C. R. Rao, Criteria of estimation in large samples, Sankhya Ser. A **25**, 189 (1963).

[61] J. K. Ghosh and K. Subramanyam, Second order efficiency of maximum likelihood estimators, Sankhya Ser. A **36**, 325 (1974).

[62] J. Berkson, Minimum Chi-Square, not maximum likelihood!, Ann. Stat. **8**, 457 (1980).

[63] J. B. S. Haldane and S. M. Smith, The sampling distribution of a maximum-likelihood estimate, Biometrika **43**, 96 (1956).

[64] M. Abramowitz and I. A. Stegun, *Handbook of Mathematical Functions: With Formulas, Graphs and Mathematical Tables* (Dover, New York, 1972).

[65] E. W. Weisstein, Series reversion, https://mathworld.wolfram.com/SeriesReversion.html.

[66] F. Ouimet, General formulas for the central and non-central moments of the multinomial distribution, Stats **4**, 18 (2021).

[67] M. Tsang, Conservative classical and quantum resolution limits for incoherent imaging, J. Mod. Opt. **65**, 1385 (2018).

[68] Y. Ye and X.-M. Lu, Quantum Cramér-Rao bound for quantum statistical models with parameter-dependent rank, Phys. Rev. A **106**, 022429 (2022).

[69] B. Efron, Defining the curvature of a statistical problem (with applications to second order efficiency), Ann. Statist. **3**, 1189 (1975).

[70] Y. Tsuda, Bhattacharyya inequality for quantum state estimation, J. Phys. A: Math. Theor. **40**, 793 (2007).

[71] Y. Tsuda and K. Matsumoto, Quantum estimation for non-differentiable models, J. Phys. A: Math. Gen. **38**, 1593 (2005).

[72] K. R. Parthasarathy, On the philosophy of Cramér-Rao-Bhattacharya Inequalities in quantum statistics, Sankhya A **83**, 521 (2021).

[73] D. C. Brody and L. P. Hughston, Geometry of quantum statistical inference, Phys. Rev. Lett. **77**, 2851 (1996).

[74] D. C. Brody and L. P. Hughston, Generalised Heisenberg relations for quantum statistical estimation, Phys. Lett. A **236**, 257 (1997).

[75] D. C. Brody and L. P. Hughston, Statistical geometry in quantum mechanics, Proc. R. Soc. Lond. A **454**, 2445 (1998).

[76] A. J. Belfield and D. C. Brody, Higher-order uncertainty bounds for mixed states, J. Phys. A: Math. Theor. **54**, 435302 (2021).

[77] L. J. Fiderer, T. Tufarelli, S. Piano, and G. Adesso, General expressions for the quantum Fisher information matrix with applications to discrete quantum imaging, PRX Quantum **2**, 020308 (2021).

[78] L. O. Conlon, J. Suzuki, P. K. Lam, and S. M. Assad, Efficient computation of the Nagaoka-Hayashi bound for multiparameter estimation with separable measurements, npj Quantum Inf. **7**, 110 (2021).

[79] M. Hayashi and Y. Ouyang, Tight Cramér-Rao type bounds for multiparameter quantum metrology through conic programming, Quantum **7**, 1094 (2023).

[80] M. Hayashi and Y. Ouyang, Finding the optimal probe state for multiparameter quantum metrology using conic programming, npj Quantum Inf. **10**, 111 (2024).

[81] L. O. Conlon, J. Suzuki, P. K. Lam, and S. M. Assad, Role of the extended Hilbert space in the attainability of the quantum Cramér–Rao bound for multiparameter estimation, Phys. Lett. A **542**, 130445 (2025).

[82] W.-K. Tung, *Group Theory in Physics* (World Scientific, Singapore, 1985).

2.2 Project 2: Majora constellation and robust states for SU(2) sensing

As introduced in the mathematical preliminaries section, the Majorana representation offers a visual and intuitive description of the states of a spin-S system. In turn, the multipole distribution provides an SU(2)-invariant quantification of the constellation's geometry. The geometry of this constellation is closely related to the metrological properties of the state. In particular, states whose constellation is more uniformly distributed over the sphere prove to be the most suitable for the estimation of arbitrary rotations.

The first paper presented in this chapter delves into the connection between the Majorana representation and the multipole distribution for several paradigmatic states: coherent states, N00N states, and king states. Coherent states, being quasi-classical in nature, serve as a standard benchmark in the evaluation of estimation protocols. Meanwhile, N00N states are optimal for estimating rotations around a fixed axis, whereas king states are optimal when the rotation axis is arbitrary. Among the main results, an analytical expression is derived for the evolution of the multipoles during the transition from a coherent to a N00N state. This analysis reveals that the even-order multipoles remain invariant, while the odd-order multipoles characterize the transition between the two states.

In the second paper, a new family of random states is introduced and characterized, generated by randomly selecting Majorana stars on the surface of a sphere. The properties of these states are exhaustively studied from a numerical perspective, analyzing their multipole distribution, their QFI, the associated precision bound (QCRB), and their resilience to noise, and are compared to those of other random state families. The results demonstrate that these states are remarkably robust to noise and maintain a high performance for rotation estimation. Finally, the feasibility of their implementation and their practical application to rotation estimation was demonstrated experimentally by a collaborating experimental group.

Note: In the experimental part of the collaboration, my contribution was limited to the visualization and representation of the data. The main focus of my work was on the numerical aspects of the first part.

Multipoles from Majorana constellations

J. L. Romero [1], A. B. Klimov [2], A. Z. Goldberg [3,4], G. Leuchs [5,6] and L. L. Sánchez-Soto [1,5]

[1]*Departamento de Óptica, Facultad de Física, Universidad Complutense, 28040 Madrid, Spain*
[2]*Departamento de Física, Universidad de Guadalajara, 44420 Guadalajara, Jalisco, Mexico*
[3]*National Research Council of Canada, Ottawa, Ontario, Canada K1N 5A2*
[4]*Department of Physics, University of Ottawa, Ottawa, Ontario, Canada K1N 6N5*
[5]*Max-Planck-Institut für die Physik des Lichts, 91058 Erlangen, Germany*
[6]*Institut für Optik, Information und Photonik, Friedrich-Alexander-Universität Erlangen-Nürnberg, 91058 Erlangen, Germany*

(Received 22 May 2023; revised 22 September 2023; accepted 2 January 2024; published 22 January 2024)

Majorana stars, the $2S$ spin coherent states that are orthogonal to a spin-S state, offer an elegant method to visualize quantum states, disclosing their intrinsic symmetries. These states are naturally described by the corresponding multipoles. These quantities can be experimentally determined and allow for an SU(2)-invariant analysis. We investigate the relationship between Majorana constellations and state multipoles, thus providing insights into the underlying symmetries of the system. We illustrate our approach with some relevant and informative examples.

DOI: 10.1103/PhysRevA.109.012214

I. INTRODUCTION

Completely symmetric states aptly describe numerous phenomena [1]. These states play a crucial role in the characterization of spinor Bose gases [2,3], whose dynamics have been observed with spin-1 [4,5], spin-2 [6], and even spin-3 [7,8] condensates. They have also been used for the characterization of entanglement [9–14] in those boson systems.

A salient feature of this family is that any state of spin S can be described as a permutation-symmetric n-qubit state, with $n = 2S$. This is the basis of the elegant representation devised by Majorana [15], in which a spin S is depicted by $2S$ points (called the stars) on the Bloch sphere. Although the subject attracted some attention in relation to the quantum theory of angular momentum [16–19], it remained quiescent until 1969, when Penrose reinterpreted Majorana stars as principal null directions in spinor theory [20] and brought it to wider attention in his celebrated book [21].

Apart from indisputable mathematical advantages [22], this picture builds a bridge between the abstract Hilbert space (where the states live) and the simple geometry of the Bloch sphere. Consequently, this representation rapidly meets the increasing interest in high-dimensional quantum systems and, several decades after its conception, is being used in fields as diverse as polarization [23–27], spinor Bose gases [28–31], multiqubit systems [32–38], metrology [39–43], geometric phases [44–51], non-Hermitian lattices [52], and algebraic quantum models such as the Lipkin-Meshkov-Glick model [53,54].

The distribution of Majorana stars conveys complete information and can be directly computed when the quantum state is known. But this notion has far-reaching advantages: by visualizing in a crystal-clear manner the intrinsic symmetries of the state, one can perceive connections with other intriguing questions. Examples include geometrical measures of entanglement [55–57], spherical t-designs [58,59], and the Thomson [60–65] and Tammes [66–68] problems. Moreover, a number of states with remarkable properties, such as queens [69] and kings of quantumness [70], maximally entangled states [71], k-uniform states [72–74], and states with maximal Wehrl entropy [75], can be aptly understood in terms of the properties of their corresponding constellations [76].

Distributing points on a sphere is a mathematical problem with a long history and with a variety of optimal configurations depending on the cost function one tries to optimize [77–80]. This suggests exploring those arrangements of points distinguished by some extremal properties. Then a natural question arises: if one knows the locations of the Majorana stars, what can one say about the state, in particular, about its multipolar distribution? That is precisely our main goal here.

For a system of point charges on the sphere, the most suitable way of capturing the progressively finer angular features of the system is the standard multipolar expansion [81]. Such an expansion can often be truncated, meaning that to a good approximation only the first terms need to be retained. We propose here to carry out a similar procedure for the Majorana constellation: the resulting multipoles constitute a basic tool for problems with an SU(2) invariance [82,83] and, in addition, they can be experimentally determined with simple procedures [84,85].

The paper is organized as follows. In Sec. II we introduce the basic notions needed to understand the Majorana constellations, whereas in Sec. III we show how to calculate the multipoles from a given Majorana constellations. Our

insight is to apply the time-honored Vieta formulas [86] to the polynomial defining the constellation, which provides a shortcut between the stars and other representations of the state. In Sec. IV we thoroughly examine how the method works in a series of relevant examples. Further physical implications are discussed in Sec. V and, finally, our conclusions are summarized in Sec. VI.

II. MAJORANA CONSTELLATIONS

We will deal with any pure system living in a finite-dimensional Hilbert space of dimension $2S+1$, which can be formally regarded as a spin S. The corresponding space $\mathcal{H}_S$, spanned by the standard angular momentum basis $\{|S,m\rangle \mid m=-S,\ldots,S\}$, is the carrier of the irreducible representation (irrep) of spin S of SU(2) and is isomorphic to $\mathbb{C}^{2S+1}$. Since any two vectors in $\mathcal{H}_S$ differing by a phase represent the same physical state, the manifold of physical states is the projective space $\mathbb{C}\mathbf{P}^{2S}$ [87].

The merit of Majorana was to show that points in $\mathbb{C}\mathbf{P}^{2S}$ are in one-to-one correspondence with unordered sets of (possibly coincident) $2S$ points on the unit sphere $\mathcal{S}_2$. There are various ways to see why this is so, but probably the most direct one is in terms of coherent states.

The spin (or Bloch) coherent states live in $\mathcal{H}_S$ and are displaced versions of a fiducial state, much the same as for the canonical coherent states on the plane. This fiducial state is chosen so as to minimize the variance of the Casimir operator $\mathbf{S}^2=S_x^2+S_y^2+S_z^2$, where (S_x,S_y,S_z) are the angular momentum operators, which generate the algebra $\mathfrak{su}(2)$. The minimum-variance states are $|S,\pm S\rangle$ and they guarantee that their displaced versions are the closest to classical states. The displacement operator on $\mathcal{S}_2$ is $D(\theta,\phi)=\exp(i\phi S_z)\exp(i\theta S_y)=\exp[\frac{1}{2}\theta(S_+e^{-i\phi}-S_-e^{i\phi})]$, where $S_\pm=S_x\pm iS_y$ are raising and lowering operators. Disentangling this displacement allows us to express the coherent states $|\theta,\phi\rangle=D(\theta,\phi)|S,-S\rangle$ as [88,89]

$$|\theta,\phi\rangle\equiv|z\rangle=\frac{1}{(1+|z|^2)^S}\exp(zS_+)|S,-S\rangle, \tag{2.1}$$

where the label $z=\tan(\theta/2)e^{-i\phi}$ corresponds to an inverse stereographic projection from the south pole, mapping the point $z\in\mathbb{C}$ onto the point $(\theta,\phi)\in\mathcal{S}_2$ [90].

On expanding the exponential, we can write the coherent states in terms of the basis states of the irrep:

$$|z\rangle=\frac{1}{(1+|z|^2)^S}\sum_{m=-S}^{S}\binom{2S}{S+m}^{\frac{1}{2}}z^{S+m}|S,m\rangle, \tag{2.2}$$

or, employing again the stereographic projection,

$$|z\rangle=\sum_{m=-S}^{S}\binom{2S}{S+m}^{\frac{1}{2}}[\sin(\theta/2)]^{S+m}[\cos(\theta/2)]^{S-m}\times e^{-i(S+m)\phi}|S,m\rangle. \tag{2.3}$$

The system of spin coherent states is complete, but the states are not mutually orthogonal; their overlap is

$$\langle z|z'\rangle=\frac{(1+z^*z')^{2S}}{[(1+|z|^2)(1+|z'|^2)]^S}. \tag{2.4}$$

They allow for a resolution of the unity in the form

$$\int_{\mathbb{C}}d\mu_S(z)\,|z\rangle\langle z|=\mathbb{1}, \tag{2.5}$$

with the invariant measure given by

$$d\mu_S(z)=\frac{2S+1}{\pi}\frac{d^2z}{(1+|z|^2)^2}. \tag{2.6}$$

With this completeness relation one is able to decompose an arbitrary pure state over the coherent states. If we denote $\psi(z^*)=\langle z|\psi\rangle$, by using the basis $\{|S,m\rangle\}$, we define the stellar function $f_\psi(z)$ of the state $|\psi\rangle$ as

$$f_\psi(z)=(1+|z|^2)^S\psi(z)=\sum_{m=-S}^{S}\binom{2S}{S+m}^{\frac{1}{2}}\psi_m\,z^{S+m}=\sum_{k=0}^{2S}\binom{2S}{k}^{\frac{1}{2}}\psi_{k-S}\,z^k, \tag{2.7}$$

with $\psi_m=\langle S,m|\psi\rangle$, and in the second line we have made the relabeling $S+m\mapsto k$. Interestingly, in this representation the wave function is a polynomial in z of order $r\leqslant 2S$. In consequence, the roots $z_k\in\mathbb{C}$ of $f_\psi(z)$ fully characterize the state. These roots define, via an inverse stereographic map, $2S$ points on the unit sphere $\mathcal{S}_2$. This is the Majorana constellation, and each one of these points constitutes one star of the constellation. Note that an SU(2) rotation corresponds to a solid rotation of the constellation; therefore, states with the same constellation, irrespective of their relative orientation, have the same physical properties.

The stellar function is directly related to the Husimi Q function [91,92]:

$$Q_\psi(z)=(1+|z|^2)^{2S}|f_\psi(z^*)|^2, \tag{2.8}$$

which clearly shows that the zeros of the Husimi Q_ψ function are the complex conjugates of the zeros of f_ψ. These can then be observed in the laboratory by measuring where the Husimi function vanishes [93].

Let us examine a few relevant examples to illustrate how these constellations look. The first one is that of a spin coherent state $|z_0\rangle$, whose stellar representation is direct from Eq. (2.4):

$$f_{z_0}(z)=\frac{(1+z_0z)^{2S}}{(1+|z_0|^2)^S} \tag{2.9}$$

so it has a single zero at $z=-1/z_0$ with multiplicity $2S$. In consequence, the constellation collapses in this case to a single point diametrically opposed to the maximum z_0.

Another relevant set of states is that of the so-called NOON states, defined as [94]

$$|\mathrm{NOON}\rangle=\frac{1}{\sqrt{2}}(|S,S\rangle-|S,-S\rangle). \tag{2.10}$$

They are known to have the highest sensitivity for a fixed excitation S to small rotations about the S_z axis [95]. The associated polynomial reads

$$f_{\mathrm{NOON}}(z)=\frac{1}{\sqrt{2}}(z^{2S}-1). \tag{2.11}$$

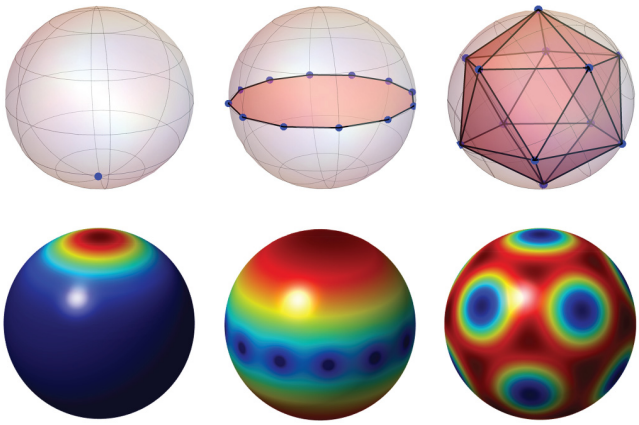

FIG. 1. Top: Majorana constellations for, from left to right, a spin coherent state, a NOON state, and a king of quantumness, all of them for the same dimension with $S = 6$. Bottom: Density plots of the corresponding Husimi functions, with a scale that goes from blue (minimum) to red (maximum).

The zeros are thus the $2S$ roots of unity, so the Majorana constellations have $2S$ stars placed around the equator with equal angular separation between each star. A rotation around the S_z axis of angle $\pi/(2S)$ renders the state orthogonal to itself, justifying their optimality.

Finally, we consider kings of quantumness, initially dubbed anticoherent states [96]. In a sense they are the opposite of spin coherent states: whereas the latter correspond as nearly as possible to a classical spin vector pointing in a given direction, the former *point nowhere*; i.e., the average angular momentum vanishes and the fluctuations up to given order M are isotropic [97]. Their symmetrical Majorana constellations herald their isotropic angular momentum properties [98] and correspond to the vertices of Platonic solids in some particular dimensions. In Fig. 1 we show the constellation associated to the examples aforementioned for the case of spin $S = 6$.

III. STATE MULTIPOLES FROM A CONSTELLATION

So far, we have shown how to compute the constellation when the state is given. In this section, we attack the inverse problem: what information can we extract from a given constellation. To this end, we first recall that every polynomial $P(z)$ of degree n can be represented in terms of its zeros ζ_k using the classical Vieta formulas [86], which can be expressed in the form

$$P(z) = \sum_{k=0}^{n} a_k z^k = a_n \sum_{k=0}^{n} (-1)^{n-k} e_{n-k}(\boldsymbol{\zeta})\, z^k, \tag{3.1}$$

where $e_j(\boldsymbol{\zeta}) \equiv e_j(\zeta_1, \zeta_2, \ldots, \zeta_n)$ are the elementary symmetric polynomials [99] defined as

$$\begin{aligned} e_0(\zeta_1, \zeta_2, \ldots, \zeta_n) &= 1, \\ e_1(\zeta_1, \zeta_2, \ldots, \zeta_n) &= \sum_{1 \leqslant j \leqslant n} \zeta_j, \\ e_2(\zeta_1, \zeta_2, \ldots, \zeta_n) &= \sum_{1 \leqslant j < k \leqslant n} \zeta_j \zeta_k, \\ &\vdots \\ e_n(\zeta_1, \zeta_2, \ldots, \zeta_n) &= \zeta_1 \zeta_2 \ldots \zeta_n. \end{aligned} \tag{3.2}$$

Using this fundamental result, the Majorana stellar function can be expressed in the compact form

$$f_\psi(z) = \sum_{k=0}^{2S} \mathfrak{f}_k(\boldsymbol{\zeta})\, z^k, \tag{3.3}$$

where we have introduced the notation

$$\mathfrak{f}_k(\boldsymbol{\zeta}) = (-1)^{2S-k}\, \psi_S\, e_{2S-k}(\boldsymbol{\zeta}), \tag{3.4}$$

and the coefficient ψ_S is fixed by the normalization condition

$$\psi_S(\boldsymbol{\zeta}) = \left(\sum_{k=0}^{2S} \frac{|e_{2S-k}(\zeta)|^2}{\binom{2S}{k}} \right)^{-1/2}. \tag{3.5}$$

In this way, the state coefficients are simply related to the coefficients of the Majorana polynomial, and we can calculate them as a function of the stars:

$$\psi_{k-S}(\boldsymbol{\zeta}) = \frac{\mathfrak{f}_k(\boldsymbol{\zeta})}{\sqrt{\binom{2S}{k}}}. \tag{3.6}$$

For many purposes, expanding in the basis $|S, m\rangle$ is not a good choice. Instead, if one considers the associated density matrix $\varrho = |\psi\rangle\langle\psi|$, it proves more convenient to use the irreducible tensors [83]. They are defined as

$$T_{Kq} = \sqrt{\frac{2K+1}{2S+1}} \sum_{m,m'=-S}^{S} C^{Sm'}_{Sm,Kq}\, |S, m'\rangle\langle S, m|, \tag{3.7}$$

with $C^{Sm'}_{Sm,Kq}$ being the Clebsch-Gordan coefficients that couple a spin S and an integer spin K ($0 \leqslant K \leqslant 2S$) to a total spin S [100]. These tensors constitute an orthonormal basis $\mathrm{Tr}(T_{Kq}\, T^\dagger_{K'q'}) = \delta_{KK'}\delta_{qq'}$ and have the correct transformation properties under rotations.

The corresponding expansion coefficients $\varrho_{Kq} = \mathrm{Tr}(\varrho\, T^\dagger_{Kq})$ are known as state multipoles. Actually, ϱ_{Kq} can be related to the Kth powers of the generators. The monopole $\varrho_{00} = 1/\sqrt{2S+1}$ is trivially fixed by normalization; the dipole ϱ_{1q} is the first-order moment of $\mathbf{S}$ and thus corresponds to the classical picture, in which the state is represented by its average value on the Bloch sphere. However, the complete characterization of a state demands the knowledge of the other multipoles that account for higher-order fluctuations. The hermiticity of ϱ imposes the conditions $\varrho_{K-q} = (-1)^q\, \varrho^*_{Kq}$.

The multipoles can be expressed in terms of the state amplitudes ψ_m, which, in turn, can be computed from the constellation. This allows us to calculate ϱ_{Kq} as a function of the constellation in a very compact form:

$$\varrho_{Kq} = \sqrt{\frac{2K+1}{2S+1}} \sum_{m=-S}^{S} C^{S,m+q}_{Sm,Kq}\, \psi^*_{m+q}(\boldsymbol{\zeta})\, \psi_m(\boldsymbol{\zeta}). \tag{3.8}$$

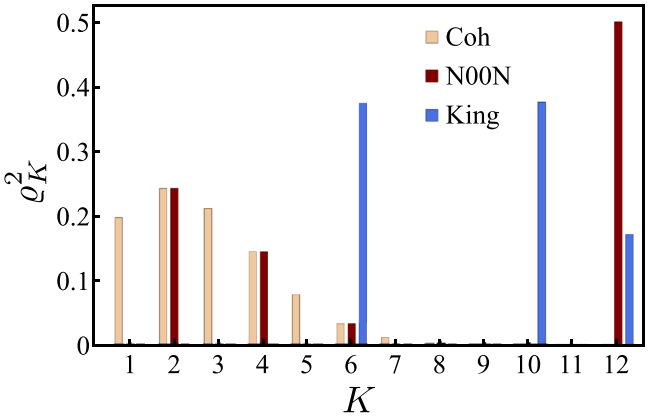

FIG. 2. Multipole lengths for the three constellations depicted in Fig. 1, as a function of the order K.

It will prove convenient to characterize the multipoles by their effective length:

$$\varrho_K^2 = \sum_{q=-K}^{K} |\varrho_{Kq}|^2, \tag{3.9}$$

which gauges the state overlapping with the Kth multipole pattern and is unchanged via SU(2) rotations of the state. Note that, for pure states we are considering, $\sum_{K=0}^{2S} \varrho_K^2 = 1$. These coefficients ϱ_K^2 have been used as measures of localization [101]; as quantifiers of quantumness [76], which is useful for applications such as rotation sensing [43]; and to quantify mode-decomposition-independent entanglement properties [14].

IV. EXAMPLES

To check how the method works we consider the constellations depicted in Fig. 1, corresponding to the states worked out in Sec. II, namely, coherent, NOON, and king of quantumness for $S = 6$. In Fig. 2 we represent the corresponding ϱ_K^2 as a function of the order K (excluding the monopole, as it is always trivial). Similar patterns emerge for other S. For completeness, in Fig. 3 we also plot the distribution of ϱ_K^2 as a function of the order K and the spin S for the same three states.

In the Bloch sphere, constellations having their points arranged as symmetrically as possible are the most quantum, whereas the opposite occurs for coherent states. As we can appreciate, the coherent state conveys all the relevant information in the lowest-order multipoles, which is in agreement with its classical character. Only for high values of S, one can see a tiny contribution of higher-order multipoles. In the limit of large S, we can fit a Gaussian distribution to these multipoles. Since the distributions are unchanged by rotations of the Bloch sphere, we can choose the coherent state with $z = 0$ to find

$$\varrho_{K,\mathrm{coh}}^2 = \frac{(2K+1)(2S)!^2}{(2S-K)!(2S+K+1)!}. \tag{4.1}$$

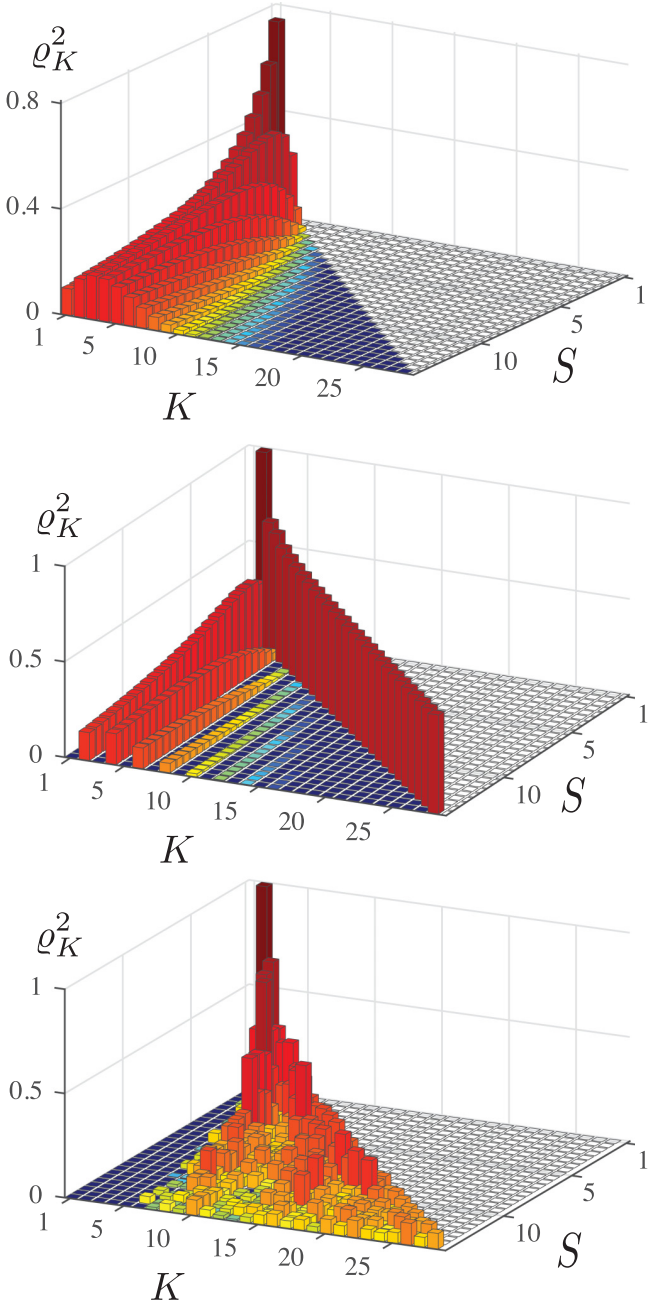

FIG. 3. Multipole lengths as a function of the order K and the system spin S for (upper panel) spin coherent states, (middle panel) NOON states, and (lower panel) kings of quantumness. Since the value of the monopole depends on the dimension, we normalized the rest of the multipole lengths to add up to 1. This allows us to compare their values for different S.

The maximum of this distribution is at $K_{\max} = \sqrt{S+1/2} - 1/2$. In the limit of large S, this peaks at $\varrho_{K_{\max}}^2 \approx 1/\sqrt{Se}$, with a variance $S/2$.

The NOON state has only even multipoles which, surprisingly, are identical with the corresponding ones from the coherent state. We thus could regard the NOON state as a coherent state wherein the information from the odd multipoles has been transferred to the highest-order one. In the limit of high S only that multipole is relevant (see Fig. 3),

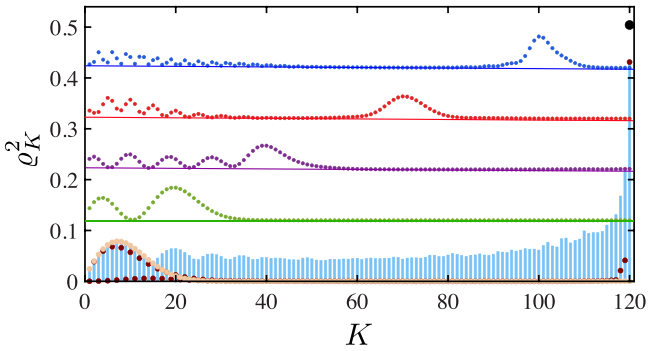

FIG. 4. Maximum multipole length for each order K, selected from randomly generated states (blue bars). Different states maximize the multipoles for different values of K, so the dotted curves represent the multipoles of the states maximizing a certain region, except for the orange dots, which denote the distribution of the coherent state. The black dot above the last multipole is the value corresponding to the NOON state. Note that the distribution for the coherent state and the state maximizing the last multipole are shown in front of the maximum values, and the rest are vertically displaced for clarity.

confirming that NOON states are more quantum for higher S. The significant contribution of the NOON state to the final multipole raises the question of the maximum value that a state can achieve in its highest-order multipole. To explore this question, we numerically generated 6×10^4 random constellations for various values of S: none of them exhibited a larger highest-order multipole than the NOON state. This brings the question of the maximum value for the Kth multipole length.

The results are shown in Fig. 4 for $S = 60$. Unexpectedly, it appears that the coherent state is the unique state with the maximal multipole ϱ_K^2 for all values of K up to a certain point. After this, another state maximizes the Kth multipole for a different region of larger K values and so on. The multipolar distribution of these states is bell shaped near the multipole it maximizes and exhibits a wiggling behavior at the first multipoles. We can also observe how, as K increases, this wiggling evolves to a distribution very similar to that of the NOON state. This supports the hypothesis that the NOON state is the one with the highest contribution to its final multipole and allows a discrete transition between states maximizing low-order multipoles (coherent) and those maximizing high-order ones (NOON).

The king of quantumness shows the absence of lower-order multipoles, which is the origin of the isotropic behavior of their higher-order fluctuations. However, the significance of the strength of the first nonzero multipole is not clear.

We can also gain some general intuition from our calculations. If one has a constellation and makes a change, such as adding, removing, or moving a star, what happens to the multipoles? Upon the addition of a new star ζ_{new} to the constellation, for example, the elementary symmetric polynomials change as $e_k \mapsto \zeta_{\text{new}} e_{k-1} + e_k$ for $k > 0$ and the rest of the calculations proceed as above. Supposing further that the original constellation corresponded to a coherent state at $z = 0$, the addition of a star at ζ_{new} makes the multipoles transform to

$$\varrho_K^2 = c(K,S)\left[4S^2 + 4S|\zeta_{\text{new}}|^2 + \frac{\left(K^2+K-2S\right)^2}{4S^2}|\zeta_{\text{new}}|^4\right], \tag{4.2}$$

with

$$c(K,S) = \frac{(2K+1)(2S-1)!^2|\psi_S|^4}{(2S-K)!(2S+K+1)!}. \tag{4.3}$$

V. DISCUSSION

We explore in this section some nontrivial consequences of our method. A first direct result is to compute Stokes operators [102] from the constellation. Choosing the S_z operator, for example, all of its moments may now be computed as

$$\langle S_z^n\rangle = |\mathfrak{f}_{2S}(\boldsymbol{\zeta})|^2 \sum_{m=0}^{2S}(m-S)^n \binom{2S}{m}^{-1} |e_{2S-m}(\boldsymbol{\zeta})|^2; \tag{5.1}$$

all other moments may be found by rigidly rotating the constellation to highlight any other operator axis. Knowledge of the Stokes vector $\mathbf{S} = (\langle S_x\rangle, \langle S_y\rangle, \langle S_z\rangle)^\top$ (the superscript $\top$ denoting the transpose) and $2S-1$ of the stars provides an overcomplete set of three equations for finding the location of the remaining star. With two stars' locations unknown, the covariances between the Stokes parameters provide sufficient information to determine the four unknown angular coordinate parameters, and so on for higher-order moments and determining the unknown locations of more stars. The inversion process involves nonlinear functions and tends to require numerical solutions.

The results may also be used to make contact with spherical t designs, which are sets of points on the sphere that may be used for averaging polynomial functions over the entire sphere [58,59]. For a set of points to be a one-design, their vectors must sum to the zero vector. In terms of the stereographic projection, this constrains the points to obey

$$\sum_j \frac{\zeta_j}{1+|\zeta_j|^2} = 0, \quad \sum_j \frac{1-|\zeta_j|^2}{1+|\zeta_j|^2} = 0. \tag{5.2}$$

More connections to designs with $t > 1$ are the subject of future study.

We can further explore the significance of the elementary symmetric polynomials, as they have not yet been used to our knowledge for studying our quantum states. Consider that a Majorana constellation can always be rotated such that one of the stars is at the north pole with $\theta = 0$. This makes the highest-order polynomial e_{2S} vanish. Then, the vanishing of the next polynomial e_{2S-1} implies that a second star is also at the north pole. With each subsequent polynomial that vanishes, another star is added to the north pole, up to the condition that $e_j = 0\,\forall\, j > 0$ implies that all $2S$ stars are at the north pole and the state is a spin coherent state. The maximal degeneracy of any star in the constellation is then equal to the maximum number of consecutive highest-order symmetric polynomials that vanish, where the latter is maximized over rigid rotations of the stars that perform a known transformation of the roots.

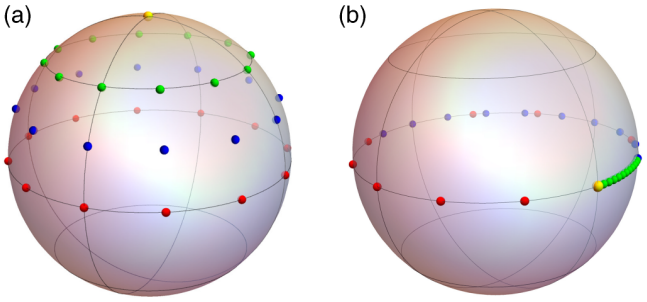

FIG. 5. Two visualizations of how a Majorana constellation can smoothly evolve between classical (coherent) and quantum (NOON) states. On the left, the stars are always at equal polar angles to each other and are equally spaced from each other, while the circle they are spaced on transitions between the north pole (coherent) and the equator (NOON). On the right, the stars spread or coalesce around the equator, with equal azimuthal angles between each star and the subsequent star; the final star goes around the equator to come closer to (NOON) or farther from (coherent) wrapping around to reach the initial star from the other side.

Specifying which polynomials $e_j(\boldsymbol{\zeta})$ vanish significantly constrains a state. In quantifying quantumness, the vanishing of low-order multipoles is a sign of nonclassicality, while here the vanishing of all higher-order polynomials seems to imply an increase in classicality. We are led to consider an interesting case: what if all of the *lower*-order polynomials vanish, such that the state retains $e_{2S} \neq 0$ while $e_j(\boldsymbol{\zeta}) = 0\,\forall 0 < j < 2S$? This includes, for example, the NOON states, which are considered highly quantum by many measures. Since NOON states have all of their stars equally spaced around the equator, the roots all obey $|\zeta_j| = |\zeta_k|$ and are directly equal to roots of unity $\zeta_j = \exp(i\pi j/S)$. Summing all $2S$ such roots gives $e_1(\boldsymbol{\zeta}) = \sum_{j=1}^{2S} \exp(i\pi j/S) = 0$; summing all $\binom{2S}{2}$ products of such roots gives

$$e_2(\boldsymbol{\zeta}) = \sum_{j<k}^{2S} \exp[i\pi(j+k)/S] = \frac{1}{2}\sum_{j\neq k}^{2S} \exp[i\pi(j+k)/S] = 0, \tag{5.3}$$

and so on for all higher-order $e_j(\boldsymbol{\zeta})$ other than

$$e_{2S}(\boldsymbol{\zeta}) = \exp\left(i\pi \sum_{j=1}^{2S} \frac{j}{S}\right) = (-1)^{2S+1} \neq 0. \tag{5.4}$$

We can visually and mathematically explore the transition between NOON states and coherent states by the migration of stars from the equator to the north pole and by the vanishing of $e_{2S}(\boldsymbol{\zeta})$, respectively. Consider the transition as sketched in Fig. 5(a), where the $2S$ points in the constellation are equally spaced around a circle other than the equator, sharing the polar angle θ. The symmetric polynomials take the same form as before, with $e_j(\boldsymbol{\zeta})$ multiplied by $\tan^j(\theta/2)$, so all of the lowest polynomials vanish other than

$$e_{2S} = (-1)^{2S+1} \tan^{2S}(\theta/2). \tag{5.5}$$

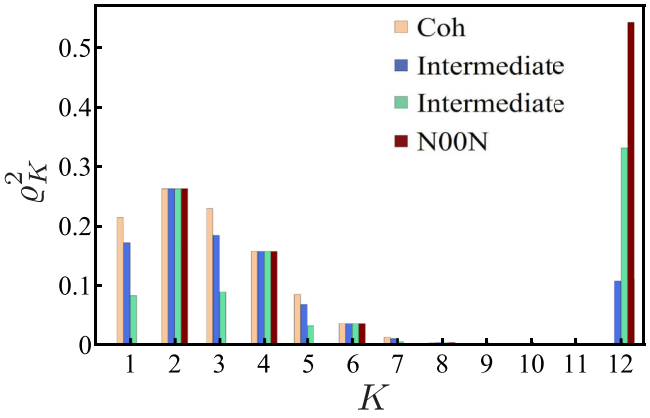

FIG. 6. Evolution of the multipole lengths corresponding to Fig. 5(a). The position of the stars in the figure is for illustrative purposes only, as the transition occurs when the stars are very close to the equator.

This codifies the gradual progression: as the circle on which the stars lie gets smaller and smaller, from a NOON to a coherent state, the one nonzero polynomial (other than $e_0 = 1$) goes to zero as $\tan^{2S}(\theta/2)$. The magnitude of this highest-order polynomial, after a rigid rotation that makes the rest of the polynomials vanish, directly encodes the quantumness of the state. Note that it is the deviation of the magnitude of e_{2S} from unity that matters: there is a coherent state at $\theta = 0$ and π.

We can also obtain exact expressions for the multipoles as a function of θ:

$$\varrho_K^2 = \varrho_{K,\mathrm{coh}}^2 \left[\frac{\tan^{4S}(\theta/2) - 1}{\tan^{4S}(\theta/2) + 1}\right]^2, \quad K = 1, 3, \ldots, 2S-1, \tag{5.6}$$

whereas $\varrho_K^2 = \varrho_{K,\mathrm{coh}}^2$ for $K = 2, 4, \ldots, 2S-2$. This transition from coherent to NOON is very abrupt, even for low values of S, due to the power of $4S$ in the tangent. The multipoles look much like a coherent state up until the stars are very close to the equator. This shows the vulnerability of the NOON state to a small displacement of its stars.

As previously argued, the NOON state maximizes the last multipole. With the help of the previous expressions we can obtain this value:

$$\varrho_{2S,\mathrm{NOON}}^2 = \begin{cases} \frac{1}{2} + \binom{4S}{2S}^{-1} & S = 1, 2, \ldots \\ \frac{1}{2} & S = \frac{1}{2}, \frac{3}{2}, \ldots \end{cases}, \tag{5.7}$$

which tends to $1/2$ as S becomes large. Note that this does not contradict the results in Fig. 3, for the multipoles are normalized therein.

We can observe how the multipole lengths change in the aforementioned transition between coherent and NOON states in Fig. 6. This transition can be enacted by evolution under the highly nontrivial Hamiltonian

$$H_{\mathrm{NOON}\leftrightarrow\mathrm{coh}} = -i|S, S\rangle\langle S, -S| + i|S, -S\rangle\langle S, S| \tag{5.8}$$

that manifestly breaks degeneracies between Majorana stars.

Further consider the alternative transition as in Fig. 5(b), where the stars spread around the equator ($\theta = \pi/2$) smoothly

between NOON- and coherent-state configurations. Now we consider the coherent state to have $\zeta = 1$, such that its polynomials take the form $e_j(\boldsymbol{\zeta}) = \binom{2S}{j}$. We choose the spreading rate such that all stars arrive in place at the same time, with $\zeta_j(t) = \exp(i\pi t j/S)$ and $t \in (0, 1)$ with $t = 0$ and 1 corresponding to coherent and NOON states, respectively. Then

$$\begin{aligned} e_1[\boldsymbol{\zeta}(t)] &= \exp\left[i\pi\frac{(2S+1)}{2S}t\right]\frac{\sin(\pi t)}{\sin\left(\frac{\pi t}{2S}\right)}, \\ e_2[\boldsymbol{\zeta}(t)] &= \frac{1}{2!}\{e_1[\boldsymbol{\zeta}(t)]^2 - e_1[\boldsymbol{\zeta}(2t)]\}, \\ e_3[\boldsymbol{\zeta}(t)] &= \frac{1}{3!}\{e_1[\boldsymbol{\zeta}(t)]^3 - 3e_1[\boldsymbol{\zeta}(t)]e_1[\boldsymbol{\zeta}(2t)] + 2e_1[\boldsymbol{\zeta}(3t)]\}, \end{aligned} \tag{5.9}$$

and so on. For small t, these equal

$$e_j[\boldsymbol{\zeta}(t)] = \binom{2S}{j} - \binom{2S}{j+1}\pi^2\frac{2S+1}{4S^2}t^2 + \mathcal{O}(t^4). \tag{5.10}$$

The Hamiltonian required to enact this transition is much more complicated, as the stars all rotate around the z axis but no Hamiltonian of the form S_z^n can do anything other than rotate the NOON state.

Finally, consider the symmetric transition where the stars spread in both directions along the equator, with pairs moving at equal speeds. For example, with $2S$ odd, we can set $\zeta_0 = 1$, $\zeta_j(t) = \exp(i\pi t j/S)$ for $0 < j \leqslant S - 1/2$, and relabel the remainder as $\zeta_{-j}(t) = \exp(-i\pi t j/S)$ for $0 < j \leqslant S - 1/2$. The spacings between all of the stars are the same as when all of the stars traveled in the same direction, merely offset by a relative phase, which symmetrizes the expressions to

$$\begin{aligned} e_1[\boldsymbol{\zeta}(t)] &= \frac{\sin(\pi t)}{\sin\left(\frac{\pi t}{2S}\right)}, \\ e_2[\boldsymbol{\zeta}(t)] &= \frac{1}{2!}\{e_1[\boldsymbol{\zeta}(t)]^2 - e_1[\boldsymbol{\zeta}(2t)]\}, \end{aligned} \tag{5.11}$$

and so on. We can thus use the symmetric polynomials to observe the transitions between highly quantum and highly classical states, in accordance with the geometric picture of the Majorana constellation.

VI. CONCLUDING REMARKS

The Majorana representation provides a valuable geometric tool to characterize quantum states with SU(2) symmetry. The visualization of quantum states as a constellation in the unit sphere is finding new applications in quantum information science. On the other hand, the multipolar expansion is especially germane to capture the state invariant properties and, in addition, the resulting multipoles can be measured in the laboratory.

We have extensively explored how to go from Majorana constellations to multipolar distributions and back, illustrating this through a variety of examples. For instance, we have elucidated the changes in the multipolar distribution when the Majorana constellation transitions from a classical (concentrated) to a highly quantum state (spread out). Additionally, we have delved into the consequences of adding new stars to the constellation and examined states with the greatest contribution to the higher-order multipole, among many other aspects. Interestingly, the formalism can be manifestly extended to other symmetries [103]: this is more than an academic curiosity, and work in this direction is ongoing.

ACKNOWLEDGMENTS

We are indebted to G. Björk, P. de la Hoz, M. Grassl, L. Villanueva, and Ł. Rudnicki for discussions. A.Z.G. acknowledges that the NRC headquarters is located on the traditional unceded territory of the Algonquin Anishinaabe and Mohawk people. We acknowledge financial support from the European Union QUANTERA program (project ApresSF) and the Spanish Research Agency (Grant No. PID2021-127781NB-I00). A.Z.G. acknowledges funding from the Natural Sciences and Engineering Research Council PDF program.

[1] K. Eckert, J. Schliemann, D. Bruß, and M. Lewenstein, Quantum correlations in systems of indistinguishable particles, Ann. Phys. **299**, 88 (2002).

[2] Y. Kawaguchi and M. Ueda, Spinor Bose-Einstein condensates, Phys. Rep. **520**, 253 (2012).

[3] D. M. Stamper-Kurn and M. Ueda, Spinor Bose gases: Symmetries, magnetism, and quantum dynamics, Rev. Mod. Phys. **85**, 1191 (2013).

[4] M. H. Anderson, J. R. Ensher, M. R. Matthews, C. E. Wieman, and E. A. Cornell, Observation of Bose-Einstein condensation in a dilute atomic vapor, Science **269**, 198 (1995).

[5] K. B. Davis, M.-O. Mewes, M. R. Andrews, N. J. van Druten, D. S. Durfee, D. M. Kurn, and W. Ketterle, Bose-Einstein condensation in a gas of sodium atoms, Phys. Rev. Lett. **75**, 3969 (1995).

[6] M. S. Chang, C. D. Hamley, M. D. Barrett, J. A. Sauer, K. M. Fortier, W. Zhang, L. You, and M. S. Chapman, Observation of spinor dynamics in optically trapped ^{87}Rb Bose-Einstein condensates, Phys. Rev. Lett. **92**, 140403 (2004).

[7] A. Griesmaier, J. Werner, S. Hensler, J. Stuhler, and T. Pfau, Bose-Einstein condensation of chromium, Phys. Rev. Lett. **94**, 160401 (2005).

[8] Q. Beaufils, R. Chicireanu, T. Zanon, B. Laburthe-Tolra, E. Maréchal, L. Vernac, J. C. Keller, and O. Gorceix, All-optical production of chromium Bose-Einstein condensates, Phys. Rev. A **77**, 061601(R) (2008).

[9] A. R. Usha Devi, R. Prabhu, and A. K. Rajagopal, Characterizing multiparticle entanglement in symmetric n-qubit states via negativity of covariance matrices, Phys. Rev. Lett. **98**, 060501 (2007).

[10] T. Bastin, S. Krins, P. Mathonet, M. Godefroid, L. Lamata, and E. Solano, Operational families of entanglement classes for symmetric n-qubit states, Phys. Rev. Lett. **103**, 070503 (2009).

[11] J. Martin, O. Giraud, P. A. Braun, D. Braun, and T. Bastin, Multiqubit symmetric states with high geometric entanglement, Phys. Rev. A **81**, 062347 (2010).

[12] M. Aulbach, Classification of entanglement in symmetric states, Int. J. Quantum Inform. **10**, 1230004 (2012).

[13] A. Mandilara, T. Coudreau, A. Keller, and P. Milman, Entanglement classification of pure symmetric states via spin coherent states, Phys. Rev. A **90**, 050302(R) (2014).

[14] A. Z. Goldberg, M. Grassl, G. Leuchs, and L. L. Sánchez-Soto, Quantumness beyond entanglement: The case of symmetric states, Phys. Rev. A **105**, 022433 (2022).

[15] E. Majorana, Atomi orientati in campo magnetico variabile, Nuovo Cim. **9**, 43 (1932).

[16] F. Bloch and I. I. Rabi, Atoms in variable magnetic fields, Rev. Mod. Phys. **17**, 237 (1945).

[17] H. Salwen, Resonance transitions in molecular beam experiments. I. General theory of transitions in a rotating magnetic field, Phys. Rev. **99**, 1274 (1955).

[18] A. Meckler, Majorana formula, Phys. Rev. **111**, 1447 (1958).

[19] J. Schwinger, The Majorana formula, Trans. NY Acad. Sci. **38**, 170 (1977).

[20] R. Penrose, A spinor approach to general relativity, Ann. Phys. **10**, 171 (1960).

[21] R. Penrose, *The Emperor's New Mind* (Oxford University, New York, 1989).

[22] H. Bacry, *Group Theory and Constellations* (Publibook, Paris, 2004).

[23] J. H. Hannay, The Majorana representation of polarization, and the Berry phase of light, J. Mod. Opt. **45**, 1001 (1998).

[24] G. Björk, A. B. Klimov, P. de la Hoz, M. Grassl, G. Leuchs, and L. L. Sánchez-Soto, Extremal quantum states and their Majorana constellations, Phys. Rev. A **92**, 031801(R) (2015).

[25] A. Z. Goldberg, Quantum theory of polarimetry: From quantum operations to Mueller matrices, Phys. Rev. Res. **2**, 023038 (2020).

[26] A. Z. Goldberg, P. de la Hoz, G. Björk, A. B. Klimov, M. Grassl, G. Leuchs, and L. L. Sánchez-Soto, Quantum concepts in optical polarization, Adv. Opt. Photon. **13**, 1 (2021).

[27] A. Z. Goldberg, Quantum polarimetry, Prog. Opt. **67**, 185 (2022).

[28] R. Barnett, D. Podolsky, and G. Refael, Geometrical approach to hydrodynamics and low-energy excitations of spinor condensates, Phys. Rev. B **80**, 024420 (2009).

[29] A. Lamacraft, Low-energy dynamics of spinor condensates, Phys. Rev. B **81**, 184526 (2010).

[30] B. Lian, T.-L. Ho, and H. Zhai, Searching for non-Abelian phases in the Bose-Einstein condensate of dysprosium, Phys. Rev. A **85**, 051606(R) (2012).

[31] X. Cui, B. Lian, T.-L. Ho, B. L. Lev, and H. Zhai, Synthetic gauge field with highly magnetic lanthanide atoms, Phys. Rev. A **88**, 011601(R) (2013).

[32] H. Mäkelä and A. Messina, *N*-qubit states as points on the Bloch sphere, Phys. Scr. **2010**, 014054 (2010).

[33] P. Ribeiro and R. Mosseri, Entanglement in the symmetric sector of *n* qubits, Phys. Rev. Lett. **106**, 180502 (2011).

[34] A. R. U. Devi, Sudha, and A. K. Rajagopal, Majorana representation of symmetric multiqubit states, Quantum Inf. Process. **11**, 685 (2012).

[35] C. Chryssomalakos, L. Hanotel, E. Guzmán-González, D. Braun, E. Serrano-Ensástiga, and K. Życzkowski, Symmetric multiqudit states: Stars, entanglement, and rotosensors, Phys. Rev. A **104**, 012407 (2021).

[36] C.-F. Kam and R.-B. Liu, Three-tangle of a general three-qubit state in the representation of majorana stars, Phys. Rev. A **101**, 032318 (2020).

[37] X. Lu, L.-Y. Zhan, J. Chen, H.-D. Liu, L.-B. Fu, and X.-G. Wang, Many-body anticommutator and its applications in the normalization of completely symmetric states with Majorana's stellar representations, Phys. Rev. A **104**, 012203 (2021).

[38] A. Burchardt, J. Czartowski, and K. Życzkowski, Entanglement in highly symmetric multipartite quantum states, Phys. Rev. A **104**, 022426 (2021).

[39] F. Bouchard, P. de la Hoz, G. Björk, R. W. Boyd, M. Grassl, Z. Hradil, E. Karimi, A. B. Klimov, G. Leuchs, J. Řeháček, and L. L. Sánchez-Soto, Quantum metrology at the limit with extremal Majorana constellations, Optica **4**, 1429 (2017).

[40] C. Chryssomalakos and H. Hernández-Coronado, Optimal quantum rotosensors, Phys. Rev. A **95**, 052125 (2017).

[41] A. Z. Goldberg and D. F. V. James, Quantum-limited Euler angle measurements using anticoherent states, Phys. Rev. A **98**, 032113 (2018).

[42] J. Martin, S. Weigert, and O. Giraud, Optimal detection of rotations about unknown axes by coherent and anticoherent states, Quantum **4**, 285 (2020).

[43] A. Z. Goldberg, A. B. Klimov, G. Leuchs, and L. L. Sánchez-Soto, Rotation sensing at the ultimate limit, J. Phys. Photonics **3**, 022008 (2021).

[44] J. H. Hannay, The Berry phase for spin in the Majorana representation, J. Phys. A **31**, L53 (1998).

[45] P. Bruno, Quantum geometric phase in Majorana's stellar representation: Mapping onto a many-body Aharonov-Bohm phase, Phys. Rev. Lett. **108**, 240402 (2012).

[46] H. D. Liu and L. B. Fu, Representation of Berry phase by the trajectories of Majorana stars, Phys. Rev. Lett. **113**, 240403 (2014).

[47] C. Yang, H. Guo, L.-B. Fu, and S. Chen, Characterization of symmetry-protected topological phases in polymerized models by trajectories of Majorana stars, Phys. Rev. B **91**, 125132 (2015).

[48] H. D. Liu and L. B. Fu, Berry phase and quantum entanglement in Majorana's stellar representation, Phys. Rev. A **94**, 022123 (2016).

[49] F. Yao, D. Li, H. Liu, L. Fu, and X. Wang, The exact curve equation for Majorana stars, Sci. Rep. **7**, 15558 (2017).

[50] C.-F. Kam and R.-B. Liu, Berry phases of higher spins due to internal geometry of Majorana constellation and relation to quantum entanglement, New J. Phys. **23**, 073020 (2021).

[51] V. Mittal, K. S. Akhilesh, and S. K. Goyal, Geometric decomposition of geodesics and null-phase curves using Majorana star representation, Phys. Rev. A **105**, 052219 (2022).

[52] J. Bartlett, H. Hu, and E. Zhao, Illuminating the bulk-boundary correspondence of a non-Hermitian stub lattice with Majorana stars, Phys. Rev. B **104**, 195131 (2021).

[53] P. Ribeiro, J. Vidal, and R. Mosseri, Thermodynamical limit of the Lipkin-Meshkov-Glick model, Phys. Rev. Lett. **99**, 050402 (2007).

[54] P. Ribeiro, J. Vidal, and R. Mosseri, Exact spectrum of the Lipkin-Meshkov-Glick model in the thermodynamic limit and finite-size corrections, Phys. Rev. E **78**, 021106 (2008).

[55] D. J. H. Markham, Entanglement and symmetry in permutation-symmetric states, Phys. Rev. A **83**, 042332 (2011).

[56] Z. Wang and D. Markham, Nonlocality of symmetric states, Phys. Rev. Lett. **108**, 210407 (2012).

[57] W. Ganczarek, M. Kuś, and K. Życzkowski, Barycentric measure of quantum entanglement, Phys. Rev. A **85**, 032314 (2012).

[58] P. Delsarte, J. M. Goethals, and J. J. Seidel, Spherical codes and designs, Geom. Dedicata **6**, 363 (1977).

[59] R. H. Hardin and N. J. A. Sloane, New spherical 4-designs, Discrete Math. **106-107**, 255 (1992).

[60] J. J. Thomson, On the structure of the atom: An investigation of the stability and periods of oscillation of a number of corpuscles arranged at equal intervals around the circumference of a circle; with application of the results to the theory of atomic structure, Philos. Mag. Ser. **7**, 37265 (1904).

[61] T. H. Melnyk, O. Knop, and W. R. Smith, Extremal arrangements of points and unit charges on a sphere: Equilibrium configurations revisited, Can. J. Chem. **55**, 1745 (1977).

[62] N. Ashby and W. E. Brittin, Thomson's problem, Am. J. Phys. **54**, 776 (1986).

[63] T. Erber and G. M. Hockney, Equilibrium configurations of n equal charges on a sphere, J. Phys. A **24**, L1369 (1991).

[64] J. R. Edmundson, The distribution of point charges on the surface of a sphere, Acta Cryst. **A48**, 46 (1992).

[65] A. Baecklund and I. Bengtsson, Four remarks on spin coherent states, Phys. Scr. **2014**, 014012 (2014).

[66] P. M. L. Tammes, On the origin of number and arrangement of places of exit on the surface of pollen grains, Recueil Trav. Bot. Néerl. **27**, 1 (1930).

[67] L. Fejes Tóth, *Lagerungen in der Ebene, auf der Kugel und in Raum* (Springer-Verlag, Berlin, 1953).

[68] J. Leech, Equilibrium of sets of particles on a sphere, Math. Gaz. **41**, 81 (1957).

[69] O. Giraud, P. Braun, and D. Braun, Quantifying quantumness and the quest for queens of quantumness, New J. Phys. **12**, 063005 (2010).

[70] G. Björk, M. Grassl, P. de la Hoz, G. Leuchs, and L. L. Sánchez-Soto, Stars of the quantum universe: Extremal constellations on the Poincaré sphere, Phys. Scr. **90**, 108008 (2015).

[71] M. Aulbach, D. Markham, and M. Murao, The maximally entangled symmetric state in terms of the geometric measure, New J. Phys. **12**, 073025 (2010).

[72] L. Arnaud and N. J. Cerf, Exploring pure quantum states with maximally mixed reductions, Phys. Rev. A **87**, 012319 (2013).

[73] D. Goyeneche and K. Życzkowski, Genuinely multipartite entangled states and orthogonal arrays, Phys. Rev. A **90**, 022316 (2014).

[74] M.-S. Li and Y.-L. Wang, k-uniform quantum states arising from orthogonal arrays, Phys. Rev. A **99**, 042332 (2019).

[75] E. H. Lieb and J. P. Solovej, Proof of an entropy conjecture for Bloch coherent spin states and its generalizations, Acta Math. **212**, 379 (2014).

[76] A. Z. Goldberg, A. B. Klimov, M. Grassl, G. Leuchs, and L. L. Sánchez-Soto, Extremal quantum states, AVS Quantum Science **2**, 044701 (2020).

[77] L. L. Whyte, Unique arrangements of points on a sphere, Am. Math. Monthly **59**, 606 (1952).

[78] E. B. Saff and A. B. J. Kuijlaars, Distributing many points on a sphere, Math. Intell. **19**, 5 (1997).

[79] A. Katanforoush and M. Shahshahani, Distributing points on the sphere, I, Exp. Math. **12**, 199 (2003).

[80] J. S. Brauchart and P. J. Grabner, Distributing many points on spheres: Minimal energy and designs, J. Complexity **31**, 293 (2015).

[81] J. D. Jackson, *Classical Electrodynamics*, 3rd ed. (Wiley, New York, 1999).

[82] U. Fano and G. Racah, *Irreducible Tensorial Sets* (Academic, New York, 1959).

[83] K. Blum, *Density Matrix Theory and Applications* (Plenum, New York, 1981).

[84] G. Björk, J. Söderholm, Y. S. Kim, Y. S. Ra, H. T. Lim, C. Kothe, Y. H. Kim, L. L. Sánchez-Soto, and A. B. Klimov, Central-moment description of polarization for quantum states of light, Phys. Rev. A **85**, 053835 (2012).

[85] A. Z. Goldberg, A. B. Klimov, H. deGuise, G. Leuchs, G. S. Agarwal, and L. L. Sánchez-Soto, From polarization multipoles to higher-order coherences, Opt. Lett. **47**, 477 (2022).

[86] H. G. Funkhouser, A short account of the history of symmetric functions of roots of equations, Am. Math. Monthly **37**, 357 (1930).

[87] I. Bengtsson and K. Życzkowski, *Geometry of Quantum States* (Cambridge University, Cambridge, England, 2006).

[88] A. Perelomov, *Generalized Coherent States and their Applications* (Springer-Verlag, Berlin, 1986).

[89] J.-P. Gazeau, *Coherent States in Quantum Physics* (Wiley, New York, 2009).

[90] H. S. M. Coxeter, *Introduction to Geometry* (Wiley, New York, 1969).

[91] K. Husimi, Some formal properties of the density matrix, Proc. Phys. Math. Soc. Jpn. **22**, 264 (1940).

[92] Y. Kano, A new phase-space distribution function in the statistical theory of the electromagnetic field, J. Math. Phys. **6**, 1913 (1965).

[93] C. R. Müller, C. Peuntinger, T. Dirmeier, I. Khan, U. Vogl, C. Marquardt, G. Leuchs, L. L. Sánchez-Soto, Y. S. Teo, Z. Hradil, and J. Řeháček, Evading Vacuum Noise: Wigner Projections or Husimi Samples? Phys. Rev. Lett. **117**, 070801 (2016).

[94] J. P. Dowling, Quantum optical metrology: The lowdown on high-N00N states, Contemp. Phys. **49**, 125 (2008).

[95] J. J. Bollinger, W. M. Itano, D. J. Wineland, and D. J. Heinzen, Optimal frequency measurements with maximally correlated states, Phys. Rev. A **54**, R4649(R) (1996).

[96] J. Zimba, "Anticoherent" spin states via the Majorana representation, Electron. J. Theor. Phys. **3**, 143 (2006).

[97] P. de la Hoz, A. B. Klimov, G. Björk, Y. H. Kim, C. Müller, C. Marquardt, G. Leuchs, and L. L. Sánchez-Soto, Multipolar hierarchy of efficient quantum polarization measures, Phys. Rev. A **88**, 063803 (2013).

[98] http://polarization.markus-grassl.de.

[99] B. van der Waerden, *Algebra* (Springer-Verlag, Berlin, 1991), Vol. 1.

[100] D. A. Varshalovich, A. N. Moskalev, and V. K. Khersonski, *Quantum Theory of Angular Momentum* (World Scientific, Singapore, 1988).

[101] M. J. W. Hall, Universal geometric approach to uncertainty, entropy, and information, Phys. Rev. A **59**, 2602 (1999).

[102] A. Luis and L. L. Sánchez-Soto, Quantum phase difference, phase measurements and Stokes operators, Prog. Opt. **41**, 421 (2000).

[103] N. Fabre, A. B. Klimov, R. Murenzi, J.-P. Gazeau, and L. L. Sánchez-Soto, Majorana stellar representation of twisted photons, Phys. Rev. Res. **5**, L032006 (2023).

Robust quantum metrology with random Majorana constellations

IOP Publishing Quantum Sci. Technol. 10 (2025) 015053 https://doi.org/10.1088/2058-9565/ad9ac7

Quantum Science and Technology

OPEN ACCESS

RECEIVED
24 June 2024

REVISED
16 October 2024

ACCEPTED FOR PUBLICATION
5 December 2024

PUBLISHED
23 December 2024

PAPER

Robust quantum metrology with random Majorana constellations

Aaron Z Goldberg[1], **Jose R Hervas**[2], **Angel S Sanz**[2], **Andrei B Klimov**[3], **Jaroslav Řeháček**[4], **Zdeněk Hradil**[4], **Markus Hiekkamäki**[5], **Matias Eriksson**[5], **Robert Fickler**[5], **Gerd Leuchs**[6] and **Luis L Sánchez-Soto**[6,*]

[1] National Research Council of Canada, 100 Sussex Drive, Ottawa, Ontario K1N 5A2, Canada
[2] Departamento de Óptica, Facultad de Física, Universidad Complutense, 28040 Madrid, Spain
[3] Departamento de Física, Universidad de Guadalajara, 44420 Guadalajara, Jalisco, Mexico
[4] Department of Optics, Palacký University, 17. listopadu 12, 771 46 Olomouc, Czech Republic
[5] Physics Unit, Photonics Laboratory, Tampere University, 33720 Tampere, Finland
[6] Max-Planck-Institut für die Physik des Lichts, 91058 Erlangen, Germany
[*] Author to whom any correspondence should be addressed.

E-mail: lsanchez@ucm.es

Keywords: Robust, quantum, metrology, Majorana, constellations

Supplementary material for this article is available online

Abstract

Even the most classical states are still governed by quantum theory. A number of physical systems can be described by their Majorana constellations of points on the surface of a sphere, where concentrated constellations and highly symmetric distributions correspond to the least and most quantum states, respectively. If these points are chosen randomly, how quantum will the resultant state be, on average? We explore this simple conceptual question in detail, investigating the quantum properties of the resulting random states. We find these states to be far from the norm, even in the large-number-of-particles limit, where classical intuition often replaces quantum properties, making random Majorana constellations peculiar and intriguing. Moreover, we study their usefulness in the context of rotation sensing and find numerical evidence of their robustness against dephasing and particle loss. We realize these states experimentally using light's orbital angular momentum degree of freedom and implement arbitrary unitaries with a multiplane light conversion setup to demonstrate the rotation sensing. Our findings open up new possibilities for quantum-enhanced metrology.

1. Introduction

Random matrices sampled from an ensemble with a specific symmetry were introduced by Wigner [1, 2] and Dyson [3–5] to describe spectral properties of quantum many-body systems, such as atomic nuclei [6]. Since then, random matrix theory [7–9] has found applications in fields as diverse as black holes [10–13] and gravity [14], quantum chaos [15], transport in disordered systems [16, 17], spin glasses [18], neural networks [19, 20], and even finance [21]. Quantum information is definitely one of the most recent applications, and a very natural one, too [22–24].

Random quantum states can be seen as arising from the time evolution of arbitrary initial states of quantum analogues of classically chaotic systems [25]. Furthermore, these states emerge when not much is known about a state and one wants to ask about its generic properties, characteristic of a 'typical' state [26–28]. Given a random quantum state, one may then ask how quantum is this state: does it exhibit classical behavior in the large-number-of-particles regime? If one had access to a black box that prepared random states, how much would it be worth and what would its applications be? These questions and more motivate the present study.

When considering the set of pure states living in an N-dimensional complex vector space, the manifold of physical states is the projective space $\mathbb{C}\mathbf{P}^N$ [29], wherein there is a unique normalized measure invariant under all unitary transformations: the associated Haar measure [30]. One can reasonably call this measure the uniform distribution over the unit sphere [31].

The geometrical properties of quantum states are essential to understanding where classical intuitions break down and where the next quantum advantage may lie [32–34]. In phase space, localization is a clear signature of the state quantumness [35, 36], as it has been demonstrated with several indicators, such as Rényi–Wehrl entropies [37], inverse participation ratio [38], or Husimi extrema [39]. However, while these notions provide effective analytical tools, the geometry of $\mathbb{C}\mathbf{P}^N$ is not very intuitive and so it is difficult to visualize and to gain insights into the nature of those states.

Here, we propose a novel class of random states based upon a mapping onto a many-qubit system (which, in some cases, might be fictitious). Actually, any system with a finite-dimensional Hilbert space of dimension $N = 2S + 1$ can be thought of as a spin S [40]. The space manifold $\mathbb{C}\mathbf{P}^N$ admits an appealing representation due to Majorana [41], which maps any pure state onto $2S$ points on the unit sphere $\mathcal{S}_2$; the state's stellar representation. This picture makes it natural to consider the states associated with random points on the sphere. We conduct a detailed study of these states from an SU(2)-invariant perspective. Notably, we find that, in the limit of a large number of particles, they do not converge to a classical state and preserve their quantumness.

In addition, these new random Majorana (RM) states belong to the symmetric (bosonic) subspace. It has been recognized that symmetric states offer significant advantages from a metrological perspective [42–45]. We find numerical evidence that the usefulness of RM states for rotation-sensing-style tasks, like magnetometry and ellipsometry, is robust against the loss of a finite number of particles and dephasing. This is in stark contrast to other relevant states, such as Greenberger–Horne–Zeilinger (GHZ) states [46] (equivalent to the NOON states [47] in optical interferometry), which completely lose their (otherwise ideal) sensitivity upon loss of just a single particle. Finally, we experimentally generate these states by utilizing light's orbital angular momentum and implement arbitrary unitaries using a multiplane light conversion setup to showcase rotation sensing.

This paper is organized as follows. In section 2 we address the basic notions of the Majorana stellar representation and its physical interpretation. In section 3 we raise the ideas behind RM constellations and characterize their properties by resorting to a multipole expansion. Subsequently, in section 4 we use these multipoles to compare our method with alternative ways of obtaining random states. In section 5 we introduce the setting of quantum parameter estimation. Utilizing the quantum Fisher information, we investigate the performance and robustness of the RM states under the influence of noise and particle loss. Finally, in section 6 we introduce the experimental setup used to study these states with respect to rotation sensing and analyze the obtained results. We conclude our work in section 7.

2. Majorana constellations

Let us consider a pure spin-S state $|\psi\rangle$ living in the $2S+1$-dimensional Hilbert space $\mathcal{H}_S$ spanned by the standard angular momentum basis $\{|S, m\rangle \mid m = -S, \ldots, S\}$, which is the carrier of the irreducible representation (irrep) of spin S of SU(2). This space is isomorphic to $\mathbb{C}^{2S+1}$, but since any two vectors in $\mathcal{H}_S$ differing by a phase represent the same physical state, the manifold of physical states is the projective space $\mathbb{C}\mathbf{P}^{2S}$ [29].

The merit of Majorana was to show that points in $\mathbb{C}\mathbf{P}^{2S}$ are in one-to-one correspondence with unordered sets of (possibly coincident) $2S$ points on the unit sphere $\mathcal{S}_2$. In other words, spin-S states can be obtained as fully symmetrized states of a system of $2S$ spins $1/2$ (or qubits). These systems have many physical applications, ranging from quantum computation to quantum sensing and metrology [48–52]. This idea is also at the heart of the Schwinger map [53, 54], which realizes the set of angular momentum operators in terms of polynomials of bosonic operators.

There are various ways to see why this is so, but probably the most direct one is to notice that the state $|\psi\rangle$ can always be written as

$$|\psi\rangle = \frac{1}{\mathcal{N}} \prod_{i=1}^{2S} a^\dagger_{-\mathbf{u}_i} |\mathrm{vac}\rangle, \tag{2.1}$$

where $\mathbf{u}_i$ is a unit direction of spherical coordinates (θ_i, ϕ_i), the rotated bosonic operators are

$$a^\dagger_{\mathbf{u}} = \cos(\theta/2)\, a^\dagger_+ + \mathrm{e}^{\mathrm{i}\phi} \sin(\theta/2)\, a^\dagger_- , \tag{2.2}$$

with $a^\dagger_+$ and $a^\dagger_-$ creating excitations in two modes (denoted by $+$ and $-$) from the two-mode vacuum $|\mathrm{vac}\rangle$, and $\mathcal{N}$ is a normalization factor of no interest for our purposes here and whose explicit expression can be found, e.g. in [55].

The set of $2S$ (non-necessarily distinct) unit vectors $\{\mathbf{u}_1, \ldots, \mathbf{u}_{2S}\}$ defines the Majorana constellation of the state. Alternatively, the state (2.1) can be expressed as

$$|\psi\rangle = P_\psi(a_+^\dagger, a_-^\dagger)|\text{vac}\rangle\,, \tag{2.3}$$

where $P_\psi(a_+^\dagger, a_-^\dagger)$ is a homogeneous polynomial of degree $2S$ in the variables $a_+^\dagger$ and $a_-^\dagger$ that can be factorized (up to an unessential factor) in the above form.

In particular, the states

$$|\mathbf{n}\rangle = \frac{1}{\sqrt{(2S)!}}\left(a_{\mathbf{n}}^\dagger\right)^{2S}|\text{vac}\rangle \tag{2.4}$$

are precisely the spin-S coherent states (CS) [56]. The definition shows that the associated constellations consist of only one single point in the antipodal direction $-\mathbf{n}$. It is natural to introduce the CS representation by $\psi(\mathbf{n}) \equiv \langle \mathbf{n}|\psi\rangle$: this is a *bona fide* wave function over the unit sphere $\mathcal{S}_2$. Simple algebraic manipulations yield

$$\psi(\mathbf{n}) = \prod_{i=1}^{2S}\left[\tfrac{1}{2}(1-\mathbf{n}\cdot\mathbf{u}_i)\ \mathrm{e}^{i\Sigma(\mathbf{n},-\mathbf{u}_i)}\right], \tag{2.5}$$

where $\Sigma(\mathbf{n}, -\mathbf{u}_i)$ is the oriented area of the spherical triangle with vertices $(\mathbf{z}, \mathbf{n}, -\mathbf{u}_i)$, with $\mathbf{z}$ the unit vector in the direction of the axis Z. This confirms that the Majorana constellation consists of the zeros of $\psi(\mathbf{n})$.

The CS wavefunction induces a probability distribution

$$Q_\psi(\mathbf{n}) \equiv |\langle \mathbf{n}|\psi\rangle|^2\,, \tag{2.6}$$

which is the Husimi function [57], and whose zeros are also the Majorana constellation.

Because the Majorana representation facilitates a useful geometrical interpretation of quantum states, it has found an increasing number of applications in recent years, with prominent examples being polarimetry and magnetometry [58], Bose–Einstein condensates [59, 60], Berry phases [61–63], and studies of entanglement [64].

3. Random Majorana constellations

Since points on the sphere $\mathcal{S}_2$ correspond uniquely to pure states via the Majorana representation, one is immediately led to the simplest idea of how to generate RM states: they correspond to sets of random points on $\mathcal{S}_2$. Interestingly, the question of distributing points uniformly over a sphere has inspired substantial mathematical research [65–67], as has the question of random polynomials [68–71], in addition to attracting the attention of physicists working in a variety of fields.

We randomize each of the spherical coordinates (θ_i, ϕ_i) independently using the Haar measure $\sin\theta_i\,\mathrm{d}\theta_i\,\mathrm{d}\phi_i/4\pi$ for $\mathcal{S}_2$. Equivalently, the resulting RM states can be viewed as arising from the action of a random operator $U \in \mathrm{SU}(2)^{\otimes 2S}$ on the ground state of $2S$ qubits, followed by projection onto the symmetric subspace and normalization. This is fundamentally tied to the most robust deterministic technique for creating arbitrary bipartite states of light, which uses beam splitters and post selection to sequentially add a photon's coordinates on its Poincaré sphere as a new point to a state's existing Majorana constellation [72, 73]. When the states of the single photons are randomized, the resulting state immediately takes the form of equation (2.1) with random spherical coordinates. This basic scheme can then be used to create random states in the light's polarization degree of freedom for tasks like polarimetry.

The intrinsic SU(2) symmetry suggests using the germane notion of multipoles [74, 75] to characterize the resulting states. To this end, we expand the density matrix of the system as

$$\varrho = \sum_{K=0}^{2S}\sum_{q=-K}^{K}\varrho_{Kq}T_{Kq}\,, \tag{3.1}$$

where T_{Kq} are the spherical tensor operators, defined as [75]

$$T_{Kq} = \sqrt{\frac{2K+1}{2S+1}}\sum_{m,m'=-S}^{S} C_{Sm,Kq}^{Sm'}|S,m'\rangle\langle S,m|\,, \tag{3.2}$$

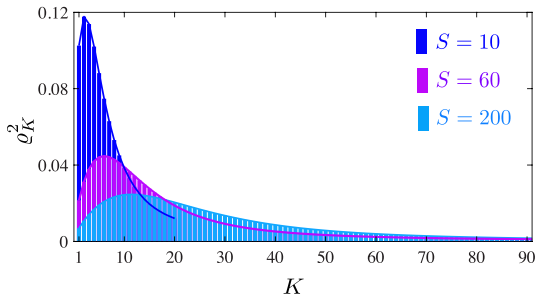

Figure 1. Mutipole distribution ϱ_K^2 for RM states with the values of S indicated in the inset.

with $C^{Sm'}_{Sm,Kq}$ being the Clebsch–Gordan coefficients that couple a spin S and a spin K ($0 \leqslant K \leqslant 2S$) to a total spin S. These tensors are an orthonormal basis

$$\mathrm{Tr}\left(T_{Kq}\, T^{\dagger}_{K'q'}\right) = \delta_{KK'}\delta_{qq'} \tag{3.3}$$

that transform appropriately under rotations $R(\mathbf{\Omega}) \in \mathrm{SU}(2)$:

$$R\left(\mathbf{\Omega}\right)\, T_{Kq}\, R^{\dagger}\left(\mathbf{\Omega}\right) = \sum_{p} D^{S}_{pq}\left(\mathbf{\Omega}\right)\, T_{Kp}\,, \tag{3.4}$$

where $D^{S}_{mn}(\mathbf{\Omega}) = \langle S, m|R(\mathbf{\Omega})|S, n\rangle$ are the usual Wigner D matrices [76].

The expansion coefficients are scalar values that are precisely the state multipoles. Alternatively, they can be computed as [48]

$$\varrho_{Kq} = C_K \int_{\mathcal{S}_2} \mathrm{d}^2\mathbf{n}\, Q_{\varrho}\left(\mathbf{n}\right)\; Y_{Kq}\left(\mathbf{n}\right)\,, \tag{3.5}$$

where C_K is a constant, $Y_{Kq}(\mathbf{n})$ the standard spherical harmonics, and $\mathrm{d}^2\mathbf{n} = \sin\theta \mathrm{d}\theta\mathrm{d}\phi$ the invariant measure on $\mathcal{S}_2$. The multipoles thus appear as the standard ones in electrostatics, but replacing the charge density by $Q_{\varrho}(\mathbf{n})$ and distances by directions [77]. They are the Kth directional moments of the state and, therefore, they resolve progressively finer angular features with increasing K.

Since $Y_{Kq}(\mathbf{n})$ constitute an orthonormal basis on $\mathcal{S}_2$, we can immediately invert equation (3.5):

$$Q_{\varrho}\left(\mathbf{n}\right) = \mathcal{C}_K^{-1} \sum_{Kq} \varrho_{Kq} Y_{Kq}\left(\mathbf{n}\right)\,, \tag{3.6}$$

so the multipoles represent the state's Q distribution on the sphere in its natural basis of spherical harmonics. As the Q function determines the Majorana constellation, these coefficients ϱ_{Kq} can also be directly computed from the constellation, as was recently explained in [78].

For each value of S, we average over 1.5×10^6 samples. In figure 1 we show the resulting multipoles plotted in terms of the multipole squared length

$$\varrho_K^2 = \sum_{q=-K}^{K} |\varrho_{Kq}|^2 \tag{3.7}$$

which are SU(2) invariant and thus serve as an effective tool for studying the states, treating all states related by an SU(2) transformation (a rigid rotation of the constellation) as equivalent. As we can see, only multipoles with small K contribute significantly. The maximally contributing multipole K_{max} smoothly increases with S: a least-squares fitting gives that, for large S, $K_{\mathrm{max}} = a\sqrt{S}$, with $a \simeq 0.8$.

To gain further insight into this behavior, in figure 2 we plot the average multipoles for RM states with $S = 60$. The broken lines delimit the corresponding variances, which are clearly not uniform. Since the individual multipole distributions are non-Gaussian, the variances give only partial information. To complete the picture, in the background we display a density plot representing the number of states with a given value of the Kth multipole. Notice that we use a logarithmic scale in order to better appreciate the behavior of higher Ks, which have exceedingly small values. We see the emergence of a striking multipeaked structure. The multipoles with significant yellow areas (i.e. a strong concentration of samples) are those with less variance.

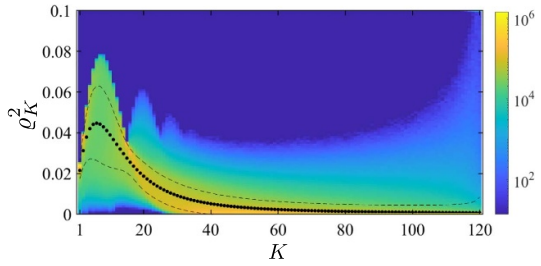

Figure 2. The dots represent the average multipoles for RM states with S 60. The broken lines delimit the associated variances. The density plot in the back (with the logarithmic scale shown at the right) is the number of trials having the corresponding value of the multipole.

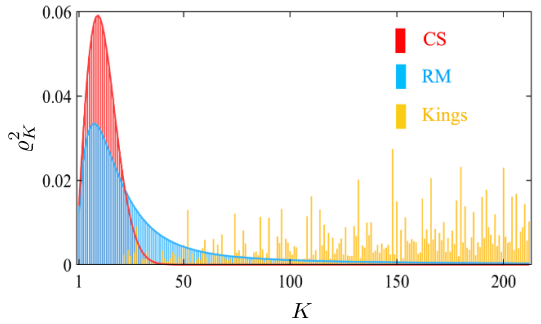

Figure 3. Multipole distribution for CS, RM, and Kings of Quantumness for $S = 106$. The colors in the inset indicate the corresponding states.

One sensible set of quantities in this scenario is the set of cumulative multipole distributions, defined as

$$A_M = \sum_{K=1}^{M} \varrho_K^2 . \tag{3.8}$$

Note that we ignore the 0th multipole as it corresponds only to normalization. For CS this quantity reaches the value

$$A_M^{\mathrm{CS}} = \frac{2S}{2S+1} - \frac{\left[\Gamma\left(2S+1\right)\right]^2}{\Gamma\left(2S-M\right)\Gamma\left(2S+M+2\right)} , \tag{3.9}$$

and it has been proven that this is indeed maximal for every $M \in \{1, \ldots, 2S\}$ [79]. At the opposite extreme we have states whose multipoles vanish up to the highest M: they have been dubbed as Kings of Quantumness [80] and they are maximally unpolarized. For each total spin S, there exists a maximal order M to which a state can be unpolarized; the state(s) satisfying this condition of $A_M = 0$ are the Kings. Therefore, A_M is a good measure of the quantum properties of a state through its *hidden polarization* features [81] that are stored in high-order multipoles.

To appreciate the different behaviors, in figure 3 we have plotted the multipole distributions for the most quantum (Kings of Quantumness), the least quantum (CS), and RM states for $S = 106$. The differences speak for themselves. A RM constellation is markedly different from a classical state: although the maximal contributions arise from roughly the same multipoles for both states (actually, for CS a quick estimate gives $K_{\max} \simeq \sqrt{S} - 1/2$), RM states have much heavier tails, thus hiding their quantum information in higher-order multipoles than CS. This makes them useful for metrological applications, even in the large-S limit, where quantum effects may be expected to vanish. Additionally, such RM states are far from the most quantum states, certifying the rarity of the Kings of Quantumness and the effort required for creating them. This behavior is confirmed by the cumulative multipole distribution A_M for the same states, as plotted in figure 4.

4. Comparison to other random distributions

If a pure state is expressed in the angular momentum basis as $|\psi\rangle = \sum_m \psi_m |S, m\rangle$, one could instead consider states with randomized probability amplitudes ψ_m. This can be achieved with a random unitary

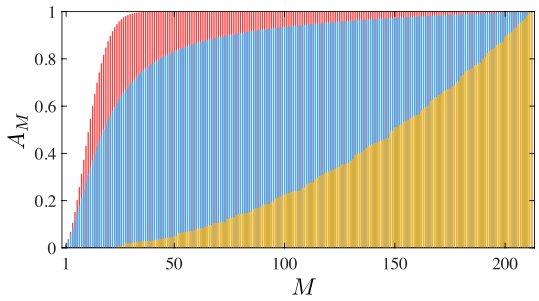

Figure 4. Cumulative multipole distribution for CS, RM, and Kings of Quantumness states for $S = 106$. The colors are the same as in figure 3.

$U \in \mathrm{SU}(2S+1)$ acting on the state, which is often called the circular unitary ensemble (CUE) [4]. These random unitaries were considered in [82] and [37], who found the Rényi–Wehrl entropies of the resulting random CUE states to be highly quantum. Moreover, in [45] it was demonstrated that such random CUE states are useful and robust for metrology.

Actually, we can calculate the expectation value of the cumulative multipole moments $\mathcal{A}_M = \int A_M \, \mathrm{d}U$ for a variety of normalized Haar measures $\mathrm{d}U$, through

$$\mathcal{A}_M = \sum_{K=1}^{M} \sum_{q=-K}^{K} \frac{2K+1}{2S+1} \sum_{m,m'=-S}^{S} C^{Sm+q}_{Sm,Kq} C^{Sm'+q}_{Sm',Kq} I_{m,m',q}, \tag{4.1}$$

with $I_{m,m',q} = \int \psi_{m+q} \psi^*_m \psi^*_{m'+q} \psi_{m'} \mathrm{d}U$, and $C^{Sm}_{S_1 m_1, S_2 m_2}$ the Clebsch–Gordan coefficients [76] that vanish unless the usual angular momentum coupling rules are satisfied: $m_1 + m_2 = m$, $0 \leqslant K \leqslant 2S$, and $-K \leqslant q \leqslant K$.

For example, if we express our random unitaries by $U \in \mathrm{SU}(2S+1)$, these integrals can be obtained exactly using random-matrix theory [83, 84] (see Supplemental Material). But there is another intuitive method: all of the nonzero integrals take the form $\int |\psi_m|^2 |\psi_n|^2 \mathrm{d}U$ and the distribution for each ψ_i is the same, so we know immediately that $I_{m,m',q} \propto \delta_{q,0} + \delta_{m,m'}$, such that

$$\mathcal{A}_{M,\,\mathrm{SU}(2S+1)} = \frac{M(M+2)}{(2S+1)(2S+2)}. \tag{4.2}$$

This means that states with random coefficients ψ_m have $\sum_{q=-K}^{K} |\varrho_{Kq}|^2 \propto 2K+1$, making them much more quantum than RM states and according with other results for this distribution [37, 82]. This is in stark contrast to the notion that both forms of randomness approach each other in the limit of large S in terms of the distance between arbitrary pairs of random states [85], stressing the differences maintained between the forms of randomness for all but $S = 1/2$.

Another possibility of obtaining a random spin-S state is to take a state of $2S$ random qubits. We employ the same procedure as used for the RM, beginning with the $2S$ qubits, but without normalizing the states initially. The resulting state is normalized at the end, ensuring that each state carries a weight proportional to its overlap with the symmetric subspace. This contrasts with the RM, where all states are assigned equal weight. This is not a unitary operation, instead creating the states from equation (2.1) with the replacement of the normalization constant by a state-independent factor $\mathcal{N} \to \sqrt{(2S)!}$, but it facilitates an analytical calculation whose cumbersome expression we show in the Supplemental Material.

Because each state in the ensemble has a different normalization due to having inhomogeneous likelihoods of being produced, the statistical properties derived for them should be understood as being weighted by the probabilities of finding the different projected states. These probabilities are proportional to $\mathcal{N}$ and their normalization can be found from the 0th order multipole. After normalizing the final results, we find that their multipolar distribution is very similar to that of CS. Intuitively, one can conclude that it is far more likely for such a projection method to produce a state close to CS than to produce a highly quantum state. The RM states may be thought of as states randomly chosen after the projection method succeeds, while the projected states are the result of randomization prior to the projection. In other words, if the RM can be thought of as a die with n equally likely sides, the projected states are the same die, but with each side having a different probability.

In figure 5 we display the conspicuous differences between the multipole distributions for these different randomized states.

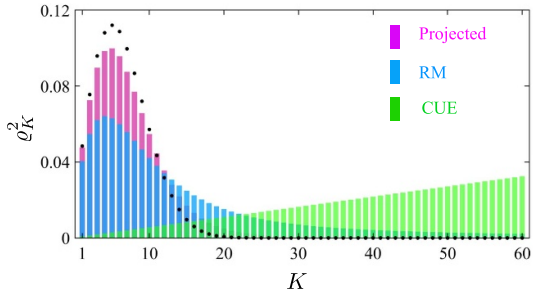

Figure 5. Multipole distribution for RM, CUE, and projected random qubits, all of them for $S = 30$. For comparison, the dots represent the multipoles for a CS.

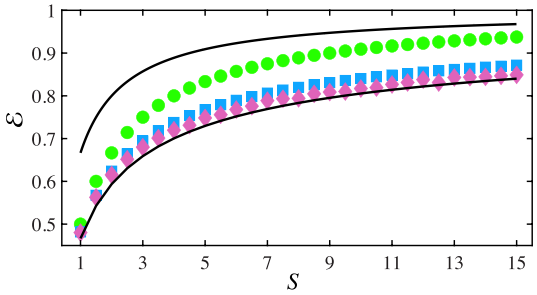

Figure 6. Quantumness $\mathcal{E}$ for the same random states considered in figure 5 as a function of S. The two continuous lines give the limit values of $\mathcal{E}$: the upper one is $2S/(2S+1)$, whereas the lower one corresponds to the CS.

The conclusion from the discussion thus far is that classical states convey their information in lower multipoles, whereas the opposite occurs for extremal quantum states. However, to assess this behavior in a quantitative way, we need a proper measure of quantumness. Since our analysis has been largely based on multipoles, we will use a recent proposal defined precisely in terms of them [86]; viz.,

$$\mathcal{E}(\varrho) = 1 - \sum_{K=0}^{2S} \frac{\varrho_K^2}{2K+1}\,. \tag{4.3}$$

$\mathcal{E}(\rho)$ takes an entanglement monotone for a particular decomposition of Hilbert space, the linear entropy of the pure state when decomposed over the modes $a_{\mathbf{u}}$ and $a_{-\mathbf{u}}$, then averages this over all possible two-mode decompositions that come from rotating the unit vector $\mathbf{u}$. We stress though that this metric is an entanglement monotone only for pure states. Equation (4.3) provides a mode-decomposition-agnostic measure of quantumness that is entanglement averaged over easy-to-perform entangling operations. Larger values of $\mathcal{E}$ signify more quantum states. This quantity emerges when looking at symmetric superpositions of two-mode states: it turns out that they can be entangled or separable, but this property can change after the Majorana constellation undergoes a rigid rotation. To properly account for this possibility, one can consider their linear entropy of entanglement averaged over all rotated partitions of the two-mode Hilbert space: the final result is precisely (4.3).

In figure 6 we calculate this measure for the different states discussed before for various values of S. We see that RM constellations are more quantum than states of random qubits projected onto the symmetric subspace, but less quantum than CUE states with random coefficients in the angular momentum basis. Impressively, the CUE states have $\mathcal{E}_{\rm CUE} = 2S/(2S+2)$ on average, which is very close to the maximum value for a single pure state: $2S/(2S+1)$. The lower continuous line in the figure corresponds to the values of $\mathcal{E}$ for CS, which are the least quantum ones.

This confirms the fact that the overwhelming majority of CUE random states are extremely close to the maximally entangled state [87] and that a significant portion of the RM states are entangled, which seems very counterintuitive. Moreover, we observe that for many functions defined over $\mathcal{H}_S$, the majority of vectors take a value of the function very close to the average value as $S \to \infty$. This observation, collectively, is referred to as the concentration of measure phenomenon [88].

5. Metrology with random states

We look next at the possibility of sensing rotations using random states. A general rotation is characterized by three parameters: the two angular coordinates fixing the rotation axis $\mathbf{u}(\Theta,\Phi)$ and the angle ω rotated around that axis [89]. In the space $\mathcal{H}_S$ the action of this rotation is represented by the operator [90]

$$R(\mathbf{\Omega}) = \exp(i\omega\,\mathbf{S}\cdot\mathbf{u})\,, \tag{5.1}$$

where we have used the notation $\mathbf{\Omega}(\omega,\mathbf{u}) = (\omega,\Theta,\Phi)$ to denote the three parameters and $\mathbf{S}$ is the vector comprising the three components of the angular momentum; the generators of the algebra $\mathfrak{su}(2)$.

The restriction of working in a single irrep is reasonable, since maximal precision will be obtained by concentrating all of the resources into a single subspace corresponding to the average total number of particles. This is true in the local regime, where prior information about the parameter in question is known [91], in sharp contrast to the global regime, where minimum error in estimating a completely unknown parameter requires coherences between irreps [92].

For the time being, we assume the rotation axis $\mathbf{u}$ to be known; the task is thus to estimate the rotation angle ω. A canonical scenario requires ω to be imprinted on a (preferably pure) probe state $|\psi\rangle$, in which the latter is shifted by applying a rotation $R(\omega)\in\mathrm{SU}(2)$ that encodes the angle ω. A set of measurements is then performed on the output state $|\psi_\omega\rangle = R(\omega)|\psi\rangle$, with the measurements represented by a positive operator-valued measure (POVM) [93] $\{\Pi_x\}$, where the POVM elements are labeled by an index x (discrete or continuous) that represents the possible outcomes of the measurement according to Born's rule $p(x|\omega) = \langle\psi_\omega|\Pi_x|\psi_\omega\rangle$. Afterward, what remains is to infer the angle via an estimator $\hat{\omega}$ [94], whose performance is usually assessed in terms of the variance. The ultimate limit for any possible POVM is given by the quantum Cramér–Rao bound (QCRB), which reads [33]

$$\mathrm{Var}_\psi(\hat{\omega}) \geqslant \frac{1}{\nu\,\mathsf{Q}_\psi(\omega)}\,, \tag{5.2}$$

where ν is the number of independent times the experiment is repeated. To assess the ultimate sensitivity per experimental trial, we take henceforth $\nu = 1$. Here, $\mathsf{Q}_\psi(\omega)$ is the quantum Fisher information (QFI), which depends exclusively on the initial probe state. We briefly recall that an explicit way to compute $\mathsf{Q}_\varrho(\omega)$ is as $\mathsf{Q}_\varrho(\omega) = \mathrm{Tr}(\varrho_\omega L_\omega^2)$ and L_ω is the so-called symmetric logarithmic derivative, defined implicitly via [95–97]

$$\frac{\partial\varrho_\omega}{\partial\theta} = \frac{1}{2}\{\varrho_\omega, L_\omega\}\,, \tag{5.3}$$

and $\{\cdot,\cdot\}$ stands for the anticommutator $\{A,B\} = AB + BA$. For pure initial states we have the simple result

$$\mathsf{Q}_\psi(\omega) = 4\,\mathrm{Var}_\psi(\mathbf{S}\cdot\mathbf{u})\,. \tag{5.4}$$

although generalizations to general density matrices are possible [98]. Convexity of the variance is responsible for a single irrep conferring maximal precision per number of particles. The QFI is thus maximal for pure states that maximize the variance of the generator $\mathbf{S}\cdot\mathbf{u}$: these are the states $|\mathbf{u}\rangle + |-\mathbf{u}\rangle)/\sqrt{2}$, which are the rotated versions of the time-honoured NOON states [47], defined as

$$|\mathrm{NOON}\rangle = \frac{1}{\sqrt{2}}(|S,S\rangle + |S,-S\rangle)\,. \tag{5.5}$$

One may be interested in a probe state with the best average performance for any $\mathbf{u}$ rather than creating a distinct state for every axis. To this end, we consider the average QFI defined as

$$\bar{\mathsf{Q}}_\varrho(\omega) = \frac{1}{4\pi}\int_0^\pi \mathrm{d}\Theta\,\sin\Theta\int_0^{2\pi}\mathrm{d}\Phi\,\mathsf{Q}_\varrho(\omega)\,. \tag{5.6}$$

This average has been used in different issues of quantum information [99]. An exemplary context is magnetometry, where the magnitude of the magnetic field being sensed can be more important than its orientation. Then, $\bar{\mathsf{Q}}_\varrho(\omega)$ gives an upper bound on the attainable precision for a quantum state ϱ, if the direction of the magnetic field is chosen randomly based on a uniform distribution.

The maximum average QFI is achieved by states whose angular momentum projection vanishes in all directions; i.e.

$$\mathrm{Tr}(\varrho_\omega\mathbf{S}) = \mathbf{0}\,, \tag{5.7}$$

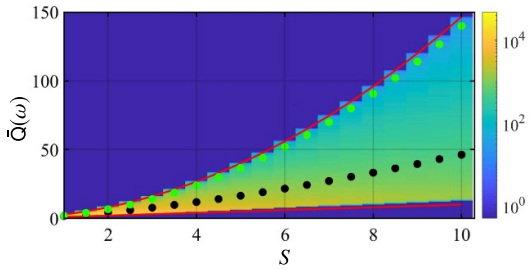

Figure 7. Average QFI as a function of the spin S. The black (green) dots denote the average value (over 60k trials) of the RM (CUE) states. The density plot in the back is the number of trials having the corresponding value of the average QFI for RM. The red lines indicate the maximum and minimum achiveable values of the QFI, corresponding to first-order unpolarized and CS, respectively.

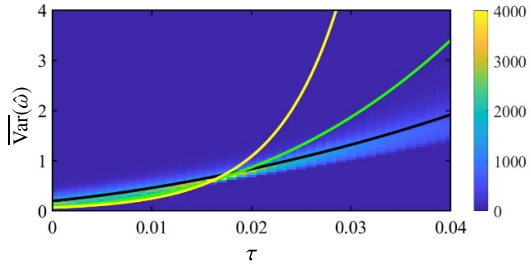

Figure 8. Average variance for RM (black line), CUE (green line) and King of Quantumness (yellow line) states as a function of the dimensionless time $\tau = \gamma t$ when the system experiences dephasing according to the model in equation (5.8). In all cases, $S = 3$. The density plot in the back is the same as in previous plots.

with a maximum value $\bar{\mathsf{Q}}_{\max} = \frac{4}{3}S(S+1)$. They correspond to first-order unpolarized states (which, among others, include the NOON states). In this sense, the most sensitive probe states are those whose classical angular momentum features are hidden [100, 101].

In figure 7 we plot the average $\bar{\mathsf{Q}}_{\varrho}(\omega)$ for both, RM and CUE states as a function of S. We also include the extremal values of this quantity, which are for first-order unpolarized and CS, respectively. The random states always lie in between these two lines, although CUE are closer to optimal. Some of the random states have QFI close to the maximum values, but most of them are concentrated below its average value.

In view of these results, one might wonder about the usefulness of random states. Intuition suggests that they should be more robust against imperfections than very fragile entangled states, as is the case for CUE states with certain types of loss [45]. To confirm this point, let us first consider the case of depolarization. We use the model devised in [102] for an SU(2)-invariant dephasing, which is appropriate for our case. The time evolution of the state is given by

$$\varrho(t) = \exp\left(-2\gamma t \mathbf{S}^2\right) \sum_{n=0}^{\infty} \sum_{j=x,y,z} \frac{(2\gamma t)^n}{n!} S_j^n \varrho(0) S_j^n \,, \tag{5.8}$$

where γ is a constant determining the strength of the dephasing, which we set to 1 without loss of generality. The results of the evolution under this dephasing are summarized in figure 8 for the case of $S = 3$, where we plot the minimum average variance of the angle estimator $\hat{\omega}$ as a function of the dimensionless time evolution (that can be easily converted to, e.g. traveled distance), for RM, CUE, and Kings of Quantumness states. The Kings are the optimal states to sense an arbitrary rotation when quantified by the highest QFI averaged over all rotations and by the lowest inverse QFI when averaged over all rotations [52], and, as expected, are very vulnerable to dephasing, and become much worse than the random, not only in their average values, but for most of their individual trials. Interestingly, RM are more robust than CUE and similar behavior is observed for other dimensions.

We next examine the case where a photon loss occurs. To analyze this scenario, we employ a simple SU(2)-invariant model that consists of mapping each state to an incoherent superposition of the states resulting from the removal of one particle, which in general is a mixed state in the space of spin $S - \frac{1}{2}$. In other words, we create $2S$ states by the removal of each one of the creation operators in equation (2.1) and add them incoherently, to explicitly look at random Majorana constellations that randomly lose a star; this is different from mode-agnostic removal of a particle [103] and is more in line with a preparation error where

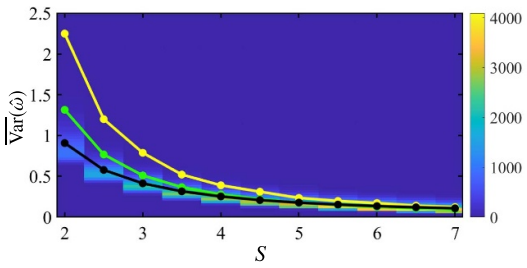

Figure 9. Average variance for RM (black line), CUE (green line) and King of Quantumness (yellow line) states as a function of S after losing one particle. The density plot in the back is the same as in previous plots.

one of the inputs is randomly neglected. The results are shown in figure 9, for the same states as in the previous figure. One can observe that for low S, random states exhibit again a clear advantage over Kings of Quantumness, albeit it diminishes as S increases.

The measurement saturating the QCRB has been characterized [52], but its experimental implementation may be challenging. Easier is to project the rotated state onto a set of coherent states for various directions and to reconstruct the rotation parameters from these measurements. Using the same basic principles applied to geographical positioning systems (GPS) [104], five projections are sufficient for this orientation problem, as has been recently demonstrated [105]. This is particularly useful in the context of random-state metrology, where we seek a single measurement scheme that is useful for all input states; while it cannot generally attain the averaged QFI, due to the QFI allowing for a different measurement for each term being averaged over, it can often perform very well, as demonstrated experimentally below.

6. Experimental results

The results of section 5 suggests that random states should perform well in rotation sensing tasks, in systems with imperfections. Hence, as a last step, we set out to test the suitability of random states for rotation sensing in the laboratory, where experimental imperfections can never be avoided. In these measurements, we used multiple different random states in the GPS-like measurement protocol mentioned above.

In our experimental implementation, we used the transverse-spatial degree of freedom of light. More specifically, we construct our Hilbert space $\mathcal{H}_S$ from a set of Laguerre–Gauss (LG) modes LG_ℓ^p, only choosing modes with a zero radial index $p=0$ and orbital angular momentum indices ℓ corresponding to the m index in the standard angular momentum basis $|S,m\rangle$. This is a standard system for probing SU(2) dynamics, even though it can also be analyzed with classical optics [107]. The beam radius was around 520 μm for the LG modes used to prepare the probe state. For both RM and CUE states, we follow the generation procedure described in sections 3 and 4, respectively, and translate the resulting states to our laboratory encoding using a set of $(2S+1)$ LG modes. We then constructed the rotation $R(\mathbf{\Omega})$, within this Hilbert space, using a multiplane light conversion (MPLC) device [108, 109]. For the measurements, Hilbert spaces with dimensions 5 and 7, corresponding to spins $S=2$ and $S=3$, respectively, were used.

The experimental setup is shown in figure 10 and can be divided into three distinct parts: probe state generation, unitary rotation of the probe state, and measurement of the rotated state. We used a CW laser at roughly 808.4 nm, for all of the measurements. The random probe states were created as coherent superpositions of the chosen set of LG modes by shaping an initial Gaussian field with an amplitude and phase modulating mask [110] on a spatial light modulator (SLM, Holoeye Pluto-2). An additional Gaussian correction was added to the masks [111, 112], and all of the SLMs used in the experiment had an added phase profile for aberration correction that was retrieved using the method introduced in [113].

In the second part of the experimental setup, an MPLC system, with five phase modulations, transforms the probe field according to the rotation transformation $R(\mathbf{\Omega})$. The phase modulations were performed on a single SLM, and each pair of consecutive modulations was separated by 800 mm of free-space propagation. The MPLC device is capable, in principle, of performing an arbitrary unitary mapping between spatial modes [108, 114].

A set of five phase modulating masks had to be designed, through a process called wavefront matching [115], for each of the 10 rotation angles $[(0, 36, \ldots, 324)$ degrees], in both the 5- and 7-dimensional systems. The rotation axis was kept fixed in each dimension. The third and final SLM was used to measure the rotated probe state by projecting it onto a transverse field structure [106].

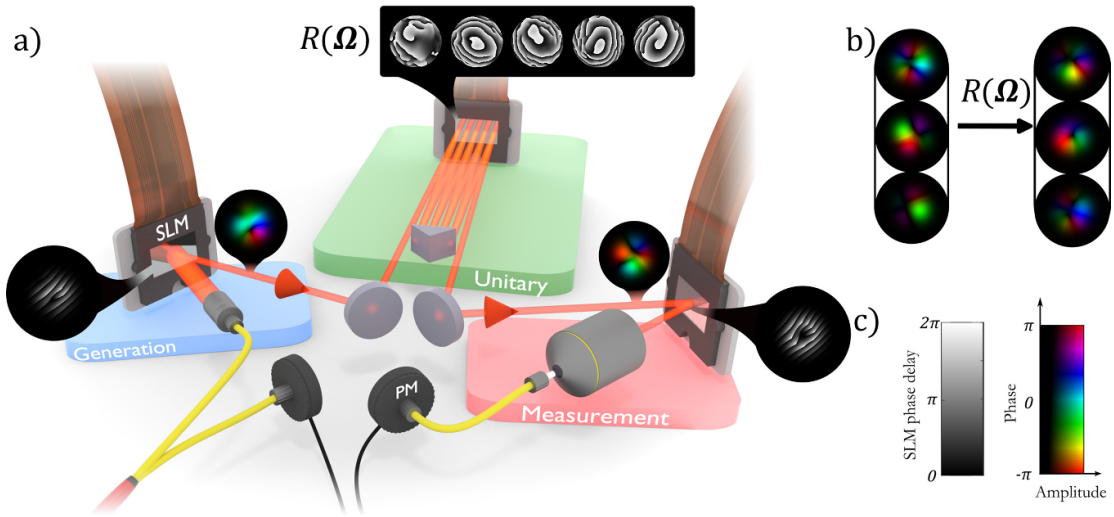

Figure 10. A simplified sketch of the experimental system is shown in (a). The initial laser output is split into two using a fiber beamsplitter with half of its power being directed onto a power meter (PM). The rest is collimated and sent onto the first of three SLMs. The Gaussian beam coming out of the single-mode fiber (SMF, yellow) is shaped into one of the chosen random states by the first SLM. The prepared probe state is then sent to the MPLC device that performs a unitary rotation operation $R(\mathbf{\Omega})$. After the MPLC, the rotated probe state is sent to the third SLM to be measured. The third SLM, together with a final single-mode fiber (SM), perform a projective measurement onto a state by first shaping the phase and amplitude of the beam and then coupling the first diffraction order of the SLM into the SMF using a 10 × microscope objective [106]. Non-magnifying 4*f* lens systems imaging each SLM onto the next one are omitted from the figure. The insets correspond to field structures (in color) and phase mask structures (in gray scale). Colorbars explaining the mode structure and gray-scale colormaps are given in (c). The holographic measurement mask shown in (a) filters for one of the chosen coherent states in the 5-dimensional Hilbert space. The field structure insets in (a) show an example of a state with a randomly distributed Majorana constellation for $S = 2$ and the same transverse field structure after the rotation unitary. In (b), more examples of states with random constellations are shown, along with their rotated counterparts. In the sketch of the experiment, the grating terms have been removed from the phase masks of the unitary and only the field structure at the first-diffraction orders from each phase mask are shown.

To perform the GPS-like measurement mentioned before, we probed each rotated random state $|\psi_{\mathbf{\Omega}}\rangle$ by projecting it onto a set of five coherent states, as described in detail in [105]. The explicit form of the FI matrix for this measurement is computed in [52]. Effectively, our measurements produced the quantities

$$\mathcal{Q}_{\mathbf{n}} = |\langle \mathbf{n}|\psi_{\mathbf{\Omega}}\rangle|^2 = \frac{P_{\langle \mathbf{n}|\psi_{\mathbf{\Omega}}\rangle}}{P_{\langle \psi_{\mathbf{\Omega}}|\psi_{\mathbf{\Omega}}\rangle}} \frac{\eta_{\psi_{\mathbf{\Omega}}}}{\eta_{\mathbf{n}}}, \tag{6.1}$$

where $P_{\langle \mathbf{n}|\psi_{\mathbf{\Omega}}\rangle}$ was the relative power coupled into the final SMF when projecting the rotated random state $|\psi_{\mathbf{\Omega}}\rangle$ onto the coherent state $|\mathbf{n}\rangle$, and $P_{\langle \psi_{\mathbf{\Omega}}|\psi_{\mathbf{\Omega}}\rangle}$ was the power coupled when projecting the rotated random state onto itself. The efficiencies $\eta_{\psi_{\mathbf{\Omega}}}$ and $\eta_{\mathbf{n}}$ are measured estimates of the state-dependent projection efficiencies: $\eta_{\psi_{\mathbf{\Omega}}}$ is the projection efficiency for the rotated random state measurement mask in question and similarly $\eta_{\mathbf{n}}$ is the efficiency of the CS projection.

The projection efficiencies were measured by first shaping the light field to the structure we want to project on in the generation, the MPLC was made to image the field structures, and the power of the field was measured both before the last SLM and after the last fiber. The efficiency was then estimated as the power after the fiber divided by the power before the measurement mask. The power measurements were normalized by dividing them with the power measured before the first spatial mode manipulation, as shown in figure 10. This was done to minimize the effects of changes in laser power throughout the measurements.

As mentioned before, the probe states used in the experiment were both RM and CUE states. In our specific experimental implementation, where transverse spatial modes are used to encode different types of random states, the primary challenge in preparing, modulating, and measuring the states with minimal errors arises from the increasing dimensionality of the state space. This difficulty stems from the increasingly intricate transverse phase and amplitude structures, coupled with the limited resolution of our devices. Consequently, all types of states can be considered equally challenging to work with, regardless of their specific nature.

However, since the difficulty of generating states will vary across different systems, it is essential to weight the ease of generating each type of state against its metrological power. Generally, we anticipate that the more entangled a state is on average, such as CUE or NOON states, the harder it will be to generate them accurately. This suggests that RM states may serve as a valuable and powerful alternative.

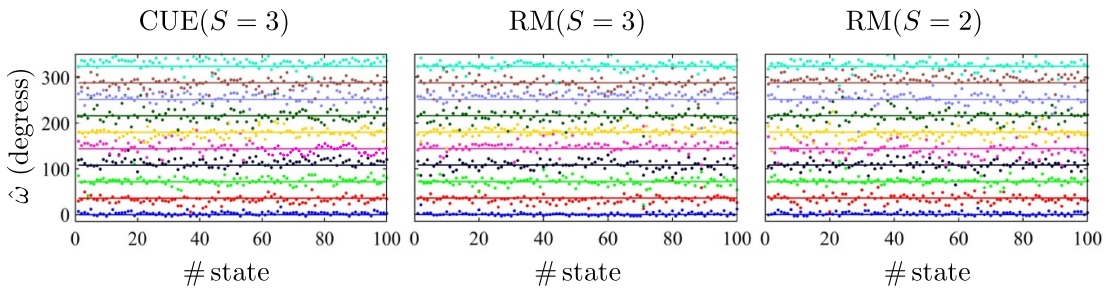

Figure 11. The dots are the estimated values of the rotation angle $\hat{\omega}$ for the CUE and RM states indicated in the upper labels. The horizontal axis labels the 100 random states used in each one of the experiments. The rotation axes used are given in equation (6.2). The true values of ω are $0, 36, \ldots, 324$ degrees and are indicated by horizontal lines.

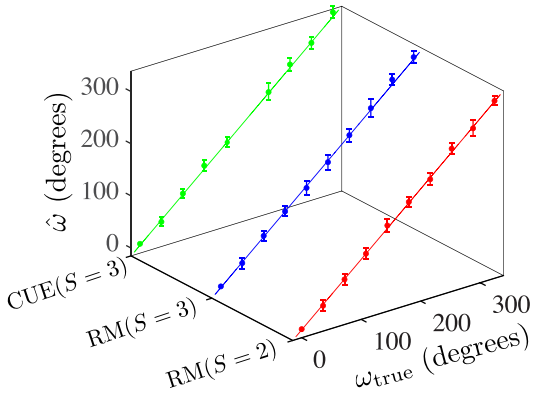

Figure 12. Statistics of the measurement for the states considered before in figure 11. The error bars represent standard deviations. The estimation procedure is local: the same states can be used for estimating a wide range of parameter values, but prior information about those parameters is essential to obtain the sensitivity limits dictated by local estimation theory.

It is important to stress that in our experimental setup there is no need to perform any projection onto the symmetric subspace, as the states are directly generated in $\mathcal{H}_S$. The concept of a symmetric subspace does not apply here, since our $\mathcal{H}_S$ does not originate from $2S$ qubits.

We performed the rotation measurement with 100 different random states of each type, with $\nu = 100$ repetitions of each relative-power measurement. The rotation axis $\mathbf{u}(\Theta, \Phi)$ was arbitrarily chosen for each value of S:

$$\mathbf{u}(\Theta,\Phi) = \begin{cases} \Theta = 34.9674^\circ, \Phi = 296.4448^\circ & S = 2, \\ \Theta = 157.948^\circ, \Phi = 137.361^\circ & S = 3\,. \end{cases} \tag{6.2}$$

Three different kinds of generalized maximum likelihood estimators were formed from this data set to verify the excellent rotational sensitivity of the fiducial states, following standard procedures [116, 117]. The estimator of the rotated angle ω reads

$$\hat{\omega} = \arg\max_{\omega} \sum_{j=1}^{5} \mathfrak{q}_j \log \frac{\mathcal{Q}_j}{\sum_{j'} \mathcal{Q}_{j'}}\,, \tag{6.3}$$

where $\mathfrak{q}_j$ is the measured value of $\mathcal{Q}_j = |\langle \mathbf{n}_j | \psi_{\mathbf{\Omega}} \rangle|^2$. This is equivalent to a quantum measurement where there are five meaningful outcomes, the measurement is repeated ν times, and the frequency with which each outcome occurs is proportional to $\mathfrak{q}_j$. The results appear in figure 11. The estimated values of ω show small fluctuations around the true values with very small typical standard deviations and negligible biases. The three cases look very similar.

To check the quality of our estimators, in figure 12 we have plotted the true values of ω versus the estimated ones. For each estimated point, we have included error bars determined by the corresponding standard deviation. The agreement emphasizes the excellent performance of the method. Moreover, figure 12 corroborates a unique property of random states: due to their typicality [118], they can unambigously

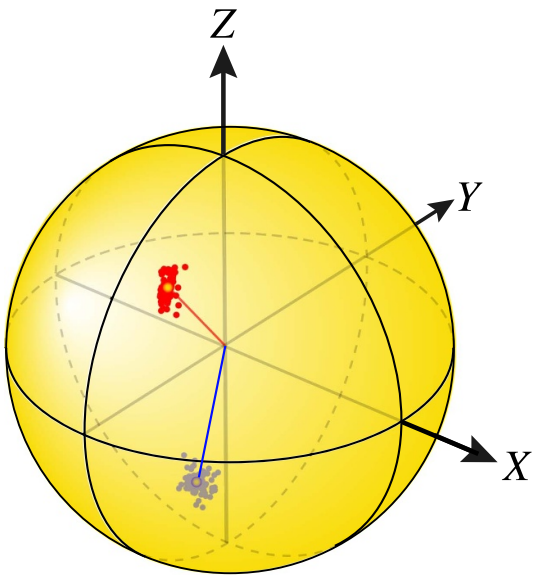

Figure 13. Estimated rotation axes for RM with $S = 2$ (red points) and $S = 3$ (blue points) using the data from figure 11.

estimate any rotation angle within a 2π range. This is in sharp contrast with other states such as NOON or of Quantumness that can distinguish angles within a range $\pi/(2S)$ [80].

Turning the assumptions around, we can take now the set of rotation angles as fixed, while assuming no prior knowledge of the rotation axis. The orientation of this axis can be estimated globally as follows

$$\hat{\mathbf{u}} = \arg\max_{\mathbf{u}} \sum_k \sum_j \mathfrak{q}_{jk} \log \frac{\mathcal{Q}_{jk}}{\sum_{k'} \sum_{j'} \mathcal{Q}_{k'j'}}, \tag{6.4}$$

where now $\mathcal{Q}_{jk} = |\langle \mathbf{n}_j | \psi_{k,\Omega} \rangle|^2$. This time, there is a bigger set of outcomes: each of the five quantum measurement outcomes for each of the rotation angles. Using this on the ensemble of 100 input RM states gives the statistics of inferred axis directions :

$$\hat{\mathbf{u}}(\hat{\Theta}, \hat{\Phi}) = \begin{cases} \hat{\Theta} = 35.31^\circ \pm 4.0^\circ, \hat{\Phi} = 295.8^\circ \pm 2.9^\circ & S = 2, \\ \\ \hat{\Theta} = 138.4^\circ \pm 2.9^\circ, \hat{\Phi} = 157.2^\circ \pm 3.9^\circ & S = 3\,. \end{cases} \tag{6.5}$$

All the target true values are comfortably accommodated within those uncertainty regions. This estimation is nicely visualized on the sphere $\mathcal{S}_2$, as sketched in figure 13. The results for CUE random states are similar, although a bit less reliable due to experimental difficulties in getting the corresponding data.

These values can be compared with the best possible results respectively for the variances of $\hat{\Theta}$ and $\hat{\Phi}$ for a single measurement with a CS, which are (albeit for different orientations of CS)

$$\mathrm{Var}_{\mathrm{CS}}(\hat{\Theta}) = \mathrm{Var}_{\mathrm{CS}}(\hat{\Phi}) = \frac{1}{2S} \tag{6.6}$$

and the variances with Kings of Quantumness

$$\begin{aligned} \mathrm{Var}_{\mathrm{Kings}}(\hat{\Theta}) &= \frac{3}{16S(S+1)\sin^2(\omega/2)}, \\ \mathrm{Var}_{\mathrm{Kings}}(\hat{\Phi}) &= \frac{3}{16S(S+1)\sin^2(\omega/2)\sin^2\Theta}. \end{aligned} \tag{6.7}$$

When performing such a multiparameter estimation, the achievable uncertainties tend to depend on the actual values of the parameters. This dependence can be removed by choosing an appropriate weight matrix for combining the covariances of the different parameters: using the metric tensor for the group as the weight matrix allows all of the results to be independent from the parameter values and the chosen parametrization [119]. As in [105], such a figure of merit when estimating the angular coordinates of a unit vector is

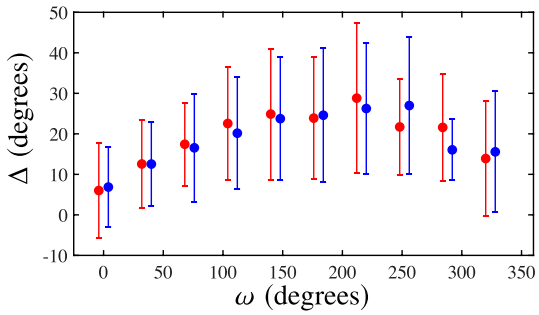

Figure 14. Deviation Δ between the true rotation and the estimated rotation for RM states with $S=2$ (red) and $S=3$ (blue), determined by the angle of rotation one would require to convert between the true and estimated rotation, as a function of the angle. The large error bars on the deviations make these results compatible with both quantum advantages (small deviations) and lack of demonstrated quantum advantages (large deviations); in all cases, the measurement method is demonstrated to be viable for determining all three parameters of a rotation.

$\Delta^2\hat{\Theta}+\sin^2\hat{\Theta}\Delta^2\hat{\Phi}$, here 0.00 488 634 and 0.00 257 369, as compared to the best possible values with a single coherent state of

$$\frac{1}{2S}\frac{2\cos\omega+\csc^2(\omega/2)+2}{2\sqrt{2}\sin\omega+\cos\omega+3}>\frac{0.3758}{2S}\,. \tag{6.8}$$

Finally, our detection scheme projecting onto five coherent states has a redundancy that makes possible to estimate simultaneously the axis of rotation and the angle of rotation. This implies maximizing the objective function

$$\{\hat{\omega},\hat{\mathbf{u}}\}=\arg\max_{\{\omega,\mathbf{u}\}}\sum_{j=1}^{5}\mathfrak{q}_j\log\frac{\mathcal{Q}_j}{\sum_{j'}\mathcal{Q}_{j'}}\,, \tag{6.9}$$

which requires global optimization tools [120]. Again, we are using a classical system to simulate a quantum measurement by taking the frequency of quantum measurement outcomes to be proportional to the relative power received for each of the five settings, then finding the variances of the maximum likelihood estimators that we take to be distributed according to the underlying probability distribution for the true parameters.

Errors of the inferred three parameters of the rotations can be quantified by considering the deviation Δ between the true rotation and the estimated rotation, determined by the angle of rotation one would require to convert between the true and estimated rotation, as $\Delta=\arg R(-\mathbf{\Omega})R(\hat{\mathbf{\Omega}})$, which can be found from the Hilbert-Schmidt norm as $\cos\Delta S+\sin\Delta S/\tan(\Delta/2)=\mathrm{Tr}[R(-\mathbf{\Omega})R(\hat{\mathbf{\Omega}})]$ [105]. This way, we find the average deviations

$$\Delta=\begin{cases}19.3^\circ\pm15.2^\circ & S=2\,,\\ 18.9^\circ\pm15.1^\circ & S=3\,.\end{cases} \tag{6.10}$$

The results are plotted for RM states in figure 14. These can be compared with the best possible results for measurement with a single CS as a probe state, which can never be used to estimate all three parameters of a rotation due to CS only depending on two coordinates that define the state's spin. Comparisons of schemes that split all of the trials into different subsets that each involve the same respective probe state can be found in the recent [121]. This allows us to conclude that the high rotational sensitivity of the RM states has been experimentally verified.

Although in our experiment the rotations have been artificially encoded using an MPLC system, the coherent-state projections used for the detection offer a range of advantages, including compactness, versatility, high efficiency, flexibility, and real-time adaptability. As already demonstrated in [105], this scheme is broad enough to apply to any other rotation-sensing application.

7. Concluding remarks

We have explored random Majorana constellations that arise as sets of points uniformly distributed on the sphere $\mathcal{S}_2$. The concept of state multipoles, intimately linked with the inherent SU(2) symmetry, has served as our main diagnostic tool to capture the amazing properties of these states. Additionally, these multipoles are sensible and experimentally-realizable quantities.

The family of symmetric states contains many metrologically useful states, including GHZ, NOON, and Dicke states, among others. However, all of them are extremely fragile resources. In contradistinction, random Majorana states, from their very same definition, are robust against imperfections such as dephasing and particle losses.

We have experimentally demonstrated the usefulness of these random constellations in protocols of quantum metrology. Apart from their incontestable geometrical beauty, there surely is plenty of room for the application of these states in a variety of physical contexts.

Data availability statement

All data that support the findings of this study are included within the article (and any supplementary files).

Acknowledgments

We are indebted to M Grassl, H Ferretti, A Steinberg, and K Życzkowski for discussions. This work was supported by the European Union's Horizon 2020 research and innovation programme under the QuantERA programme through the Project ApresSF. AZG acknowledges that the NRC headquarters is located on the traditional unceded territory of the Algonquin Anishinaabe and Mohawk people and support from NRC's Quantum Sensors Challenge Program and an NSERC Postdoctoral Fellowship. ABK acknowledges the Mexican CONAHCyT (Grant CBF2023-2024-50). MH acknowledges the Doctoral School of Tampere University, the Magnus Ehrnrooth Foundation, and the Emil Aaltonen Foundation. RF acknowledges support from the Academy of Finland through the Academy Research Fellowship (Decision 332399). ME, MH, RF acknowledge the support of the Academy of Finland through the Photonics Research and Innovation Flagship (PREIN-decision 320165). LLSS acknowledges support from Ministerio de Ciencia e Innovación (Grant PID2021-127781NB-I00).

ORCID iDs

Aaron Z Goldberg https://orcid.org/0000-0002-3301-7672
Jose R Hervas https://orcid.org/0000-0003-4499-7378
Angel S Sanz https://orcid.org/0000-0001-8617-5976
Andrei B Klimov https://orcid.org/0000-0001-8493-721X
Jaroslav Řeháček https://orcid.org/0000-0002-4969-2760
Zdeněk Hradil https://orcid.org/0000-0001-8732-4638
Markus Hiekkamäki https://orcid.org/0000-0002-3496-7338
Matias Eriksson https://orcid.org/0000-0002-3227-8037
Robert Fickler https://orcid.org/0000-0001-6251-753X
Gerd Leuchs https://orcid.org/0000-0003-1967-2766
Luis L Sánchez-Soto https://orcid.org/0000-0002-7441-8632

References

[1] Wigner E P 1955 Characteristic vectors of bordered matrices with infinite dimensions *Ann. Math.* **62** 548
[2] Wigner E P 1967 Random matrices in physics *Soc. Ind. Appl. Math. Rev.* **9** 1
[3] Dyson F J 1962 Statistical theory of the energy levels of complex systems. I *J. Math. Phys.* **3** 140
[4] Dyson F J 1962 Statistical theory of the energy levels of complex systems. II *J. Math. Phys.* **3** 157
[5] Dyson F J 1962 Statistical theory of the energy levels of complex systems. III *J. Math. Phys.* **3** 166
[6] Brody T A, Flores J, French J B, Mello P A, Pandey A and Wong S S M 1981 Random-matrix physics: spectrum and strength fluctuations *Rev. Mod. Phys.* **53** 385
[7] Mehta M L 2004 *Random Matrices* (Elsevier)
[8] Tao T 2012 *Topics in Random Matrix Theory* vol 132 (American Mathematical Society)
[9] Livan G, Novaes M and Vivo P 2018 *Introduction to Random Matrices: Theory and Practice* (Springer)
[10] Page D N 1993 Average entropy of a subsystem *Phys. Rev. Lett.* **71** 1291
[11] Page D N 1993 Information in black hole radiation *Phys. Rev. Lett.* **71** 3743
[12] Sen S 1996 Average entropy of a quantum subsystem *Phys. Rev. Lett.* **77** 1
[13] Renner R and Wang J The black hole information puzzle and the quantum de Finetti theorem 2021 (arXiv:2110.14653 [hep-th])
[14] Francesco P D, Ginsparg P and Zinn-Justin J 1995 2D gravity and random matrices *Phys. Rep.* **254** 1
[15] Bohigas O, Giannoni M J and Schmit C 1984 Characterization of chaotic quantum spectra and universality of level fluctuation laws *Phys. Rev. Lett.* **52** 1
[16] Mello P A 1990 Averages on the unitary group and applications to the problem of disordered conductors *J. Phys. A: Math. Gen.* **23** 4061
[17] Beenakker C W J 1997 Random-matrix theory of quantum transport *Rev. Mod. Phys.* **69** 731
[18] Cugliandolo L F, Kurchan J, Parisi G and Ritort F 1995 Matrix models as solvable glass models *Phys. Rev. Lett.* **74** 1012
[19] Sompolinsky H, Crisanti A and Sommers H J 1988 Chaos in random neural networks *Phys. Rev. Lett.* **61** 259

[20] Wainrib G and Touboul J 2013 Topological and dynamical complexity of random neural networks *Phys. Rev. Lett.* **110** 118101
[21] Bouchaud J and Potters M 2000 *Theory of Finance Risks: From Statistical Physics to Risk Management* (Cambridge University Press)
[22] Collins B and Nechita I 2015 Random matrix techniques in quantum information theory *J. Math. Phys.* **57** 015215
[23] Russell N J, Chakhmakhchyan L, O'Brien J L and Laing A 2017 Direct dialling of Haar random unitary matrices *New J. Phys.* **19** 033007
[24] Boixo S, Isakov S V, Smelyanskiy V N, Babbush R, Ding N, Jiang Z, Bremner M J, Martinis J M and Neven H 2018 Characterizing quantum supremacy in near-term devices *Nat. Phys.* **14** 595
[25] Haake F 1991 *Quantum Signatures of Chaos* (Springer)
[26] Wootters W K 1990 Random quantum states *Found. Phys.* **20** 1365
[27] Hayden P, Leung D, Shor P W and Winter A 2004 Randomizing quantum states: constructions and applications *Commun. Math. Phys.* **250** 371
[28] Życzkowski K, Penson K A, Nechita I and Collins B 2011 Generating random density matrices *J. Math. Phys.* **52** 062201
[29] Bengtsson I and Życzkowski K 2017 *Geometry of Quantum States: an Introduction to Quantum Entanglement* (Cambridge University Press)
[30] Alfsen E M 1963 A simplified constructive proof of the existence and uniqueness of Haar measure *Math. Scand.* **12** 106
[31] Życzkowski K and Kuś M 1994 Random unitary matrices *J. Phys. A: Math. Gen.* **27** 4235
[32] Mielnik B 1968 Geometry of quantum states *Commun. Math. Phys.* **9** 55
[33] Braunstein S L and Caves C M 1994 Statistical distance and the geometry of quantum states *Phys. Rev. Lett.* **72** 3439
[34] Nielsen M A, Dowling M R, Gu M and Doherty A C 2006 Quantum computation as geometry *Science* **311** 1133
[35] Goldberg A Z, Klimov A B, Grassl M, Leuchs G and Sánchez-Soto L L 2020 Extremal quantum states *AVS Quantum Sci.* **2** 044701
[36] Rudziński M, Burchardt A and Życzkowski K 2024 Orthonormal bases of extreme quantumness *Quantum* **8** 1234
[37] Gnutzmann S and Życzkowski K 2001 Rényi-Wehrl entropies as measures of localization in phase space *J. Phys. A: Math. Gen.* **34** 10123
[38] Wobst A, Ingold G-L, Hänggi P and Weinmann D 2003 Phase-space signatures of the Anderson transition *Phys. Rev.* B **68** 085103
[39] Marian P and Marian T A 2020 A geometric measure of non-classicality *Phys. Scr.* **95** 054005
[40] Ganczarek W, Kuś M and Życzkowski K 2012 Barycentric measure of quantum entanglement *Phys. Rev.* A **85** 032314
[41] Majorana E 1932 Atomi orientati in campo magnetico variabile *Nuovo Cimento* **9** 43
[42] Hyllus P, Gühne O and Smerzi A 2010 Not all pure entangled states are useful for sub-shot-noise interferometry *Phys. Rev.* A **82** 012337
[43] Benatti F and Braun D 2013 Sub–shot-noise sensitivities without entanglement *Phys. Rev.* A **87** 012340
[44] Apellaniz I, Lücke B, Peise J, Klempt C and Tóth G 2015 Detecting metrologically useful entanglement in the vicinity of Dicke states *New J. Phys.* **17** 083027
[45] Oszmaniec M, Augusiak R, Gogolin C, Kołodyński J, Acín A and Lewenstein M 2016 Random bosonic states for robust quantum metrology *Phys. Rev.* X **6** 041044
[46] Greenberger D M, Horne M A and Zeilinger A 1989 *Going Beyond Bell's Theorem* (Springer) pp 69–72
[47] Dowling J P 2008 Quantum optical metrology–the lowdown on high-N00N states *Contemp. Phys.* **49** 125
[48] Bouchard F *et al* 2017 Quantum metrology at the limit with extremal Majorana constellations *Optica* **4** 1429
[49] Chryssomalakos C and Hernández-Coronado H 2017 Optimal quantum rotosensors *Phys. Rev.* A **95** 052125
[50] Goldberg A Z and James D F V 2018 Quantum-limited Euler angle measurements using anticoherent states *Phys. Rev.* A **98** 032113
[51] Martin J, Weigert S and Giraud O 2020 Optimal detection of rotations about unknown axes by coherent and anticoherent states *Quantum* **4** 285
[52] Goldberg A Z, Klimov A B, Leuchs G and Sánchez-Soto L L 2021 Rotation sensing at the ultimate limit *J. Phys: Photon.* **3** 022008
[53] Schwinger J 1965 On angular momentum *Quantum Theory of Angular Momentum* ed L C Biedenharn and H Dam (Academic)
[54] Chaturvedi S, Marmo G, Mukunda N, SIMON R and ZAMPINI A 2006 The Schwinger representation of a group: concept and applications *Rev. Math. Phys.* **18** 887
[55] Liu H D and Fu L B 2014 Representation of Berry phase by the trajectories of Majorana stars *Phys. Rev. Lett.* **113** 240403
[56] Perelomov A 1986 *Generalized Coherent States and Their Applications* (Springer)
[57] Husimi K 1940 Some formal properties of the density matrix *Proc. Phys. Math. Soc. Japan* **22** 264
[58] Goldberg A Z 2019 Quantum theory of polarimetry: from quantum operations to Mueller matrices *Phys. Rev. Res.* **2** 023038
[59] Lian B, Ho T-L and Zhai H 2012 Searching for non-Abelian phases in the Bose-Einstein condensate of dysprosium *Phys. Rev.* A **85** 051606
[60] Cui X, Lian B, Ho T-L, Lev B L and Zhai H 2013 Synthetic gauge field with highly magnetic lanthanide atoms *Phys. Rev.* A **88** 011601
[61] Hannay J H 1998 The Majorana representation of polarization and the Berry phase of light *J. Mod. Opt.* **45** 1001
[62] Hannay J H 1998 The Berry phase for spin in the Majorana representation *J. Phys. A: Math. Gen.* **31** L53
[63] Bruno P 2012 Quantum geometric phase in Majorana's stellar representation: mapping onto a many-body Aharonov-Bohm phase *Phys. Rev. Lett.* **108** 240402
[64] Liu H D and Fu L B 2016 Berry phase and quantum entanglement in Majorana's stellar representation *Phys. Rev.* A **94** 022123
[65] Saff E B and Kuijlaars A B J 1997 Distributing many points on a sphere *Math. Intell.* **19** 5
[66] Brauchart J S and Grabner P J 2015 Distributing many points on spheres: minimal energy and designs *J. Complexity* **31** 293
[67] Alishahi K and Zamani M 2015 The spherical ensemble and uniform distribution of points on the sphere *Electron. J. Probab.* **20** 1
[68] Bharucha-Reid A T and Sambandham M 1986 *Random Polynomials* (Academic)
[69] Hannay J H 1996 Chaotic analytic zero points: exact statistics for those of a random spin state *J. Phys. A: Math. Gen.* **29** L101
[70] Prosen T 1996 Exact statistics of complex zeros for Gaussian random polynomials with real coefficients *J. Phys. A: Math. Gen.* **29** 4417
[71] Bogomolny E, Bohigas O and Leboeuf P 1996 Quantum chaotic dynamics and random polynomials *J. Stat. Phys.* **85** 639
[72] Fiurasek J 2002 Conditional generation of *n*-photon entangled states of light *Phys. Rev.* A **65** 053818
[73] Kok P, Lee H and Dowling J P 2002 Creation of large-photon-number path entanglement conditioned on photodetection *Phys. Rev.* A **65** 052104
[74] Fano U and Racah G 1959 *Irreducible Tensorial Sets* (Academic)
[75] Blum K 1981 *Density Matrix Theory and Applications* (Plenum)
[76] Varshalovich D A, Moskalev A N and Khersonski V K 1988 *Quantum Theory of Angular Momentum* (World Scientific)
[77] Jackson J D 1999 *Classical Electrodynamics* 3rd edn (Wiley)

[78] Romero J L, Klimov A B, Goldberg A Z, Leuchs G and Sánchez-Soto L L 2024 Multipoles from Majorana constellations *Phys. Rev.* A **109** 012214
[79] Björk G, Klimov A B, de la Hoz P, Grassl M, Leuchs G and Sánchez-Soto L L 2015 Extremal quantum states and their Majorana constellations *Phys. Rev.* A **92** 031801
[80] Björk G, Grassl M, de la Hoz P, Leuchs G and Sánchez-Soto L L 2015 Stars of the quantum Universe: extremal constellations on the Poincaré sphere *Phys. Scr.* **90** 108008
[81] Klyshko D 1992 Multiphoton interference and polarization effects *Phys. Lett.* A **163** 349
[82] Słomczyński W and Życzkowski K 1998 Mean dynamical entropy of quantum maps on the sphere diverges in the semiclassical limit *Phys. Rev. Lett.* **80** 1880
[83] Weingarten D 1978 Asymptotic behavior of group integrals in the limit of infinite rank *J. Math. Phys.* **19** 999
[84] Gorin T and López G V 2008 Monomial integrals on the classical groups *J. Math. Phys.* **49** 013503
[85] Życzkowski K and Slomczynski W 2001 The Monge metric on the sphere and geometry of quantum states *J. Phys. A: Math. Gen.* **34** 6689
[86] Goldberg A Z, Grassl M, Leuchs G and Sánchez-Soto L L 2021 Quantumness beyond entanglement: the case of symmetric states *Phys. Rev.* A **105** 022433
[87] Hayden P, Leung D W and Winter A 2006 Aspects of generic entanglement *Commun. Math. Phys.* **265** 95
[88] Singh U, Zhang L and Pati A K 2016 Average coherence and its typicality for random pure states *Phys. Rev.* A **93** 032125
[89] Grafarend E W and Kühnel W 2011 A minimal atlas for the rotation group so(3) *Int. J. Geomath.* **2** 113
[90] Cornwell J F 1984 *Group Theory in Physics* vol II (Academic)
[91] Kolenderski P and Demkowicz-Dobrzanski R 2008 Optimal state for keeping reference frames aligned and the platonic solids *Phys. Rev.* A **78** 052333
[92] Chiribella G, D'Ariano G M, Perinotti P and Sacchi M F 2004 Efficient use of quantum resources for the transmission of a reference frame *Phys. Rev. Lett.* **93** 180503
[93] Helstrom C W 1976 *Quantum Detection and Estimation Theory* (Academic)
[94] Kay S M 1993 *Fundamentals of Statistical Signal Processing* vol 1 (Prentice Hall)
[95] Szczykulska M, Baumgratz T and Datta A 2016 Multi-parameter quantum metrology *Adv. Phys.* X **1** 621
[96] Sidhu J S and Kok P 2020 Geometric perspective on quantum parameter estimation *AVS Quantum Sci.* **2** 014701
[97] Albarelli F, Barbieri M, Genoni M G and Gianani I 2020 A perspective on multiparameter quantum metrology: from theoretical tools to applications in quantum imaging *Phys. Lett.* A **384** 126311
[98] Fiderer L J, Fraïsse J M E and Braun D 2019 Maximal quantum Fisher information for mixed states *Phys. Rev. Lett.* **123** 250502
[99] Tóth G and Apellaniz I 2014 Quantum metrology from a quantum information science perspective *J. Phys. A: Math. Theor.* **47** 424006
[100] Goldberg A Z, de la Hoz P, Björk G, Klimov A B, Grassl M, Leuchs G and Sánchez-Soto L L 2020 Quantum concepts in optical polarization *Adv. Opt. Photon.* **13** 1
[101] Serrano-Ensástiga E, Chryssomalakos C and Martin J 2024 Quantum metrology of rotations with mixed spin states (arXiv:2404.15548)
[102] Rivas A and Luis A 2013 SU(2)-invariant depolarization of quantum states of light *Phys. Rev.* A **88** 052120
[103] Goldberg A Z 2024 Correlations for subsets of particles in symmetric states: what photons are doing within a beam of light when the rest are ignored *Opt. Quantum* **2** 14
[104] Hofmann-Wellenhof B, Lichtenegger H and Collins J 2001 *Global Positioning System* (Springer)
[105] Eriksson M, Goldberg A Z, Hiekkamäki M, Bouchard F, Rehacek J, Hradil Z, Leuchs G, Fickler R and Sánchez-Soto L L 2023 Sensing rotations with multiplane light conversion *Phys. Rev. Appl.* **20** 024052
[106] Bouchard F, Valencia N H, Brandt F, Fickler R, Huber M and Malik M 2018 Measuring azimuthal and radial modes of photons *Opt. Express* **26** 31925
[107] D'Ambrosio V, Spagnolo N, Del Re L, Slussarenko S, Li Y, Kwek L C, Marrucci L, Walborn S P, Aolita L and Sciarrino F 2013 Photonic polarization gears for ultra-sensitive angular measurements *Nat. Commun.* **4** 2432
[108] Morizur J F, Nicholls L, Jian P, Armstrong S, Treps N, Hage B, Hsu M, Bowen W, Janousek J and Bachor H-A 2010 Programmable unitary spatial mode manipulation *J. Opt. Soc. Am.* A **27** 2524
[109] Labroille G, Denolle B, Jian P, Genevaux P, Treps N and Morizur J-F 2014 Efficient and mode selective spatial mode multiplexer based on multi-plane light conversion *Opt. Express* **22** 15599
[110] Bolduc E, Bent N, Santamato E, Karimi E and Boyd R W 2013 Exact solution to simultaneous intensity and phase encryption with a single phase-only hologram *Opt. Lett.* **38** 3546
[111] Plachta S Z D, Hiekkamäki M, Yakaryılmaz A and Fickler R 2022 Quantum advantage using high-dimensional twisted photons as quantum finite automata *Quantum* **6** 752
[112] Hiekkamäki M, Barros R F, Ornigotti M and Fickler R 2022 Observation of the quantum Gouy phase *Nat. Photon.* **16** 1
[113] Jesacher A, Schwaighofer A, Fürhapter S, Maurer C, Bernet S and Ritsch-Marte M 2007 Wavefront correction of spatial light modulators using an optical vortex image *Opt. Express* **15** 5801
[114] Brandt F, Hiekkamäki M, Bouchard F, Huber M and Fickler R 2020 High-dimensional quantum gates using full-field spatial modes of photons *Optica* **7** 98
[115] Fontaine N K, Ryf R, Chen H, Neilson D T, Kim K and Carpenter J 2019 Laguerre-Gaussian mode sorter *Nat. Commun.* **10** 1
[116] Hradil Z, Mogilevtsev D and Řeháček J 2006 Biased tomography schemes: an objective approach *Phys. Rev. Lett.* **96** 230401
[117] Řeháček J, Mogilevtsev D and Hradil Z 2008 Tomography for quantum diagnostics *New J. Phys.* **10** 043022
[118] Garnerone S, de Oliveira T R and Zanardi P 2010 Typicality in random matrix product states *Phys. Rev.* A **81** 032336
[119] Goldberg A Z, Sánchez-Soto L L and Ferretti H 2021 Intrinsic sensitivity limits for multiparameter quantum metrology *Phys. Rev. Lett.* **127** 110501
[120] Horst R and Pardalos P M 1995 *Handbook of Global Optimization* (Springer)
[121] Ferretti H, Batuhan Yilmaz Y, Bonsma-Fisher K, Goldberg A Z, Lupu-Gladstein N, Pang A O T, Rozema L A and Steinberg A M 2024 Generating a 4-photon tetrahedron state: toward simultaneous super-sensitivity to non-commuting rotations *Opt. Quantum* **2** 91

2.3 Project 3: Multi-parameter estimation and super-resolution

The Rayleigh resolution criterion holds notable historical importance in optics and imaging. While its original formulation provides a useful rule, it is crucial to understand that it functions more as a heuristic guideline than as an absolute threshold. The loss of resolution between two point sources is not an abrupt event that occurs upon reaching a specific separation, but a gradual process. Nevertheless, the Rayleigh criterion reveals a fundamental and ineluctable aspect of wave optics: due to the phenomenon of diffraction, as two light sources draw closer, their respective point spread functions (PSFs) begin to overlap, making their "resolution" progressively more difficult.

In its original sense, "resolving," as per the Rayleigh criterion, refers primarily to the ability to discern whether an observation corresponds to a single light source or to two distinct sources. More generally, the problem of characterizing a system composed of two sources can be conceptually divided into two fundamental tasks. Consider an astronomical observation via a telescope, where a region of diffuse light of uncertain origin is perceived. The first task consists of determining the number of sources present in said region. The second, once the number of sources has been established, lies in assigning them coordinates—that is, in locating them spatially. In the context of this thesis, the analysis will focus on the two-source scenario, for which a particularly useful one-dimensional parameterization is given by the separation between them and the position of their centroid, as illustrated in Fig. 2.1.

The first of these tasks, determining the number of sources, falls within the domain of hypothesis testing, an essential discipline in statistical inference. While not addressed in this thesis, it is crucial for making optimal decisions when choosing between alternative hypotheses—in this case, whether there is one source or two. It can be shown mathematically that the difficulty of this decision increases as the sources become closer [226], a fact that represents a mathematical manifestation of the Rayleigh criterion. In the present work, we will assume that this detection stage has already been resolved; that is, we will start from the premise that the presence of two sources has been established, and our objective is their spatial localization.

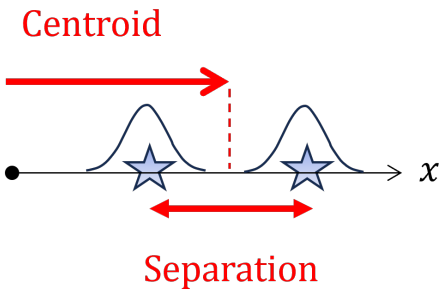

Figure 2.1: Centroid and separation coordinates

Before proceeding, it is worth clarifying two important points. Generally, the Rayleigh criterion is formulated for the case of two incoherent sources of identical intensity, which is the scenario that will be addressed in this work. However, the concept can be generalized to systems with more than two

sources, different degrees of coherence, or unequal intensities.

There is another fundamental subtlety that must be clarified. Suppose an idealized, noise-free scenario where the presence of two sources has been determined and the image observed on a detector is as shown in Fig. 2.2. In such a case, there would be no difficulty in determining the spatial coordinates of the sources. If the shape of the PSF is known—a common assumption—a one-to-one correspondence exists between the observed image and the coordinates of the sources. As illustrated in the figure, only a specific configuration of the model (red dots) exactly reproduces the observed signal. In other words, a one-to-one correspondence would exist between the model and physical reality.

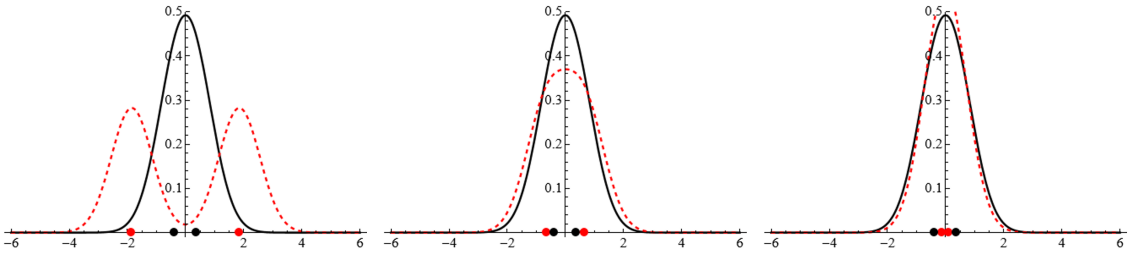

Figure 2.2: Comparison of an observed intensity profile (solid black line) with a theoretical model (dashed red line). Black dots on the x-axis mark the true source positions, while red dots mark the positions assumed by the model.

However, this idealized scenario ignores an ineluctable element: noise. In a real experimental situation, the presence of noise, as shown in Fig. 2.3, precludes this direct, one-to-one inversion. In this work, we will consider a fundamental source of noise: photon shot noise. This means that technical noise sources, such as electronic noise, are disregarded, and only the randomness inherent in the corpuscular nature of light is considered.

Analogously to the difficulty in choosing between the two hypotheses, it can be shown mathematically that the precision in estimating the separation, in the presence of photon shot noise, is also compromised as the sources draw closer. The Cramér-Rao bound for the estimation of the separation diverges in this limit, a phenomenon that has been termed the "Rayleigh curse" to distinguish it from the hypothesis testing problem. Formally, this translates to the classical Fisher information $F(\mathfrak{s})$ tending to zero as the separation $\mathfrak{s}$ approaches zero: $F(\mathfrak{s}) \to 0$.

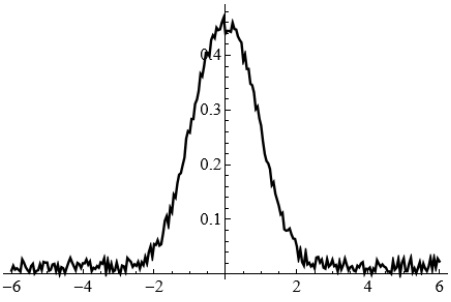

Figure 2.3: Intensity profile for two incoherent sources when noise is present

However, a seminal paper published in 2016 by M. Tsang et al. [227] achieved a significant breakthrough by reconsidering this problem from the perspective of quantum metrology. By treating

light as a quantum system, and under certain assumptions, they demonstrated that, through the use of an optimal measurement, the precision in estimating the separation not only does not degrade but in fact remains constant, regardless of the sources' proximity. This precision is, in fact, equal to that which would be obtained in the ideal classical scenario where the sources are infinitely separated.

$$Q(\rho(\mathfrak{s})) = \text{const} = F(\infty) \tag{2.5}$$

This finding indicates that the "Rayleigh curse" is not an intrinsic limitation of light, but rather an artifact of the conventional detection method. It should be noted that an analysis of the hypothesis testing task from a quantum perspective reveals an analogous phenomenon.

Since its publication, this influential paper has served as a foundation for hundreds of articles that expand on its original ideas, generalize its findings, or explore new facets of the problem. An important observation is that most of these subsequent investigations have predominantly focused on the estimation of the separation, often assuming the centroid's position to be already determined. However, in a realistic scenario, both parameters—separation and centroid—are, in general, unknown and must be estimated simultaneously.

The present work builds upon previous attempts, which were primarily numerical, aimed at determining the optimal measurement strategies for the joint estimation of both parameters. The core contribution of this research is the derivation of analytical expressions for these optimal measurements, capable of simultaneously extracting the maximum possible information about both the separation and the centroid. Furthermore, these measurements offer the advantage of being tunable, allowing for the prioritization of information extraction for one parameter over the other, depending on experimental requirements. Moreover, their dependence on a free parameter renders them non-unique, affording considerable flexibility for their practical implementation.

Optimizing measurement tradeoffs in multiparameter spatial superresolution

J. R. Hervas [1], L. L. Sánchez-Soto [1,2,3], A. Z. Goldberg [4,5], Z. Hradil [6], and J. Řeháček [6]

[1]*Departamento de Óptica, Facultad de Física, Universidad Complutense, 28040 Madrid, Spain*
[2]*Institute for Quantum Studies, Chapman University, Orange, California 92866, USA*
[3]*Max-Planck-Institut für die Physik des Lichts, 91058 Erlangen, Germany*
[4]*National Research Council of Canada, 100 Sussex Drive, Ottawa, Ontario, Canada K1N 5A2*
[5]*Department of Physics, University of Ottawa, 25 Templeton Street, Ottawa, Ontario, Canada K1N 6N5*
[6]*Department of Optics, Palacký University, 17. listopadu 12, 771 46 Olomouc, Czech Republic*

(Received 4 July 2024; accepted 12 September 2024; published 23 September 2024)

The quantum Cramér-Rao bound for the joint estimation of the centroid and the separation between two incoherent point sources cannot be saturated. As such, the optimal measurements for extracting maximal information about both at the same time are not known. In this paper, we ascertain these optimal measurements for an arbitrary point spread function, in the most relevant regime of a small separation between the sources. Our measurement can be adjusted within a set of tradeoffs, allowing more information to be extracted from the separation or the centroid while ensuring that the total information is the maximum possible.

DOI: 10.1103/PhysRevA.110.033716

I. INTRODUCTION

The Rayleigh criterion [1] is a commonly accepted standard that specifies the minimum separation between two incoherent point sources using a linear imaging system. It was widely believed that this represents a fundamental limitation inherent to the nature of light.

Recently, Tsang and co-workers [2–5] challenged this Rayleigh *curse*. They resorted to the concepts of quantum Fisher information (QFI) and the associated Cramér-Rao bound (QCRB) [6] to quantify how well the separation between two point sources can be estimated. When only the intensity at the image is measured, the Fisher information falls to zero as the separation between the sources decreases and the classical Cramér-Rao bound (CCRB) diverges accordingly. However, when the QFI for the complete field is calculated, it stays constant and so does the QCRB. This clearly reveals that the Rayleigh limit is not intrinsic to the problem.

Since then, a plethora of publications have arisen from this idea: experimental implementations [7–12], generalizations [13–21], effects of noise [22–26], and coherence [27–31]. A comprehensive review can be found in Ref. [32] and an updated list of references in Ref. [33].

An optimal method, dubbed spatial mode demultiplexing (SPADE), was designed to estimate the separation between two point sources. This involves passively projecting the collected light onto an orthonormal basis of spatial modes, which is accomplished using a mode-sorting device that couples each spatial mode to a specific intensity-resolving detector. However, SPADE requires prior knowledge of the centroid of these sources and the alignment of the device with the centroid [2,34]. This prior information can be easily obtained because direct imaging is accurate in estimating the centroid. An adaptive two-stage detection scheme that dynamically allocates the resources between the centroid estimation and the separation estimation has been proposed [35], demonstrating that it still outperforms direct imaging. The impact of misalignment on separation estimation has been also considered [36].

At a fundamental level, this is a multiparameter problem. It is well known that in this scenario the QCRB suffers from the incompatibility issue of quantum measurements [37–43]. It has been noticed [44] that the optimal measurements for individually estimating the centroid and the separation of two incoherent point sources are maximally incompatible. Actually, reaching the quantum limit in one, inevitably, reduces the information of the other to zero [45].

However, this does not prevent one from a joint estimation of both quantities: It is possible to achieve acceptable performance in both variables without necessarily reaching the quantum limit in either. In Ref. [46], the authors numerically pursued optimal measurements that approached the tradeoff relation and came remarkably close to achieving it. In the same vein, Ref. [47] proposed an adaptive sequential protocol that uses optimal measurements (that have to be found numerically) to simultaneously estimate both parameters.

In this paper, which serves as a seamless extension of preceding efforts, we analytically demonstrate the ideal measurement strategy as the sources get very close. This strategy hinges on a parameter whose manipulation enables us to glean enhanced insights from both centroid and separation metrics. In this way, we saturate the tradeoff relation and extract the maximum possible information from the two variables at the same time.

This paper is organized as follows. In Sec. II, we describe the mathematical formulation of our estimation problem. In Sec. III, we derive our measurement scheme and demonstrate that the centroid and the separation can, in principle, be estimated simultaneously. Section IV studies the performance of our scheme for the relevant case of a Gaussian point spread function (PSF), showing that the measurements works over a wide range of separations. Finally, our conclusions are summarized in Sec. V.

II. MODEL AND ASSOCIATED MULTIPARAMETER CRAMÉR-RAO BOUND

We assume quasimonochromatic paraxial waves with one specified polarization and one spatial dimension x denoting the image-plane coordinate. For a linear spatially invariant system the corresponding object-plane coordinates can be obtained via the lateral magnification, which we take as unity without loss of generality.

We phrase what follows in a quantum notation that will facilitate the calculations. A wave of complex amplitude $U(x) \in L^2(\mathbb{R})$ can then be assigned to a ket $|U\rangle$, in such a way that $U(x) = \langle x|U\rangle$, with $|x\rangle$ representing an ideal point source localized exactly at x.

The normalized amplitude response of the system to a point source will be denoted by $\Psi(x) = \langle x|\Psi\rangle$. The corresponding intensity response, usually called the point spread function (PSF) [48], can thus be written as $I(x) = |\Psi(x)|^2$.

Two point sources of equal intensities and separated by a distance $\mathfrak{s}$ are imaged by that system. Since they are incoherent with respect to each other, the total signal must be written as a density operator

$$\varrho_{\mathfrak{s}} = \tfrac{1}{2}(\varrho_+ + \varrho_-), \tag{2.1}$$

where the total intensity is normalized to unity. The individual components $\varrho_\pm = |\Psi_\pm\rangle\langle\Psi_\pm|$ are just x-displaced PSF states, that is, $\langle x|\Psi_\pm\rangle = \langle x - \mathfrak{s}_0 \mp \mathfrak{s}/2|\Psi\rangle$, so that they are symmetrically located around the position of the geometric centroid $\mathfrak{s}_0$. If we recall that the momentum operator (which in the x representation acts as a derivative $P \mapsto -i\partial_x$) generates displacements in the x variable, we can write

$$|\Psi_\pm\rangle = \exp[-i(\mathfrak{s}_0 \pm \mathfrak{s}/2)P]|\Psi\rangle. \tag{2.2}$$

The density matrix (2.1) depends on both the centroid $\mathfrak{s}_0$ and the separation $\mathfrak{s}$. This is indicated by the vector $\boldsymbol{\mathfrak{s}} = (\mathfrak{s}_0, \mathfrak{s})^\top$. Our task is to estimate the values of $\boldsymbol{\mathfrak{s}}$ from the outcomes of some measurement performed on $\varrho_{\boldsymbol{\mathfrak{s}}}$.

Let us assume a real and symmetric PSF. This implies that $\langle\Psi|\,P^{2n+1}\,|\Psi\rangle = 0$ and we denote $\wp_{2n} = \langle\Psi|\,P^{2n}\,|\Psi\rangle$ for $n = 0, 1, \ldots$. Our first step is to define an orthonormal computational basis: This can be achieved by orthonormalizing the PSF state and its successive derivatives [13]. For our purposes here, we consider only the first three elements of that basis, all centered at an educated guess $\hat{\mathfrak{s}}_0$ for the centroid $|\Psi_{\mathfrak{s}_0}\rangle = \exp(-i\hat{\mathfrak{s}}_0 P)\,|\Psi\rangle$:

$$\begin{aligned}
|\Phi_1\rangle &= \left|\Psi_{\hat{\mathfrak{s}}_0}\right\rangle, \\
|\Phi_2\rangle &= -\frac{i}{\sqrt{\wp_2}}\,P\left|\Psi_{\hat{\mathfrak{s}}_0}\right\rangle, \\
|\Phi_3\rangle &= \frac{1}{\sqrt{\wp_4 - \wp_2^2}}(\wp_2 - P^2)\left|\Psi_{\hat{\mathfrak{s}}_0}\right\rangle.
\end{aligned} \tag{2.3}$$

Next, we construct an optimal positive operator-valued measure (POVM) [49]. Since we need to simultaneously estimate two parameters, the optimal POVM must contain three outputs (the third one to ensure normalization). To this end, we introduce two vectors using a set of real-valued parameters a_j, b_j and making one vector orthogonal to the signal PSF state:

$$\begin{aligned}
|\pi_1\rangle &= a_2\,|\Phi_2\rangle + a_3\,|\Phi_3\rangle\,, \\
|\pi_2\rangle &= b_1\,|\Phi_1\rangle + b_2\,|\Phi_2\rangle + b_3\,|\Phi_3\rangle\,.
\end{aligned} \tag{2.4}$$

Then a family of three-element POVMs is designed as follows:

$$\Pi_1 = |\pi_1\rangle\langle\pi_1|\,, \quad \Pi_2 = |\pi_2\rangle\langle\pi_2|\,, \quad \Pi_3 = 1 - \Pi_1 - \Pi_2. \tag{2.5}$$

As we shall see in Sec. III, the coefficients a_j and b_j have to be properly chosen in order to optimize the POVM.

Since our goal is to estimate small deviations of the signal state $\varrho_{\mathfrak{s}}$ from the nominal PSF state $|\Psi\rangle\langle\Psi|$, we expand the signal state components in the small quantities $\delta_\pm = \mathfrak{x}_0 \pm \mathfrak{s}/2$,

$$|\Psi_\pm\rangle \approx \left(1 - i\delta_\pm P - \frac{1}{2}\delta_\pm^2 P^2 + \frac{i}{6}\delta_\pm^3 P^3\right)\left|\Psi_{\hat{\mathfrak{s}}_0}\right\rangle, \tag{2.6}$$

where $\mathfrak{x}_0 = (\mathfrak{s}_0 - \hat{\mathfrak{s}}_0)$ is the small deviation between the initial guess and the true centroid. This makes it possible to compute the probabilities $p(j|\boldsymbol{\mathfrak{s}}) = \mathrm{Tr}(\varrho_{\boldsymbol{\mathfrak{s}}}\Pi_j)$ of observing Π_j for true signal parameters $\boldsymbol{\mathfrak{s}}$. From these probabilities we can calculate the classical Fisher information (CFI) matrix associated to this measurement. The calculations are straightforward and we get

$$\begin{aligned}
&\mathsf{F}(\boldsymbol{\mathfrak{s}}) \\
&= \begin{pmatrix}
4\wp_2\left(\varepsilon_{\mathfrak{s}_0}^2 + \dfrac{\varepsilon_{\mathfrak{s}}^2}{1+\mathfrak{r}}\right) + \mathcal{O}(\mathfrak{s}^2) & \dfrac{4\varepsilon_{\mathfrak{s}}^2}{4\mathfrak{r} + 1/\mathfrak{r}} + \mathcal{O}(\mathfrak{s}) \\
\dfrac{4\varepsilon_{\mathfrak{s}}^2}{4\mathfrak{r} + 1/\mathfrak{r}} + \mathcal{O}(\mathfrak{s}) & \wp_2\,\varepsilon_{\mathfrak{s}}^2\dfrac{\mathfrak{r}}{1+\mathfrak{r}} + \mathcal{O}(\mathfrak{s}^2)
\end{pmatrix},
\end{aligned} \tag{2.7}$$

where we have enforced $a_2, b_1, b_2 > 0$ and the parameters

$$\varepsilon_{\mathfrak{s}}^2 = a_2^2, \quad \varepsilon_{\mathfrak{s}_0}^2 = \frac{b_2^2}{1 - b_1^2}, \quad \varepsilon_{\mathfrak{s}}^2, \varepsilon_{\mathfrak{s}_0}^2 \leqslant 1. \tag{2.8}$$

We also set

$$\mathfrak{r} = \frac{1}{4}\frac{\mathfrak{s}^2}{\mathfrak{x}_0^2}. \tag{2.9}$$

Similar to the intuition from postselected metrology [50], quantum measurements effectively allow one to zoom in on a parameter range and there obtain enhanced sensitivity; this

means, to harness the advantages, one must have prior information about the region to magnify, so we henceforth consider $\mathfrak{r} \gg 1$. This allows us to consider the CCRB,

$$\mathsf{C}(\hat{\mathfrak{s}}) \succcurlyeq \mathsf{F}^{-1}(\mathfrak{s}), \tag{2.10}$$

where the matrix inequality $\mathsf{A} \succcurlyeq \mathsf{B}$ means that $\mathsf{A} - \mathsf{B}$ is a positive semidefinite matrix. Here, $\mathsf{C}_\Psi(\hat{\mathfrak{s}})$ is the covariance matrix of the unbiased estimator $\hat{\mathfrak{s}}$.

In quantum estimation theory, we often consider the QFI matrix instead of the classical version to evaluate the error bound. It is known that the $\mathsf{F}(\mathfrak{s})$ for a given measurement scheme is bounded from above by the QFI matrix $\mathsf{Q}(\mathfrak{s})$, that is

$$\mathsf{F}(\mathfrak{s}) \preccurlyeq \mathsf{Q}(\mathfrak{s}). \tag{2.11}$$

If there exists a measurement that achieves the upper bound in (2.11), it is the optimal measurement. As a rank-2 state [51], elements of the QFI can be found analytically from the purity of the state and the variance of P, giving

$$\begin{aligned}\mathsf{Q}_{\mathfrak{s}_0\mathfrak{s}_0} &= 4[\wp_2 - |\langle\Psi_+|\Psi_-\rangle|^2(1 - |\langle\Psi_+|\Psi_-\rangle|^2)/4] \\ &\approx 4\wp_2(1 - \mathfrak{s}^2/4).\end{aligned} \tag{2.12}$$

By convexity properties of the QFI and its further relation to variances [52], we can immediately bound $\mathsf{Q}_{\mathfrak{s}\mathfrak{s}} \leqslant \wp_2$. In our case, since our CFI matrix is diagonal as $\mathfrak{r} \to \infty$ and $\mathfrak{s} \to 0$, we have

$$\mathsf{F}_{jj} = \varepsilon_j^2 \mathsf{Q}_{jj}, \tag{2.13}$$

where the subscript j runs the values $\mathfrak{s}$ and $\mathfrak{s}_0$. The same applies to the inverse diagonal elements of the corresponding inverse matrices, which set the classical and quantum bounds.

III. OPTIMAL MEASUREMENT

Any three-element POVM of the form (2.4) with $a_2, b_1, b_2 > 0$ generates, in the limit of small separations, information about centroid and separation, which differs from the corresponding quantum bounds by constant factors, which amounts to lifting the Rayleigh curse. This can be checked using the explicit form Eq. (2.7).

The next step is optimizing POVM with respect to a_j and b_j. Unfortunately, the obvious choice $a_2 = 1$ and $b_1^2 = 1 - b_2^2$, which (apparently) saturates the QCRB fails, as it is not consistent with Π_3 being positive semidefinite. Considering the projector $A = |\Phi_1\rangle\langle\Phi_1| + |\Phi_2\rangle\langle\Phi_2|$ and imposing $\Pi_3 \geqslant 0$ on this subspace gives

$$1 - \det(A\,\Pi_3\,A) = a_2^2\big(1 - b_1^2\big) + b_1^2 + b_2^2 \leqslant 1. \tag{3.1}$$

Using Eq. (2.8) and rearranging, we get the tradeoff relation

$$\varepsilon_{\mathfrak{s}}^2 + \varepsilon_{\mathfrak{s}_0}^2 \leqslant 1 \tag{3.2}$$

that places limits on how the total information can be distributed between the centroid and separation variables. For example, letting $\varepsilon_{\mathfrak{s}}^2 = \varepsilon_{\mathfrak{s}_0}^2 \leqslant 1/2$, the price to pay for having a "uniform" access to both centroid and separation in a multiparameter estimation amounts to minimally doubling their mean-square errors with respect to single-parameter cases. This is consistent with the tradeoff relation introduced in Ref. [45] for the so-called information regrets, defined as

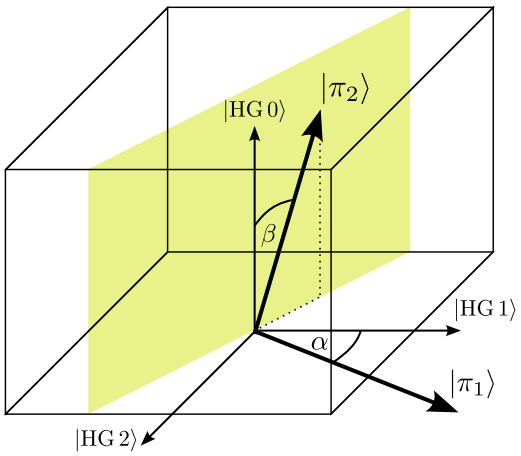

FIG. 1. The geometry of optimal measurements. Aligning modes $|\pi_1\rangle$ or $|\pi_2\rangle$ along any coordinate axis must be avoided to not invalidate the optimality conditions. We denote the axis by $|\mathrm{HG}\,i\rangle$ in reference to the common case of a Gaussian PSF. For non-Gaussian PSFs the HG modes are replaced with the corresponding three lowest-order orthonormalized PSF derivatives $|\Phi_i\rangle$.

$$\Delta_j = \sqrt{\frac{\mathsf{Q}_{jj} - \mathsf{F}_{jj}}{\mathsf{Q}_{jj}}}, \tag{3.3}$$

which in the limit of small separations take the form [46]

$$\Delta_{\mathfrak{s}}^2 + \Delta_{\mathfrak{s}_0}^2 \geqslant 1. \tag{3.4}$$

For our POVM, we have $\Delta_j^2 = 1 - \varepsilon_j^2$, and in the limit of small separation, (3.2) is equivalent to (3.4).

One particular way of saturating those tradeoffs is by choosing

$$|\pi_1\rangle = \begin{pmatrix} 0 \\ \cos\alpha \\ \sin\alpha \end{pmatrix}, \quad |\pi_2\rangle = \begin{pmatrix} \cos\beta \\ \sin\alpha\sin\beta \\ -\cos\alpha\sin\beta \end{pmatrix}, \tag{3.5}$$

so that $\varepsilon_{\mathfrak{s}}^2 = \cos^2\alpha$ and $\varepsilon_{\mathfrak{s}_0}^2 = \sin^2\alpha$, ensuring we have explicitly found the best measurement possible for very small separations—the only interesting regime.

Visualizing $|\pi_1\rangle$ and $|\pi_2\rangle$ as vectors in a real three-dimensional (3D) space, whose z, x, and y coordinates (in this order) are given by the coefficients a_ℓ and b_ℓ ($\ell \in \{1, 2, 3\}$) as in Eq. (2.4), the states on which to project are as follows: $|\pi_1\rangle$ lies in the xy plane making an angle α with the x axis. This angle α determines how the information is distributed between the centroid and the separation estimates according to (3.2). The second projection lies in a plane perpendicular to $|\pi_1\rangle$, while its orientation in this plane, i.e., angle β, can be chosen arbitrarily. This is indicated in Fig. 1. In particular, rotating the POVM so as to move $|\pi_1\rangle$ closer to $|\Phi_1\rangle$ (the first PSF derivative) improves the estimation of separation while moving it closer to $|\Phi_2\rangle$ (the second PSF derivative) improves the estimation of the centroid. In both cases this is at the expense of worsening the estimates of the other variable.

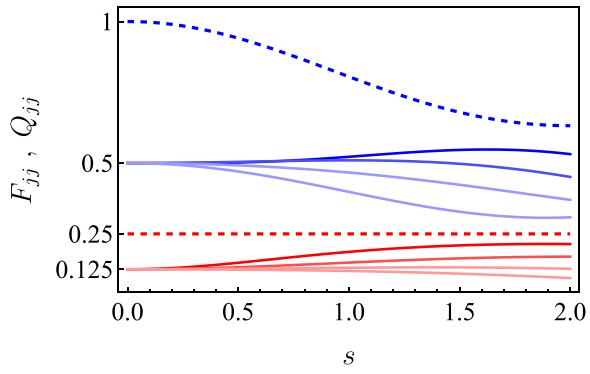

FIG. 2. The diagonal elements of the CFI (solid lines) and the QFI (dashed lines) matrices for the centroid (blue, upper portion of the plot) and the separation (red, lower portion of the plot) variables. The curves correspond to decreasing values of the parameter $\beta = \pi/12, \pi/6, \pi/4, \pi/3$, with the lowest value represented by the uppermost lines in each set.

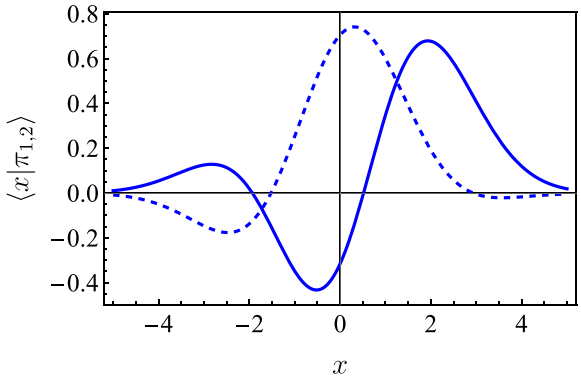

FIG. 3. Optimal measurement modes $|\pi_1\rangle$ (solid) and $|\pi_2\rangle$ (dashed) with $\alpha = \pi/4$ and $\beta = \pi/6$.

IV. GAUSSIAN PSF

The freedom of rotating $|\pi_2\rangle$ about $|\pi_1\rangle$ by (almost) any angle β without compromising the small-separation performance of the optimal POVM is a useful feature. First, projections on some sets of modes may offer easier or more robust implementation in a laboratory and some POVM orientations may be preferred over others for this reason. Second, different settings of β alter the higher-order terms of the CFI matrix expansion. This becomes important when extending the range of metrology to larger separations.

This will be demonstrated with a conceptually simple yet practically important case of a Gaussian PSF of variance σ (which we set to unity without loss of generality):

$$\Psi(x) = \langle x|\Psi\rangle = \frac{1}{(2\pi\sigma^2)^{\frac{1}{4}}} \exp\left(-\frac{x^2}{4\sigma^2}\right). \tag{4.1}$$

Here, the computational basis $|\Phi_j\rangle$, obtained by orthonormalizing $\Psi(x)$ and its successive derivatives, becomes the Hermite-Gauss (HG) modes, which are well-known solutions to the paraxial wave equation commonly used to describe the transverse profile of laser beams [53]. The POVM elements in Fig. 1 are labeled using these modes.

Going for balanced resolutions in both variables, we set $\alpha = \pi/4$ and compare the performances of POVMs with different β settings to their respective quantum limits. The results appear in Fig. 2. For very small separations, the β setting is irrelevant, as we already concluded. Making the separation larger gives a clear advantage to small β values, for which the resolution in separation actually gets close to the quantum limit at some points. Figure 3 provides a visualization of one pair of such optimal modes. There is no point in extending the analysis to even larger separations, because there the two signal components spatially separate, Rayleigh's curse does not apply, and direct intensity detection starts to rule.

V. CONCLUDING REMARKS

We have introduced an optimal measurement, valid for an arbitrary PSF, that allows extracting the maximum possible information from the centroid and the separation of two incoherent point sources when they are very close. This measurement can be adjusted at will, allowing us to extract more information from the centroid or the separation, ensuring that it always extracts the maximum total information. We have also demonstrated, for a Gaussian PSF, the good performance of this measurement for small and moderate separations.

ACKNOWLEDGMENTS

We acknowledge discussions with M. Tsang at an early stage of this work. This publication has received financial support from the QuantEra program (project ApresSF) and from the Agencia Estatal de Investigación (Grant No. PID2021-127781NB-I00). A.Z.G. acknowledges that the NRC headquarters is located on the traditional unceded territory of the Algonquin Anishinaabe and Mohawk people, as well as support from the NSERC PDF program and the NRC Quantum Sensors Challenge program. L.L.S.S. was supported in part by Grant No. NSF PHY-1748958 to the Kavli Institute for Theoretical Physics (KITP).

[1] L. Rayleigh, Investigations in optics, with special reference to the spectroscope, Philos. Mag. **8**, 261 (1879).

[2] M. Tsang, R. Nair, and X.-M. Lu, Quantum theory of superresolution for two incoherent optical point sources, Phys. Rev. X **6**, 031033 (2016).

[3] R. Nair and M. Tsang, Far-field superresolution of thermal electromagnetic sources at the quantum limit, Phys. Rev. Lett. **117**, 190801 (2016).

[4] S. Z. Ang, R. Nair, and M. Tsang, Quantum limit for two-dimensional resolution of two incoherent optical point sources, Phys. Rev. A **95**, 063847 (2017).

[5] M. Tsang, Subdiffraction incoherent optical imaging via spatial-mode demultiplexing, New J. Phys. **19**, 023054 (2017).

[6] C. W. Helstrom, *Quantum Detection and Estimation Theory* (Academic, New York, 1976).

[7] M. Paur, B. Stoklasa, Z. Hradil, L. L. Sanchez-Soto, and J. Rehacek, Achieving the ultimate optical resolution, Optica **3**, 1144 (2016).

[8] F. Yang, A. Taschilina, E. S. Moiseev, C. Simon, and A. I. Lvovsky, Far-field linear optical superresolution via heterodyne detection in a higher-order local oscillator mode, Optica **3**, 1148 (2016).

[9] W.-K. Tham, H. Ferretti, and A. M. Steinberg, Beating Rayleigh's curse by imaging using phase information, Phys. Rev. Lett. **118**, 070801 (2017).

[10] Y. Zhou, J. Yang, J. D. Hassett, S. M. H. Rafsanjani, M. Mirhosseini, A. N. Vamivakas, A. N. Jordan, Z. Shi, and R. W. Boyd, Quantum-limited estimation of the axial separation of two incoherent point sources, Optica **6**, 534 (2019).

[11] X.-J. Tan, L. Qi, L. Chen, A. J. Danner, P. Kanchanawong, and M. Tsang, Quantum-inspired superresolution for incoherent imaging, Optica **10**, 1189 (2023).

[12] L. Santamaria, F. Sgobba, and C. Lupo, Single-photon sub-Rayleigh precision measurements of a pair of incoherent sources of unequal intensity, Opt. Quantum **2**, 46 (2024).

[13] J. Rehacek, M. Paúr, B. Stoklasa, Z. Hradil, and L. L. Sánchez-Soto, Optimal measurements for resolution beyond the Rayleigh limit, Opt. Lett. **42**, 231 (2017).

[14] J. Rehacek, Z. Hradil, B. Stoklasa, M. Paúr, J. Grover, A. Krzic, and L. L. Sánchez-Soto, Multiparameter quantum metrology of incoherent point sources: Towards realistic superresolution, Phys. Rev. A **96**, 062107 (2017).

[15] M. Parniak, S. Borówka, K. Boroszko, W. Wasilewski, K. Banaszek, and R. Demkowicz-Dobrzański, Beating the Rayleigh limit using two-photon interference, Phys. Rev. Lett. **121**, 250503 (2018).

[16] E. Bisketzi, D. Branford, and A. Datta, Quantum limits of localisation microscopy, New J. Phys. **21**, 123032 (2019).

[17] S. Zhou and L. Jiang, Modern description of Rayleigh's criterion, Phys. Rev. A **99**, 013808 (2019).

[18] C. Napoli, S. Piano, R. Leach, G. Adesso, and T. Tufarelli, Towards superresolution surface metrology: Quantum estimation of angular and axial separations, Phys. Rev. Lett. **122**, 140505 (2019).

[19] M. Tsang, Semiparametric estimation for incoherent optical imaging, Phys. Rev. Res. **1**, 033006 (2019).

[20] K. Prakash, B. Diederich, R. Heintzmann, and L. Schermelleh, Super-resolution microscopy: A brief history and new avenues, Philos. Trans. R. Soc. A **380**, 20210110 (2022).

[21] E. F. Matlin and L. J. Zipp, Imaging arbitrary incoherent source distributions with near quantum-limited resolution, Sci. Rep. **12**, 2810 (2022).

[22] S. Kurdzialek, Back to sources–the role of losses and coherence in super-resolution imaging revisited, Quantum **6**, 697 (2022).

[23] S. Kurdziałek and R. Demkowicz-Dobrzański, Measurement noise susceptibility in quantum estimation, Phys. Rev. Lett. **130**, 160802 (2023).

[24] M. Gessner, C. Fabre, and N. Treps, Superresolution limits from measurement crosstalk, Phys. Rev. Lett. **125**, 100501 (2020).

[25] K. Schlichtholz, T. Linowski, M. Walschaers, N. Treps, Ł. Rudnicki, and G. Sorelli, Practical tests for sub-Rayleigh source discriminations with imperfect demultiplexers, Opt. Quantum **2**, 29 (2024).

[26] F. Albarelli, I. Gianani, M. G. Genoni, and M. Barbieri, Fisher information susceptibility for multiparameter quantum estimation, arXiv:2312.02035 [Phys. Rev. A (to be published)].

[27] W. Larson and B. E. A. Saleh, Resurgence of Rayleigh's curse in the presence of partial coherence, Optica **5**, 1382 (2018).

[28] M. Tsang and R. Nair, Resurgence of Rayleigh's curse in the presence of partial coherence: comment, Optica **6**, 400 (2019).

[29] Z. Hradil, J. Řeháček, L. Sánchez-Soto, and B.-G. Englert, Quantum Fisher information with coherence, Optica **6**, 1437 (2019).

[30] S. A. Wadood, K. Liang, Y. Zhou, J. Yang, M. A. Alonso, X. F. Qian, T. Malhotra, S. M. Hashemi Rafsanjani, A. N. Jordan, R. W. Boyd, and A. N. Vamivakas, Experimental demonstration of superresolution of partially coherent light sources using parity sorting, Opt. Express **29**, 22034 (2021).

[31] S. De, J. Gil-Lopez, B. Brecht, C. Silberhorn, L. L. Sánchez-Soto, Z. Hradil, and J. Řeháček, Effects of coherence on temporal resolution, Phys. Rev. Res. **3**, 033082 (2021).

[32] M. Tsang, Resolving starlight: A quantum perspective, Contemp. Phys. **60**, 279 (2019).

[33] M. Tsang, https://blog.nus.edu.sg/mankei/superresolution/.

[34] S. Prasad and Z. Yu, Quantum-limited superlocalization and superresolution of a source pair in three dimensions, Phys. Rev. A **99**, 022116 (2019).

[35] M. R. Grace, Z. Dutton, A. Ashok, and S. Guha, Approaching quantum-limited imaging resolution without prior knowledge of the object location, J. Opt. Soc. Am. A **37**, 1288 (2020).

[36] J. O. de Almeida, J. Kołodyński, C. Hirche, M. Lewenstein, and M. Skotiniotis, Discrimination and estimation of incoherent sources under misalignment, Phys. Rev. A **103**, 022406 (2021).

[37] H. Zhu, Information complementarity: A new paradigm for decoding quantum incompatibility, Sci. Rep. **5**, 14317 (2015).

[38] T. Heinosaari, T. Miyadera, and M. Ziman, An invitation to quantum incompatibility, J. Phys. A: Math. Theor. **49**, 123001 (2016).

[39] S. Ragy, M. Jarzyna, and R. Demkowicz-Dobrzański, Compatibility in multiparameter quantum metrology, Phys. Rev. A **94**, 052108 (2016).

[40] M. Szczykulska, T. Baumgratz, and A. Datta, Multi-parameter quantum metrology, Adv. Phys. X **1**, 621 (2016).

[41] J. S. Sidhu and P. Kok, Geometric perspective on quantum parameter estimation, AVS Quantum Sci. **2**, 014701 (2020).

[42] J. Liu, H. Yuan, X.-M. Lu, and X. Wang, Quantum Fisher information matrix and multiparameter estimation, J. Phys. A: Math. Theor. **53**, 023001 (2020).

[43] A. Z. Goldberg, L. L. Sánchez-Soto, and H. Ferretti, Intrinsic sensitivity limits for multiparameter quantum metrology, Phys. Rev. Lett. **127**, 110501 (2021).

[44] A. Chrostowski, R. Demkowicz-Dobrzański, M. Jarzyna, and K. Banaszek, On superresolution imaging as a multiparameter estimation problem, Int. J. Quantum Inf. **15**, 1740005 (2017).

[45] X.-M. Lu and X. Wang, Incorporating Heisenberg's uncertainty principle into quantum multiparameter estimation, Phys. Rev. Lett. **126**, 120503 (2021).

[46] J. Shao and X.-M. Lu, Performance-tradeoff relation for locating two incoherent optical point sources, Phys. Rev. A **105**, 062416 (2022).

[47] M. Kimizu, F. Tanaka, and A. Fujiwara, Adaptive quantum state estimation for two optical point sources, Phys. Rev. A **109**, 032434 (2024).

[48] J. W. Goodman, *Introduction to Fourier Optics* (Roberts and Company, Englewood, CO, 2004).

[49] A. S. Holevo, *Probabilistic and Statistical Aspects of Quantum Theory*, 2nd ed. (North-Holland, Amsterdam, 2003).

[50] J. H. Jenne and D. R. M. Arvidsson-Shukur, Unbounded and lossless compression of multiparameter quantum information, Phys. Rev. A **106**, 042404 (2022).

[51] G. Toth, Lower bounds on the quantum Fisher information based on the variance and various types of entropies, arXiv:1701.07461.

[52] G. Tóth and F. Fröwis, Uncertainty relations with the variance and the quantum Fisher information based on convex decompositions of density matrices, Phys. Rev. Res. **4**, 013075 (2022).

[53] A. Siegman, *Lasers* (Oxford University Press, Oxford, UK, 1986).

3

Conclusions and Future Outlook

Conclusions

Quantum metrology is a discipline that has attained a remarkable maturity, with high-impact applications already in practice. Nevertheless, fundamental theoretical and experimental challenges persist. This thesis contributes to the collective effort to address three of these challenges: the analysis of precision beyond the asymptotic limit, the design of robust quantum states, and the simultaneous estimation of incompatible parameters.

The three projects comprising this thesis tackle these challenges through the development of analytical tools and the generation of numerical results. The main contributions of each project are summarized below, followed by an outline of the future research directions that emerge from this work.

The first project investigated the asymptotic nature of the quantum Cramér-Rao bound (QCRB), which is insufficient for describing performance with finite resources and for discriminating between strategies that are equivalent in the $\nu \to \infty$ limit. The main contribution was the analytical derivation of corrections of order $1/\nu^2$ and higher to the mean squared error (MSE) within the frequentist paradigm. It was shown that these corrections break the degeneracy of the QCRB, as they explicitly depend on the implemented quantum measurement and the higher-order moments of the state. This result provides a highly practical criterion for selecting optimal strategies in the pre-asymptotic regime.

The second project focused on two interconnected objectives: on the one hand, the search for robust quantum states for SU(2) rotation sensing; on the other, a deeper understanding of the multipole distribution as a tool to characterize the geometry of these states. Within this framework, a new family of states, the Random Majorana (RM) states, was proposed and characterized, numerically

demonstrating their high robustness and excellent metrological performance. Furthermore, the connection between the Majorana constellation and the multipole distribution was investigated in detail for several paradigmatic states. The proposal of RM states was experimentally validated through a collaboration that successfully generated these states and used them for rotation sensing.

Finally, the third project addressed a paradigmatic problem in multi-parameter estimation: the simultaneous estimation of the centroid and separation of two incoherent sources, for which the optimal measurements are incompatible. In contrast to previous, predominantly numerical approaches, the fundamental contribution of this work was the analytical derivation of a family of measurements that extract the maximum joint information about both parameters. These expressions are valid for arbitrary point spread functions (PSFs), allow for tuning the trade-off between centroid and separation precision, and depend on a free parameter that offers flexibility for their experimental implementation.

Future Outlook

The research conducted in this thesis motivates a series of future lines of work. The prospects arising from the results of each project are outlined below.

Corrections to the quantum Cramér-Rao bound

The formalism of higher-order asymptotics, is a fertile field for future research.

- Define a quantum analogue of the $\Gamma(\theta)$ function. In the same way that the QFI is obtained by optimizing the CFI, one could seek a "second-order QFI" that optimizes this correction term over the family of measurements that already saturate the QFI. In parallel, assess whether the measurements identified by this criterion also exhibit sufficient experimental robustness.

- Apply this formalism to non-unitary transformations and mixed initial states, enabling the analysis of finite-resource performance in the presence of noise and decoherence.

- Characterize the general structure of POVMs that saturate the QFI ($F = Q$), further investigate the role of POVM extensions, and develop general expressions for the case of vanishing probabilities. Likewise, investigating higher-order versions of $\Gamma(\theta)$ ($1/\nu^3$ and beyond) could unequivocally reveal the advantage of states with isotropic higher-order moments.

Majorana constellation and robust states for SU(2) sensing

- Find analytical expressions that relate the Majorana constellation to the multipole distribution. This would allow for a more precise understanding of the exact sense in which the multipole distribution captures the state's geometry.

- Develop analytical tools to study RM states. Unlike other random states, such as CUE states, RM states do not arise from the simple application of a symmetry group, which makes their mathematical treatment with standard methods difficult. If analytical formulas for their statistical properties were obtained, one could rigorously prove their robustness and their scaling with the total spin.

Multi-parameter estimation and super-resolution

- Design an optical setup that implements the proposed family of measurements and experimentally demonstrate the ability to tune the trade-off between centroid and separation estimation.
- Extend the analysis to determine the optimal measurements for the N-point-source scenario, exploring the structure of incompatibilities in a higher-dimensional multi-parameter system.

In conclusion, this work has contributed analytical tools and solutions to specific problems in quantum metrology, focusing on scenarios that extend beyond common idealizations. It is hoped that the results presented here will contribute to the development of more precise and robust estimation protocols, and that the future lines of research proposed herein will stimulate new investigations.

Bibliography

[1]S. Colombo, E. Pedrozo-Peñafiel, and V. Vuletić, "Entanglement-enhanced optical atomic clocks", Appl. Phys. Lett. **121**, 210502 (2022).

[2]J. M. Robinson, M. Miklos, Y. M. Tso, C. J. Kennedy, T. Bothwell, D. Kedar, J. K. Thompson, and J. Ye, "Direct comparison of two spin-squeezed optical clock ensembles at the 10-17 level", Nat. Phys. **20**, 208–213 (2024).

[3]A. Cao, W. J. Eckner, T. Lukin Yelin, A. W. Young, S. Jandura, L. Yan, K. Kim, G. Pupillo, J. Ye, N. Darkwah Oppong, and A. M. Kaufman, "Multi-qubit gates and Schrödinger cat states in an optical clock", Nature **634**, 315–320 (2024).

[4]H. Shi, Z. Zhang, S. Pirandola, and Q. Zhuang, "Entanglement-Assisted Absorption Spectroscopy", Phys. Rev. Lett. **125**, 180502 (2020).

[5]A. Belsley, "Quantum-Enhanced Absorption Spectroscopy with Bright Squeezed Frequency Combs", Phys. Rev. Lett. **130**, 133602 (2023).

[6]D. I. Herman, M. Walsh, M. K. Kreider, N. Lordi, E. J. Tsao, A. J. Lind, M. Heyrich, J. Combes, J. Genest, and S. A. Diddams, "Squeezed dual-comb spectroscopy", Science **387**, 653–658 (2025).

[7]Z. Zhang, X. Zhang, J. Liu, and H. Dong, "Quantum-Enhanced Weak Absorption Estimation with Correlated Photons", Phys. Rev. Lett. **134**, 133604 (2025).

[8]Z. Huang, C. Schwab, and C. Lupo, "Ultimate limits of exoplanet spectroscopy: A quantum approach", Phys. Rev. A **107**, 022409 (2023).

[9]Z. Ibarra-Borja, C. Sevilla-Gutiérrez, R. Ramírez-Alarcón, H. Cruz-Ramírez, and A. B. U'Ren, "Experimental demonstration of full-field quantum optical coherence tomography", Photonics Res. **8**, 51 (2020).

[10]Y. Zhang, Z. He, X. Tong, D. C. Garrett, R. Cao, and L. V. Wang, "Quantum imaging of biological organisms through spatial and polarization entanglement", Sci. Adv. **10**, eadk1495 (2024).

[11] J. Bordes, J. R. Brown, D. P. Watts, M. Bashkanov, K. Gibson, R. Newton, and N. Zachariou, "First Detailed Study of the Quantum Decoherence of Entangled Gamma Photons", Phys. Rev. Lett. **133**, 132502 (2024).

[12] K. Stolzenberg, C. Struckmann, S. Bode, R. Li, A. Herbst, V. Vollenkemper, D. Thomas, A. Rajagopalan, E. M. Rasel, N. Gaaloul, and D. Schlippert, "Multi-Axis Inertial Sensing with 2D Matter-Wave Arrays", Phys. Rev. Lett. **134**, 143601 (2025).

[13] Q. d'Armagnac De Castanet, C. Des Cognets, R. Arguel, S. Templier, V. Jarlaud, V. Ménoret, B. Desruelle, P. Bouyer, and B. Battelier, "Atom interferometry at arbitrary orientations and rotation rates", Nat. Commun. **15**, 6406 (2024).

[14] "NRL Charters Navy's Quantum Inertial Navigation Path To Reduce Drift", U.S. Nav. Res. Lab.

[15] K. A. Gilmore, M. Affolter, R. J. Lewis-Swan, D. Barberena, E. Jordan, A. M. Rey, and J. J. Bollinger, "Quantum-enhanced sensing of displacements and electric fields with two-dimensional trapped-ion crystals", Science **373**, 673–678 (2021).

[16] K. Bian, W. Zheng, X. Zeng, X. Chen, R. Stöhr, A. Denisenko, S. Yang, J. Wrachtrup, and Y. Jiang, "Nanoscale electric-field imaging based on a quantum sensor and its charge-state control under ambient condition", Nat. Commun. **12**, 2457 (2021).

[17] H. Wang, K. L. Tiwari, K. Jacobs, M. Judy, X. Zhang, D. R. Englund, and M. E. Trusheim, "A spin-refrigerated cavity quantum electrodynamic sensor", Nat. Commun. **15**, 10320 (2024).

[18] B. Stray et al., "Quantum sensing for gravity cartography", Nature **602**, 590–594 (2022).

[19] M. Tsang, "Resolving starlight: a quantum perspective", Contemp. Phys. **60**, 279–298 (2019).

[20] Z. A. Kudyshev, D. Sychev, Z. Martin, O. Yesilyurt, S. I. Bogdanov, X. Xu, P.-G. Chen, A. V. Kildishev, A. Boltasseva, and V. M. Shalaev, "Machine learning assisted quantum super-resolution microscopy", Nat. Commun. **14**, 4828 (2023).

[21] Z. He, Y. Zhang, X. Tong, L. Li, and L. V. Wang, "Quantum microscopy of cells at the Heisenberg limit", Nat. Commun. **14**, 2441 (2023).

[22] X. Yue, H. Wu, J. Wang, and Z. He, "Quantum super-resolution imaging: a review and perspective", Nanophotonics **14**, 1961–1974 (2025).

[23] M. Jiang, H. Su, A. Garcon, X. Peng, and D. Budker, "Search for axion-like dark matter with spin-based amplifiers", Nat. Phys. **17**, 1402–1407 (2021).

[24] Y. Wang, H. Su, M. Jiang, Y. Huang, Y. Qin, C. Guo, Z. Wang, D. Hu, W. Ji, P. Fadeev, X. Peng, and D. Budker, "Limits on Axions and Axionlike Particles within the Axion Window Using a Spin-Based Amplifier", Phys. Rev. Lett. **129**, 051801 (2022).

[25]D. Hartley, C. Käding, R. Howl, and I. Fuentes, "Quantum-enhanced screened dark energy detection", The Eur. Phys. J. C **84**, 49 (2024).

[26]M. Jiang, T. Hong, D. Hu, Y. Chen, F. Yang, T. Hu, X. Yang, J. Shu, Y. Zhao, X. Peng, and J. Du, "Long-baseline quantum sensor network as dark matter haloscope", Nat. Commun. **15**, 3331 (2024).

[27]D. DeMille, N. R. Hutzler, A. M. Rey, and T. Zelevinsky, "Quantum sensing and metrology for fundamental physics with molecules", Nat. Phys. **20**, 741–749 (2024).

[28]S. Bose, I. Fuentes, A. A. Geraci, S. M. Khan, S. Qvarfort, M. Rademacher, M. Rashid, M. Toroš, H. Ulbricht, and C. C. Wanjura, "Massive quantum systems as interfaces of quantum mechanics and gravity", Rev. Mod. Phys. **97**, 015003 (2025).

[29]J. Ye and P. Zoller, "Essay: Quantum Sensing with Atomic, Molecular, and Optical Platforms for Fundamental Physics", Phys. Rev. Lett. **132**, 190001 (2024).

[30]C. W. Bauer et al., "Quantum Simulation for High-Energy Physics", PRX Quantum **4**, 027001 (2023).

[31]A. Abbas et al., "Challenges and Opportunities in Quantum Optimization", Nat. Rev. Phys. **6**, 718–735 (2024).

[32]B. Fauseweh, "Quantum many-body simulations on digital quantum computers: State-of-the-art and future challenges", Nat. Commun. **15**, 2123 (2024).

[33]S. Pirandola et al., "Advances in Quantum Cryptography", Adv. Opt. Photonics **12**, 1012 (2020).

[34]V. Zapatero, T. Van Leent, R. Arnon-Friedman, W.-Z. Liu, Q. Zhang, H. Weinfurter, and M. Curty, "Advances in device-independent quantum key distribution", npj Quantum Inf. **9**, 10 (2023).

[35]S. K. Sahu and K. Mazumdar, "State-of-the-art analysis of quantum cryptography: applications and future prospects", Front. Phys. **12**, 1456491 (2024).

[36]K. Bharti, A. Cervera-Lierta, T. H. Kyaw, T. Haug, S. Alperin-Lea, A. Anand, M. Degroote, H. Heimonen, J. S. Kottmann, T. Menke, W.-K. Mok, S. Sim, L.-C. Kwek, and A. Aspuru-Guzik, "Noisy intermediate-scale quantum algorithms", Rev. Mod. Phys. **94**, 015004 (2022).

[37]O. Ezratty, "Mitigating the quantum hype", arXiv:2202.01925 (2022).

[38]M. Tse et al., "Quantum-Enhanced Advanced LIGO Detectors in the Era of Gravitational-Wave Astronomy", Phys. Rev. Lett. **123**, 231107 (2019).

[39]H. Grote, K. Danzmann, K. L. Dooley, R. Schnabel, J. Slutsky, and H. Vahlbruch, "First Long-Term Application of Squeezed States of Light in a Gravitational-Wave Observatory", Phys. Rev. Lett. **110**, 181101 (2013).

[40]S. M. Kay, *Fundamentals of statistical signal processing*, Prentice Hall Signal Processing Series (Prentice-Hall PTR, Englewood Cliffs, N.J, 1993).

[41]E. L. Lehmann and G. Casella, *Theory of point estimation*, 2nd ed, Springer Texts in Statistics (Springer, New York, 1998).

[42]H. L. Van Trees, *Detection, estimation, and modulation theory* (Wiley, New York, 2001).

[43]G. Casella and R. L. Berger, *Statistical inference*, 2. ed (Duxbury, Pacific Grove, Calif, 2002).

[44]A. Papoulis and S. U. Pillai, *Probability, random variables, and stochastic processes*, 4th ed (McGraw-Hill, Boston, 2002).

[45]D. R. Cox, *Principles of statistical inference* (Cambridge University Press, Cambridge New York, 2006).

[46]J. Unkelbach, M. Alber, M. Bangert, R. Bokrantz, T. C. Y. Chan, J. O. Deasy, A. Fredriksson, B. L. Gorissen, M. Van Herk, W. Liu, H. Mahmoudzadeh, O. Nohadani, J. V. Siebers, M. Witte, and H. Xu, "Robust radiotherapy planning", Phys. Med. & Biol. **63**, 22TR02 (2018).

[47]M. G. A. Paris, "Quantum Estimation for Quantum Technology", Int. J. Quantum Inf. **07**, 125–137 (2009).

[48]R. Demkowicz-Dobrzański, M. Jarzyna, and J. Kołodyński, "Quantum Limits in Optical Interferometry", in *Progress in Optics*, Vol. 60 (Elsevier, 2015), pp. 345–435.

[49]J. S. Sidhu and P. Kok, "Geometric perspective on quantum parameter estimation", AVS Quantum Sci. **2**, 014701 (2020).

[50]M. Barbieri, "Optical Quantum Metrology", PRX Quantum **3**, 010202 (2022).

[51]J. M. E. Fraisse, "New concepts in quantum-metrology: From coherent averaging to Hamiltonian extensions", PhD thesis (University of Tübingen, 2017).

[52]W. Górecki, "Heisenberg Limit beyond Quantum Fisher Information", PhD thesis (Faculty of Physics, University of Warsaw, 2023).

[53]L. Conlon, "Quantum Multiparameter Estimation: Exploring Fundamental Limits and Testing Quantum Mechanics", PhD thesis (The Australian National University, 2023).

[54]C. Mukhopadhyay, V. Montenegro, and A. Bayat, "Current trends in global quantum metrology", J. Phys. A: Math. Theor. **58**, 063001 (2025).

[55]X.-M. Lu and X. Wang, "Incorporating Heisenberg's Uncertainty Principle into Quantum Multiparameter Estimation", Phys. Rev. Lett. **126**, 120503 (2021).

[56]I. Bengtsson and K. Zyczkowski, *Geometry of Quantum States: An Introduction to Quantum Entanglement* (Cambridge University Press, Cambridge, 2006).

[57]A. R. U. Devi, Sudha, and A. K. Rajagopal, "Majorana representation of symmetric multiqubit states", Quantum Inf. Process. **11**, 685–710 (2012).

[58]L. L. Sánchez-Soto, A. B. Klimov, P. De La Hoz, and G. Leuchs, "Quantum versus classical polarization states: when multipoles count", J. Phys. B: At. Mol. Opt. Phys. **46**, 104011 (2013).

[59]P. De La Hoz, G. Björk, A. B. Klimov, G. Leuchs, and L. L. Sánchez-Soto, "Unpolarized states and hidden polarization", Phys. Rev. A **90**, 043826 (2014).

[60]S. Shabbir, "Majorana Representation in Quantum Optics : SU(2) Interferometry and Uncertainty Relations", PhD thesis (KTH, School of Engineering Sciences (SCI), Applied Physics, Quantum Electronics and Quantum Optics, QEO., 2017).

[61]A. Z. Goldberg, A. B. Klimov, M. Grassl, G. Leuchs, and L. L. Sánchez-Soto, "Extremal quantum states", AVS Quantum Sci. **2**, 044701 (2020).

[62]A. Z. Goldberg, P. De La Hoz, G. Björk, A. B. Klimov, M. Grassl, G. Leuchs, and L. L. Sánchez-Soto, "Quantum concepts in optical polarization", Adv. Opt. Photonics **13**, 1 (2021).

[63]A. Z Goldberg, A. B Klimov, G. Leuchs, and L. L Sánchez-Soto, "Rotation sensing at the ultimate limit", J. Physics: Photonics **3**, 022008 (2021).

[64]L. Pezzè, A. Smerzi, M. K. Oberthaler, R. Schmied, and P. Treutlein, "Quantum metrology with nonclassical states of atomic ensembles", Rev. Mod. Phys. **90**, 035005 (2018).

[65]L. Pezze' and A. Smerzi, "Quantum theory of phase estimation", arXiv:1411.5164 (2014).

[66]J. F. Haase, A. Smirne, S. F. Huelga, J. Kołodynski, and R. Demkowicz-Dobrzanski, "Precision Limits in Quantum Metrology with Open Quantum Systems", Quantum Meas. Quantum Metrol. **5**, 13–39 (2016).

[67]D. Braun, G. Adesso, F. Benatti, R. Floreanini, U. Marzolino, M. W. Mitchell, and S. Pirandola, "Quantum-enhanced measurements without entanglement", Rev. Mod. Phys. **90**, 035006 (2018).

[68]S. Pirandola, B. R. Bardhan, T. Gehring, C. Weedbrook, and S. Lloyd, "Advances in photonic quantum sensing", Nat. Photonics **12**, 724–733 (2018).

[69]K. C. Tan and H. Jeong, "Nonclassical light and metrological power: An introductory review", AVS Quantum Sci. **1**, 014701 (2019).

[70]R. Demkowicz-Dobrzański, W. Górecki, and M. Guţă, "Multi-parameter estimation beyond quantum Fisher information", J. Phys. A: Math. Theor. **53**, 363001 (2020).

[71]F. Albarelli, M. Barbieri, M. Genoni, and I. Gianani, "A perspective on multiparameter quantum metrology: From theoretical tools to applications in quantum imaging", Phys. Lett. A **384**, 126311 (2020).

[72]S. E. Crawford, R. A. Shugayev, H. P. Paudel, P. Lu, M. Syamlal, P. R. Ohodnicki, B. Chorpening, R. Gentry, and Y. Duan, "Quantum Sensing for Energy Applications: Review and Perspective", Adv. Quantum Technol. **4**, 2100049 (2021).

[73]J. J. Meyer, "Fisher Information in Noisy Intermediate-Scale Quantum Applications", Quantum **5**, 539 (2021).

[74]Z. Zhang and Q. Zhuang, "Distributed quantum sensing", Quantum Sci. Technol. **6**, 043001 (2021).

[75]J. Liu, M. Zhang, H. Chen, L. Wang, and H. Yuan, "Optimal Scheme for Quantum Metrology", Adv. Quantum Technol. **5**, 2100080 (2022).

[76]H. I. Nurdin and M. Guţă, "Parameter estimation and system identification for continuously-observed quantum systems", Annu. Rev. Control. **54**, 295–304 (2022).

[77]V. Montenegro, C. Mukhopadhyay, R. Yousefjani, S. Sarkar, U. Mishra, M. G. Paris, and A. Bayat, "Review: Quantum metrology and sensing with many-body systems", Phys. Reports **1134**, 1–62 (2025).

[78]E. Bisketzi, "Quantum limits in microscopy and spectroscopy", PhD thesis (University of Warwick, 2021).

[79]H. Ferretti, "Quantum parameter estimation in the laboratory", PhD thesis (University of Toronto, 2022).

[80]A. Z. Goldberg, "Disquisitions on quantum-enhanced polarimetry", PhD thesis (University of Toronto, 2021).

[81]T. Ilias, "Application of quantum many-body physics in quantum metrology", PhD thesis (Ulm University, 2023).

[82]J. R. Jimenez, "Non-asymptotic quantum metrology", PhD thesis (University of Sussex, 2019).

[83]L. Seveso, "Advances in quantum parameter estimation and other topics", PhD thesis (University of Milan, 2018).

[84]J. Sidhu, "Quantum Metrology of Grid Deformations and Squeezed Light: With applications in quantum imaging & quantum information", PhD thesis (University of Sheffield, 2018).

[85]E. Köse, "High-resolution imaging with multi-parameter quantum metrology in passive remote sensing", PhD thesis (University of Tübingen, 2023).

[86]S. Zhou, "Error-corrected quantum metrology", PhD thesis (Yale University, 2021).

[87]C. W. Helstrom, "Quantum detection and estimation theory", J. Stat. Phys. **1**, 231–252 (1969).

[88]A. S. Cholevo and A. S. Cholevo, *Probabilistic and statistical aspects of quantum theory*, North Holland Series in Statistics and Probability 1 (North-Holland Publ. Co, Amsterdam u.a, 1982).

[89]O. D. Aguiar, "Past, present and future of the Resonant-Mass gravitational wave detectors", Res. Astron. Astrophys. **11**, 1–42 (2011).

[90]P. R. Saulson, "Josh Goldberg and the physical reality of gravitational waves", Gen. Relativ. Gravit. **43**, 3289–3299 (2011).

[91]R. P. Giffard, "Ultimate sensitivity limit of a resonant gravitational wave antenna using a linear motion detector", Phys. Rev. D **14**, 2478–2486 (1976).

[92]C. M. Caves, K. S. Thorne, R. W. P. Drever, V. D. Sandberg, and M. Zimmermann, "On the measurement of a weak classical force coupled to a quantum-mechanical oscillator. I. Issues of principle", Rev. Mod. Phys. **52**, 341–392 (1980).

[93]C. M. Caves, "Quantum-mechanical noise in an interferometer", Phys. Rev. D **23**, 1693–1708 (1981).

[94]R. S. Bondurant and J. H. Shapiro, "Squeezed states in phase-sensing interferometers", Phys. Rev. D **30**, 2548–2556 (1984).

[95]M. J. Holland and K. Burnett, "Interferometric detection of optical phase shifts at the Heisenberg limit", Phys. Rev. Lett. **71**, 1355–1358 (1993).

[96]N. Christensen and R. Meyer, "Parameter estimation with gravitational waves", Rev. Mod. Phys. **94**, 025001 (2022).

[97]B. P. Abbott et al., "Observation of Gravitational Waves from a Binary Black Hole Merger", Phys. Rev. Lett. **116**, 061102 (2016).

[98]R. Demkowicz-Dobrzański, K. Banaszek, and R. Schnabel, "Fundamental quantum interferometry bound for the squeezed-light-enhanced gravitational wave detector GEO 600", Phys. Rev. A **88**, 041802 (2013).

[99]LIGO Scientific Collaboration, "Quantum-enhanced advanced LIGO detectors in the era of gravitational-wave astronomy", Phys. Rev. Lett. **123**, 231107 (2019).

[100]L. McCuller, C. Whittle, D. Ganapathy, K. Komori, M. Tse, A. Fernandez-Galiana, L. Barsotti, P. Fritschel, M. MacInnis, F. Matichard, K. Mason, N. Mavalvala, R. Mittleman, H. Yu, M. E. Zucker, and M. Evans, "Frequency-Dependent Squeezing for Advanced LIGO", Phys. Rev. Lett. **124**, 171102 (2020).

[101]E. Capote et al., "Advanced LIGO detector performance in the fourth observing run", Phys. Rev. D **111**, 062002 (2025).

[102]T. L. S. Collaboration, "Enhancing the sensitivity of the LIGO gravitational wave detector by using squeezed states of light", Nat. Photonics **7**, 613–619 (2013).

[103]B. Yurke, S. L. McCall, and J. R. Klauder, "SU(2) and SU(1,1) interferometers", Phys. Rev. A **33**, 4033–4054 (1986).

[104]V. Giovannetti, S. Lloyd, and L. Maccone, "Quantum-enhanced measurements: beating the standard quantum limit", Science **306**, 1330–1336 (2004).

[105]V. Giovannetti, S. Lloyd, and L. Maccone, "Quantum Metrology", Phys. Rev. Lett. **96**, 010401 (2006).

[106]M. Hayashi, *Quantum Information: An Introduction*, SpringerLink Bücher (Springer Berlin Heidelberg, Berlin, Heidelberg, 2006).

[107]V. Giovannetti, S. Lloyd, and L. Maccone, "Advances in quantum metrology", Nat. Photonics **5**, 222–229 (2011).

[108]R. Demkowicz-Dobrzański, J. Kołodyński, and M. Guţă, "The elusive Heisenberg limit in quantum-enhanced metrology", Nat. Commun. **3**, 1063 (2012).

[109]A. W. Chin, S. F. Huelga, and M. B. Plenio, "Quantum Metrology in Non-Markovian Environments", Phys. Rev. Lett. **109**, 233601 (2012).

[110]A. Smirne, J. Kołodyński, S. F. Huelga, and R. Demkowicz-Dobrzański, "Ultimate Precision Limits for Noisy Frequency Estimation", Phys. Rev. Lett. **116**, 120801 (2016).

[111]R. Demkowicz-Dobrzański and L. Maccone, "Using Entanglement Against Noise in Quantum Metrology", Phys. Rev. Lett. **113**, 250801 (2014).

[112]W. Dür, M. Skotiniotis, F. Fröwis, and B. Kraus, "Improved Quantum Metrology Using Quantum Error Correction", Phys. Rev. Lett. **112**, 080801 (2014).

[113]S. Zhou, M. Zhang, J. Preskill, and L. Jiang, "Achieving the Heisenberg limit in quantum metrology using quantum error correction", Nat. Commun. **9**, 78 (2018).

[114]D. Layden, S. Zhou, P. Cappellaro, and L. Jiang, "Ancilla-Free Quantum Error Correction Codes for Quantum Metrology", Phys. Rev. Lett. **122**, 040502 (2019).

[115]W. Gorecki, S. Zhou, L. Jiang, and R. Demkowicz-Dobrzanski, "Optimal probes and error-correction schemes in multi-parameter quantum metrology", Quantum **4**, 288 (2020).

[116]S. Zhou and L. Jiang, "Asymptotic Theory of Quantum Channel Estimation", PRX Quantum **2**, 010343 (2021).

[117]S. Zhou, "Limits of Noisy Quantum Metrology with Restricted Quantum Controls", Phys. Rev. Lett. **133**, 170801 (2024).

[118]W. Górecki, R. Demkowicz-Dobrzański, H. M. Wiseman, and D. W. Berry, "π -Corrected Heisenberg Limit", Phys. Rev. Lett. **124**, 030501 (2020).

[119]W. Górecki and R. Demkowicz-Dobrzański, "Multiple-Phase Quantum Interferometry: Real and Apparent Gains of Measuring All the Phases Simultaneously", Phys. Rev. Lett. **128**, 040504 (2022).

[120]M. Szczykulska, T. Baumgratz, and A. Datta, "Multi-parameter quantum metrology", Adv. Physics: X **1**, 621–639 (2016).

[121]J. Liu, H. Yuan, X.-M. Lu, and X. Wang, "Quantum Fisher information matrix and multiparameter estimation", J. Phys. A: Math. Theor. **53**, 023001 (2020).

[122]Z. Hou, Z. Zhang, G.-Y. Xiang, C.-F. Li, G.-C. Guo, H. Chen, L. Liu, and H. Yuan, "Minimal Tradeoff and Ultimate Precision Limit of Multiparameter Quantum Magnetometry under the Parallel Scheme", Phys. Rev. Lett. **125**, 020501 (2020).

[123]P. C. Humphreys, M. Barbieri, A. Datta, and I. A. Walmsley, "Quantum Enhanced Multiple Phase Estimation", Phys. Rev. Lett. **111**, 070403 (2013).

[124]J.-D. Yue, Y.-R. Zhang, and H. Fan, "Quantum-enhanced metrology for multiple phase estimation with noise", Sci. Reports **4**, 5933 (2014).

[125]M. D. Vidrighin, G. Donati, M. G. Genoni, X.-M. Jin, W. S. Kolthammer, M. Kim, A. Datta, M. Barbieri, and I. A. Walmsley, "Joint estimation of phase and phase diffusion for quantum metrology", Nat. Commun. **5**, 3532 (2014).

[126]T. Baumgratz and A. Datta, "Quantum Enhanced Estimation of a Multidimensional Field", Phys. Rev. Lett. **116**, 030801 (2016).

[127]S. Pang and T. A. Brun, "Quantum metrology for a general Hamiltonian parameter", Phys. Rev. A **90**, 022117 (2014).

[128]A. Chrostowski, R. Demkowicz-Dobrzański, M. Jarzyna, and K. Banaszek, "On super-resolution imaging as a multiparameter estimation problem", Int. J. Quantum Inf. **15**, 1740005 (2017).

[129]C. W. Helstrom, "Minimum mean-squared error of estimates in quantum statistics", Phys. Lett. A **25**, 101–102 (1967).

[130]C. Helstrom, "The minimum variance of estimates in quantum signal detection", IEEE Trans. on Inf. Theory **14**, 234–242 (1968).

[131]H. Yuen and M. Lax, "Multiple-parameter quantum estimation and measurement of nonselfadjoint observables", IEEE Trans. on Inf. Theory **19**, 740–750 (1973).

[132]L. Pezzè, M. A. Ciampini, N. Spagnolo, P. C. Humphreys, A. Datta, I. A. Walmsley, M. Barbieri, F. Sciarrino, and A. Smerzi, "Optimal Measurements for Simultaneous Quantum Estimation of Multiple Phases", Phys. Rev. Lett. **119**, 130504 (2017).

[133]J. Suzuki, Y. Yang, and M. Hayashi, "Quantum state estimation with nuisance parameters", J. Phys. A: Math. Theor. **53**, 453001 (2020).

[134]P. Horodecki, Ł. Rudnicki, and K. Życzkowski, "Five Open Problems in Quantum Information Theory", PRX Quantum **3**, 010101 (2022).

[135]H. Chen, Y. Chen, and H. Yuan, "Incompatibility measures in multiparameter quantum estimation under hierarchical quantum measurements", Phys. Rev. A **105**, 062442 (2022).

[136]B. Wang, K. Zheng, Q. Xie, A. Zhang, L. Xu, and L. Zhang, "Achieving the Multiparameter Quantum Cramér-Rao Bound with Antiunitary Symmetry", Phys. Rev. Lett. **133**, 210801 (2024).

[137]L. O. Conlon, J. Suzuki, P. K. Lam, and S. M. Assad, "Role of the extended Hilbert space in the attainability of the quantum Cramér–Rao bound for multiparameter estimation", Phys. Lett. A **542**, 130445 (2025).

[138]H. I. Nurdin, "Saturability of the Quantum Cramér–Rao Bound in Multiparameter Quantum Estimation at the Single-Copy Level", IEEE Control. Syst. Lett. **8**, 376–381 (2024).

[139]S. Ragy, M. Jarzyna, and R. Demkowicz-Dobrzański, "Compatibility in multiparameter quantum metrology", Phys. Rev. A **94**, 052108 (2016).

[140]M. Tsang, "The Holevo Cramér-Rao bound is at most thrice the Helstrom version", arXiv.1911.08359 (2021).

[141]A. Candeloro, Z. Pazhotan, and M. G. A. Paris, "Dimension matters: precision and incompatibility in multi-parameter quantum estimation models", arXiv.2403.07106 (2024).

[142]L. O. Conlon, J. Suzuki, P. K. Lam, and S. M. Assad, "The gap persistence theorem for quantum multiparameter estimation", arXiv.2208.07386 (2024).

[143]A. Holevo, *Probabilistic and Statistical Aspects of Quantum Theory* (Edizioni della Normale, Pisa, 2011).

[144]K. Matsumoto, "A new approach to the Cramér-Rao-type bound of the pure-state model", J. Phys. A: Math. Gen. **35**, 3111–3123 (2002).

[145]A. Das, L. O. Conlon, J. Suzuki, S. K. Yung, P. K. Lam, and S. M. Assad, "Holevo Cramér-Rao bound: How close can we get without entangling measurements?", arXiv.2405.09622 (2024).

[146]J. W. Gardner, T. Gefen, S. A. Haine, J. J. Hope, and Y. Chen, "Achieving the Fundamental Quantum Limit of Linear Waveform Estimation", Phys. Rev. Lett. **132**, 130801 (2024).

[147]M. Zhou, H. Ma, L. Chen, W. Zhang, and C.-H. Yuan, "Holevo Cramér-Rao bound for multi-parameter estimation in nonlinear interferometers", arXiv.2502.02855 (2025).

[148]K. Yamagata, A. Fujiwara, and R. D. Gill, "Quantum local asymptotic normality based on a new quantum likelihood ratio", The Ann. Stat. **41**, 10.1214/13-AOS1147 (2013).

[149]Y. Yang, G. Chiribella, and M. Hayashi, "Attaining the Ultimate Precision Limit in Quantum State Estimation", Commun. Math. Phys. **368**, 223–293 (2019).

[150]L. O. Conlon, J. Suzuki, P. K. Lam, and S. M. Assad, "Efficient computation of the Nagaoka–Hayashi bound for multiparameter estimation with separable measurements", npj Quantum Inf. **7**, 110 (2021).

[151]L. O. Conlon, T. Vogl, C. D. Marciniak, I. Pogorelov, S. K. Yung, F. Eilenberger, D. W. Berry, F. S. Santana, R. Blatt, T. Monz, P. K. Lam, and S. M. Assad, "Approaching optimal entangling collective measurements on quantum computing platforms", Nat. Phys. **19**, 351–357 (2023).

[152]L. O. Conlon, J. Suzuki, P. K. Lam, and S. M. Assad, "Role of the extended Hilbert space in the attainability of the Quantum Cramér-Rao bound for multiparameter estimation", arXiv.2404.01520 (2024).

[153]F. Albarelli, J. F. Friel, and A. Datta, "Evaluating the Holevo Cramér-Rao Bound for Multiparameter Quantum Metrology", Phys. Rev. Lett. **123**, 200503 (2019).

[154]J. S. Sidhu, Y. Ouyang, E. T. Campbell, and P. Kok, "Tight Bounds on the Simultaneous Estimation of Incompatible Parameters", Phys. Rev. X **11**, 011028 (2021).

[155]P. Mironowicz, "Semi-definite programming and quantum information", J. Phys. A: Math. Theor. **57**, 163002 (2024).

[156]S. Boyd and L. Vandenberghe, *Convex Optimization*, 1st ed. (Cambridge University Press, Mar. 2004).

[157]M. Hayashi and Y. Ouyang, "Tight Cramér-Rao type bounds for multiparameter quantum metrology through conic programming", Quantum **7**, 1094 (2023).

[158]M. Hayashi and Y. Ouyang, "Finding the optimal probe state for multiparameter quantum metrology using conic programming", npj Quantum Inf. **10**, 111 (2024).

[159]S. K. Yung, L. O. Conlon, J. Zhao, P. K. Lam, and S. M. Assad, "Comparison of estimation limits for quantum two-parameter estimation", Phys. Rev. Res. **6**, 033315 (2024).

[160]H. Chen, L. Wang, and H. Yuan, "Simultaneous measurement of multiple incompatible observables and tradeoff in multiparameter quantum estimation", npj Quantum Inf. **10**, 1–10 (2024).

[161]S. Zhou and S. Chen, "Randomized measurements for multi-parameter quantum metrology", arXiv:2502.03536 (2025).

[162]E. T. Jaynes, *Probability theory: the logic of science*, edited by G. L. Bretthorst (Cambridge University Press, Cambridge, 2003).

[163]Y. Li, L. Pezzè, M. Gessner, Z. Ren, W. Li, and A. Smerzi, "Frequentist and Bayesian Quantum Phase Estimation", Entropy **20**, 628 (2018).

[164]U. Von Toussaint, "Bayesian inference in physics", Rev. Mod. Phys. **83**, 943–999 (2011).

[165]S. Personick, "Application of quantum estimation theory to analog communication over quantum channels", IEEE Trans. on Inf. Theory **17**, 240–246 (1971).

[166]C. Helstrom and R. Kennedy, "Noncommuting observables in quantum detection and estimation theory", IEEE Trans. on Inf. Theory **20**, 16–24 (1974).

[167]A. Holevo, "Statistical decision theory for quantum systems", J. Multivar. Anal. **3**, 337–394 (1973).

[168]M. Tsang, "Ziv-Zakai Error Bounds for Quantum Parameter Estimation", Phys. Rev. Lett. **108**, 230401 (2012).

[169]X.-M. Lu and M. Tsang, "Quantum Weiss-Weinstein bounds for quantum metrology", Quantum Sci. Technol. **1**, 015002 (2016).

[170]D. W. Berry, M. Tsang, M. J. W. Hall, and H. M. Wiseman, "Quantum Bell-Ziv-Zakai Bounds and Heisenberg Limits for Waveform Estimation", Phys. Rev. X **5**, 031018 (2015).

[171]Y.-R. Zhang and H. Fan, "Quantum metrological bounds for vector parameters", Phys. Rev. A **90**, 043818 (2014).

[172]E. Martínez-Vargas, C. Pineda, F. Leyvraz, and P. Barberis-Blostein, "Quantum estimation of unknown parameters", Phys. Rev. A **95**, 012136 (2017).

[173]M. A. C. Rossi, F. Albarelli, D. Tamascelli, and M. G. Genoni, "Noisy Quantum Metrology Enhanced by Continuous Nondemolition Measurement", Phys. Rev. Lett. **125**, 200505 (2020).

[174]J. Boeyens, S. Seah, and S. Nimmrichter, "Uninformed Bayesian quantum thermometry", Phys. Rev. A **104**, 052214 (2021).

[175]M. R. Jørgensen, J. Kołodyński, M. Mehboudi, M. Perarnau-Llobet, and J. B. Brask, "Bayesian quantum thermometry based on thermodynamic length", Phys. Rev. A **105**, 042601 (2022).

[176]M. Mehboudi, M. R. Jørgensen, S. Seah, J. B. Brask, J. Kołodyński, and M. Perarnau-Llobet, "Fundamental Limits in Bayesian Thermometry and Attainability via Adaptive Strategies", Phys. Rev. Lett. **128**, 130502 (2022).

[177]K. K. Lee, C. Gagatsos, S. Guha, and A. Ashok, "Quantum Multi-Parameter Adaptive Bayesian Estimation and Application to Super-Resolution Imaging", arXiv:2202.09980 (2022).

[178]M. Overton, J. Rubio, N. Cooper, D. Baldolini, D. Johnson, J. Anders, and L. Hackermüller, "Substantial precision enhancements via adaptive symmetry-informed Bayesian metrology", arXiv:2410.10615 (2025).

[179]J. Wei, J. Huang, and C. Lee, "Adaptive robust high-precision atomic gravimetry", Phys. Rev. Res. **7**, L012064 (2025).

[180]V. Cimini, E. Polino, M. Valeri, N. Spagnolo, and F. Sciarrino, "Benchmarking Bayesian quantum estimation", Quantum Sci. Technol. **9**, 035035 (2024).

[181]J. Rubio, "Quantum scale estimation", Quantum Sci. Technol. **8**, 015009 (2023).

[182]J. Rubio, "First-principles construction of symmetry-informed quantum metrologies", Phys. Rev. A **110**, L030401 (2024).

[183]J. Boeyens, J. Glatthard, E. Gandar, S. Nimmrichter, L. A. Correa, and J. Rubio, "On the role of symmetry and geometry in global quantum sensing", arXiv:2502.14817 (2025).

[184]R. Lecamwasam, S. Assad, J. J. Hope, P. K. Lam, J. Thompson, and M. Gu, "Relative Entropy of Coherence Quantifies Performance in Bayesian Metrology", PRX Quantum **5**, 030303 (2024).

[185]J. Bavaresco, P. Lipka-Bartosik, P. Sekatski, and M. Mehboudi, "Designing optimal protocols in Bayesian quantum parameter estimation with higher-order operations", Phys. Rev. Res. **6** (2024).

[186]J. Rubio, J. Anders, and L. A. Correa, "Global Quantum Thermometry", Phys. Rev. Lett. **127**, 190402 (2021).

[187]Z.-Y. Zhou, J.-T. Qiu, and D.-J. Zhang, "Strict hierarchy of optimal strategies for global estimations: Linking global estimations with local ones", Phys. Rev. Res. **6**, L032048 (2024).

[188]V. Montenegro, U. Mishra, and A. Bayat, "Global Sensing and Its Impact for Quantum Many-Body Probes with Criticality", Phys. Rev. Lett. **126**, 200501 (2021).

[189]C. Mukhopadhyay and A. Bayat, "Modular Many-Body Quantum Sensors", Phys. Rev. Lett. **133**, 120601 (2024).

[190]J. J. Meyer, S. Khatri, D. S. França, J. Eisert, and P. Faist, "Quantum metrology in the finite-sample regime", arXiv:2307.06370 (2023).

[191]M. Hayashi, "Heisenberg scaling based on population coding", Quantum **9**, 1648 (2025).

[192]P. Mehta, M. Bukov, C.-H. Wang, A. G. R. Day, C. Richardson, C. K. Fisher, and D. J. Schwab, "A high-bias, low-variance introduction to Machine Learning for physicists", Phys. Reports, A High-Bias, Low-Variance Introduction to Machine Learning for Physicists **810**, 1–124 (2019).

[193]G. Carleo, I. Cirac, K. Cranmer, L. Daudet, M. Schuld, N. Tishby, L. Vogt-Maranto, and L. Zdeborová, "Machine learning and the physical sciences", Rev. Mod. Phys. **91**, 045002 (2019).

[194]J. Huang, M. Zhuang, J. Zhou, Y. Shen, and C. Lee, "Quantum Metrology Assisted by Machine Learning", Adv. Quantum Technol. **8**, 2300329 (2025).

[195]S. Nolan, A. Smerzi, and L. Pezzè, "A machine learning approach to Bayesian parameter estimation", npj Quantum Inf. **7**, 169 (2021).

[196]L. J. Fiderer, J. Schuff, and D. Braun, "Neural-Network Heuristics for Adaptive Bayesian Quantum Estimation", PRX Quantum **2**, 020303 (2021).

[197]A. Lumino, E. Polino, A. S. Rab, G. Milani, N. Spagnolo, N. Wiebe, and F. Sciarrino, "Experimental Phase Estimation Enhanced by Machine Learning", Phys. Rev. Appl. **10**, 044033 (2018).

[198]F. Belliardo, F. Zoratti, F. Marquardt, and V. Giovannetti, "Model-aware reinforcement learning for high-performance Bayesian experimental design in quantum metrology", Quantum **8**, 1555 (2024).

[199]V. Cimini, M. Valeri, E. Polino, S. Piacentini, F. Ceccarelli, G. Corrielli, N. Spagnolo, R. Osellame, and F. Sciarrino, "Deep reinforcement learning for quantum multiparameter estimation", Adv. Photonics **5**, 016005 (2023).

[200]G. Buonaiuto and C. Lupo, "Machine learning with sub-diffraction resolution in the photon-counting regime", Quantum Mach. Intell. **7**, 28 (2025).

[201]D. Šafránek, "Discontinuities of the quantum Fisher information and the Bures metric", Phys. Rev. A **95**, 052320 (2017).

[202]L. Seveso, F. Albarelli, M. G. Genoni, and M. G. A. Paris, "On the discontinuity of the quantum Fisher information for quantum statistical models with parameter dependent rank", J. Phys. A: Math. Theor. **53**, 02LT01 (2020).

[203]Y. Ye and X.-M. Lu, "Quantum Cramér-Rao bound for quantum statistical models with parameter-dependent rank", Phys. Rev. A **106**, 022429 (2022).

[204]A. T. Rezakhani, M. Hassani, and S. Alipour, "Continuity of the quantum Fisher information", Phys. Rev. A **100**, 032317 (2019).

[205]Y. Yang, V. Montenegro, and A. Bayat, "Overcoming Quantum Metrology Singularity through Sequential Measurements", arXiv:2501.02784 (2025).

[206]A. Z. Goldberg, J. L. Romero, Á. S. Sanz, and L. L. Sánchez-Soto, "Taming singularities of the quantum Fisher information", Int. J. Quantum Inf. **19**, 2140004 (2021).

[207]I. Gianani, M. G. Genoni, and M. Barbieri, "Assessing Data Postprocessing for Quantum Estimation", IEEE J. Sel. Top. Quantum Electron. **26**, 1–7 (2020).

[208]V. Cimini, M. G. Genoni, I. Gianani, N. Spagnolo, F. Sciarrino, and M. Barbieri, "Diagnosing Imperfections in Quantum Sensors via Generalized Cramér-Rao Bounds", Phys. Rev. Appl. **13**, 024048 (2020).

[209]D. R. M. Arvidsson-Shukur, N. Yunger Halpern, H. V. Lepage, A. A. Lasek, C. H. W. Barnes, and S. Lloyd, "Quantum advantage in postselected metrology", Nat. Commun. **11**, 3775 (2020).

[210]J. H. Jenne and D. R. M. Arvidsson-Shukur, "Unbounded and lossless compression of multiparameter quantum information", Phys. Rev. A **106**, 042404 (2022).

[211]J. Yang, "Theory of Compression Channels for Postselected Quantum Metrology", Phys. Rev. Lett. **132**, 250802 (2024).

[212]F. Girotti, A. Godley, and M. Guţă, "Optimal estimation of pure states with displaced-null measurements", J. Phys. A: Math. Theor. **57**, 245304 (2024).

[213]J. Jae, J. Lee, M. S. Kim, K.-G. Lee, and J. Lee, "Contextual quantum metrology", npj Quantum Inf. **10**, 68 (2024).

[214]I. Frérot and T. Roscilde, "Symmetry: A Fundamental Resource for Quantum Coherence and Metrology", Phys. Rev. Lett. **133**, 260402 (2024).

[215]K. Herb and C. L. Degen, "Quantum Speed Limit in Quantum Sensing", Phys. Rev. Lett. **133**, 210802 (2024).

[216]L. Seveso and M. G. A. Paris, "Estimation of general Hamiltonian parameters via controlled energy measurements", Phys. Rev. A **98**, 032114 (2018).

[217]L. Seveso, M. A. C. Rossi, and M. G. A. Paris, "Quantum metrology beyond the quantum Cramér-Rao theorem", Phys. Rev. A **95**, 012111 (2017).

[218]M. Tsang, F. Albarelli, and A. Datta, "Quantum Semiparametric Estimation", Phys. Rev. X **10**, 031023 (2020).

[219]K. Yamagata, "Maximum logarithmic derivative bound on quantum state estimation as a dual of the Holevo bound", J. Math. Phys. **62**, 062203 (2021).

[220]J. Escandón-Monardes, D. Uzcátegui, M. Rivera-Tapia, S. P. Walborn, and A. Delgado, "Estimation of high-dimensional unitary transformations saturating the Quantum Cramér-Rao bound", Quantum **8**, 1405 (2024).

[221]Y. S. Teo, S. U. Shringarpure, H. Jeong, N. Prasannan, B. Brecht, C. Silberhorn, M. Evans, D. Mogilevtsev, and L. L. Sánchez-Soto, "Evidence-Based Certification of Quantum Dimensions", Phys. Rev. Lett. **133**, 050204 (2024).

[222]J.-L. Zhao, Y.-H. Zhou, D.-X. Chen, Q.-P. Su, X.-L. Zong, Q.-C. Wu, M. Yang, and C.-P. Yang, "Quantum Fisher information power of quantum evolutions", J. Phys. A: Math. Theor. **57**, 275304 (2024).

[223]M. Zhang, H.-M. Yu, H. Yuan, X. Wang, R. Demkowicz-Dobrzański, and J. Liu, "QuanEstimation: An open-source toolkit for quantum parameter estimation", Phys. Rev. Res. **4**, 043057 (2022).

[224]B. MacLellan, P. Roztocki, S. Czischek, and R. G. Melko, "End-to-end variational quantum sensing", npj Quantum Inf. **10**, 118 (2024).

[225]Z. Zou, J. Gong, and W. Chen, "Enhancing Quantum Metrology by Quantum Resonance Dynamics", arXiv:2502.01462 (2025).

[226]Z. Huang and C. Lupo, "Quantum Hypothesis Testing for Exoplanet Detection", Phys. Rev. Lett. **127**, 130502 (2021).

[227]M. Tsang, R. Nair, and X.-M. Lu, "Quantum Theory of Superresolution for Two Incoherent Optical Point Sources", Phys. Rev. X **6**, 031033 (2016).